



**Universidade do Minho**  
Escola de Engenharia

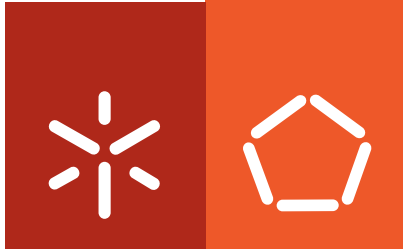
Albino Manuel Pereira Martins

**Development of electrospun nanofibrous-based scaffolds for bone regeneration.**

Albino Manuel Pereira Martins **Development of electrospun nanofibrous-based scaffolds for bone regeneration.**

UMinho | 2009

Dezembro 2009



**Universidade do Minho**  
Escola de Engenharia

Albino Manuel Pereira Martins

**Development of electrospun  
nanofibrous-based scaffolds  
for bone regeneration.**

Tese no Programa de Doutoramento em  
Engenharia de Tecidos, Medicina Regenerativa e  
Células Estaminais

Trabalho efectuado sob a orientação do  
**Professor Nuno João Meleiro Alves das Neves**  
e do  
**Professor Rui Luís Gonçalves dos Reis**

Dezembro 2009

É AUTORIZADA A REPRODUÇÃO INTEGRAL DESTA TESE APENAS PARA EFEITOS DE INVESTIGAÇÃO,  
MEDIANTE DECLARAÇÃO ESCRITA DO INTERESSADO, QUE A TAL SE COMPROMETE;

Universidade do Minho, \_\_\_/\_\_\_/\_\_\_\_\_

Assinatura:

---

## Acknowledgements

During the course of my PhD, several people contributed to accomplish this thesis, both professionally and personally. To them, I would like to deeply express my gratitude and dedicate this dissertation.

First of all, I would like to acknowledge my thesis supervisor, Professor Nuno M. Neves, for his constructive criticism, for supporting new ideas and intellectual property protection, clarifying my ideas about the importance of scientific policy, and the scientific brainstormings. He is meticulous in planning the experiments, in the evaluation and discussion of the experimental data, and in the drawing of conclusions (good or not so good) from the data generated. I herein gratefully acknowledge him for believing in me, trust in my scientific contribution of the 'Naturally Nano' project. Indeed, this project was of utmost importance for my PhD work. I also thank the possibility given to be involved in other parallel projects, which made me feel more responsible and were of utmost importance for my researcher career.

I also thank Professor Rui L. Reis for giving me the opportunity to join the 3B's Research Group and to be the co-supervisor of my PhD work. He is an example to follow in leadership and intelligence, capacity to motivate people and scientific policy; he is an inspiration and mentor. I should also remember his benevolence to me and to my family.

I should also present my gratitude to Alexandra P. Marques for her guidance and reviewing criticism of biological data. I am also grateful to Susana Faria for her help on all the statistical analysis performed, making the results more statistically sound and correctly analysed.

I would like to dedicate a special thank to my colleagues José V. Araújo, Marta Alves da Silva, Ana C. Guimarães, Sangwon Chung, Iva Pashkuleva, Ana Rita C. Duarte, Vitor M. Correlo, Adriano J. Pedro and Rui A. Sousa, and to my friends Elisabete D. Pinho and Pedro Costa, who significantly contributed to the success of my experimental work and scientific inventiveness.

I also appreciated the technical support of Eng. José Cunha and Mr. Américo Rodrigues in the development of the electrospinning apparatus, the patience of Elsa Ribeiro during the SEM/EDS analysis, and of Camen Serra from C.A.C.T.I. at the University of Vigo for the interferometric optical profilometry and XPS measurements and data interpretation.

To finalize my professional acknowledgements, I would like to dedicate a special thanks to the worldwide spread 3B's colleagues.

I should also acknowledge the Portuguese Foundation for Science and Technology (FCT) for my PhD grant SFRH/BD/24382/2005, the 'Naturally Nano' project (POCI/EME/58982/2004) and the European Integrated Project GENOSTEM (LSH-STREP-CT-2003-503161) for the initial scholarship.

No domínio pessoal, gostaria de reconhecer e demonstrar a importância da minha esposa e do meu filhote (apesar de alheio a tudo o que se passa) no decorrer proveitoso do Doutoramento. Eles constituíram, constituem e constituirão a minha motivação para a vida pessoal e profissional.

Aos meus queridos pais e irmão agradeço toda a dedicação como família berço, a confiança no 'filho mais velho', o apoio financeiro aos meus estudos de licenciatura, o amor e carinho para toda a vida.

Aos meus sogros agradeço todo o auxílio que têm proporcionado à minha família.

# Development of electrospun nanofibrous-based scaffolds for bone regeneration

## Abstract

Biomaterials and scaffolds play a significant role in many strategies followed in regenerative medicine and tissue engineering. Those systems are intended and designed to help and guide the cells to contribute for the tissue regeneration process. To achieve that goal, the system needs to actively participate in the signaling process for the cells. It is widely believed that a successful scaffold should mimic the main properties and structure of the extracellular matrix of the tissue of interest.

The fibrous nature of the natural extracellular matrix (ECM) has led many researchers to focus on the development of fiber-based scaffolds. Electrospinning has emerged as a very promising technology enabling to produce synthetic polymeric ultrafine fibers. These fibers in mesh-like structure have diameters in the submicron range which results in a high surface area-to-volume ratio and high porosity. The meshes have a typically random distribution or, in some special cases, some preferential directions of alignment. Despite the claim similarity to the morphology of natural ECM, the surface chemical properties of electrospun nanofibers must be optimized. It is herein shown that defined plasma treatments are able to improve the proliferation of different cell types (fibroblastic, chondrogenic and osteogenic) when seeded at the surface of those meshes.

Bone ECM is a complex ordered hierarchical structure, as a result of the assembling of collagen fibrils at several length scales, ranging from macro to the nanoscale. To test the interest of those morphologies, patterned nanofiber meshes were developed, having areas of uniaxial/parallel alignment and areas of orthogonal/random distribution of fibers. Those patterned nanofiber meshes, not only induced human bone marrow mesenchymal stem cell (hBMSCs) guidance at the early culture periods, but also influence the cell ECM deposition along the predefined fiber direction.

Electrospun nanofibrous structures, due to the inherent planar structure, could compromise a successful reconstruction or regeneration of thick tissues. Two alternative strategies are proposed to overcome this limitation and allowing developing complex ordered fibrous structures that may mimic the hierarchical organization of bone. One structure involves aligned microfibers processed by a 3D rapid prototyping technique, intercalated by electrospun nanofiber meshes. Human osteoblastic-like cells showed significantly higher proliferation and maturation when dynamically seeded on these hierarchical fibrous scaffolds, adhering preferentially to the nanofiber meshes. The other structure developed is

composed by randomly distributed microfibers reinforced by electrospun chitosan nanofibers, processed by melt extrusion and assembled by fiber bonding. The PBS/Cht-based composite scaffolds sustained ECM deposition and mineralization, as suggested by the increased amount of calcium phosphates produced by the hBMSCs under osteogenic induction conditions.

Among the very interesting properties of electrospun nanofiber meshes, their morphological similarity to the natural ECM is very attractive for tissue engineering applications. However, the small size of the pores constitutes a limitation for the infiltration of cells into the inner regions of the fibrous scaffold, hindering its application for thicker 3D tissues. Herein, we propose the electrospinning of a dual composition nanofiber mesh to solve the low cell infiltration capacity on random electrospun nanofiber meshes. The production is followed by the selective dissolution of one fraction of the dual mesh to generate open porosity. The obtained meshes showed statistically significant larger pores, without inducing significant alterations on their morphology. Those highly porous meshes allow human osteoblastic cells infiltration into the full thickness of the mesh structure, showing enhanced viability and proliferation.

The properties of electrospun nanofiber meshes were also explored as bioactive agent release systems. Based in large surface area of the meshes, the release rate of a drug/bioactive agent may be modulated by the concentration of loading in the system. We intended to promote the release of the bioactive agent close to the cells to maximize its efficacy. An osteogenic differentiation factor, dexamethasone, was incorporated into electrospun nanofiber meshes at different concentrations (5, 10, 15 and 20 wt.% polymer), in a single-step process. The 15 wt.% nanofibrous system was selected for the cell studies because of its typical morphology and the sustained release of a biologically relevant dexamethasone concentration. An increased alkaline phosphatase concentration and deposition of mineralized matrix was observed on dexamethasone releasing nanofibrous system, cultured with hBMSCs in dexamethasone-absent osteogenic differentiation medium, showing the potential of this strategy for bone related applications.

We proposed herein different ways to overcome some of the limitations of the electrospun meshes for bone tissue engineering related applications. The strategies enabled showing that, by systematically facing its limitations, we could generate structures that have many more possibilities, enabling also its application in many different problems in the context of tissue engineering and regenerative medicine.

# **Desenvolvimento de estruturas de suporte ao crescimento celular à base de nanofibras produzidas por ‘electrospinning’ para regeneração de osso**

## **Resumo**

Os biomateriais e as estruturas de suporte ao crescimento celular, ou ‘scaffolds’, desempenham um papel importante em inúmeras estratégias de medicina regenerativa e engenharia de tecidos. Esses sistemas são projectados e desenhados a fim de auxiliar e guiar as células durante a regeneração tecidual. De forma a alcançar este objectivo, o ‘scaffold’ deve imitar as propriedades e estrutura da matriz extra-celular (ECM) do tecido alvo.

A natureza fibrosa da ECM tem direccionado os investigadores no desenvolvimento de ‘scaffolds’ fibrosos. O ‘electrospinning’ é uma das tecnologias mais promissoras na produção de fibras poliméricas sintéticas ultra-finas. Essas fibras organizadas numa estrutura semelhante a uma malha têm diâmetros sub-micrométricos, resultando numa elevada área de superfície e porosidade. As malhas têm, tipicamente, uma distribuição aleatória ou, em alguns casos especiais, direcções preferenciais de alinhamento. Apesar da similaridade morfológica destas malhas com a ECM nativa, as propriedades químicas da superfície das nanofibras devem ser optimizadas. Demonstra-se nesta tese que tratamentos de plasma específicos podem melhorar a proliferação de diferentes tipos celulares (fibroblásticos, condrogénicos e osteogénicos) quando semeados à superfície dessas malhas.

A ECM do osso é uma estrutura hierárquica organizada e complexa, resultante do arranjo espacial de fibrilos de colagénio a diversas escalas, partindo da dimensão nanométrica. Para testar a relevância dessa morfologia, foram desenvolvidas malhas de nanofibras com padrão definidos, contendo áreas de alinhamento uniaxial/paralelo e áreas de distribuição ortogonal/aleatória das fibras. Essas malhas de nanofibras padronizadas induzem não só a orientação de células estaminais mesenquimais de medula óssea humana (hBMSCs) para tempos de cultura curtos, mas também influenciam favoravelmente a deposição de ECM ao longo das fibras com alinhamento predefinido.

Estruturas produzidas por ‘electrospinning’, devido à sua estrutura planar, poderão comprometer o sucesso da reconstrução ou regeneração de tecidos espessos. Duas estratégias alternativas foram aqui propostas para ultrapassar esta limitação e permitir o desenvolvimento de estruturas fibrosas ordenadas complexas que podem recapitular a organização hierárquica do osso. Uma estrutura envolve microfibras alinhadas processadas por uma técnica de prototipagem tridimensional, intercaladas por malhas de nanofibras produzidas por ‘electrospinning’. Células

osteoblásticas humanas demonstraram níveis de proliferação e maturação significativamente mais elevadas, quando semeadas dinamicamente nesses 'scaffolds' fibrosos hierárquicos, aderindo preferencialmente às malhas nanofibras. Uma outra estrutura desenvolvida é composta por microfibras aleatoriamente distribuídas reforçadas por nanofibras de quitosano produzidas por 'electrospinning', processadas por extrusão e aglomeradas por compressão a quente. Estes 'scaffolds' compósitos à base de PBS/Cht reforçados sustentam uma acrescida deposição de ECM e mineralização, como sugerido pelo aumento de fosfatos de cálcio produzidos pelas hBMSCs cultivadas em condições de indução osteogénica.

A semelhança morfológica das malhas de nanofibras com a ECM é muito atraente para várias aplicações em engenharia de tecidos. No entanto, a pequena dimensão dos poros constitui uma limitação à infiltração de células, prejudicando a sua aplicação na geração de tecidos mais espessos. Nesta tese, propõe-se a produção de uma malha nanofibrosa com dupla composição para solucionar a baixa capacidade de infiltração celular em malhas aleatórias. A subsequente dissolução selectiva de uma das fracções da malha permite obter maiores porosidades. As malhas obtidas demonstraram um aumento estatisticamente significativo do tamanho dos poros, sem alteração da sua morfologia. Demonstrou-se que estas malhas altamente porosas permitem a infiltração das células osteoblásticas humanas em todo o volume da sua estrutura, apresentando maior viabilidade e proliferação celular.

As malhas produzidas por 'electrospinning' foram também exploradas como sistemas de libertação de agentes bioactivos. Pretendia-se uma libertação do agente bioactivo directamente na vizinhança das células, de modo a maximizar a sua eficácia. Um componente indutor da diferenciação osteogénica, dexametasona, foi incorporado nas malhas nanofibras em diferentes concentrações (5, 10, 15 and 20 wt.% polymer), num passo único. A concentração de fosfatase alcalina e a deposição de matriz mineralizada aumentadas foram observadas em sistemas nanofibrosos com libertação de dexametasona cultivados com hBMSCs em meio de diferenciação osteogénica sem dexametasona, demonstrando o potencial desta estratégia em aplicações ósseas.

Neste trabalho propusemos diferentes possibilidades para obviar a importantes limitações das malhas produzidas por 'electrospinning' quando aplicadas em estratégias de regeneração de tecido ósseo. Estas estratégias permitiram demonstrar que, encarando sistematicamente essas limitações, foi possível desenvolver estruturas com maiores potencialidades e funcionalidades acrescidas. Estes desenvolvimentos podem ainda estender o seu potencial a outras aplicações em engenharia de tecidos e medicina regenerativa.

## Table of contents

<b>Acknowledgments</b>	iii
<b>Abstract</b>	v
<b>Resumo</b>	vii
<b>List of abbreviations</b>	xvii
<b>List of figures</b>	xxi
<b>List of tables</b>	xxviii
<b>List of schemes</b>	xxix
<b>Structure of the thesis</b>	xxx

## Section I – REVIEW OF THE LITERATURE

### 1. Chapter 1 - Electrospinning: processing technique for tissue engineering scaffolding

<b>1.1. Abstract</b>	4
<b>1.2. Introduction</b>	4
<b>1.3. Electrospinning process</b>	8
1.3.1. <i>Electrospinning apparatus</i>	9
1.3.2. <i>Processing parameters</i>	10
1.3.3. <i>Recent developments on electrospinning process</i>	13
<b>1.4. Tissue engineering/Biomedical applications of electrospun nanofibers</b>	17
1.4.1. <i>Wound dressing</i>	18
1.4.2. <i>Medical prostheses</i>	20
1.4.3. <i>Drug delivery systems</i>	22
1.4.4. <i>DNA release</i>	26
1.4.5. <i>Tissue templates/scaffolds</i>	27
<b>1.5. Desired properties of electrospun nanofibers as scaffolds</b>	34
<b>1.6. Future perspectives</b>	37

<b>1.7. Conclusions</b>	41
<b>1.8. References</b>	42

## **Section II – DETAILED DESCRIPTION OF EXPERIMENTAL TESTING AND MATERIALS**

### **2. Chapter 2 - Materials & Methods**

#### **2.1. Materials**

<i>2.1.1. Polycaprolactone</i>	66
<i>2.1.2. Poly(ethylene Oxide)</i>	67
<i>2.1.3. Starch-Polycaprolactone blend</i>	68
<i>2.1.4. Poly(butylene succinate)</i>	69
<i>2.1.5. Chitosan</i>	70
2.1.5.1. Purification of chitosan	71
2.1.5.2. Determination of the viscosity average molecular weight	71
2.1.5.3. Determination of the degree deacetylation	73

#### **2.2. Scaffolds Fabrication**

<i>2.2.1. Electrospinning</i>	77
2.1.1.1. Processing of chitosan nanofiber meshes	79
2.1.1.2. Processing of dual composition nanofiber meshes	80
2.1.1.3. Processing of polycaprolactone nanofiber meshes	80
<i>2.2.2. Rapid Prototyping</i>	81
<i>2.2.3. Melt Fiber Extrusion – Fiber Bonding</i>	83

#### **2.3. Modification of PCL Nanofiber Meshes Surface by Plasma Treatment**

#### **2.4. Dexamethasone Kinetic Release Studies**

#### **2.5. Scaffolds Characterization**

<i>2.5.1. Physical Characterization</i>	
2.5.1.1. Scanning Electron Microscopy	87
2.5.1.2. Interferometric Optical Profilometry	88

2.5.1.3.	Micro-computed Tomography	89
2.5.1.4.	Differential Scanning Calorimetry	90
<i>2.5.2. Chemical Characterization</i>		
2.5.2.1.	Fourier Transform Infra-red Spectroscopy	91
2.5.2.2.	X-ray Photoelectron Spectroscopy	92
2.5.2.3.	Contact Angle measurements	93
<b>2.6. Biological assays</b>		
2.6.1.	<i>Cell Lines</i>	93
2.6.2.	<i>Seeding and Culture of the Cell Lines onto Electrospun Nanofiber Meshes</i>	94
2.6.3.	<i>Primary Cultures of Human Bone Marrow Mesenchymal Stem Cells</i>	95
2.6.4.	<i>hBMSCs Culture, Seeding and Differentiation into the Osteogenic Lineage</i>	96
2.6.5.	<i>Evaluation of Cell Morphology and Distribution</i>	97
2.6.6.	<i>Cell Viability Assay</i>	99
2.6.7.	<i>Cell Proliferation Assay</i>	100
2.6.8.	<i>Alkaline Phosphatase Quantification</i>	101
2.6.9.	<i>Alizarin Red Staining</i>	102
2.6.10.	<i>Immunodetection of Bone-specific Proteins</i>	103
2.6.11.	<i>RNA isolation and Real-Time Quantitative Polymerase Chain Reaction</i>	104
<b>2.7. Statistical Analysis</b>		106
<b>2.8. References</b>		107

### **Section III – ENHANCING THE FUNCTIONALITY OF ELECTROSPUN NANOFIBER MESHES**

#### **3. Chapter 3 - Surface Modification of Electrospun Polycaprolactone Nanofiber Meshes by Plasma Treatment to Enhance Biological Performance**

<b>3.1. Abstract</b>	120
----------------------	-----

<b>3.2. Introduction</b>	120
<b>3.3. Materials &amp; Methods</b>	
3.3.1. <i>Electrospinning process</i>	122
3.3.2. <i>Surface Modification by Plasma Treatment</i>	123
3.3.3. <i>Surface Characterization of Untreated and Plasma-Treated PCL Nanofiber Meshes</i>	
3.3.3.1. Scanning Electron Microscopy	123
3.3.3.2. Interferometric Optical Profilometry	123
3.3.3.3. Contact Angle Measurements	124
3.3.3.4. X-ray Photoelectron Spectroscopy	124
3.3.4. <i>Biological Assays</i>	
3.3.4.1. Cell Lines	125
3.3.4.2. Cell Seeding	125
3.3.4.3. Evaluation of Cell Morphology	126
3.3.4.4. Metabolic Activity Analysis (MTS Assay)	126
3.3.5. <i>Statistical Analysis</i>	126
<b>3.4. Results</b>	
3.4.1. <i>Morphological Characterization of Plasma-Treated Electrospun Nanofibers</i>	127
3.4.2. <i>Hydrophilicity of Plasma-Treated Electrospun Nanofibers</i>	128
3.4.3. <i>Chemical Composition of Plasma-Treated Electrospun Nanofibers</i>	130
3.4.4. <i>Cellular Performance over Plasma-Treated Electrospun Nanofibers</i>	131
<b>3.5. Discussion</b>	139
<b>3.6. Conclusions</b>	143
<b>3.7. References</b>	144

## Section IV – COMPLEX ORDERED FIBROUS STRUCTURES

### 4. Chapter 4 - Differentiated Human Bone Marrow Stem Cells are Sensitive to Patterned Nanofiber Meshes?

<b>4.1. Abstract</b>	154
<b>4.2. Introduction</b>	154
<b>4.3. Materials &amp; Methods</b>	
4.3.1. <i>Production of Patterned Nanofiber Meshes</i>	157
4.3.2. <i>Characterization of Patterned Nanofiber Meshes</i>	157
4.3.3. <i>Expansion, Seeding and Osteogenic Differentiation of Human Bone Marrow Mesenchymal Stem Cells</i>	157
4.3.4. <i>Cell Morphology and Distribution</i>	158
4.3.5. <i>Cell Viability and Proliferation (MTS assay and DNA content)</i>	159
4.3.6. <i>Alkaline Phosphatase quantification and Immunodetection of Bone-specific Proteins</i>	159
4.3.7. <i>RNA isolation and Real-Time Quantitative Polymerase Chain Reaction</i>	161
4.3.8. <i>Statistical Analysis</i>	162
<b>4.4. Results and Discussion</b>	
4.4.1. <i>Morphological Characterization of Patterned Nanofiber Meshes</i>	162
4.4.2. <i>Phenotypic Characterization of Differentiated hBMSCs on Patterned Nanofiber Meshes</i>	164
4.4.3. <i>Genotypic Characterization of Differentiated hBMSCs on Patterned Nanofiber Meshes</i>	169
<b>4.5. Conclusions</b>	171
<b>4.6. References</b>	172
<b>5. Chapter 5 - Hierarchical Starch-based Fibrous Scaffold for Bone Tissue Engineering Applications</b>	
<b>5.1. Abstract</b>	178
<b>5.2. Introduction</b>	178
<b>5.3. Materials &amp; Methods</b>	
5.3.1. <i>Scaffold Fabrication</i>	180
5.3.2. <i>Scaffold Characterization</i>	180
5.3.3. <i>Cell Seeding and Culture</i>	181
5.3.4. <i>Evaluation of Cell Adhesion, Morphology and Distribution</i>	182

5.3.5. <i>Cell Viability Assay</i>	182
5.3.6. <i>DNA Quantification</i>	182
5.3.7. <i>Alkaline Phosphatase (ALP) Quantification</i>	183
5.3.8. <i>Statistical analysis</i>	183
<b>5.4. Results &amp; Discussion</b>	184
<b>5.5. Conclusions</b>	188
<b>5.6. References</b>	189

## **6. Chapter 6 - Biodegradable Nanofiber-Reinforced Microfibrous Composite Scaffolds for Bone Tissue Engineering Applications**

<b>6.1. Abstract</b>	194
<b>6.2. Introduction</b>	194
<b>6.3. Materials &amp; Methods</b>	
6.3.1. <i>Production of the Nanofiber-Reinforced Microfibrous Composite Scaffolds</i>	197
6.3.2. <i>Characterization of the Nanofiber-reinforced Microfibrous Composite Scaffolds</i>	198
6.3.3. <i>Expansion, Seeding and Osteogenic Differentiation of Human Bone Marrow Mesenchymal Stem Cells</i>	199
6.3.4. <i>Analysis of Cell Morphology and Distribution, and ECM Mineralization</i>	199
6.3.5. <i>Cell Viability and Proliferation Assessment</i>	200
6.3.6. <i>Alkaline Phosphatase Quantification</i>	200
6.3.7. <i>RNA isolation and Real-Time Quantitative Polymerase Chain Reaction</i>	201
6.3.8. <i>Statistical Analysis</i>	202
<b>6.4. Results</b>	
6.4.1. <i>Morphology of the Nanofibers Reinforced Microfibrous Composite Scaffolds</i>	203
6.4.2. <i>Morphology, Viability and Proliferation of Human Bone Marrow Mesenchymal Stem Cells on Nanofiber-reinforced Microfibrous Composite Scaffolds</i>	204
6.4.3. <i>Osteogenic Differentiation of Human Bone Marrow Mesenchymal Stem</i>	

<i>Cells on Nanofiber-Reinforced Microfibrous Composite Scaffolds</i>	208
<b>6.5. Discussion</b>	210
<b>6.6. Conclusions</b>	213
<b>6.7. References</b>	213

## **Section V – 2<sup>ND</sup> GENERATION ELECTROSPUN SCAFFOLDS**

### **7. Chapter 7 - Solving Cell Infiltration Limitations of Electrospun Nanofiber Meshes for Tissue Engineering Applications**

<b>7.1. Abstract</b>	222
<b>7.2. Introduction</b>	222
<b>7.3. Materials &amp; Methods</b>	
<i>7.3.1. Electrospinning processing</i>	226
<i>7.3.2. Physical characterization</i>	227
<i>7.3.3. Biological assays</i>	228
<i>7.3.4. Statistical analysis</i>	230
<b>7.4. Results</b>	
<i>7.4.1. Physical characterization</i>	233
<i>7.4.2. Biological assays</i>	237
<b>7.5. Discussion</b>	243
<b>7.6. Conclusions</b>	247
<b>7.7. References</b>	248

### **8. Chapter 8 - hBMSCs Osteogenic Induction by Electrospun Scaffolds with Dexamethasone Release Functionality**

<b>8.1. Abstract</b>	256
<b>8.2. Introduction</b>	256
<b>8.3. Materials &amp; Methods</b>	
<i>8.3.1. Production of Nanofiber Meshes Loaded with Dexamethasone</i>	259
<i>8.3.2. Characterization of Dexamethasone-loaded PCL Nanofiber Meshes</i>	260

8.3.3. <i>Dexamethasone Kinetic Release Studies</i>	260
8.3.4. <i>Expansion, Seeding and Osteogenic Differentiation of Human Bone Marrow Mesenchymal Stem Cells</i>	261
8.3.5. <i>Cell Morphology and Distribution, and Chemistry of Deposited Matrix</i>	262
8.3.6. <i>Alkaline Phosphatase Quantification</i>	263
8.3.7. <i>Alizarin Red Staining</i>	263
8.3.8. <i>Immunodetection of Bone-specific Proteins</i>	263
8.3.9. <i>RNA isolation and Real-Time Quantitative Polymerase Chain Reaction</i>	264
8.3.10. <i>Statistical Analysis</i>	265
<b>8.4. Results</b>	
8.4.1. <i>Physicochemical Properties of the Dexamethasone-loaded Electrospun PCL Nanofiber Meshes</i>	266
8.4.2. <i>Release Kinetics of Dexamethasone from the Electrospun PCL Nanofiber Meshes</i>	268
8.4.3. <i>Biological Activity of the Dexamethasone Released from the Electrospun Nanofiber Meshes</i>	270
<b>8.5. Discussion</b>	
8.5.1. <i>Electrospun PCL Nanofiber Meshes Incorporating and Releasing Dexamethasone</i>	276
8.5.2. <i>Bioactivity of the Dexamethasone Released from the Electrospun Nanofiber Meshes</i>	278
<b>8.6. Conclusions</b>	280
<b>8.7. References</b>	281

## **Section VI – GENERAL CONCLUSIONS AND FURTHER WORK**

### **9. Chapter 9 - Concluding Remarks**

<b>9.1. Conclusions</b>	290
<b>9.2. Future work</b>	295

## List of abbreviations and nomenclature

### A

AcOH - acetic acid  
ALP - alkaline phosphatase  
AA - ascorbic acid  
AFM - atomic force microscopy

### B

BMSCs - bone marrow stromal cells  
BMP-2 - bone morphogenetic protein 2  
BSP - Bone sialoprotein  
BACs - bovine articular chondrocytes  
BCAECs - bovine coronary artery endothelial cells

### C

CMs - cardiomyocytes  
Cht - chitosan  
Cht NFM - chitosan nanofiber meshes  
COL – collagen  
CFU - colony-forming unit  
cDNA – complementary deoxyribonucleic acid  
CT - computed tomography  
CAD - computer aided design  
CAE - Constant Analyzer Energy  
*Cbfa1/Runx2* - core binding factor  $\alpha$  1/runt-related gene  
SPCL - com starch - polycaprolactone blend

### D

DD - degree deacetylation  
DNA - deoxyribonucleic acid  
DEX - Dexamethasone  
DAPI - 4,6-diamidino-2-phenylindole, dilactate  
DAB – diaminobenzidine  
DC - Dichloromethane  
DSC - Differential Scanning Calorimetry  
DTA - differential thermal analysis  
MTS - 3-(4,5-dimethylthiazol-2-yl)-5-(3-carboxymethoxyphenyl)-2-(4-sulfonyl)-2H-tetrazolium, inner salt  
dsDNA - double-stranded DNA  
DMEM - Dulbecco's modified Eagle's medium

### E

ECs - endothelial cells  
ESCA - electron spectroscopy for chemical analysis  
EDS - energy dispersive spectrometer  
EPR - enhanced permeability and retention  
 $\Delta H$  - enthalpy  
 $\Delta S$  - entropy  
E-SEM - environmental scanning electron microscopy  
EO - ethylene oxide

ECM - extracellular matrix

## **F**

FBS - fetal bovine serum

FITC-BSA - fluorescein isothiocyanate  
labelled bovine serum albumin

FDA - Food and Drug Administration

FTIR - Fourier transform infra-red

FDM - fused deposition modeling

## **G**

*GAPDH* - glyceraldehydes-3-  
phosphate-dehydrogenase gene

$T_g$  - glass transition temperature

GAGs - glycosaminoglycans

GBR - guided bone regeneration

## **H**

HPLC - high performance liquid  
chromatography

HVPS - high voltage power supply

$K_H$  - Huggins coefficient

hBMSCs - human bone marrow  
mesenchymal stem cells

HEPM - human embryonic palatal  
mesenchymal cells

hMSCs - human mesenchymal stem  
cells

Saos-2 - human primary osteosarcoma  
cell line

HSCs - human satellite cells

HUVECs - human umbilical vein  
endothelial cells

HLF - human ligament fibroblast

HA - hyaluronic acid

HAp - hydroxyapatite

HMPC - hydroxypropylmethylcellulose

## **I**

IC - Informed Consent

IMR - International Materials Reviews

$[\eta]$  - intrinsic viscosity

## **K**

$K_K$  - Kraemer coefficient

## **M**

$T_m$  - melting temperature

MSC - mesenchymal stem cells

mRNA - messenger ribonucleic acid

$\alpha$ -MEM - minimum essential medium  
alpha

$M_w$  - molecular weight

ATDC5 - mouse chondrocyte  
teratocarcinoma-derived cell line

L929 - mouse lung fibroblastic cell line

## **N**

NFM(s) - nanofiber mesh(es)

nHAP - nanoparticles of hydroxyapatite

NIR - near infrared

NGF - nerve growth factor

NSC - neural stem cells

NADH - nicotinamide adenine dinucleotide  
NADPH - nicotinamide adenine dinucleotide phosphate  
pnPP - nitrophenyl phosphate disodium salt  
NHK - normal human keratinocytes  
NMR - nuclear magnetic resonance

## O

OC - osteocalcin  
OP - osteopontin  
*Osx* – *Osterix* gene

## P

P-NFM - patterned PCL nanofiber meshes  
PBS - phosphate buffer saline  
PAA - poly(acrylic acid)  
PANI/PEO - polyaniline/poly(ethylene oxide)  
PNmPh - poly[bis(*p*-methylphenoxy)phosphazene]  
PBS - poly(butylene succinate)  
PBS/Cht - (poly(butylene succinate)/Chitosan (50:50 wt.%) microparticulate composite  
PCL - poly(caprolactone)  
PCL NFM - polycaprolactone nanofiber meshes  
PCLEEP - poly( $\epsilon$ -caprolactone-*co*-ethyl ethylene phosphate)

PDMS - poly(dimethylsiloxane)  
PEUU - poly(ester urethane) urea  
PEVA - poly(ethylene-*co*-vinylacetate)  
EVOH - poly(ethylene-*co*-vinyl alcohol)  
PEG - poly(ethylene glycol)  
PEG-*g*-CHN - poly(ethylene glycol)-*g*-chitosan  
PEO – poly(ethylene oxide)  
PET - polyethylene terephthalate  
PGA - poly(glycolic acid)  
PLA - poly(lactic acid)  
PLLA - poly(L-lactic acid)  
PLCL - poly(L-lactide-*co*- $\epsilon$ -caprolactone)  
P(LLA-CL) - poly(L-lactic acid)-*co*-poly( $\epsilon$ -caprolactone)  
LEL - poly(lactide)-*b*-poly(ethylene glycol)-*b*-poly(lactide)  
PLGA - poly(lactide-*co*-glycolide)  
PMMA - poly(methyl methacrylate)  
PPX - poly(*p*-xylene)  
PTFE - polytetrafluoroethylene  
PU – polyurethane  
PVA - poly(vinyl alcohol)  
PVP - polyvinylpyrrolidone  
pNP - *p*-nitrophenol

## R

RF - radio frequency  
RP - rapid prototyping

rhBMP-2 - recombinant human bone morphogenetic protein 2  
 $\eta_r$  - relative viscosity  
RT - reverse transcriptase  
RNA - ribonucleic acid  
RMS - root mean square  
 $Rq$  – RMS roughness  
 $Ra$  - roughness average

## **S**

SEM - scanning electron microscopy  
SF - silk fibroin  
ssDNA - single-stranded DNA  
SMCs - smooth muscle cells  
AcONa - sodium acetate  
 $\eta_{sp}$  - specific viscosity

## **T**

TGA – thermogravimetric analysis  
3D - three-dimensional  
ToF/SIMS - Time-of-Flight Secondary Ion Mass Spectrometry

TCPS - tissue culture polystyrene  
TGF $\beta$ -1 - transforming growth factor  $\beta$ 1  
TEM - transmission electron microscopy  
TFA - trifluoroacetic acid

## **U**

UV - ultraviolet  
UV-Vis ou UV/Vis - ultraviolet-visible spectrophotometry

## **V**

VSMCs - vascular smooth muscle cells  
VSI - vertical scanning interferometry  
 $M_v$  - viscosity average molecular weight

## **W**

WLI - white light interferometer

## **X**

XPS - X-ray Photoelectron Spectroscopy

## List of figures

<b>Figure 1.1</b> - SEM micrograph of polycaprolactone (PCL) nanofibers in a mesh, produced by electrospinning.	9
<b>Figure 1.2</b> - Schematic representation of electrospinning apparatus.	10
<b>Figure 1.3</b> - SEM micrograph of polyvinylpyrrolidone (PVP) nanofibers with beads in its structure.	12
<b>Figure 1.4</b> – (A) Schematic illustration of the setup for electrospinning nanofibers having a core/sheath structure. The system is based in a spinneret with two coaxial capillaries. (B) SEM micrograph of a uniaxially aligned array of TiO <sub>2</sub> hollow fibers after both mineral oil extraction from the core and calcination.	14
<b>Figure 1.5</b> - SEM micrographs of PLLA fibers with pores at the surface obtained via electrospinning of a solution of PLLA in dichloromethane.	15
<b>Figure 1.6</b> - A, B and C) Schematic illustration of collectors based in gold electrodes deposited over insulating substrates. D, E and F micrographs obtained by dark-field optical microscopy of PVP nanofibers collected between the electrodes A, B and C, respectively.	17
<b>Figure 1.7</b> - Mouse lung fibroblasts (L929 cell line) adhered on plasma-modified PCL nanofiber meshes.	19
<b>Figure 1.8</b> - Fabricated bilayered tubular construct composed of a polyurethane tube with the interior surface coated with collagen.	21
<b>Figure 1.9</b> - SEM micrographs of electrospun poly( $\epsilon$ -caprolactone) nanofiber meshes after biomimetic calcium phosphate coating, keeping the porous morphology (A). Morphology of Saos-2 cells cultured for 14 days on PCL nanofiber meshes coated with a biomimetic coating (B).	30
<b>Figure 1.10</b> – Image from the electrospinning process embedding living cells in the fiber structure.	39
<b>Figure 2.1</b> - Chemical structure of polycaprolactone.	66
<b>Figure 2.2</b> – Chemical structure of poly(ethylene oxide).	67
<b>Figure 2.3</b> - Chemical structures of the amylase (A) and amylopectin (B) molecules.	68

<b>Figure 2.4</b> - Chemical structure of chitosan.	70
<b>Figure 2.5</b> - Linear regressions obtained by plotting $\eta_{sp}/c$ or $\ln \eta_r/c$ against $c$ , according to the Huggins or Kraemer equations, respectively.	73
<b>Figure 2.6</b> - Identification of the chitosan $^1\text{H-NMR}$ spectra peaks.	75
<b>Figure 2.7</b> - Photographs of the electrospinning apparatus components: the semi-commercial high voltage power supply (A); the single syringe infusion pump (B); and a grounded metallic collector located inside a cuboid acrylic structure, with a vertical position holder of the syringe pump, lodge in a chemical hood (C).	78
<b>Figure 2.8</b> - SEM micrographs showing the morphology of electrospun PCL random (A) and patterned (B) nanofiber meshes, and chitosan (C) nanofiber meshes.	81
<b>Figure 2.9</b> – SEM micrographs of of the starch-based rapid prototyped (6RP) (A) and hierarchical fibrous scaffolds (6RP+5NFM) (B).	83
<b>Figure 2.10</b> - Design of the micro-extruder.	84
<b>Figure 2.11</b> – SEM micrographs of the PBS-based (A) and PBS/Cht-based microfibrinous scaffolds (B).	85
<b>Figure 3.1</b> - SEM micrographs of untreated and plasma-treated PCL nanofiber meshes.	127
<b>Figure 3.2</b> - Optical profilometry images of the untreated PCL nanofiber meshes (A), Oxygen-treated at 30W during 10 minutes (B) and Argon-treated at 20W during 5 minutes (C).	128
<b>Figure 3.3</b> - Glycerol Contact Angle values of untreated and plasma modified PCL nanofiber meshes as function of the time.	129
<b>Figure 3.4</b> - High resolution C1s core level signals of untreated (A) and Oxygen-treated electrospun PCL nanofiber meshes at 30W during 5 minutes (B).	131
<b>Figure 3.5</b> - SEM micrographs of L929 cells growing onto plasma-treated and untreated PCL nanofiber meshes, after 1 day of culture.	132
<b>Figure 3.6</b> - SEM micrographs of ATDC5 cells growing onto plasma-treated and	

untreated PCL nanofiber meshes, after 1 day of culture.	133
<b>Figure 3.7</b> - SEM micrographs of Saos-2 cells growing onto plasma-treated and untreated PCL nanofiber meshes, after 1 day of culture.	134
<b>Figure 3.8</b> - Box plot of MTS assay results for fibroblasts (L929 cell line) cultured on untreated and plasma treated PCL nanofiber meshes during 1, 3, 7 and 14 days.	135
<b>Figure 3.9</b> - Box plot of MTS assay results for chondrocytes (ATDC5 cell line) cultured on untreated and plasma treated PCL nanofiber meshes during 1, 3, 7 and 14 days.	137
<b>Figure 3.10</b> - Box plot of MTS assay results for osteoblasts (Saos-2 cell line) cultured on plasma treated and untreated PCL nanofiber meshes during 1, 3, 7 and 14 days.	138
<b>Figure 4.1</b> - SEM micrographs (A-D) and optical profilometric images (E-H) of the typical random (A and E) and patterned (B and F) nanofiber meshes (P-NFM). P-NFM comprise areas of parallel/uniaxial (C and G) and orthogonal (D and H) alignment of the fibers.	163
<b>Figure 4.2</b> - SEM micrographs of undifferentiated hBMSCs cultured on patterned nanofiber meshes, at the random/orthogonal area of alignment (A) and at the parallel/uniaxial fibers (B). SEM micrographs (C, F and H) and fluorescence images (D, E, G and I) of hBMSCS induced to differentiate into the osteogenic lineage at days 7 (C-E), 14 (F-G) and 21 (H-I) of culture.	165
<b>Figure 4.3</b> – Box plot of DNA content of hBMSCS induced to differentiate into the osteogenic lineage during 21 days, cultured on random and patterned nanofiber meshes.	166
<b>Figure 4.4</b> – Box plot of ALP quantification from hBMSCS induced to differentiate into the osteogenic lineage during 21 days, cultured on random and patterned nanofiber meshes.	167
<b>Figure 4.5</b> - Optical images of immunodetected osteogenic markers, namely osteopontin (A-C), bone sialoprotein (D-F) and osteocalcin (G-I), expressed by hBMSCS, induced to differentiate into the osteogenic lineage and cultured on patterned nanofiber meshes during 7 (A, D and G), 14 (B, E and H) and 21 (C,	

F and I) days.	168
<b>Figure 4.6</b> – Relative expression of bone-specific transcripts, namely <i>Alkaline Phosphatase</i> , <i>Osteopontin</i> , <i>Bone Sialoprotein</i> , <i>Osteocalcin</i> , <i>Runx2</i> and <i>Osterix</i> , by hBMSCs induced to differentiate into the osteogenic lineage during 21 days, cultured on random and patterned nanofiber meshes.	170
<b>Figure 5.1</b> - SEM and $\mu$ -CT micrographs of the starch-based rapid prototyped, 6RP (A and C), and hierarchical fibrous scaffolds, 6RP+5NFM (B and D).	184
<b>Figure 5.2</b> – SEM micrographs of rapid prototyped (A, C, E and G) and hierarchical fibrous (B, D, F and H) scaffolds cultured with human osteoblast-like cells (Saos-2 cell line) during 1 (A-D) and 7 days (E-H).	186
<b>Figure 5.3</b> - Box plot of cell viability results of human osteoblastic cells cultured on rapid prototyped (6RP) and hierarchical fibrous (6RP+5NFM) scaffolds, during 1 and 7 days.	186
<b>Figure 5.4</b> - Box plot of DNA content of osteoblast-like cells cultured on rapid prototyped (6RP) and hierarchical fibrous (6RP+5NFM) scaffolds, during 1 and 7 days.	187
<b>Figure 5.5</b> - Box plot of ALP activity, normalized against dsDNA amount, from osteoblastic cells (Saos-2 cell line) cultured on rapid prototyped (6RP) and hierarchical fibrous (6RP+5NFM) scaffolds, during 1 and 7 days.	188
<b>Figure 6.1</b> - Morphology and architecture of the electrospun chitosan nanofibers reinforced (A, C, E and G) and non-reinforced (B, D, F and H) microfibrinous scaffolds on photomicrographs from scanning electron microscopy (A-D) and 3D models from micro-computed tomography (E-H).	203
<b>Figure 6.2</b> - SEM photomicrographs of nanofibers reinforced (A, C, E, G, I and K) and non-reinforced (B, D, F, H, J and L) microfibrinous scaffolds cultured with hBMSCs during 7 (A-D), 14 (E-H) and 21 days (I-L), under osteogenic conditions.	204
<b>Figure 6.3</b> - EDS spectra for electrospun nanofibers reinforced (i.e. <i>PBS/Cht-R</i> ) (A) and non-reinforced <i>PBS/Cht</i> (B) scaffolds seeded with hBMSCs and cultured under osteogenic conditions, after 14 and 21 days.	205
<b>Figure 6.4</b> - Box plot of the hBMSCs viability cultured in <i>PBS-R</i> , <i>PBS</i> , <i>PBS/Cht-</i>	

<i>R</i> and <i>PBS/Cht</i> , under osteogenic conditions.	206
<b>Figure 6.5</b> - Box plot of the hBMSCs proliferation, cultured on <i>PBS-R</i> , <i>PBS</i> , <i>PBS/Cht-R</i> and <i>PBS/Cht</i> scaffolds under osteogenic conditions.	207
<b>Figure 6.6</b> - Box plot of the alkaline phosphatase (ALP) from hBMSCs cultured on <i>PBS-R</i> , <i>PBS</i> , <i>PBS/Cht-R</i> and <i>PBS/Cht</i> scaffolds under osteogenic conditions.	208
<b>Figure 6.7</b> - Relative expression of osteoblastic transcripts, namely <i>Alkaline Phosphatase</i> , <i>Osteopontin</i> , <i>Bone Sialoprotein</i> , <i>Osteocalcin</i> , <i>Runx2</i> and <i>Osterix</i> , by hBMSCs cultured on <i>PBS-R</i> , <i>PBS</i> , <i>PBS/Cht-R</i> and <i>PBS/Cht</i> scaffolds under osteogenic conditions.	209
<b>Figure 7.1</b> - SEM micrographs of electrospun dual composition PCL-PEO NFM, produced with different applied tensions, from lower (A) to higher (C), without dissolution (1), after 2 hours (2) and 24 hours of dissolution (3) at 37 °C.	232
<b>Figure 7.2</b> - SEM micrographs (A) and Interferometric Optical Profilometry images (B) of electrospun control PCL NFM (1), dual composition PCL-PEO NFM (2) and PCL-PEO NFM, after PEO dissolution (3).	233
<b>Figure 7.3</b> - Box plot of fiber diameter for control PCL NFM, dual composition PCL-PEO NFM and PCL-PEO NFM, after dissolution.	234
<b>Figure 7.4</b> - Box plot of pores size on control PCL NFM, dual composition PCL-PEO NFM and PCL-PEO NFM, after dissolution.	234
<b>Figure 7.5</b> - Box plot of roughness parameters, namely <i>R<sub>a</sub></i> (average roughness) and <i>R<sub>q</sub></i> (root mean square roughness), on control PCL NFM, dual composition PCL-PEO NFM and PCL-PEO NFM, after dissolution.	235
<b>Figure 7.6</b> - Box plot of water contact angle values for control PCL NFM, dual composition PCL-PEO NFM and PCL-PEO NFM, after PEO dissolution NFM, as a function of time.	236
<b>Figure 7.7</b> - SEM micrographs of electrospun control PCL NFM (A) and PCL-PEO NFM, after PEO dissolution (B), and opposite face of control PCL NFM (C) and PCL-PEO NFM, after PEO dissolution (D) cultured with human osteoblastic cells during 1 (1), 3 (2), 7 (3) and 14 days (4).	238
<b>Figure 7.8</b> - Laser scanning confocal microscopy images of electrospun control	

PCL NFM (A) and PCL-PEO NFM, after PEO dissolution (B), after 1 (1) and 7 days (2) of human osteoblastic-like cells culture.	239
<b>Figure 7.9</b> - Box plot of human osteoblast-like cells viability cultured on control PCL NFM control and PCL-PEO NFM, after PEO dissolution.	241
<b>Figure 7.10</b> - Box plot of cell proliferation on control PCL NFM and PCL-PEO NFM, after PEO dissolution, estimated according to the DNA quantification assay.	242
<b>Figure 8.1</b> – Morphological characterization of a typical electrospun PCL nanofiber mesh (A) and the electrospun nanofiber meshes incorporating different concentrations of dexamethasone.	266
<b>Figure 8.2</b> - FTIR spectra of raw dexamethasone, control PCL NFMs, DEX-loaded PCL NFMs at 10 wt.%, 15 wt.% and 20 wt.%.	267
<b>Figure 8.3</b> – DSC thermogram of control PCL NFMs (black line) and raw dexamethasone (grey line) (A), and DEX-loaded PCL nanofibers at 5 wt.%, 10 wt.%, 15.wt % and 20.wt % (B).	268
<b>Figure 84</b> – Release profile of the different dexamethasone concentrations incorporated into the electrospun PCL nanofiber meshes during 360h (A). A zoom up of the initial 24h of dexamethasone release (B).	269
<b>Figure 8.5</b> – Box plot of the hBMSCs viability (MTS assay) cultured on <i>NFM_Osteo</i> , <i>NFM_Basal</i> , <i>NFM+DEX_Osteo</i> and <i>NFM+DEX_Basal</i> , after 7, 14 and 21 days.	270
<b>Figure 8.6</b> – Box plot of the hBMSCs proliferation (DNA concentration) cultured on <i>NFM_Osteo</i> , <i>NFM_Basal</i> , <i>NFM+DEX_Osteo</i> and <i>NFM+DEX_Basal</i> , after 7, 14 and 21 days.	271
<b>Figure 8.7</b> – Box plot of the alkaline phosphatase (ALP) produced by hBMSCs cultured on <i>NFM_Osteo</i> , <i>NFM_Basal</i> , <i>NFM+DEX_Osteo</i> and <i>NFM+DEX_Basal</i> , after 7, 14 and 21 days.	272
<b>Figure 8.8</b> – SEM micrographs of hBMSCs cultured on DEX-loaded NFMs during 7 (A), 14 (B) and 21 days (C). Higher magnifications are shown to evidence the mineralization nodules produced by the hBMSCs. Alizarin red staining of the DEX-loaded NFMs-hBMSCs constructs after 14 (D) and 21 days	

(E). Energy dispersive spectrometer (EDS) spectra of the calcium phosphates nodules produced by hBMSCs cultured on DEX-loaded NFMs after 14 and 21 days (F). 273

**Figure 8.9** – Immunodetection of some bone-specific proteins, namely Osteopontin, Bone Sialoprotein and Osteocalcin, expressed by hBMSCs cultured on DEX-loaded NFMs during 7, 14 and 21 days. 275

**Figure 8.10** - Relative expression of bone-specific transcripts, namely *Alkaline Phosphatase*, *Osteopontin*, *Bone Sialoprotein*, *Osteocalcin*, *Runx2* and *Osterix*, by hBMSCs cultured on *NFM\_Osteo*, *NFM+DEX\_Osteo* and *NFM+DEX\_Basal*, after 7, 14 and 21 days. 276

## List of tables

<b>Table 2.1</b> - Calibration curves to determine the DD using the FTIR spectrum of chitosan that make use of different combinations of bands and baselines.	76
<b>Table 2.2</b> - List of primer sets for bone-specific genes.	105
<b>Table 3.1</b> - Surface roughness parameters of some plasma-treated and untreated electrospun PCL nanofiber meshes.	128
<b>Table 3.2</b> - Elemental composition of some plasma-treated and untreated electrospun PCL nanofiber meshes.	130
<b>Table 4.1</b> - Primers list of osteogenic markers.	161
<b>Table 6.1</b> - Primers list of osteogenic markers.	202
<b>Table 8.1</b> - Primers list of osteogenic markers.	265

## List of schemes

<b>Scheme 2.1</b> - Schematic representation of the electrospinning apparatus.	77
<b>Scheme 2.2</b> - Schematic representation (lateral and top view) of the fixing system used in the biologic assay.	95
<b>Scheme 7.1</b> - Schematic representation of the fixing system used in the biologic assay.	228

## **Structure of the thesis**

The present thesis is divided in 6 sections, organized according with the defined aims, the nature of the experiments performed and the results obtained. The level of complexity of the problem being studied and the biological assays used to characterize the developed systems were the main parameters taken into account in the organization and sequence of those sections. The sub-division in chapters is based in a series of related papers published in international journals or submitted for publication, which are identified in the front page of each chapter. Therefore, each thesis chapter is presented in an adapted version of the published or submitted manuscript style, keeping its contents, but intended to have a consistent structure between the various thesis chapters.

The first section consists of a comprehensive and detailed literature review about the development of electrospun nanofiber meshes for tissue engineering applications. This literature review begins with an in depth description of the electrospinning apparatus, governing parameters, and recent developments and potentialities of this technology.

The second section of the thesis includes a detailed analysis of the materials used, the processing techniques, the techniques used for the scaffolds physicochemical characterization. The biological tests with both model cell lines and primary cultures of human bone marrow mesenchymal stem cells are also described. The biological assays include the analysis of the cell viability and proliferation, the quantification of an osteoblastic marker, specifically alkaline phosphatase (ALP), immunolocalization of some osteoblastic proteins and quantification of osteoblastic genes expression.

The third section reports the surface modification of electrospun PCL nanofibers by different plasma treatments. Although the electrospun nanofibers herein used are made of a synthetic biodegradable polymer, the plasma surface modifications induced an increment of the viability and proliferation of the different model cell types.

The fourth section includes 3 chapters, based on a series of related papers that present the development of complex ordered nanofibrous-based scaffolds. The first chapter of this section reports on studies using patterned nanofibrous structures produced by electrospinning. The second chapter includes 3D nanofibrous-based scaffolds consisting of electrospun nanofiber meshes intercalated between layers of rapid prototyping microfibers. In the third chapter of this section, electrospun nanofiber meshes were incorporated into melt-extruded microfibers, acting as a mechanical reinforcement. The biological relevance of those structures was tested, envisioning a more advanced bone tissue engineering strategy.

The fifth section presents significant contributions to overcome the limitations of the typical electrospun nanofiber meshes aiming at increasing their biological functionality. In the first chapter of this section it is presented a strategy to overcome the cell infiltration limitations of electrospun nanofiber meshes. The second chapter of this section, being the last research chapter of the thesis, reports on electrospun nanofibers capable of release an osteogenic differentiation factor. Its bioactivity is shown by the successful osteogenic differentiation of hBMSCs cultured in those highly functional structures.

In the final section of this thesis, the sixth, it is presented the overall conclusions obtained from the collection of research works previously presented and it is also discussed the future perspectives and lines of research to be followed.



## **Section I**

### REVIEW OF THE LITERATURE



# Chapter 1

## Electrospinning: processing technique for tissue engineering scaffolding

This chapter is based on the following publications: Martins A, Reis RL, Neves NM. *Electrospinning: processing technique for tissue engineering scaffolding*. International Materials Reviews 2008; 53(5):257-274 and Martins A, Araujo JV, Reis RL, Neves NM. *Electrospun nanostructured scaffolds for tissue engineering applications*. Nanomedicine 2007; 2(6):929-942.

## **1.1. Abstract**

Electrospinning has attracted tremendous interest in the research community as a simple and versatile technique to produce synthetic polymeric ultrafine fibers with diameters ranging from a few micrometers to tens of nanometers. Recently, some natural origin polymers have also been successfully electrospun. Owing to their very small diameter, polymeric nanofibers exhibit unusual properties such as high specific surface area, flexibility in surface functionalities and superior mechanical properties. In addition, electrospun non-woven meshes could physically mimic the extracellular matrix structure of native tissues. These remarkable properties render electrospun nanofibers useful for many applications, particularly those related to the field of biomedical engineering. The first part of this review is intended to provide a fundamental survey of the electrospinning process (e.g. apparatus, governing parameters) and of recent improvements of the technique, including associated structural modifications of polymeric nanofiber meshes. The prospective tissue engineering/biomedical applications of electrospun polymeric nanofibers are then reviewed, namely, wound dressings, medical prostheses, drug delivery systems, DNA release and tissue engineering scaffolds. The essential properties of scaffolds in terms of the structural features of electrospun nanofiber meshes are discussed. Finally, the future perspectives for applications of electrospun nanofibers, particularly in the field of tissue engineering, are considered.

## **1.2. Introduction**

Nanostructures and the nanotechnologies to produce them have been a subject of intensive research due to the unique properties that can be obtained and their potential applications in many areas. A large number of technologies have already been demonstrated as being able to generate nanostructures in the form of fibers [1, 2], among them electrospinning. The electrospinning technique may be considered as a variation of the electrostatic spraying (or electrospraying) process [3], used in technologies such as time of flight secondary ion mass spectrometry [4] and

other spectrometric methods [5]. In electrospraying, small droplets or particles are formed as a result of the varicose break-up of the electrified jet that is often present with a solution of low viscosity [6]. In electrospinning, a solid fiber (composed of a viscous polymer solution) is produced by the generated electrical field. Subsequently, nanofibers are formed by continuous stretching, due to the electrostatic repulsion between the charged nanofibers and the evaporation of the solvent [3].

Although the term 'electrospinning', derived from 'electrostatic spinning', was proposed relatively recently (around 1994), its origin as a viable fiber spinning technique can be traced back to the mid 1930s. Formhals [7] patented, in 1934, his first invention, describing the process and the apparatus for producing artificial filaments using electric charges. In 1964, Taylor [8] developed fundamental studies on the jet formation process. The observed conical shape of the jet was later referred by other researchers as the 'Taylor Cone'. In subsequent years, the focus shifted to studying the structural morphology of nanofibers owing to the development of atomic force microscopy (AFM), transmission electron microscopy (TEM) and even scanning electron microscopy (SEM) tools. Researchers were occupied with the structural characterization of fibers and the understanding of the relationship between the structural features and process parameters [3, 9-16]. A major upsurge in electrospinning research took place due to the application potential of nanofibers in areas such as filtration systems, protective clothing, catalyst substrates, photonics, sensors and tissue engineering scaffolding [1, 17-20]. Strangely enough, although the electrospinning process has been known for more than 70 years, the mechanism by which nanofibers is formed is not fully understood. Although a number of studies have been carried out to investigate the mechanism of fiber formation in order reproducibly to control scaffold design, little theoretical understanding has been achieved.

According to the review by Huang *et al.* [1] more than 100 different polymers have been successfully spun into ultrafine fibers using this technique (most dissolved in solvents yet some electrospun from melt) for various applications. The potential applications in cell biology and tissue engineering has resulted in a large number of biodegradable polymers being electrospun into nanofibers, including poly(caprolactone) (PCL) [21-27], poly(lactic acid) [28-30] (PLA), poly(glycolic acid)

(PGA) [31, 32] and poly(lactide-co-glycolide) (PLGA) [33-36]). In addition to these synthetic biodegradable polymers, natural biopolymers, such as DNA [14, 37], silk fibroin [38-41], fibrinogen [42, 43], dextran [44], collagen [45-48] and chitosan [49, 50] have been successfully processed by electrospinning. Relative to synthetic polymers, natural origin polymers have good biocompatibility; conversely, their processability is, in general, poor.

A number of functional polymers envisaged for specific applications have been directly electrospun into nanofibers. However, many functional polymers are not suitable for use with electrospinning, because of their limited molecular weights and/or solubilities. One of the most effective strategies for solving this problem is to blend them with polymers that are well suited for electrospinning [18]. This is a feasible approach that may not only reduce the potential problem of cytotoxicity, as a result of using a chemical cross-linking reagent, but also provides a well designed solution for overcoming the shortcomings of synthetic and natural polymers. Indeed, the production of new biomaterials with good biocompatibility and improved mechanical and physical/chemical properties has been achieved [51-55].

Electrospinning is an attractive approach for polymer biomaterials processing, providing an opportunity to control morphology, porosity, and composition using relatively unsophisticated equipment. Unlike conventional fiber spinning processes that produce fibers with diameters in the micrometre range [56], electrospinning is capable of producing fibers in the nanometre diameter range, which are typically deposited in the form on non-woven fabrics. Nanofibers provide a connection between the nanoscale and the macroscale world, since although their diameters are in the nanometre range, they are very long entities, sometimes of the order of kilometers [14]. Even the largest diameters produced by electrospinning are more than 10 times smaller than those that can be extruded to manufacture textile structures and woven mats.

When the diameters of polymer fiber materials are shrunk from the micrometre (e.g. 10-100  $\mu\text{m}$ ) to the submicrometre or nanometre scale (e.g. 10-100 nm), several interesting properties arise, such as very large surface area to volume ratio (which for a nanofiber can be 1000 times of that of a microfiber), flexibility in surface

functionalities and superior mechanical performance (e.g. stiffness and tensile strength) compared with any other known form of the material [1]. It is known that the natural extracellular matrix (ECM) of various tissues is composed of randomly oriented collagen fibers with nanometre scale diameters. Indeed, the architecture of the electrospun nanofibrous structure is dimensionally, but not morphologically, similar to those of some natural ECMs [2, 19]. The non-woven mats produced have the additional advantages of controllable pore size, high porosity with interconnected pores and permeability [27, 57]. These outstanding properties make the polymer nanofibers effective candidates for many important applications, particularly for tissue engineering/biomedical applications.

The present review is organised into three main sections. First, the fundamentals of the electrospinning process are considered; this survey includes an overview of the electrospinning apparatus and the parameters governing the process (the effects of these processing parameters have been reviewed in detail previously) [58, 59]. Recent developments of the electrospinning process enabling production of different nanofibrous structures (e.g. core/sheath combinations, hollow, porous or aligned nanofibers) are also reviewed (some of these nanofiber structures have been reviewed previously) [60, 61].

The following section provides an extensive discussion of the potential tissue engineering/biomedical applications of electrospun nanofibers, such as wound dressing, medical prostheses, drug delivery systems, DNA release and tissue scaffolding, with a focus on the electrospun polymer structures and biological evidence. This approach is intended to capture the state of the art of understanding for each type of biomedical application and is the distinctive feature of the present review: a critical assessment of electrospinning as a technique to produce tissue engineered scaffolds. While similar information has been presented in other reviews [62-69], these articles have not covered these tissue engineering/biomedical applications in comparable depth.

The next section reviews scaffold target properties and the extent that these have been achieved by electrospinning nanofibers. The achievements to date and the deviations from the target properties are of utmost importance in identifying the

process improvements required to obtain the tailored nanofibrous scaffolds needed for tissue engineering applications. The review concludes with a section covering future perspectives on applications and opportunities raised by the development of electrospinning, particularly in the field of tissue engineering.

### **1.3. Electrospinning process**

Electrospinning involves applying a very high voltage to a capillary filled with the polymer solution to be spun. Mutual charge repulsion induced by the electrical field causes a force directly opposite to the surface tension of the polymer fluid. As the intensity of the electrical field is increased, the hemispherical surface of the fluid at the tip of the capillary tube elongates to form a conical shape, known as 'Taylor cone', observable in various spinning techniques. With increasing electrostatic field, a critical value is attained when the repulsive electrostatic force overcomes the surface tension of the polymer solution and a charged jet of fluid is ejected from the tip of the Taylor cone [3, 14].

As the jet progresses from the capillary towards the collector, the forces from the external electrical field accelerate and stretch the jet. Stretching and evaporation of the solvent molecules cause the jet diameter to become smaller. As the radius of the jet becomes smaller, the radial forces from the charge can become large enough to overcome the cohesive forces of the fiber and cause it to split into two or more fibers, that is, to splay. This jet division process occurs several more times in rapid succession and produces a large number of small electrically charged fibers moving toward the collector. The divided jets repels each other, thereby acquiring lateral velocities and chaotic trajectories, which gives a brush like appearance in the region beyond the point at which the jet first splays. Splaying and elongation appear to occur simultaneously in many cases [14]. However, recent observations of Yarin *et al.* [16] suggested that the jet, while moving towards the collector, undergoes a chaotic motion or bending instability, due to the repulsive forces originating from the charged ions within the electrospinning jet. Because electrospinning is a continuous process, the fibers could be as long as several kilometres. In the electrospinning process,

these long fibers can be assembled into a three-dimensional, non-woven mat as a result of bending instability of the spinning jet (Figure 1.1).

### 1.3.1. *Electrospinning apparatus*

There are basically three components to complete a functional electrospinning setup: a high voltage power supply (HVPS), a spinneret constituted by a glass capillary tube or a needle of small diameter, and a grounded metal collecting screen (Figure 1.2). The electrospinning apparatus is usually set up in a chemical hood to the exhaustion of organic vapours. In addition, a closed, non-conductive environment with temperature and humidity control is required to avoid interference from environmental factors, such as air turbulence [67]. Several groups [70-72] working on electrospinning have adopted different solutions for the polymer flow through the needle. Some have simply opted for placing the capillary perpendicularly, letting the polymer fluid dropping with help of gravity and placing the collector underneath [71]. Sometimes the capillary can be tilted at a defined angle to control the flow rate through the capillary [72]. Other authors use the capillary horizontal and a pump is used to initiate the droplet. The pump is also used in the case of vertical feeding [70]. The electrode can be inserted either in the polymer fluid or placed onto the tip of the capillary if a syringe with a metal needle is used [12]. The collector is usually a plane metal sheet or a grid that can be covered with a fabric, although rotating cylinders covered with a grounded aluminium sheet could also be used [73].

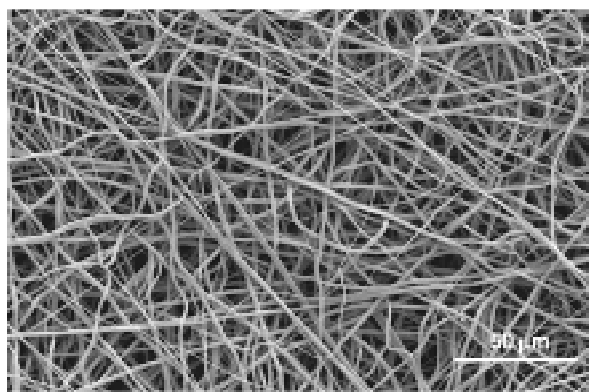


**Figure 1.1** - SEM micrograph of polycaprolactone (PCL) nanofibers in a mesh, produced by electrospinning.

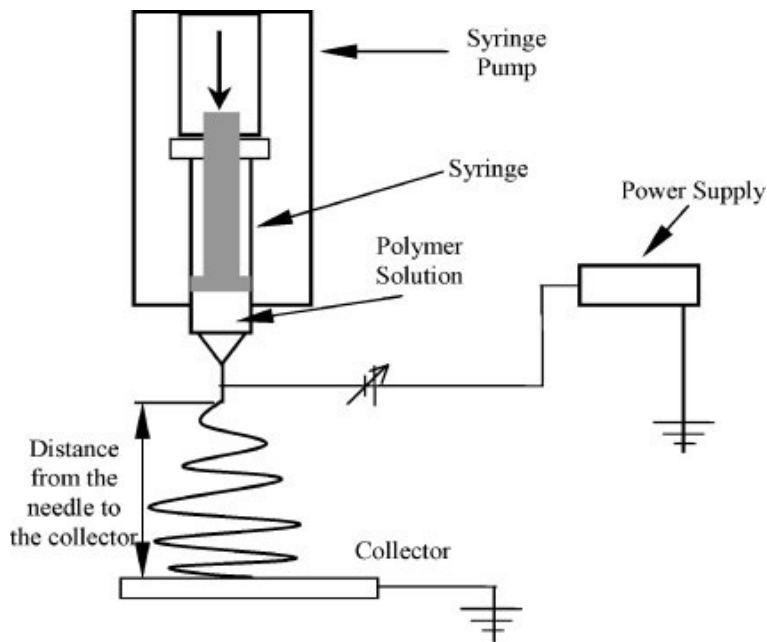


**Figure 1.2** - Schematic representation of electrospinning apparatus (*adapted from reference [25]*).

Most polymers commonly used in electrospinning are dissolved in appropriated solvents before being electrospun [1, 3, 14, 20]. Molten polymers can also be processed into nanofibers through electrospinning, usually at relatively high temperatures [74]; the polymer melt is introduced direct into the capillary tube rather than the solution. However, electrospinning of a polymer melt must be performed in a vacuum condition.

### 1.3.2. Processing parameters

The foregoing discussion suggests that the following parameters significantly affect the electrospinning process: (a) intrinsic solution properties: viscosity, elasticity, conductivity, and surface tension [3, 9, 10], (b) operational conditions: hydrostatic pressure in the capillary tube, electrical potential at the capillary tip, capillary diameter and distance between tip and collecting screen [12, 25], (c) ambient parameters such as solution temperature, humidity and air velocity in the electrospinning chamber [13, 20]. By appropriated tuning of one or more of these parameters, fibers may be

successfully electrospun from water soluble polymers, biopolymers or liquid crystalline polymers.

Generally, the polymer solution must have a concentration high enough to have sufficient number of polymer entanglements yet not so high that the viscosity prevents the polymer flow induced by the pump and the stretching caused by the electrical field. The solution must also have a surface tension low enough, a charge density high enough and a viscosity high enough to prevent the jet from coalescing into droplets before the solvent has evaporated [3]. In the electrospinning process, the properties of the solvent, such as volatility and polarity (dielectric constant), have a significant influence on the morphology and diameter of the electrospun fibers. The electrospinning of a polymer in a polar solvent generally produces ultrathin fibers with smaller average diameters, although the effect of solvent polarity on the fiber diameters has not been systematically studied [9]. Morphological changes can occur upon decreasing the distance between the spinneret and the collector. Increasing the distance or decreasing the electrical field decreases the probability of beads in the mesh, regardless of the concentration of the polymer in solution [12].

As long as a polymer can be electrospun into nanofibers, ideal targets would be: (1) the fibers diameters be uniform, consistent and controllable, (2) that the fiber surface be defectfree, (3) that continuous single nanofibers be collectable. However, to date, these three targets have proved by no means easily achievable. As long as no splitting is involved, one of the most significant parameters influencing the fiber diameter is the solution viscosity: high viscosity results in a larger fiber diameter. In general, fiber diameter tends to decrease with increasing electrospinning voltage, although the influence is not as strong as that of the polymer concentration. An additional challenge is to control the uniformity of fiber diameters with current electrospinning equipment [3, 10, 11, 13]. The base of the Taylor cone when formed is equal to the orifice diameter of the needle. Therefore, it was hypothesized that a change in the length of the base of the Taylor cone will potentially influence the forces necessary for its formation, the formation of the jet and thus the diameter of the nanofibers. As predicted, a decrease in the base of the Taylor cone (orifice diameter) caused a decrease in the average diameter of the nanofibers formed [1].

The structure and morphology of electrospun fibers is also affected by the spinneret tip to collector distance because of their dependence on the deposition time, evaporation rate and whipping or instability regions. Shorter spinneret tip collector distances tend to produce wetter fibers and beaded structures. Thus, aqueous polymer solutions require longer distances to dry fiber formation than systems that use highly volatile organic solvents. The flowrate of the polymer at the syringe is another important process parameter, since it influences jet velocity and material transfer rate. Therefore, the fiber diameters and the pore size are larger when the polymer flowrate is higher. Increased flowrate also increases the tendency to form beaded morphologies [13]. Indeed, a common problem encountered in electrospinning is the formation of structure defects, such as beads and pores caused by local excess of solvent, which may occur in polymer nanofibers (Figure 1.3) [75]. The beads may form as a result of an instability in jet initiation, which is correlated with properties of the polymer solution (viscosity and surface tension) as well as there being insufficient force to stretch the polymer jet. This effect may be due to the electrical field or to the boundary conditions such as a spinneret tip diameter. In other words, it is more likely to be possible to electrospin bead free fibers from thicker spinneret tips with higher polymer concentration solution. Fiber diameter could be significantly decreased by decreasing polymer concentration, although there is a limit to obtain uniform nanofibers without beads. Furthermore, adding filler material into a polymer solution can also result in fibers free from beads [1].

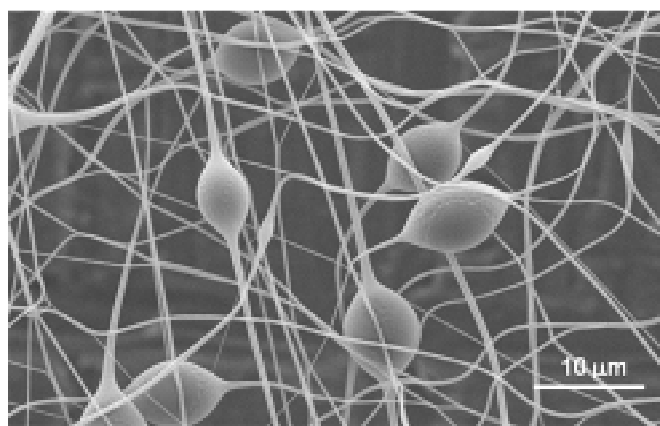


**Figure 1.3** - SEM micrograph of polyvinylpyrrolidone (PVP) nanofibers with beads in its structure.

### *1.3.3. Recent developments on electrospinning process*

Electrospinning apparatus is simple in construction and there have been no significant developments in the equipment design in the past decade. Some research groups [21, 25, 47, 54, 76-78] have improvised the basic electrospinning set-up to suit their experimental needs in terms of materials and applications. In improve control of the electrospinning process and thus, tailor the structures of resultant fibers, the set-up (in particular, the collector and the spinneret) has also been modified. In general, electrospinning is a process with limited productivity because the polymer solution has to be fed at relatively slow rates (usually less than 1 ml/h), to obtain ultrathin fibers. Productivity enhancement for commercializing products obtained by electrospinning is under active research, with emphasis on multiple spinneret designs, and alternative experimental set-ups have recently been demonstrated [76]. However, there is still debate on the potential of scaling up this technology for commercialization. From the available published literature and the current state of understanding of the electrospinning process, it is likely that commercial scaling-up of the electrospinning process will be achieved only when a more fundamental understanding of the process and better control of the instability behaviour of the jets is achieved [20].

The conventional set-up for electrospinning involves the use of a single capillary as the spinneret and thus is suitable only for generating fibers with one particular composition in each run of fabrication, exhibiting a solid interior and a smooth surface. Recent demonstrations established that nanofibers with some specific secondary structures (e.g. core/sheath or hollow, and porous) could also be prepared if appropriated processing parameters (e.g. electrical field strength, concentration of solution and feedrate of solution) or new designs of spinnerets were employed. With the use of the conventional electrospinning set-up, it is possible to fabricate core/sheath nanofibers from a polymer solution containing two polymers that will phase separate as the solvent is evaporated. Core/sheath or hollow nanofibers could also be fabricated by coelectrospinning of two different polymeric solutions through a spinneret comprising two coaxial capillaries [54, 77, 79-82] (Figure 1.4). It has thus amply been demonstrated that electrospinning is capable of fabricating

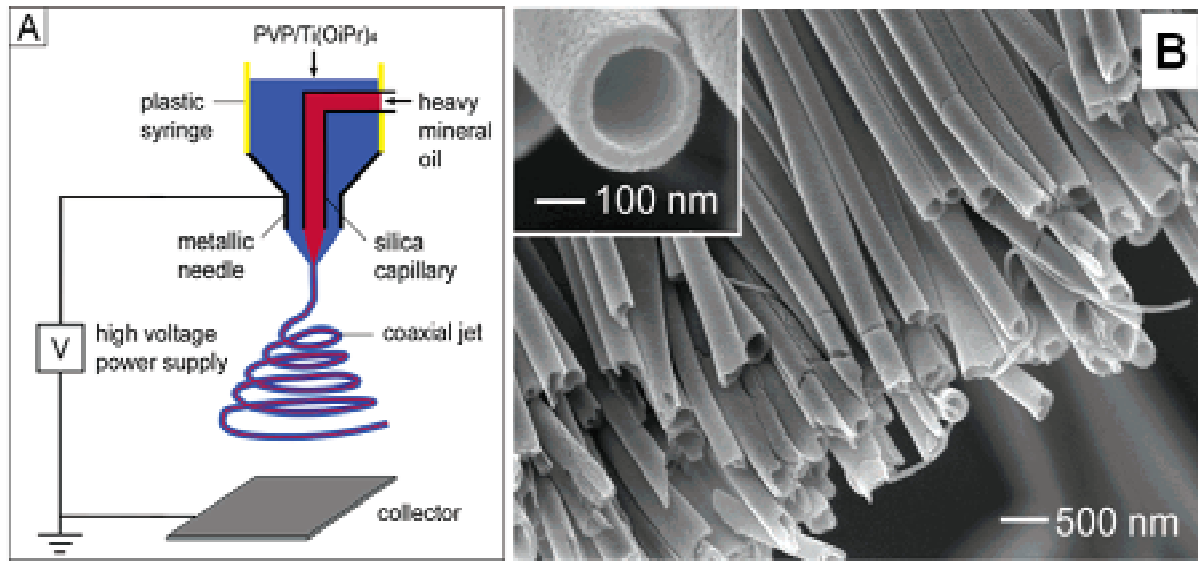


**Figure 1.4** - (A) Schematic illustration of the setup for electrospinning nanofibers having a core/sheath structure. The system is based in a spinneret with two coaxial capillaries. (B) SEM micrograph of a uniaxially aligned array of TiO<sub>2</sub> hollow fibers after both mineral oil extraction from the core and calcination (*adapted from reference [77]*).

nanostructures with complex functionalities. It is also speculated that it will be possible to fabricate hollow nanofibers with multiple walls using a spinneret composed of more than two coaxial capillaries [18].

The specific surface area of a nanofiber can be greatly increased when its structure is switched from solid to porous [82]. Increase in surface areas is beneficial to many applications that include catalysis, filtration, absorption, fuel cells, solar cells, batteries or tissue engineering. Two slightly different approaches have been reported to introduce a porous structure into the bulk of an electrospun nanofiber. One is based on the selective removal of one component used to produce nanofibers made from a two phase material, such as a composite or a blend. The other involves the use of phase separation technology during electrospinning with appropriate spinning parameters [9] (Figure 1.5).

Most nanofibers obtained to date are in the non-woven form, which can be useful for a small number of applications such as filtration, tissue engineering scaffolds, implant coating film, and wound dressing. However, by analogy with the

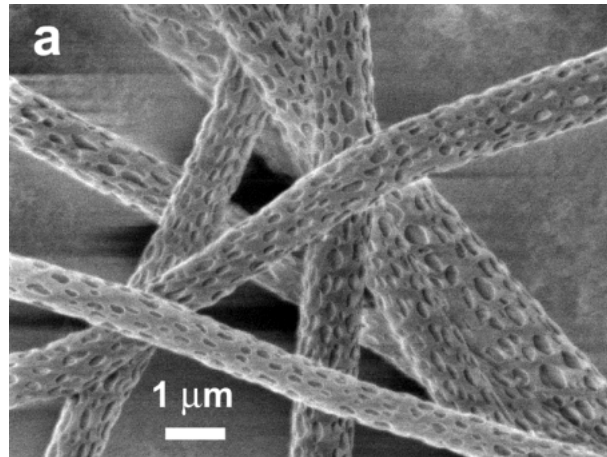


**Figure 1.5** - SEM micrographs of PLLA fibers with pores at the surface obtained via electrospinning of a solution of PLLA in dichloromethane (*adapted from reference [9]*).

traditional fiber and textile industry, only when continuous single nanofibers or uniaxial fiber bundles are obtained will their range of applications be expanded. This is a very tough target to achieve with electrospun nanofibers, because the polymer jet trajectory is a complex three-dimensional “whipping” path, caused by bending instability, rather than a straight line. To date, no continuous long fiber yarn has been reported and the publications related to aligned nanofibers are very limited [1]. It has been suggested that by rotating a cylinder collector at a very high speed (up to thousands of revolutions per minute), electrospun nanofibers could be oriented circumferentially (e.g. PGA and type I collagen) [73].

However, the fiber alignments were achieved only to some extent. The reason why a perfect alignment is difficult to achieve can be attributed to the fact that the chaotic motions of polymer jets are not likely to be coherent and are not controllable. Even so, a large amount of work has been carried out in the field of nanofiber alignment, regarding the use of rotating systems as collectors in the electrospinning process [21, 23, 83-88]. A significant advance in collecting aligned electrospun nanofibers has been made by Theron *et al.* [89], who described a novel approach to position and align individual nanofibers on a tapered and grounded wheel like bobbin. The tip like edge substantially concentrates the electrical field so that the as spun nanofibers are almost all attracted to and continuously wound onto the bobbin edge of the rotating wheel. Investigation is continuing to understand the alignment

characteristics in terms of varying the shape and size of frame rods, the distance between the frame rods, and the inclination angle of a single frame [1]. Fong *et al.* [90] obtained aligned nylon 6 fibers by rapidly oscillating a grounded frame within the electrospun polymer jets. In another approach, it was demonstrated that using a multiple field technique, the polymer jet, usually in chaotic oscillating motion as it approaches the collection target, can be straightened to some extent [11]. Li *et al.* [91] recently demonstrated that the geometrical configuration of a conductive collector had a profound effect on the orientation of electrospun nanofibers (Figure 1.6). Using a collector consisting of two conductive strips separated by a gap of variable width (up to several centimetres), electrospun fibers could be uniaxially aligned over long lengths during the spinning process [92-94]. This collecting process has been termed the 'gap method of alignment', and it results in single electrospun fibers, oriented and suspended between two collection plates. In a different strategy, copper wires spaced evenly in the form of a circular drum as a collector resulted in sheets with 1 cm wide strips of aligned nanofibers [95]. In a recent paper, Teo and Ramakrishna [65] described a simple method of obtaining a fiber bundle of micrometre scale diameter from nanofibers aligned between two parallel steel blades with a gap between them. A similar structure composed of aligned nanofibers, developed by Dalton and colleagues [96], was obtained using two grounded collection rings or circular disks equidistant from the spinneret, by rotating one of the collection rings.

It may also be possible to integrate electrospinning with conventional lithographic techniques to obtain new fabrication platforms for generating patterned microstructures from a variety of materials and a broad range of length scales. Czaplewski *et al.* [97] deposited nanofibers of poly(methyl methacrylate) as templates for the formation of functional nanomechanical devices (e.g. nanomechanical oscillators), combined with lithographically defined support structures. Afterwards, Liu and collaborators [98] developed sensor devices that utilized individual oriented polymeric nanowires of polyaniline/poly(ethylene oxide) deposited on lithographically defined microelectrodes.

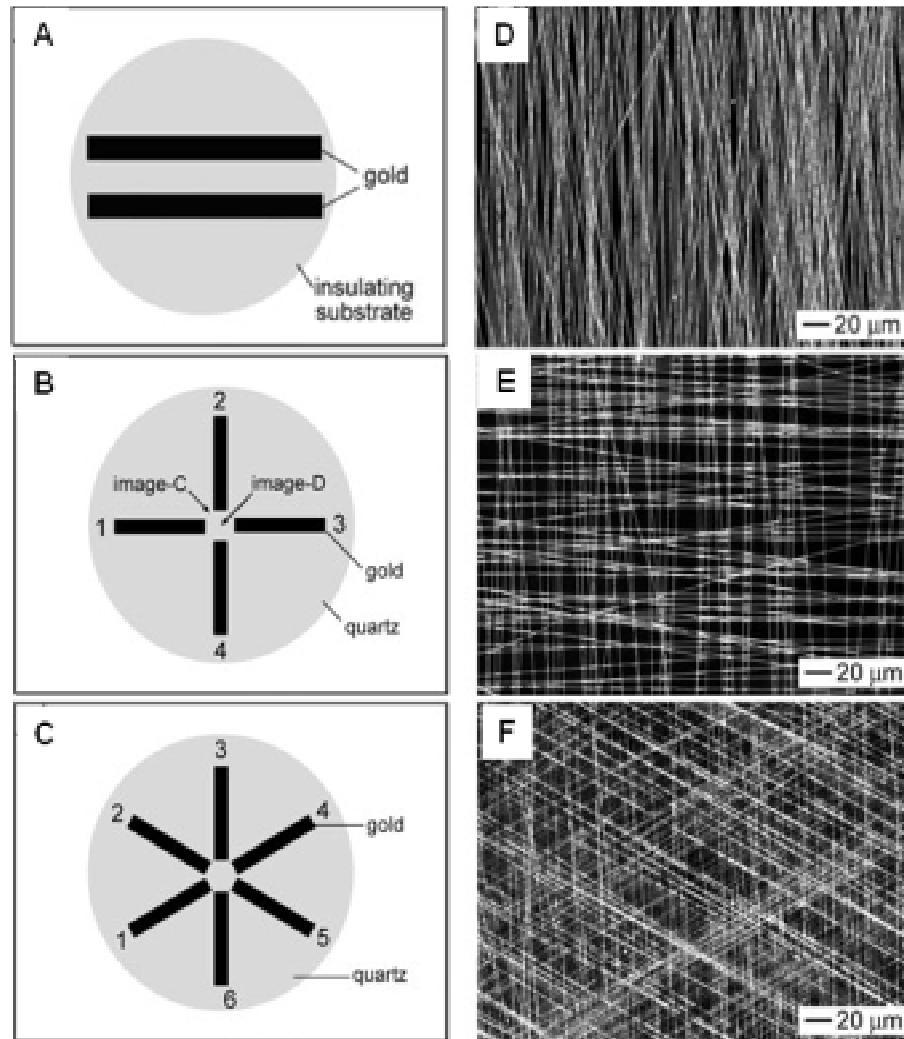


**Figure 1.6** - **A, B** and **C**) Schematic illustration of collectors based in gold electrodes deposited over insulating substrates. **D, E** and **F** micrographs obtained by dark-field optical microscopy of PVP nanofibers collected between the electrodes **A, B** and **C**, respectively (*adapted from reference [91]*).

#### 1.4. Tissue engineering/Biomedical applications of electrospun nanofibers

From a biological perspective, almost all human tissues and organs are deposited in some kind of nanofibrous form or structure [2]. Examples include, among many others, bone, collagen, cartilage and skin [99-101]. All of these are characterized by well organized hierarchical fibrous structures realigning on a nanometre scale [102]. As such, current research in electrospun polymer nanofibers

has focused extensively on biomedical products. Tissue engineering has been recognized, for some time, as a promising alternative to the use of autografts or allografts for tissue reconstruction and regeneration [103-105]. This approach utilises cells, biomaterial scaffolds and signalling molecules for the repair of disease or damage tissues. However, other applications are also envisaged, such as wound dressings and prostheses.

#### *1.4.1. Wound dressing*

An ideal dressing will cover and protect a wound, providing an environment at the surface of the wound in which healing can take place at the maximum rate, with good demosthetical appearance [66]. Modern dressings are developed to serve the purpose of facilitating wound healing apart from the basic function of covering wounds and protecting them from infections. It has been noted by several authors [43, 66, 106] that an ideal dressings is required to (1) be haemostatic, (2) be efficiency as a bacterial barrier, (3) absorb excess exudates, (4) provide and maintain a moist environment or appropriate water vapour transmission rate, and provide adequate gaseous exchange, (5) conform to the limits of the wound area, (6) adhere to healthy tissue but not to wound tissue, i. e., to show functional adhesion, (7) be painless to the patient and easy to remove, and (8) provide these qualities at an affordable cost.

Current efforts using polymer nanofibrous membranes as medical dressings are still at an early stage (Figure 1.7). Fibrinogen is a soluble protein that is present in the blood plasma and has been shown to play a key role in wound healing. Human and bovine fibrinogen nanofiber mats have been electrospun and developed for their potential use as a tissue engineered scaffold, wound dressing or haemostatic bandage [43, 106, 107]. Electrospun poly(ethylene-co-vinyl alcohol) membranes also appear to be favourable substrates for tissue engineering, wound coverage and healing; one has been shown to support the culturing of aortic smooth muscle cells and dermal fibroblasts [108]. Recently, cytocompatibility and cell behaviour of primary normal human keratinocytes (NHK) and fibroblasts cultured on silk fibroin (SF) nanofibrous membranes were also reported [40, 41]. The adhesion of cultured cell types was evaluated using type I collagen, fibronectin or laminin as substrates, which

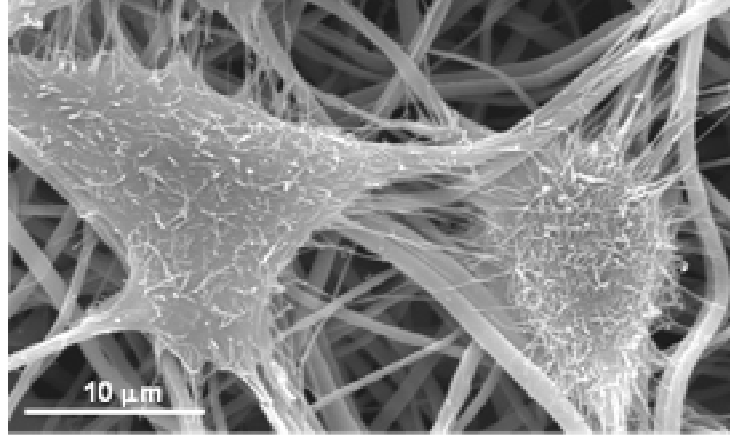


**Figure 1.7** - Mouse lung fibroblasts (L929 cell line) adhered on plasma-modified PCL nanofiber meshes.

were adsorbed onto the SF nanofibers. The results indicated that type I collagen, one of the integrin ligands, is functionally active in terms of cell adhesion onto the electrospun SF nanofibers for both keratinocytes and fibroblasts tested. In another study, the same research group produced a nanofibrous matrix of type I collagen from calfskin via electrospinning [109]. In cell activity assessment, electrospun collagen nanofibers coated with type I collagen or laminin were found to promote cell adhesion and spreading of NHK. Additionally, the effect of collagen nanofibers on open wound healing in rats and athymic mice [110] was very effective as wound healing accelerators in early stage wound healing. In those studies, SF and type I collagen nanofiber non-wovens produced by electrospinning were introduced for wound dressing and scaffolds for tissue engineering. The performance of electrospun nanofibrous polyurethane (PU) membranes as dressings was examined *in vivo* using a pig model [107]. To validate the application in the medical field, morphological properties of the membranes were characterized and wound healing was investigated. This wound dressing showed controlled evaporative water loss, excellent oxygen permeability and promoted fluid drainage owing to the presence of porous nanofibers and inherent properties of PU. Histological examination confirmed that epithelialization rate was increased and the exudate in the dermis was well controlled by covering the wound with the electrospun membrane.

#### 1.4.2. Medical prostheses

Polymer nanofibers fabricated via electrospinning have been proposed for a number of soft tissue prostheses applications, such as arterial blood vessel [111, 112] and breast [113]. Electrospun biocompatible polymer nanofibers can also be deposited as a thin porous film onto a hard tissue prosthetic device designed to be implanted into the human body [114].

The search for vascular grafts substitutes has been a half century endeavour. Although polytetrafluoroethylene [115] and polyethylene terephthalate (PET) (Dacron) [116] have been successful in treating the pathology of large diameter arteries (> 6 mm, inner diameter), no materials have been successful in replacing small diameter blood vessels (< 6 mm). The first approach using the electrospinning technique to obtain biomimetic vascular graft scaffolds was developed by Stitzel and colleagues [117]. The graft was fabricated with collagen fibers wound on a stainless mandrel and covered with electrospun PLA. The vascular construct was seeded with human aortic smooth muscle cells (SMCs) and general cellular orientation along the principal stress lines was observed. In a recent article, Venugopal *et al.* [118] reported the development of biocomposite nanofiber scaffolds of PCL and collagen types I and III. *In vitro* studies with coronary artery SMCs revealed that these biocomposites constitute promising scaffolds for the regeneration of smooth muscle tissue for blood vessel engineering.

In recent years, creating a biodegradable polymer scaffold with an endothelialized surface has become an attractive concept for replacement of small diameter blood vessels. Taking this into account, Xu *et al.* [119] cultured human vascular endothelial cells (ECs) on electrospun and solvent cast poly(L-lactic acid) (PLLA) substrates with different surface roughness and showed that EC function was enhanced on the smooth solvent cast surface relative to the rough electrospun surface of PLLA nanofibers. Interestingly, in previous works [120, 121], the same research group demonstrated that a nanofiber matrix of the block copolymer of poly(L-lactic acid)- $\omega$ -poly( $\epsilon$ -caprolactone), P(LLA-CL), could support the adhesion and proliferation of ECs and SMCs. This synthetic nanofiber matrix combined the advantages of synthetic biodegradable polymers with the biocompatible mimicking

architecture of extracellular matrix, to have great potential for blood vessel engineering. To facilitate viability, attachment and phenotypic maintenance of human coronary artery ECs, an electrospun collagen coated P(LLA-CL) nanofiber mesh was fabricated through plasma treatment followed by collagen coating [122]. The collagen coated nanofibrous structure also showed mechanical properties suitable for tissue engineered vascular grafts (Figure 1.8). A similar study was recently presented by Jeong *et al.* [123], demonstrating the effectiveness of a dynamic culture on the engineering of vascular grafts. Additionally, for prosthetic vascular grafts, directional bias of fibers with respect to the tubular axis is required to mimetically obtain anisotropic vascular grafts so as to improve burst strength. Aligned P(LLA-CL) nanofibrous scaffold have been successfully produced [87]. Cell culture results of SMCs on the nanofibrous scaffold indicated that cells adhered and migrated along the direction of aligned nanofibers, showing observed a significant improvement over polymer films.

Vascular graft scaffolds have also recently been fabricated using electrospun polymer blends of type I collagen from calf skin (45 %), elastin from ligamentum nuchae (15 %) and PLGA (40 %) [124]. The biocompatibility of the scaffolds was tested with bovine ECs and SMCs and assessed by MTT metabolic assay and neutral red assays. The biocompatibility of the electrospun vascular scaffolds was also tested

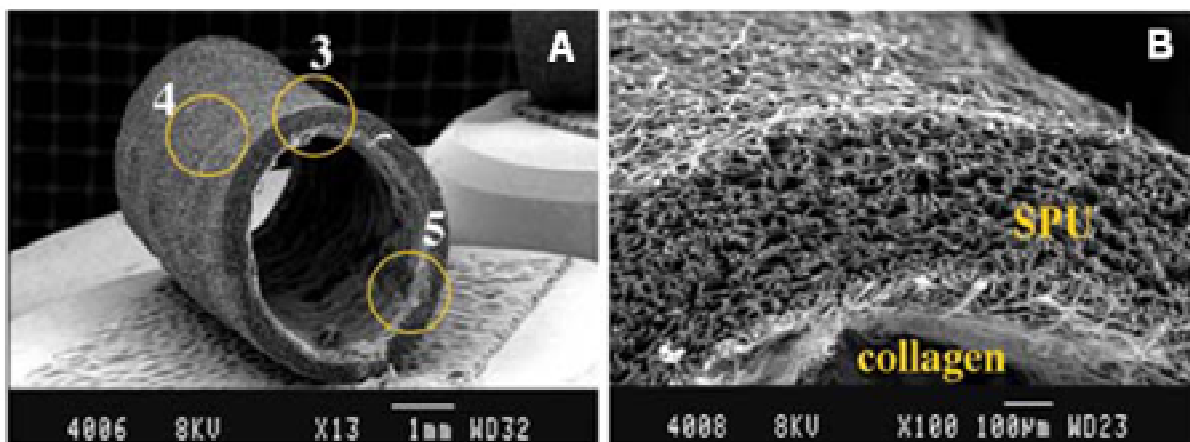


**Figure 1.8** - Fabricated bilayered tubular construct composed of a polyurethane tube with the interior surface coated with collagen. (A) SEM micrograph of the tube. (B) Magnified image of region 3 in the micrograph (*adapted from reference [153]*).

*in vivo*. Favorable interactions between SMCs and ECs on the scaffold were demonstrated by cellular morphology, histology and immunostaining. Ma *et al.* [125] processed a conventional polymer used in vascular grafts, PET, into non-woven nanofiber mat via electrospinning. To overcome the chemical and biological inertness of the PET surface, gelatin was covalently grafted onto the PET nanofibrous surface. Endothelial cells were cultured on the original and gelatin modified PET nanofiber meshes and results demonstrated an improvement of spreading and proliferation of the ECs, maintaining their phenotype. Altogether, these studies demonstrate the potential of electrospinning as a method to fabricate functional vascular grafts for clinical applications, using different biomaterials.

#### 1.4.3. Drug delivery systems

The ability to influence the fiber diameter, by changing the polymer solution concentration and/or its surface tension, and the ability to incorporate therapeutic compounds into the mats during spinning process afforded the prospect of preparing useful polymer systems for controlled drug delivery. Moreover, two potential advantages of the electrospinning approach are the avoidance of melt processing, which is especially important for heat sensitive drugs, and minimization of the initial burst. The nature of the polymer can direct the use of the electrospun fibers with water soluble polymers giving rise to immediate release dosage forms and water insoluble (i.e. biodegradable or non-biodegradable) polymers, being useful for sustained release systems. Thus, the fabrics generated with water soluble carriers could be used in oral dosage formulations by direct incorporation of the materials into a capsule or by further processing (i.e. milling of the fabrics) [126]. Covalent conjugation of drugs to polymers represents an alternative strategy for moderating the rates of drug release. This strategy, however, requires the presence of side chains/functional groups, which are generally only abundant in some hydrophilic biodegradable polymers. Unfortunately, the electrospun membranes prepared from hydrophilic polymers generally have poor mechanical strength, especially in their swollen state, and also tend to disintegrate faster *in vivo*. Moreover, chemical cross-linking is generally needed to solidify and stabilise the electrospun membranes

prepared from hydrophilic polymers, and most of those chemical reactions have potential toxicity. In addition, hydrophilic and water soluble polymers tend to leach out rapidly from the blends when incubated in an aqueous environment. Thus, it is necessary to find hydrophilic polymers that are soluble in organic solvents and insoluble in water under physiological conditions, for preparing composite electrospun membranes [52].

Drug delivery devices including polymer nanofibers are based on the principle that dissolution rate of a drug may be mediated by the surface area of both the drug and the corresponding carrier. Since drugs and carrier materials can be mixed together to produce nanofibers by electrospinning, various interaction modes in the resulting nanostructured products can be envisaged: (1) the drug as tiny particles attached to the surface of the nanofiber carriers, (2) both drugs and carriers are in nanofiber form, resulting in an interlaced structure, (3) a blend of drugs and carrier materials integrated into a single type of composite nanofibers, and (4) the carrier material is electrospun into a tubular form in which the drug particles are encapsulated. Modes (1) and (2) tend to give rise to a problem of burst release in the initial stages of incubation and therefore, modes (3) and (4) may be preferred [1].

Kenawy *et al.* [127] were the first to describe the incorporation of a drug into polymeric nanofibers. They found that electrospun poly(ethylene-co-vinylacetate) (PEVA) released 65 % of its drug (tetracycline hydrochloride) content within 120 h, whereas the 50:50 material (PEVA/PLA) released ~ 50 % over the same time period. Mats of PLA fibers exhibited some instantaneous release, most probably caused by tetracycline hydrochloride on the fiber surfaces. In addition, the percentage of tetracycline released after 5 days from electrospun PEVA was only about twice that released from Actisite (tetracycline periodontal fibers). In general, the total percentage release from the cast films was lower than that from the electrospun mats, as would be expected due to the much lower surface area of the former. In other work, bioabsorbable nanofiber membranes of PLA were used for loading an antibiotic drug, Mefoxin (cefoxitin) [128].

For potential use in topical drug administration and wound healing, poorly water soluble drugs loaded in water soluble and water insoluble nanofibrous polymer

carriers were investigated [126, 129]. Verreck *et al.* [129] reported that solvent casting and melt extrusion of hydroxypropylmethylcellulose results in samples that rapidly release itraconazole, with the solvent cast film giving more complete release. Samples produced using electrostatic spinning resulted in a complete *in vitro* release over time, but the dissolution rate was slower than for either the cast thin films or the melt extruded, milled powder. Additionally, it was shown that drug loaded polymer electrospun nanofibers were able to disperse drugs in an amorphous state, which facilitates drug dissolution.

Zeng and co-workers [130] described a perfect inclusion of Rifampin and Paclitaxel inside PLLA fibers, in that no burst release of drug was observed. These drugs are lipophilic and highly soluble in PLLA/chloroform/acetone solution. When the solution jet was rapidly elongated and the solvent evaporated quickly, the drug remained compatible with PLLA. Doxorubicin hydrochloride (a hydrophilic drug) was also used in this study and limited solubility in the electrospinning solution was reported. During the rapid evaporation of the solvent, phase separation took place quickly between the drug and PLLA. Therefore, the solubility and compatibility of the drug in the drug-polymer-solvent system was a decisive factor.

Electrospun nanofibrous meshes can also be used as carriers for hydrophilic drugs, where the drug release profile can be finely controlled by the modulation of scaffold morphology, porosity and composition. By taking advantage of the unique solubility characteristics of poly(ethylene glycol)-*g*-chitosan (PEG-*g*-CHN), Jiang and colleagues [52] prepared by electrospinning a highly porous composite membrane composed of PLGA and PEG-*g*-CHN, without the need for cross-linking. These membranes are mechanically robust and flexible, and have high porosity, hydrophilicity and capacity to sustained release of ibuprofen, rendering them suitable for direct application to atrial tissue. Kim and co-workers [131] successfully incorporated a hydrophilic antibiotic drug, Mefoxin (cefoxitin sodium), into electrospun PLGA and PLGA/PLA/PEG-*b*-PLA (80:5:15) nanofibers, without the loss of structure and bioactivity. It was demonstrated that the introduction of an amphiphilic PEG-*b*-PLA block copolymer in the polymer matrix reduced the cumulative amount of the release at earlier time points and prolonged drug release rate to 1 week. In addition,

the released cefoxitin sodium from electrospun scaffolds was found to be structurally intact as well as effective in *Staphylococcus aureus* growth inhibition, in both static and dynamic environments.

The use of electrospun fibers as drug carriers will be also promising in future biomedical applications, especially post-operative local chemotherapy. Along those lines, Katti *et al.* [132] reported the development of a novel bioresorbable, polymeric nanofiber based antibiotic delivery system for the treatment of wounds; Cefazolin was incorporated into PLGA nanofibers using the free acid form of the antibiotic. Zong *et al.* [133] examined the effect of using electrospun non-woven bioabsorbable PLGA impregnated with antibiotics (Mefoxin) as an anti-adhesion membrane based on an *in vivo* rat model. These delivery systems would potentially have two functions: as a topical/local antibiotic delivery system and as a resorbable/biodegradable gauze whose degradation products are easily metabolized by the body. A particular advantage of this delivery system would be the possibility of delivering uniform and highly controlled doses of bioactive agents at the wound site via the high surface area to volume ratio of the nanofiber system. Another advance in post-operative localised drug administration focused on vascular grafts. Sustained delivery of heparin to the localised adventitial surface of the grafted blood vessels has been shown to prevent vascular smooth muscle cells (VSMC) proliferation leading to graft occlusion and failure. Luong-Van *et al.* [134] successfully incorporated heparin into electrospun PCL fiber mats. The effect of heparin incorporation on the fiber morphology was studied, as well as heparin dispersion and release rates. A homogeneous distribution of heparin was found throughout the fiber mats and continuous diffusional release over 14 days. In addition, the fibers did not elicit a proinflammatory response, as assessed through *in vitro* macrophage assay, and the released heparin was effective in preventing the proliferation of VSMCs in culture.

A number of authors [44, 127-134] have successfully encapsulated drugs into electrospun fibers by mixing the drugs in the polymer solution to be electrospun. Fewer, however, have encapsulated proteins in electrospun polymer fibers [135-137]. Proteins such as growth factors are often the most important biochemical signalling agents for tissue engineering applications. A recent study developed by Chew *et al.*

[135] demonstrated the feasibility of encapsulating human nerve growth factor (NGF) by electrospinning it into a biodegradable fiber composed of the copolymers poly( $\epsilon$ -caprolactone) and ethyl ethylene phosphate (PCLEEP). Partially aligned protein encapsulated fibers were obtained and the protein was found to be randomly dispersed throughout the electrospun fibrous mesh in aggregate form. A sustained release of NGF from electrospun fibrous mesh for up to 3 months was observed. Additionally, it was confirmed that the NGF released at the end of this time period was, at least partially, bioactive in stimulating PC12 cells differentiation into neurons. In another study, Zeng *et al.* [137] reported the release of comparable large proteins from electrospun poly(vinyl alcohol) (PVA) nanofibers obtained by electrospinning. The release of fluorescein isothiocyanate labelled bovine serum albumin or luciferase from electrospun PVA nanofibers was demonstrated; the burst release was retarded significantly by a post-electrospinning coating of highly hydrophilic poly(*p*-xylylene). The preservation of enzyme activity and the continuous release of the intact enzyme from the immersed fibers meets a fundamental prerequisite for the application of enzymes or other sensitive agents released from electrospun nanofibers under physiological conditions.

#### 1.4.4. DNA release

Fibers produced by electrospinning form a large, interconnected porous network that is ideal for drug, gene, as well as cell delivery. Fang and Reneker [37] have previously reported on electrospinning of DNA fibers, utilising purified genomic DNA (calf thymus Na-DNA) as the polymer. Luu *et al.* [34] utilised the unique capabilities of electrospinning to develop a biologically active scaffold for gene delivery. This study appears to be the first report describing the successful dispersion of plasmid DNA into polymeric solutions of PLA-PEG and PLGA, generating biologically active composite scaffold via electrospinning. Preliminary data indicate that, by manipulating the scaffold's properties (fiber diameter, porosity or pore size), it should be possible to accurately control the release of DNA from the scaffold, and thus decrease the rate of release at earlier times and sustain a more linear release for longer time periods. Additionally, these results indicated that the DNA released from

the scaffold was not only intact, but also capable of cellular transfection. In a subsequent study, the same group [138] developed a novel core-sheath DNA nanoparticle composed of condensed plasmid DNA in a triblock copolymer of poly(lactide)-*b*-poly(ethylene glycol)-*b*-poly(lactide). The mixture of encapsulated DNA and PLGA was then electrospun to form a non-woven nanofibrous and nanocomposite scaffold. This structure was capable of controlled release bioactive plasmid DNA in an intact form and transfect preosteoblastic MC3T3 cells in culture. Together, these results demonstrated that by understanding and using the molecular interactions of block copolymers and plasmid DNA in solution, novel structures and additional functionality can emerge. A deep understanding on the molecular self-assemblies and the electrospinning process has enabled the development of an effective gene delivery vehicle.

#### 1.4.5. Tissue templates/scaffolds

A biodegradable scaffold is commonly recognized as an indispensable element in engineering living tissues. Scaffolds are used as temporary templates for cell seeding, proliferation and differentiation, to lead to the regeneration of the tissue [59, 103-105]. The design of biomaterial scaffolds for tissue engineering is an attempt to obtain functional replacement of the ECM, to support the desired cellular differentiation and maintain phenotype specific activities. Nanofibrous materials, by virtue of their morphological similarities to natural ECM, have been considered as promising scaffolds for tissue engineering applications. The difficulties with these structures include poor control of porosity and limited mechanical properties.

Diverse tissues that undergo injury could benefit from the potentialities of the nanofibrous structures produced by electrospinning. For instance, in cartilage regeneration, induction and maintenance of chondrocyte differentiation are obtained by embedding cells in agarose, or alginate, or in the form of a high density pellet. However, such cultures lack the mechanical stability provided by PCL nanofibrous scaffold, as described by Li *et al.* [22]. In subsequent work [24], it was demonstrated that electrospun nanofibers of PCL effectively support transforming growth factor  $\beta$ 1 induced chondrogenesis of adult human mesenchymal stem cells (hMSCs). The level

of differentiation appeared to be equivalent to that observed in high density pellet cultures of hMSCs. In addition, nanofibrous scaffolds allowed cells to be grown on the same surface throughout their entire course of differentiation and maturation. The same group, in another study [139], showed that PCL nanofibrous scaffolds not only support the maintenance of a chondrogenic phenotype, but also provide a suitable scaffold for the osteogenic, chondrogenic, and adipogenic differentiation of hMSCs. In a recent study, Subramanian *et al.* [140] have evaluated a novel electrospun chitosan/polyethylene oxide (PEO) mat composed of oriented submicron fibers for its tensile properties and biocompatibility with canine chondrocytes (cell attachment, viability and proliferation). The results demonstrated that the electrospun aligned fibers had a higher modulus than anisotropic cast films, and provided good chondrocyte biocompatibility. A similar biological study [141], with chitosan/PEO nanofibers deposited as a non-woven membrane or as a highly aligned bundle, was developed with human chondrocytes (HTB-94 cell line) and osteoblasts (MG-63 cell line). Experimental results showed that the nanofibrous structure promoted adhesion and maintained characteristic cell morphology and viability throughout the period of study, properties of particular interest in tissue engineering for controlled drug release and tissue remodelling. In other recent work [142], starch based nanofiber meshes were presented as support structures for bovine articular chondrocytes proliferation and maturation, as demonstrated by the formation of extracellular matrix (glycosaminoglycans quantification) and immunoexpression of collagen types I and II.

Interesting work by Yoshimoto *et al.* [27] demonstrated that electrospun PCL nanofibers are capable of supporting attachment and proliferation of rat bone marrow derived MSCs, which maintain their phenotypic shape and differentiation into osteoblastic cells under dynamic culture conditions. Shin *et al.* [143] implanted MSC-PCL constructs subcutaneously in rats and showed new bone formation at the implantation site. These results were later confirmed by Boudriot and colleagues [144], who demonstrated osteogenic differentiation of hMSCs on a three-dimensional matrix of electrospun PLLA nanofibers. Therefore, nanofibrous structures processed by electrospinning could also be promising scaffolds for bone tissue engineering. Recently, Zhang *et al.* [55] coelectrospun gelatin with PCL to produce composite

fibrous scaffolds, which exhibited improved mechanical properties (namely, elongation and deformation), as well as more favorable wettability, than nanofibers obtained from either gelatin or PCL alone. Additionally, cell culture experiments with bone marrow stromal cells (BMSCs) showed favorable interactions (i.e. attachment and spreading) and cellular migration into the fibrous structure of this artificial polymeric material. In a recent study, guided bone regeneration (GBR) composite nanofiber membranes were successfully fabricated by electrospinning of PCL/calcium carbonate ( $\text{CaCO}_3$ ) [145]. Human osteoblasts (hFOB1.19 cell line) were cultured on composite nanofibrous GBR membranes, and MTS assay and SEM observation revealed good cell attachment and proliferation. Another study [146] had also evaluated the osteoblast attachment and proliferation on composites of PCL nanofibers containing nanoparticles hydroxyapatite (nHA). Results demonstrated that cells seeded on PCL/nHA fibrous scaffolds presented higher viability than the cells seeded on scaffolds containing PCL/ $\text{CaCO}_3$  or PCL alone. That behavior was attributed to the ability of nHA to promote bone cell activities. Recently, the formation of an apatite layer has been induced over electrospun PCL nanofiber meshes, without the occurrence of pore occlusion [147]. The biological influence of this biomimetic coating on osteoblastic like cells was assessed. It was shown that PCL nanofiber meshes coated with an apatite layer support and enhance the proliferation of osteoblasts for long culture periods (Figure 1.9).

Nair and colleagues [148] recently produced non-woven nanofiber meshes from poly[bis(*p*-methylphenoxy)phosphazene] (PNmPh) by electrospinning. This biodegradable polymer is a polyphosphazene, a class of inorganic-organic polymers known for their high biocompatibility, high temperature stability and low temperature flexibility. Furthermore, the electrospun nanofiber mats were studied to evaluate the biological performance. It was found that these mats supported the adhesion of bovine coronary artery endothelial cells, as well as promoting adhesion and proliferation of osteoblastic like MC3T3-E1 cells (mouse immortalized calvarial cells). This study indicated that the PNmPh nanofiber matrices could promote cell matrix and cell-cell interactions, making them potential candidates for various biomedical applications.

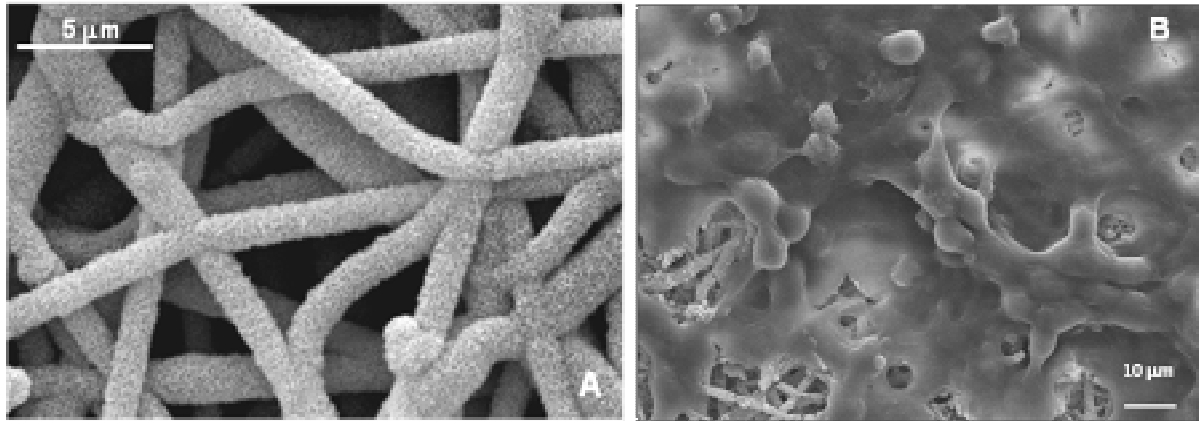


**Figure 1.9** - SEM micrographs of electrospun poly( $\epsilon$ -caprolactone) nanofiber meshes after biomimetic calcium phosphate coating, keeping the porous morphology (**A**) (*adapted from the reference [68]*). Morphology of Saos-2 cells cultured for 14 days on PCL nanofiber meshes coated with a biomimetic coating (**B**) (*adapted from the reference [147]*).

Many researchers [38-41, 149] have investigated silk proteins, mainly SF, as candidate materials for biomedical applications, because it has several distinctive properties including good biocompatibility, good oxygen and water vapour permeability, biodegradability and minimal inflammatory reaction. Jin *et al.* [38] reported the ability of electrospun silk matrices to support human BMSCs attachment, spreading and growth *in vitro*, suggesting the potential use of these biomaterial matrices as scaffolds for tissue engineering. Electrospun silk fibroin mats were comparable with other biodegradable electrospun mats using PGA [31, 41], PLGA [33-36], collagen [45-47], collagen/PEO blends [51] that were tested for use as scaffolds for tissue regeneration. In fact, smooth muscle cells were observed to infiltrate an electrospun collagen (calfskin) nanofiber matrix and were well integrated into the network within 7 days of culture [46]. Matthews [45] also performed an *in vitro* study with chondrocytes, where it was also demonstrated that electrospun collagen type II scaffolds support cell proliferation and are readily infiltrated. More recently, a comparative study of collagen, gelatin (denaturated collagen), solubilised alpha-elastin and recombinant human tropoelastin as biopolymeric materials for fabricating tissue engineering scaffolds by electrospinning was developed by Li and colleagues [150]. In contrast to collagen and gelatin, which could be spun into fibers in the

nanometre scale, the diameter of alpha-elastin and tropoelastin fibers was always in the range of microns. The characterization of the mechanical tensile moduli of electrospun fibers was also reported. Cell culture studies confirmed that these electrospun engineered protein scaffolds support attachment and growth of human embryonic palatal mesenchymal cells.

Numerous topographical and chemical strategies have been undertaken to create micro- and nanoscale enhanced features to regulate cell morphology and function [102, 151, 152]. In fact, very little was previously known about the textural effects of the fibrous matrix on tissue engineering. Park *et al.* [40] studied the cytocompatibility and human oral keratinocytes behaviour on the different textures of SF (woven matrix of microfibers, films and non-woven matrix of nanofibers). Their results indicated that the SF nanofiber matrix promotes cell adhesion and spreading, using type I collagen as substrate, better than SF film and SF microfiber matrices. In subsequent work [53], they demonstrated that a PLGA/chitin composite non-woven matrix can be a better candidate than the PLGA non-woven matrix in terms of cell adhesion and spreading for normal human keratinocytes, and that the PLGA and PLGA/chitin matrices are good matrices for normal human fibroblasts. These nanofibrous matrices showed promise for biomedical applications, such as wound dressing and scaffolds for tissue engineering. In a different topographical approach, nano- to micro-structure biodegradable poly(L-lactide-co- $\epsilon$ -caprolactone) (PLCL) fabrics were prepared by electrospinning [153]. Physical characterization revealed that a decrease in the fiber diameter of the fabric resulted in a decrease in the porosity and on the pore size. This was followed by an increase in fiber density and mechanical strength. Biological assays demonstrated that human umbilical vein endothelial cells (HUVECs) were well adhered and proliferated on the small diameter fiber fabrics (0.3-1.2  $\mu\text{m}$  in diameter), whereas markedly reduced cell adhesion, restricted cell spreading and no signs of proliferation were observed on the large diameter fiber fabric ( $\sim 7.0 \mu\text{m}$  in diameter). The discussion suggests that electrospun elastomeric nanofiber fabric may be useful as temporary functional scaffolds in cardiovascular and muscular tissue engineering.

Nanofibrous structures were recently proposed as a potential cell carrier for neural tissue engineering by Yang *et al.* [29]. Production of PLLA nanofibrous scaffolds and the biological performance of neural stem cells (NSC) when seeded into those scaffolds was described. It was concluded that this nanostructure supports neural stem cell adhesion and enable NSCs differentiation and outgrowth of neurites. Later, the production of perfectly aligned PLLA fibrous scaffolds was achieved and *in vitro* studies demonstrated the elongation and neuritis outgrowth of NCS parallel to the direction of fiber alignment [88]. Moreover, a comparative study with electrospun microfibers revealed a significant effect on the cell orientation. However, the NSC differentiation rate was higher for nanofibers than for microfibers.

Several studies on creating cardiac muscle cell constructs have also been reported [154, 155]. Studies that used a synthetic polymer scaffold typically concluded that the stiffness of the scaffold hindered tissue contractions [59, 153]. A study developed by Shin *et al.* [154] introduced an *in vitro* system for engineered myocardium using a degradable, nanofibrous scaffold made of PCL by electrostatic fiber spinning. The cardiomyocytes penetrated the entire scaffold and stained positively for cardiotypical proteins, i.e. actin, tropomyosin and cardiac troponin-I. The work presented provides an alternative approach to engineered myocardium by relying on a synthetic polymer that provides sufficient stability and low opposition to contractions. In a similar approach [155], biodegradable polymer nanofibers of PLLA and PLGA (PLA10-GA90+PLLA and PLGA+PEG-PLA) were assessed for use in heart and cardiac tissue constructs. Primary rat cardiomyocytes (CMs) were cultured onto nanofibrous scaffolds and a dense multilayer of cells was obtained. It was also observed that CMs over electrospun PLLA scaffolds developed mature contractile structures (sarcomeres).

Skeletal muscle tissue engineering represents an attractive approach to overcome problems associated with autologous transfer of muscle tissue and provide a valid alternative for tissue replacement in the enhancement of muscle regeneration. In this context, Riboldi *et al.* [156, 157] investigated the potential use of electrospun DegraPol<sup>®</sup> (degradable polyesterurethane) membranes as fibrous scaffolds for skeletal muscle tissue engineering. To evaluate their suitability for this specific

application, scaffolds were characterized with reference to their morphological, degradative and mechanical properties. Subsequently, cell viability, adhesion and differentiation on coated (with collagen, fibronectin and Matrigel<sup>®</sup> - a gelatinous protein mixture) and uncoated DegraPol electrospun membranes were investigated using murine and rat myoblast cell lines (C2C12 and L6, respectively) and primary human satellite cells. The electrospun DegraPol<sup>®</sup> membranes showed satisfactory mechanical properties (linear elastic behaviour up to 10 % deformation,  $E$  modulus in the order of megapascals) and good cellular response in preliminary adhesion and differentiation experiments (cellular adherence and proliferation on differently coated electrospun membranes, accompanied with positive staining for myosin heavy chain).

Originally, in the field of liver tissue engineering, galactosylated nanofiber meshes were suggested as potential scaffolds by Chua *et al.* [158]. In this study, highly porous nanofiber scaffolds of PCLEEP were grafted with poly(acrylic acid) and subsequently, covalently conjugated with galactose ligands. Hepatocytes, isolated from male Wister rats, cultured on galactosylated scaffolds, exhibited similar functional profile in terms of cell attachment, ammonia metabolism, albumin secretion and cytochrome P450 enzymatic activity as those on the functional two-dimensional substrate. Galactosylated PCLEEP nanofiber mesh demonstrated the unique properties of promoting hepatocyte aggregates within the mesh and around the fibers, forming an integrated spheroid nanofiber construct. Indeed, this construct would be advantageous in the design of bioartificial liver assisted devices.

Mechanical forces play a central role in the physiology of a wide variety of tissues. Several researchers [159, 160] have reported that cyclic mechanical stretch increases ECM production in cultured fibroblasts on flexible membranes. Additionally, when connective tissue cells are grown on deformable substrates and subject to an applied cyclic strain field, the cells align perpendicular to the greatest strain direction. Lee *et al.* [83] studied the effect of fiber alignment in polyurethane nanofibers and direction of mechanical stimuli on the ECM generation of human ligament fibroblast (HLF). The results indicated that HLF cultured in aligned nanofibers had a similar morphology to ligament fibroblasts *in vivo*. The aligned structure led to increased ECM production, and the aligned HLFs were more sensitive to strain in the

longitudinal direction. Consequently, aligned nanofibers can constitute a promising base material for tissue engineered ligament in that they are a biomimetic structure and provide the mechanical environment ligament fibroblasts encounter *in vivo*.

### **1.5. Desired properties of electrospun nanofibers as scaffolds**

Tissue Engineering is emerging as an alternative approach for the (re)generation of functional tissues damaged by disease or trauma, and in replacing failing or malfunctioning organs. Biomaterials play a significant role in these modern strategies of regenerative medicine and tissue engineering. They can be used to tailor the biophysical and biochemical milieu that direct cellular behaviour and function into the desired regeneration of tissues. Moreover, the scaffold should act as a template for the neovascularization of the regenerated tissue and could actively participate in the regeneration process through the release of growth/differentiation factors. Various degradable biomaterials, either natural or synthetic, have been processed into scaffolds for tissue engineering [59, 103, 104, 161-164]. Essentially, the success of tissue engineering methods is highly dependent on the properties of the scaffold. Basic scaffold design requirements include biodegradability, biocompatibility, high surface area/volume ratio (porosity and interconnectivity) and mechanical integrity [59, 165-168].

It is agreed [162, 167] that a candidate scaffold should closely mimic the structural and functional properties of the materials found in the native ECM of the host tissue. Therefore, the ultimate goal of the scaffold is the production of an ideal structure that can replace the natural ECM until host cells can repopulate and resynthesize a new natural matrix. It is well known that most natural ECMs are composed of randomly oriented fibrils of nanometer scale diameters. The morphology and architecture of the electrospun structure aims at being similar to those of some natural ECMs [2, 66]. Biological performance is regulated by the biological signals from growth factors, extracellular matrix, and also by the surrounding cells. More sophisticated efforts to mimic this natural scaffold are being pursued by many groups [169, 170] that are exploring the development of biomaterial/biochemical composites incorporating biological agents such as growth factors and other key cell regulatory

molecules. This objective has also been pursued using electrospun nanofiber meshes, although little attention has to date been given to the loading growth factors, so far [135, 136].

The pores of a tissue engineering scaffold constitute the space in which the cells reside. It is generally agreed that a highly porous microstructure with interconnected pores and a large surface area is desirable to allow cell seeding and migration throughout the material. Furthermore, the scaffolds should exhibit adequate microporosity, to encourage capillary ingrowth. High porosity provides more opportunities for cell colonization and makes the diffusion of gases, nutrients and metabolic waste between scaffold and environment more efficient. Given the importance of the pore structure of tissue engineering scaffolds, a variety of techniques have been proposed to obtain an appropriate substrate for cell culture [103, 166, 171-189]. Many of these techniques employ organic solvents or high temperature, and the preservation of biocompatibility and the crystalline structure of the polymer are problematic. To overcome the above limitations, electrospun fibrous matrices can be used as alternative scaffolds in tissue engineering applications. When nanofibers are created in the electrostatic field, they are deposited randomly on the collector, layer by layer, and a wide variety of pore diameters (distances between fibers) are formed [27, 34, 52, 57, 153]. However, the strongest limitations of nanofibrous structures are their inherent two-dimensional character and the difficulty in controlling pore size. In most TE applications it is desirable to have scaffolds with a pore size that enables migration of the cells into the inner regions of the structure. The cells must remain viable, thus requiring an efficient exchange of nutrients and metabolites with the culture medium. The porosity of the electrospun meshes hinders the migration of cells, but is suitable for diffusion of nutrients and metabolites. Thus, new developments of the technology are needed to overcome the difficulty of cell migration when seeded at the mesh surface. Furthermore, the degree of porosity always influences other properties of the scaffolds such as its mechanical stability, and its value should always be balanced with the mechanical needs of the particular tissue that is targeted.

The purpose of a scaffold is not only to provide a surface for cell residence but also to maintain mechanical stability at the host defect site. Mechanical stability is dependent primarily on the selection of the biomaterial, the architectural design of the scaffold, and the cell-material interactions [59, 166]. A well designed tissue engineered scaffold has to meet, at least, two mechanical requirements to be effective. The scaffold must retain structural integrity and stability when a physician handles and implants it into the defect site of the host. After surgery, the structure at the implant site must provide sufficient biomechanical support during the process of tissue regeneration and structure degradation. Electrospun fibers have nanostructured surface morphologies with small pores that influence mechanical properties like tensile strength and modulus [55, 122, 153, 157]. Also, aligned nanofiber composites provide better mechanical properties than a randomly aligned nanofiber composite structure [73, 190].

It is also highly desirable to use processing methods that are efficient and that can be used to regulate the chemical, biological and material properties of the fabricated matrix [59, 166]. Methods such as solvent casting [181, 184, 185], fiber bonding [56, 176, 180, 191], injection moulding [172, 173, 175, 186-188], and rapid prototyping [174, 177, 178, 183, 189], among others, have been used for the fabrication of porous scaffolds. These scaffolds were proposed for tissue engineering of various tissues including bone, cartilage, tendon, blood vessel and heart valve [100, 103, 104, 165, 192]. However, most of the scaffolds could only replace the lost tissue physically but not functionally [193]. In electroprocessing, the shape of the scaffolding and orientation of fibers within an engineered matrix can be regulated by controlling the motion of target mandrel and source polymeric solution. Presumably, the incorporation of various degrees of cross-linking into this type of nonwoven matrix can be used to further tailor the material properties of the matrix to specific applications. As a processing strategy, electrospinning is rapid, efficient and inexpensive, and can be used to fabricate complex, reliable scaffolds. For example, blends [55] or laminates [54] of different materials can be produced with this technique. Electrospinning can even be used to incorporate slight structural

adjustments into an engineered material by regulating the orientation of nanofibers within the fabricated network [46, 83, 86-88].

A significant advantage of the electrospinning process is the ability to fabricate non-woven, nanometre-scale fibrous structures [14]. The architecture of the scaffold is dynamically changed as the polymer fibers are hydrolyzed and degraded over time, which allows the colonising cells to build up their own ECM [33]. Indeed, the main goal of tissue engineering approach is to develop a biocompatible scaffold material which is degradable over a controllable time scale into non-toxic products that may disappear together with new tissue formation, leaving natural tissue replacement [167]. Thus, an electrospun structure composed of ultrafine nanofibers would be more susceptible to hydrolysis than thicker fibers when used to culture cells for tissue engineering applications, because of enhanced water contact due to the large surface area [22]. However, the molecular weight decrease during *in vitro* degradation of electrospun PCL materials were much lower than those for solvent casted PCL films, which may be due to enhanced diffusion of oligomers out of the fibers (as a result of high surface/volume ratio), which would reduce the effects of autocatalytic degradation [194]. Bolgen and colleagues [194] demonstrated a faster degradation rate *in vivo* than *in vitro*, attributed to the enzymatic degradation of PCL in addition to the hydrolytic degradation. Recently, Liang and collaborators [138] established that the biodegradation rate, as well as the hydrophilicity of the electrospun scaffolds, could be finely turned with different material compositions (PLGA or PLA-*b*-PEG-*b*-PLA triblock copolymer and DNA). It was demonstrated that the electrospun scaffold containing those four compositions, which exhibited an ideal biodegradation profile, good hydrophilicity, and stable mechanical properties in aqueous conditions, was suitable for biomedical applications including biodegradable scaffolds for tissue engineering and prevention of post-operative adhesions [28].

## 1.6. Future perspectives

Electrospinning is a relatively old technology [7], which was appeared in the literature for more than 70 years. Despite the progress made in process modification and control, considerable challenges remain.

Improved process models needed to achieve better understanding of the mechanisms and to explain observed phenomena such as nanofibers pore formation during electrospinning [9] and hollow fibers formation [77, 79-82]. Another need is to model nanofiber deposition on substrates, both stationary and moving, to improve the nanofiber alignment when using newly developed processes [11, 65, 73, 83-96], which may itself lead to the development of novel techniques. Models for multiple jet electrospinning should also be improved, as well as the modelling of jet interactions [195]. It is unclear, at this stage, as to what extent the aggregation and conformation of polymer chains are affected by the electrospinning process. Those changes are mainly related to the solvent used. The solvents have a crucial role since they are expected to solvate the polymer molecules, thus forming the electrified solution jet. A systematic study regarding the influence of the type of solvent and polymer concentration on the polymer chain conformation and, consequently, in the properties of the polymer structure and morphology in the nanofiber meshes, is needed. In summary, a fundamental experimental and theoretical analysis of the process is needed to develop flexible and reliable methods to fabricate nanofibers and their assemblies and composites [196].

To date, most of the electrospun fibers obtained have been synthetic. More attention should be given to natural biopolymers (e.g. chitin, chitosan, alginate, starch, hyaluronic acid and dextran), with the aim of achieving fibers with better biocompatibility and performance. The present authors believe that the successful conversion of natural biopolymers into ultrafine and nanofibrous structures will provide new opportunities and enhance the possibilities of their use in bioengineering and other demanding applications.

A number of authors successfully encapsulated drugs into electrospun fibers by mixing or dissolving the drugs in the electrospun polymeric solution. However, the encapsulation of proteins is yet to be studied in detail, despite their biochemical importance as signalling agents for tissue engineering applications. Core/sheath or hollow nanofibers are a more recent revolutionary product of electrospinning. Application of those structures in tissue engineering and regenerative medicine will, it is hoped, allow drugs, growth factors, enzymes, peptides or even DNA to be

embedded into the core of biodegradable polymer nanofibers, and released as required [19]. In addition, using a synthetic polymer as the core material and natural polymer as the shell material, nanofibers with strong mechanical strength and good biocompatibility should be obtained [54]. In addition, using this method, strong inflammatory reactions could be avoided. It is also possible to speculate that the fabrication of hollow nanofibers with multiple walls by using more complex spinnerets composed of more than two coaxial capillaries may be technically feasible [18].

Recently [197, 198], the possibility of producing encapsulated cells in microfibers (so-called microthreads by the authors) and meshes by the electrospinning technology has been explored (Figure 1.10). In this approach, immortalized (human brain astrocytoma cell line) and primary cells (porcine vascular and rabbit aorta smooth muscle cells) were loaded into poly(dimethylsiloxane) (PDMS) nanofibers, using a coaxial needle configuration. It was demonstrated that electrospun cells remain viable over long culture periods, showing no evidence of cellular damage. Works pioneering the incorporation of living cells into electrospun nanofibers were carried out by Lee *et al.* [199] and Salalha *et al.* [200], demonstrating efficient encapsulation of viruses (M13) and bacteria (*Escherichia coli* and

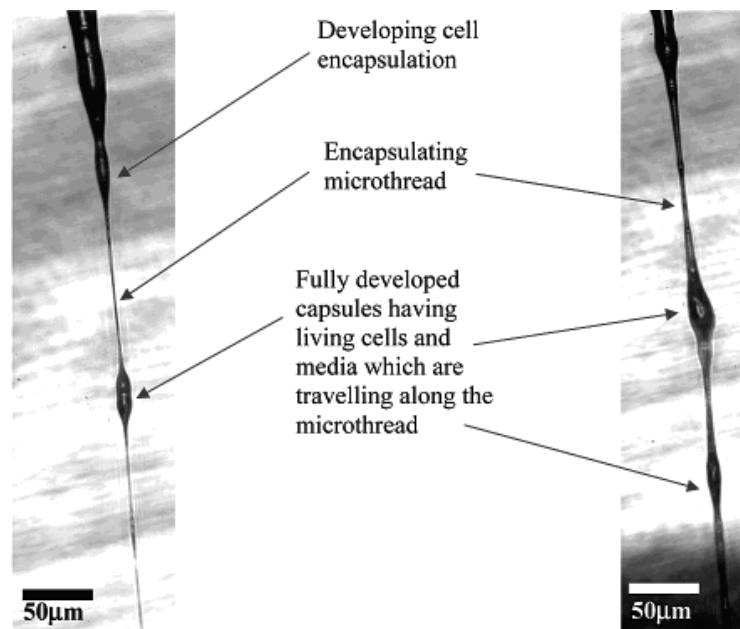


**Figure 1.10** - Image from the electrospinning process embedding living cells in the fiber structure. (*adapted from the reference [198]*).

*Staphylococcus albus*). Another approach [201, 202] used rat aorta vascular SMCs electrosprayed simultaneously with electrospun poly(ester urethane) urea to produce a hybrid tissue engineered construct. This approach, denominated by ‘cellular microintegration’, was proposed in the context of blood vessel replacement, aiming at seed the cells during the fabrication of nanofibrous tubular scaffolds. Indeed, these biomicrofabrication methods allow the production of biohybrid scaffolds with promising applications in regenerative medicine, an approach that will surely be further explored in future.

Biomaterial scaffolds are designed to support cell and tissue growth, aiming on a macroscopic level to match the properties of the organs to be replaced, without being able to recreate the complexity and nanoscale detail observed in real organs at the level of the matrix interaction [102]. The ability to engineer materials to a similar level of complexity may become a reality, through the fabrication of novel biodegradable polymeric matrices by combining electrospinning methodologies with well-established techniques for materials processing (e.g. injection moulding, solvent casting, 3D plotting). For example, a three-dimensional micro-/nanoscaffold comprising electrospun nanofibers deposited on a wet-spun microfibers scaffold has recently been developed [56] (Figure 1.11). Its biological functionality was demonstrated by the culturing of human osteoblast-like cells, bone marrow stromal

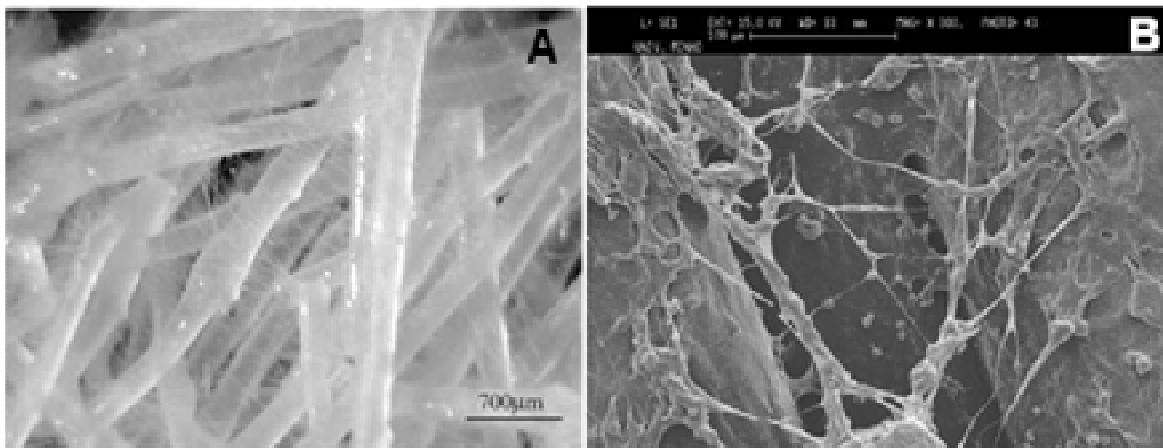


**Figure 1.11** – Optical micrograph (A) of micro-nano fiber combined scaffolds. SEM micrograph (B) of human osteoblast like cells (Saos-2) seeded on nano and micro-fiber combined scaffolds after 14 days of culture (*adapted from the reference [56]*).

cells and endothelial cells (HUVECs and microvascular endothelial cells) [56, 203, 204]. This hierarchical structure was developed to mimic the highly organized fibrous structure of bone tissue, not forgetting the vascular system. Combining nanostructured scaffolds with the incorporation of biological signals into the scaffold fabric is also likely to prove a most rewarding approach [162].

## 1.7. Conclusions

Numerous studies reported the use of electrospun fiber meshes in tissue engineering. However, some technical barriers remain uncrossed and many possible configurations of the process were not fully exploited. Despite the high level of porosity and high specific surface area of the non-woven fiber meshes, the pore size usually is too narrow to allow cell migration through the inner regions of the fiber mesh scaffolds. This is the most serious limitation of these structures, and may compromise its use in the regeneration of tissues. Variations in the electrospinning setup or in the deposition pattern may be valuable strategies to control pore size. Strategies already suggested in the literature include the use of porogen agents such as salt particles [205] or chemical blowing agent [206]. Most biological studies with electrospun nanofiber meshes show that cells tend to stay at their surfaces. This behaviour is observed even when the pore size is sufficiently large to allow cells to migrate into the inner regions of the mesh scaffolds. Coating with cell-affine materials such as collagen was proposed to facilitate cell ingrowth into the core of meshes [122, 207].

Other limitation of the electrospun nanofiber meshes in tissue engineering is the typical two-dimensional thin structure. Fibrous meshes are generally obtained as planar sheets, which may limit the applicability of those structures to the regeneration of layered tissues. During processing, the time of deposition may be increased in order to produce 3D structures. However, in practice this is not feasible, since this way it is progressively more difficult to control the fiber deposition process. By complementing or associating electrospinning with other techniques, it may be possible to obtain macroporous structures with tissue-scale motifs, this being a

promising strategy to produce scaffolds that combine good mechanical properties and adequate topography for cell fixation. In our understanding, much more effort is required to produce 3D stable macroporous structures, exploring the advantages of electrospun fiber meshes and avoiding their limitations. The production of mesh structures together with well-controlled properties and architecture of individual fibers, such as alignment, would enable the production of structures that would have a huge impact in the tissue engineering field.

Appropriate biomaterials tuned for specific cell types have also unsolved challenges. As previously mentioned, different cell types behave and react according to the fiber composition [119]. Efforts to improve cell attachment may include bulk modification [39, 146] or surface activation [31, 122, 125, 147, 208] of the fiber meshes. Both strategies have been followed to improve interactions of specific cell types with the surface of fiber meshes. Eventual residual solvent in the meshes is another subject that is not sufficiently discussed and that might considerably affect the cell viability and the efficacy of these meshes as supports for tissue engineering.

## **1.8. References**

1. Huang ZM, Zhang YZ, Kotaki M, Ramakrishna S. A review on polymer nanofibers by electrospinning and their applications in nanocomposites. *Composites Science and Technology* 2003; 63(15):2223-2253.

2. Smith LA, Ma PX. Nano-fibrous scaffolds for tissue engineering. *Colloid Surface B* 2004; 39(3):125-131.

3. Doshi J, Reneker DH. Electrospinning process and applications of electrospun fibers. *Journal of Electrostatics* 1995; 35(2-3):151-160.

4. Van Vaeck L, Adriaens A, Gijbels R. Static secondary ion mass spectrometry: (S-SIMS) part 1. Methodology and structural interpretation. *Mass Spectrometry Reviews* 1999; 18(1):1-47.

5. Briggs D. *Surface analysis of polymers by XPS and static SIMS*. Cambridge, UK: Cambridge University Press, 1998.

6. Gañán-Calvo AM, Dávila J, Barrero A. Current and droplet size in the electro spraying of liquids. Scaling laws. *Journal of Aerosol Science* 1997; 28(2):249-275.
7. Formhals A, inventor. Process and apparatus for preparing artificial threads. US Patent 1975504, 1934.
8. Taylor G. Disintegration of water drops in an electric field. *Proceedings of Royal Society A* 1964; 280:383-397.
9. Bognitzki M, Czado W, Frese T, Schaper A, Hellwig M, Steinhart M, *et al.* Nanostructured fibers via electrospinning. *Advanced Materials* 2001; 13(1):70-72.
10. Deitzel JM, Kleinmeyer J, Harris D, Beck Tan NC. The effect of processing variables on the morphology of electrospun nanofibers and textiles. *Polymer* 2001; 42(1):261-272.
11. Deitzel JM, Kleinmeyer JD, Hirvonen JK, Beck Tan NC. Controlled deposition of electrospun poly(ethylene oxide) fibers. *Polymer* 2001; 42(19):8163-8170.
12. Frenot A, Chronakis IS. Polymer nanofibers assembled by electrospinning. *Current Opinion on Colloid and Interface Science* 2003; 8(1-2):64-67.
13. Megelski S, Stephens JS, Bruce Chase D, Rabolt JF. Micro- and nanostructured surface morphology on electrospun polymer fibers. *Macromolecules* 2002; 35(22):8456-8466.
14. Reneker DH, Chun I. Nanometre diameter fibres of polymer, produced by electrospinning. *Nanotechnology* 1996; 7(3):216-223.
15. Tan SH, Inai R, Kotaki M, Ramakrishna S. Systematic parameter study for ultra-fine fiber fabrication via electrospinning process. *Polymer* 2005; 46(16):6128-6134.
16. Yarin AL, Koombhongse S, Reneker DH. Bending instability in electrospinning of nanofibers. *Journal of Applied Physics* 2001; 89(5):3018-3026.
17. Dersch R, Steinhart M, Boudriot U, Greiner A, Wendorff JH. Nanoprocessing of polymers: applications in medicine, sensors, catalysis, photonics. *Polymers for Advanced Technologies* 2005; 16(2-3):276-282.

18. Li D, Xia YN. Electrospinning of nanofibers: Reinventing the wheel? *Advanced Materials* 2004; 16(14):1151-1170.
19. Ma ZW, Kotaki M, Inai R, Ramakrishna S. Potential of nanofiber matrix as tissue-engineering scaffolds. *Tissue Engineering* 2005; 11(1-2):101-109.
20. Subbiah T, Bhat GS, Tock RW, Parameswaran S, Ramkumar SS. Electrospinning of nanofibers. *Journal of Applied Polymer Science* 2005; 96(2):557-569.
21. Baker BM, Mauck RL. The effect of nanofiber alignment on the maturation of engineered meniscus constructs. *Biomaterials* 2007; 28(11):1967-1977.
22. Li WJ, Danielson KG, Alexander PG, Tuan RS. Biological response of chondrocytes cultured in three-dimensional nanofibrous poly(epsilon-caprolactone) scaffolds. *Journal of Biomedical Materials Research, Part A* 2003; 67A(4):1105-1114.
23. Li WJ, Mauck RL, Cooper JA, Yuan X, Tuan RS. Engineering controllable anisotropy in electrospun biodegradable nanofibrous scaffolds for musculoskeletal tissue engineering. *Journal of Biomechanics* 2007; 40(8):1686-1693.
24. Li WJ, Tuli R, Okafor C, Derfoul A, Danielson KG, Hall DJ, *et al.* A three-dimensional nanofibrous scaffold for cartilage tissue engineering using human mesenchymal stem cells. *Biomaterials* 2005; 26(6):599-609.
25. Neves NM, Campos R, Pedro A, Cunha J, Macedo F, Reis RL. Patterning of polymer nanofiber meshes by electrospinning for biomedical applications. *International Journal of Nanomedicine* 2007; 2(3):1-16.
26. Pham QP, Sharma U, Mikos AG. Electrospun poly(epsilon-caprolactone) microfiber and multilayer nanofiber/microfiber scaffolds: Characterization of scaffolds and measurement of cellular infiltration. *Biomacromolecules* 2006; 7(10):2796-2805.
27. Yoshimoto H, Shin YM, Terai H, Vacanti JP. A biodegradable nanofiber scaffold by electrospinning and its potential for bone tissue engineering. *Biomaterials* 2003; 24(12):2077-2082.
28. Kim K, Yu M, Zong X, Chiu J, Fang D, Seo YS, *et al.* Control of degradation rate and hydrophilicity in electrospun non-woven poly(D,L-lactide) nanofiber scaffolds for biomedical applications. *Biomaterials* 2003; 24(27):4977-4985.

29. Yang F, Xu CY, Kotaki M, Wang S, Ramakrishna S. Characterization of neural stem cells on electrospun poly(L-lactic acid) nanofibrous scaffold. *Journal of Biomaterials Science - Polymer Edition* 2004; 15(12):1483-1497.

30. Zeng J, Chen X, Xu X, Liang Q, Bian X, Yang L, *et al.* Ultrafine fibers electrospun from biodegradable polymers. *Journal of Applied Polymer Science* 2003; 89(4):1085-1092.

31. Boland ED, Telemeco TA, Simpson DG, Wnek GE, Bowlin GL. Utilizing acid pretreatment and electrospinning to improve biocompatibility of poly(glycolic acid) for tissue engineering. *Journal of Biomedical Materials Research, Part B - Applied Biomaterials* 2004; 71B(1):144-152.

32. Boland ED, Wnek GE, Simpson DG, Pawlowski KJ, Bowlin GL. Tailoring tissue engineering scaffolds using electrostatic processing techniques: A study of poly(glycolic acid) electrospinning. *Journal of Macromolecular Sciences - Pure Applied Chemistry* 2001; 38(12):1231-1243.

33. Li WJ, Laurencin CT, Catterson EJ, Tuan RS, Ko FK. Electrospun nanofibrous structure: A novel scaffold for tissue engineering. *Journal of Biomedical Materials Research* 2002; 60(4):613-621.

34. Luu YK, Kim K, Hsiao BS, Chu B, Hadjiargyrou M. Development of a nanostructured DNA delivery scaffold via electrospinning of PLGA and PLA-PEG block copolymers. *Journal of Controlled Release* 2003; 89(2):341-353.

35. Sahoo S, Ouyang H, Goh JCH, Tay TE, Toh SL. Characterization of a novel polymeric scaffold for potential application in tendon/ligament tissue engineering. *Tissue Engineering* 2006; 12(1):91-99.

36. Xin XJ, Hussain M, Mao JJ. Continuing differentiation of human mesenchymal stem cells and induced chondrogenic and osteogenic lineages in electrospun PLGA nanofiber scaffold. *Biomaterials* 2007; 28(2):316-325.

37. Fang X, Reneker DH. DNA fibers by electrospinning. *Journal of Macromolecular Science - Physics* 1997; 36(2):169-173.

38. Jin HJ, Chen JS, Karageorgiou V, Altman GH, Kaplan DL. Human bone marrow stromal cell responses on electrospun silk fibroin mats. *Biomaterials* 2004; 25(6):1039-1047.

39. Li CM, Vepari C, Jin HJ, Kim HJ, Kaplan DL. Electrospun silk-BMP-2 scaffolds for bone tissue engineering. *Biomaterials* 2006; 27(16):3115-3124.
40. Min BM, Jeong L, Nam YS, Kim JM, Kim JY, Park WH. Formation of silk fibroin matrices with different texture and its cellular response to normal human keratinocytes. *International Journal of Biological Macromolecules* 2004; 34(5):281-288.
41. Min BM, Lee G, Kim SH, Nam YS, Lee TS, Park WH. Electrospinning of silk fibroin nanofibers and its effect on the adhesion and spreading of normal human keratinocytes and fibroblasts in vitro. *Biomaterials* 2004; 25(7-8):1289-1297.
42. McManus MC, Boland ED, Simpson DG, Barnes CP, Bowlin GL. Electrospun fibrinogen: Feasibility as a tissue engineering scaffold in a rat cell culture model. *Journal of Biomedical Materials Research, Part A* 2007; 81A(2):299-309.
43. Wnek GE, Carr ME, Simpson DG, Bowlin GL. Electrospinning of nanofiber fibrinogen structures. *Nano Letters* 2003; 3(2):213-216.
44. Jiang H, Fang D, Hsiao BS, Chu B, Chen W. Optimization and characterization of dextran membranes prepared by electrospinning. *Biomacromolecules* 2004; 5(2):326-333.
45. Matthews JA, Boland ED, Wnek GE, Simpson DG, Bowlin GL. Electrospinning of collagen type II: A feasibility study. *Journal of Bioactive and Compatible Polymers* 2003; 18(2):125-134.
46. Matthews JA, Wnek GE, Simpson DG, Bowlin GL. Electrospinning of collagen nanofibers. *Biomacromolecules* 2002; 3(2):232-238.
47. Zhong SP, Teo WE, Zhu X, Beueman RW, Ramakrishna S, Yung LYL. An aligned nanofibrous collagen scaffold by electrospinning and its effects on in vitro fibroblast culture. *Journal of Biomedical Materials Research, Part A* 2006; 79A(3):456-463.
48. Sefcik LS, Neal RA, Kaszuba SN, Parker AM, Katz AJ, Ogle RC, *et al.* Collagen nanofibres are a biomimetic substrate for the serum-free osteogenic differentiation of human adipose stem cells. *Journal of Tissue Engineering and Regenerative Medicine* 2008; 2(4):210-220.

49. Geng XY, Kwon OH, Jang JH. Electrospinning of chitosan dissolved in concentrated acetic acid solution. *Biomaterials* 2005; 26(27):5427-5432.
50. Ohkawa K, Cha DI, Kim H, Nishida A, Yamamoto H. Electrospinning of chitosan. *Macromolecular Rapid Communications* 2004; 25(18):1600-1605.
51. Huang L, Nagapudi K, Apkarian RP, Chaikof EL. Engineered collagen - PEO nanofibers and fabrics. *Journal of Biomaterials Science - Polymer Edition* 2001; 12(9):979-993.
52. Jiang HL, Fang DF, Hsiao BJ, Chu BJ, Chen WL. Preparation and characterization of ibuprofen-loaded poly(lactide-co-glycolide)/poly(ethylene glycol)-g-chitosan electrospun membranes. *Journal of Biomaterials Science - Polymer Edition* 2004; 15(3):279-296.
53. Min BM, You Y, Kim JM, Lee SJ, Park WH. Formation of nanostructured poly(lactic-co-glycolic acid)/chitin matrix and its cellular response to normal human keratinocytes and fibroblasts. *Carbohydrate Polymers* 2004; 57(3):285-292.
54. Zhang YZ, Huang ZM, Xu XJ, Lim CT, Ramakrishna S. Preparation of core-shell structured PCL-r-gelatin Bi-component nanofibers by coaxial electrospinning. *Chemistry of Materials* 2004; 16(18):3406-3409.
55. Zhang YZ, Ouyang HW, Lim CT, Ramakrishna S, Huang ZM. Electrospinning of gelatin fibers and gelatin/PCL composite fibrous scaffolds. *Journal of Biomedical Materials Research, Part B - Applied Biomaterials* 2005; 72B(1):156-165.
56. Tuzlakoglu K, Bolgen N, Salgado AJ, Gomes ME, Piskin E, Reis RL. Nano- and micro-fiber combined scaffolds: A new architecture for bone tissue engineering. *Journal Materials Science: Materials in Medicine* 2005; 16(12):1099-1104.
57. Khil MS, Bhattarai SR, Kim HY, Kim SZ, Lee KH. Novel fabricated matrix via electrospinning for tissue engineering. *Journal of Biomedical Materials Research, Part B - Applied Biomaterials* 2005; 72B(1):117-124.
58. Rutledge GC, Fridrikh SV. Formation of fibers by electrospinning. *Advanced Drug Delivery Reviews* 2007; 59(14):1384-1391.

59. Agrawal CM, Ray RB. Biodegradable polymeric scaffolds for musculoskeletal tissue engineering. *Journal of Biomedical Materials Research* 2001; 55(2):141-150.

60. Greiner A, Wendorff JH, Yarin AL, Zussman E. Biohybrid nanosystems with polymer nanofibers and nanotubes. *Applied Microbiology and Biotechnology* 2006; 71(4):387-393.

61. Murugan R, Ramakrishna S. Design Strategies of Tissue Engineering Scaffolds with Controlled Fiber Orientation. *Tissue Engineering* 2007; 13:1845-1866.

62. Ashammakhi N, Ndreu A, Piras AM, Nikkola L, Sindelar T, Ylikauppila H, *et al.* Biodegradable nanomats produced by electrospinning: Expanding multifunctionality and potential for tissue engineering. *Journal of Nanoscience and Nanotechnology* 2007; 7(3):862-882.

63. Barnes CP, Sell SA, Boland ED, Simpson DG, Bowlin GL. Nanofiber technology: Designing the next generation of tissue engineering scaffolds. *Advanced Drug Delivery Reviews* 2007; 59(14):1413-33.

64. Pham QP, Shama U, Mikos AG. Electrospinning of polymeric nanofibers for tissue engineering applications: a review. *Tissue Engineering* 2006; 12(5):1197-1211.

65. Teo WE, Ramakrishna S. Electrospun fibre bundle made of aligned nanofibres over two fixed points. *Nanotechnology* 2005; 16(9):1878-1884.

66. Zhang YZ, Lim CT, Ramakrishna S, Huang ZM. Recent development of polymer nanofibers for biomedical and biotechnological applications. *Journal of Materials Science: Materials in Medicine* 2005; 16(10):933-946.

67. Li WJ, Mauck RL, Tuan RS. Electrospun nanofibrous scaffolds: production, characterization, and applications for tissue engineering and drug delivery. *Journal of Biomedical Nanotechnology* 2005; 1:259-275.

68. Martins A, Araujo JV, Reis RL, Neves NM. Electrospun nanostructured scaffolds for tissue engineering applications. *Nanomedicine* 2007; 2(6):929-942.

69. Ndreu A, Nikkola L, Ylikauppila H, Ashammakhi N, Hasirci V. Electrospun biodegradable nanofibrous mats for tissue engineering. *Nanomedicine* 2008; 3(1):45-60.

70. Bognitzki M, Frese T, Steinhart M, Greiner A, Wendorff JH, Schaper A, *et al.* Preparation of fibers with nanoscaled morphologies: electrospinning of polymer blends. *Polymer Engineering and Science* 2001; 41(6):982-989.
71. Koombhongse S, Liu W, Reneker DH. Flat polymer ribbons and other shapes by electrospinning. *Journal of Polymer Science, Part B: Polymer Physics* 2001; 39(21):2598-2606.
72. MacDiamid AG, Jones Jr WE, Norris ID, Gao J, Johnson Jr AT, Pinto NJ, *et al.* Electrostatically-generated nanofibers of electronic polymers. *Synthetic Metals* 2001; 119(1-3):27-30.
73. Kim JS, Reneker DH. Polybenzimidazole nanofiber produced by electrospinning. *Polymer Engineering and Science* 1999; 39(5):849-854.
74. Lyons J, Li C, Ko F. Melt-electrospinning part I: Processing parameters and geometric properties. *Polymer* 2004; 45(22):7597-7603.
75. Hsu CM, Shivkumar S. Nano-sized beads and porous fiber constructs of Poly( $\epsilon$ -caprolactone) produced by electrospinning. *Journal of Materials Science* 2004; 39(9):3003-3013.
76. Fang D, Hsiao BS, Chu B. Development of multiple-jet electrospinning technology for mass production of nanofibers. 14<sup>th</sup> Annual International TANDEC Nonwovens Conference 2004; 1-11.
77. Li D, Xia YN. Direct fabrication of composite and ceramic hollow nanofibers by electrospinning. *Nano Letters* 2004; 4(5):933-938.
78. Yu JH, Fridrikh SV, Rutledge GC. Production of submicrometer diameter fibers by two-fluid electrospinning. *Advanced Materials* 2004; 16(17):1562-1566.
79. Huang ZM, Zhang Y, Ramakrishna S. Double-layered composite nanofibers and their mechanical performance. *Journal of Polymer Science, Part B: Polymer Physics* 2005; 43(20):2852-2861.
80. Jiang HL, Hu YQ, Zhao PC, Li Y, Zhu KJ. Modulation of protein release from biodegradable core-shell structured fibers prepared by coaxial electrospinning. *Journal of Biomedical Materials Research, Part B - Applied Biomaterials* 2006; 79B(1):50-57.

81. Li D, Babel A, Jenekhe SA, Xia YN. Nanofibers of conjugated polymers prepared by electrospinning with a two-capillary spinneret. *Advanced Materials* 2004; 16(22):2062-2066.
82. Loscertales IG, Barrero A, Marquez M, Spretz R, Velarde-Ortiz R, Larsen G. Electrically forced coaxial nanojets for one-step hollow nanofiber design. *Journal of the American Chemistry Society* 2004; 126(17):5376-5377.
83. Lee CH, Shin HJ, Cho IH, Kang YM, Kim IA, Park KD, *et al.* Nanofiber alignment and direction of mechanical strain affect the ECM production of human ACL fibroblast. *Biomaterials* 2005; 26(11):1261-1270.
84. Nerurkar NL, Elliott DM, Mauck RL. Mechanics of oriented electrospun nanofibrous scaffolds for annulus fibrosus tissue engineering. *Journal of Orthopaedic Research* 2007.
85. Sundaray B, Subramanian V, Natarajan TS, Xiang RZ, Chang CC, Fann WS. Electrospinning of continuous aligned polymer fibers. *Applied Physics Letters* 2004; 84(7):1222-1224.
86. Teo WE, Kotaki M, Mo XM, Ramakrishna S. Porous tubular structures with controlled fibre orientation using a modified electrospinning method. *Nanotechnology* 2005; 16(6):918-924.
87. Xu CY, Inai R, Kotaki M, Ramakrishna S. Aligned biodegradable nanofibrous structure: a potential scaffold for blood vessel engineering. *Biomaterials* 2004; 25(5):877-886.
88. Yang F, Murugan R, Wang S, Ramakrishna S. Electrospinning of nano/micro scale poly(L-lactic acid) aligned fibers and their potential in neural tissue engineering. *Biomaterials* 2005; 26(15):2603-2610.
89. Theron A, Zussman E, Yarin AL. Electrostatic field-assisted alignment of electrospun nanofibres. *Nanotechnology* 2001; 12(3):384-390.
90. Fong H, Liu W, Wang CS, Vaia RA. Generation of electrospun fibers of nylon 6 and nylon 6-montmorillonite nanocomposite. *Polymer* 2002; 43(3):775-780.
91. Li D, Wang YL, Xia YN. Electrospinning of polymeric and ceramic nanofibers as uniaxially aligned arrays. *Nano Letters* 2003; 3(8):1167-1171.

92. Dersch R, Liu TQ, Schaper AK, Greiner A, Wendorff JH. Electrospun nanofibers: Internal structure and intrinsic orientation. *Journal of Polymer Science, Part A - Polymer Chemistry* 2003; 41(4):545-553.

93. Li D, Wang YL, Xia YN. Electrospinning nanofibers as uniaxially aligned arrays and layer-by-layer stacked films. *Advanced Materials* 2004; 16(4):361-366.

94. Schnell E, Klinkhammer K, Balzer S, Brook G, Klee D, Dalton P, *et al.* Guidance of glial cell migration and axonal growth on electrospun nanofibers of poly-epsilon-caprolactone and a collagen/poly-epsilon-caprolactone blend. *Biomaterials* 2007; 28(19):3012-3025.

95. Katta P, Alessandro M, Ramsier RD, Chase GG. Continuous electrospinning of aligned polymer nanofibers onto a wire drum collector. *Nano Letters* 2004; 4(11):2215-2218.

96. Dalton PD, Klee D, Moller M. Electrospinning with dual collection rings. *Polymer* 2005; 46(3):611-614.

97. Czaplewski DA, Verbridge SS, Kameoka J, Craighead HG. Nanomechanical oscillators fabricated using polymeric nanofiber templates. *Nano Letters* 2004; 4(3):437-439.

98. Liu H, Kameoka J, Czaplewski DA, Craighead HG. Polymeric nanowire chemical sensor. *Nano Letters* 2004; 4(4):671-675.

99. Alberts B, Johnson A, Lewis J, Raff M, Roberts K, Walter P. *Molecular Biology of the Cell*. Fourth Edition ed. London, UK: Garland Science, 2002.

100. Seal BL, Otero TC, Panitch A. Polymeric biomaterials for tissue and organ regeneration. *Materials Science and Engineering: Reports* 2001; 34(4-5):147-230.

101. Zagris N. Extracellular matrix in development of the early embryo. *Micron* 2001; 32(4):427-438.

102. Stevens MM, George JH. Exploring and engineering the cell surface interface. *Science* 2005; 310(5751):1135-1138.

103. Gomes ME, Reis RL. Biodegradable polymers and composites in biomedical applications: From catgut to tissue engineering Part 1 Available systems and their properties. *International Materials Reviews* 2004; 49(5):261-273.

104. Gomes ME, Reis RL. Tissue engineering: Key elements and some trends. *Macromolecular Bioscience* 2004; 4(8):737-742.
105. Langer R, Vacanti JP. Tissue engineering. *Science* 1993; 260(5110):920-926.
106. Layman JM, Kenawy E-R, Watkins JR, Carrjr ME, Bowlin GL, Wnek GE. Development of the Biohemostat - a treatment modality for high pressure bleeding based on super absorbent polymer and electrospun membranes. *Polymer Preprints* 2003; 44:94-95.
107. Khil MS, Cha DI, Kim HY, Kim IS, Bhattarai N. Electrospun nanofibrous polyurethane membrane as wound dressing. *Journal of Biomedical Materials Research, Part B - Applied Biomaterials* 2003; 67B(2):675-679.
108. Kenawy ER, Layman JM, Watkins JR, Bowlin GL, Matthews JA, Simpson DG, *et al.* Electrospinning of poly(ethylene-co-vinyl alcohol) fibers. *Biomaterials* 2003; 24(6):907-913.
109. Rho KS, Jeong L, Lee G, Seo BM, Park YJ, Hong SD, *et al.* Electrospinning of collagen nanofibers: Effects on the behavior of normal human keratinocytes and early-stage wound healing. *Biomaterials* 2006; 27(8):1452-1461.
110. Powell HM, Supp DM, Boyce ST. Influence of electrospun collagen on wound contraction of engineered skin substitutes. *Biomaterials* 2008; 29(7):834-843.
111. How TV, inventor. Synthetic vascular grafts, and methods of manufacturing such grafts. U.S.Patent 4552707, 1985.
112. Stenoien MD, Drasler WJ, Scott RJ, Jenson ML, inventors. Silicone composite vascular graft. U.S.Patent 5866217, 1999.
113. Pinchuk L, Martin Jr JB, Maurin AA, inventors. Breast prostheses. U.S.Patent 5376117, 1994.
114. Buchko CJ, Kozloff KM, Sioshansi A, O'Shea KS, Martin DC. Electric field mediated deposition of bioactive polypeptides on neural prosthetic devices. *Materials Research Society Symposium - Proceedings*; 1996; Boston, MA, USA: Materials Research Society; 1996. p. 23-28.

115. Vinard E, Lesèche G, Andreassian B, Costagliola D. In vitro endothelialization of PTFE vascular grafts: A comparison of various substrates, cell densities, and incubation times. *Annals of Vascular Surgery* 1999; 13(2):141-150.
116. Williams SK, Jarrell BE. Tissue-engineered vascular grafts. *Nature Medicine* 1996; 2(1):32-34.
117. Stitzel JD, Pawlowski KJ, Wnek GE, Simpson DG, Bowlin GL. Arterial smooth muscle cell proliferation on a novel biomimicking, biodegradable vascular graft scaffold. *Journal of Biomaterials Applications* 2001; 16(1):22-33.
118. Venugopal J, Zhang YZ, Ramakrishna S. Fabrication of modified and functionalized polycaprolactone nanofibre scaffolds for vascular tissue engineering. *Nanotechnology* 2005; 16(10):2138-2142.
119. Xu CY, Yang F, Wang S, Ramakrishna S. In vitro study of human vascular endothelial cell function on materials with various surface roughness. *Journal of Biomedical Materials Research, Part A* 2004; 71A(1):154-161.
120. Mo XM, Xu CY, Kotaki M, Ramakrishna S. Electrospun P(LLA-CL) nanofiber: a biomimetic extracellular matrix for smooth muscle cell and endothelial cell proliferation. *Biomaterials* 2004; 25(10):1883-1890.
121. Xu CY, Inai R, Kotaki M, Ramakrishna S. Electrospun nanofiber fabrication as synthetic extracellular matrix and its potential for vascular tissue engineering. *Tissue Engineering* 2004; 10(7-8):1160-1168.
122. He W, Ma ZW, Yong T, Teo WE, Ramakrishna S. Fabrication of collagen-coated biodegradable polymer nanofiber mesh and its potential for endothelial cells growth. *Biomaterials* 2005; 26(36):7606-7615.
123. Jeong SI, Kim SY, Cho SK, Chong MS, Kim KS, Kim H, *et al.* Tissue-engineered vascular grafts composed of marine collagen and PLGA fibers using pulsatile perfusion bioreactors. *Biomaterials* 2007; 28(6):1115-1122.
124. Stitzel J, Liu L, Lee SJ, Komura M, Berry J, Soker S, *et al.* Controlled fabrication of a biological vascular substitute. *Biomaterials* 2006; 27(7):1088-1094.
125. Ma ZW, Kotaki M, Yong T, He W, Ramakrishna S. Surface engineering of electrospun polyethylene terephthalate (PET) nanofibers towards development of a new material for blood vessel engineering. *Biomaterials* 2005; 26(15):2527-2536.

126. Verreck G, Chun I, Peeters J, Rosenblatt J, Brewster ME. Preparation and characterization of nanofibers containing amorphous drug dispersions generated by electrostatic spinning. *Pharmaceutical Research* 2003; 20(5):810-817.

127. Kenawy ER, Bowlin GL, Mansfield K, Layman J, Simpson DG, Sanders EH, *et al.* Release of tetracycline hydrochloride from electrospun poly(ethylene-co-vinylacetate), poly(lactic acid), and a blend. *Journal of Controlled Release* 2002; 81(1-2):57-64.

128. Zong XH, Li S, Chen E, Garlick B, Kim KS, Fang DF, *et al.* Prevention of postsurgery-induced abdominal adhesions by electrospun bioabsorbable nanofibrous poly(lactide-co-glycolide)-based membranes. *Annals of Surgery* 2004; 240(5):910-915.

129. Verreck G, Chun I, Rosenblatt J, Peeters J, Van Dijck A, Mensch J, *et al.* Incorporation of drugs in an amorphous state into electrospun nanofibers composed of a water-insoluble, nonbiodegradable polymer. *Journal Of Controlled Release* 2003; 92(3):349-360.

130. Zeng J, Xu X, Chen X, Liang Q, Bian X, Yang L, *et al.* Biodegradable electrospun fibers for drug delivery. *Journal of Controlled Release* 2003; 92(3):227-231.

131. Kim K, Luu YK, Chang C, Fang DF, Hsiao BS, Chu B, *et al.* Incorporation and controlled release of a hydrophilic antibiotic using poly(lactide-co-glycolide)-based electrospun nanofibrous scaffolds. *Journal of Controlled Release* 2004; 98(1):47-56.

132. Katti DS, Robinson KW, Ko FK, Laurencin CT. Bioresorbable nanofiber-based systems for wound healing and drug delivery: Optimization of fabrication parameters. *Journal of Biomedical Materials Research, Part B - Applied Biomaterials* 2004; 70B(2):286-296.

133. Zong XH, Kim K, Fang DF, Ran SF, Hsiao BS, Chu B. Structure and process relationship of electrospun bioabsorbable nanofiber membranes. *Polymer* 2002; 43(16):4403-4412.

134. Luong-Van E, Grondahl L, Chua KN, Leong KW, Nurcombe V, Cool SM. Controlled release of heparin from poly(epsilon-caprolactone) electrospun fibers. *Biomaterials* 2006; 27(9):2042-2050.

135. Chew SY, Wen J, Yim EKF, Leong KW. Sustained release of proteins from electrospun biodegradable fibers. *Biomacromolecules* 2005; 6(4):2017-2024.

136. Sanders EH, Kloefkom R, Bowlin GL, Simpson DG, Wnek GE. Two-phase electrospinning from a single electrified jet: Microencapsulation of aqueous reservoirs in poly(ethylene-co-vinyl acetate) fibers. *Macromolecules* 2003; 36(11):3803-3805.

137. Zeng J, Aigner A, Czubyko F, Kissel T, Wendorff JH, Greiner A. Poly(vinyl alcohol) nanofibers by electrospinning as a protein delivery system and the retardation of enzyme release by additional polymer coatings. *Biomacromolecules* 2005; 6(3):1484-1488.

138. Liang DH, Luu YK, Kim KS, Hsiao BS, Hadjiargyrou M, Chu B. In vitro non-viral gene delivery with nanofibrous scaffolds. *Nucleic Acids Research* 2005; 33(19):1-8.

139. Li WJ, Tuli R, Huang XX, Laquerriere P, Tuan RS. Multilineage differentiation of human mesenchymal stem cells in a three-dimensional nanofibrous scaffold. *Biomaterials* 2005; 26(25):5158-5166.

140. Subramanian A, Vu D, Larsen GF, Lin HY. Preparation and evaluation of the electrospun chitosan/PEO fibers for potential applications in cartilage tissue engineering. *Journal of Biomaterials Science - Polymer Edition* 2005; 16(7):861-873.

141. Bhattarai N, Edmondson D, Veisoh O, Matsen FA, Zhang MQ. Electrospun chitosan-based nanofibers and their cellular compatibility. *Biomaterials* 2005; 26(31):6176-6184.

142. Alves da Silva M, Crawford A, Mundy J, Martins A, Araujo JV, Hatton PV, *et al.* Evaluation of extracellular matrix formation in PCL and SPCL nanofiber meshes when seeded with bovine articular chondrocytes. *Tissue Engineering, Part A* 2009, 15:377-385.

143. Shin M, Yoshimoto H, Vacanti JP. In vivo bone tissue engineering using mesenchymal stem cells on a novel electrospun nanofibrous scaffold. *Tissue Engineering* 2004; 10(1-2):33-41.

144. Boudriot U, Goetz B, Dersch R, Greiner A, Wendorff JH. Role of electrospun nanofibers in stem cell technologies and tissue engineering. *Macromolecular Symposia* 2005; 225:9-16.

145. Fujihara K, Kotaki M, Ramakrishna S. Guided bone regeneration membrane made of polycaprolactone/calcium carbonate composite nano-fibers. *Biomaterials* 2005; 26(19):4139-4147.

146. Wutticharoenmongkol P, Sanchavanakit N, Pavasant P, Supaphol P. Preparation and characterization of novel bone scaffolds based on electrospun polycaprolactone fibers filled with nanoparticles. *Macromolecular Bioscience* 2006; 6(1):70-77.

147. Araujo JV, Martins A, Leonor IB, Pinho ED, Reis RL, Neves NM. Surface Controlled Biomimetic Coating of Polycaprolactone Nanofiber Meshes to Be Used as Bone Extracellular Matrix Analogues. *Journal of Biomaterials Science - Polymer Edition* 2008, 19(10):1261-1278.

148. Nair LS, Bhattacharyya S, Bender JD, Greish YE, Brown PW, Allcock HR, *et al.* Fabrication and optimization of methylphenoxy substituted polyphosphazene nanofibers for biomedical applications. *Biomacromolecules* 2004; 5(6):2212-2220.

149. Meechaisue C, Wutticharoenmongkol P, Waraput R, Huangjing T, Ketbumrung N, Pavasant P, *et al.* Preparation of electrospun silk fibroin fiber mats as bone scaffolds: a preliminary study. *Biomedical Materials* 2007; 2(3):181-188.

150. Li MY, Mondrinos MJ, Gandhi MR, Ko FK, Weiss AS, Lelkes PI. Electrospun protein fibers as matrices for tissue engineering. *Biomaterials* 2005; 26(30):5999-6008.

151. Flemming RG, Murphy CJ, Abrams GA, Goodman SL, Nealey PF. Effects of synthetic micro- and nano-structured surfaces on cell behavior. *Biomaterials* 1999; 20(6):573-588.

152. Wang S, Cui W, Bei J. Bulk and surface modifications of polylactide. *Analytical and Bioanalytical Chemistry* 2005; 381(3):547-556.

153. Kwon IK, Kidoaki S, Matsuda T. Electrospun nano- to microfiber fabrics made of biodegradable copolyesters: structural characteristics, mechanical properties and cell adhesion potential. *Biomaterials* 2005; 26(18):3929-3939.
154. Shin M, Ishii O, Sueda T, Vacanti JP. Contractile cardiac grafts using a novel nanofibrous mesh. *Biomaterials* 2004; 25(17):3717-3723.
155. Zong XH, Bien H, Chung CY, Yin LH, Fang DF, Hsiao BS, *et al.* Electrospun fine-textured scaffolds for heart tissue constructs. *Biomaterials* 2005; 26(26):5330-5338.
156. Riboldi SA, Sadr N, Pignini L, Neuenschwander P, Simonet M, Mognol P, *et al.* Skeletal myogenesis on highly orientated microfibrous polyesterurethane scaffolds. *Journal of Biomedical Materials Research* 2008; 84(4):1094-1101.
157. Riboldi SA, Sampaolesi M, Neuenschwander P, Cossu G, Mantero S. Electrospun degradable polyesterurethane membranes: potential scaffolds for skeletal muscle tissue engineering. *Biomaterials* 2005; 26(22):4606-4615.
158. Chua KN, Lim WS, Zhang PC, Lu HF, Wen J, Ramakrishna S, *et al.* Stable immobilization of rat hepatocyte spheroids on galactosylated nanofiber scaffold. *Biomaterials* 2005; 26(15):2537-2547.
159. Berry CC, Cacou C, Lee DA, Bader DL, Shelton JC. Dermal fibroblasts respond to mechanical conditioning in a strain profile dependent manner. *Biorheology* 2002; 40(1-3):337-345.
160. Sambajon WV, Cillo Jr JE, Gassner RJ, Buckley MJ. The effects of mechanical strain on synovial fibroblasts. *Journal of Oral and Maxillofacial Surgery* 2003 ;61(6):707-712.
161. Azevedo HS, Gomes ME, Malafaya PB, Marques AP, Salgado AJ, Reis RL. Natural origin degradable polymers in biomedical applications. In: Mallapragada S, Narasimhan B, editors. *Handbook of biodegradable polymeric materials and their applications*. California: American Scientific Publishers, 2006. p. 13-31.
162. Lutolf MP, Hubbell JA. Synthetic biomaterials as instructive extracellular microenvironments for morphogenesis in tissue engineering. *Nature Biotechnology* 2005; 23(1):47-55.

163. Malafaya PB, Gomes ME, Salgado AJ, Reis RL. Polymer based scaffolds and carriers for bioactive agents from different natural origin materials. *Advances in Experimental Medicine and Biology* 2003; 534:201-233.

164. Mano JF, Silva GA, Azevedo HS, Malafaya PB, Sousa RA, Silva SS, *et al.* Natural origin biodegradable systems in tissue engineering and regenerative medicine: present status and some moving trends. *Journal of Royal Society Interface* 200; 4(17):999-1030.

165. Hutmacher DW. Scaffolds in tissue engineering bone and cartilage. *Biomaterials* 2000; 21(24):2529-2543.

166. Karande TS, Ong JL, Agrawal CM. Diffusion in musculoskeletal tissue engineering scaffolds: Design issues related to porosity, permeability, architecture, and nutrient mixing. *Annals of Biomedical Engineering* 2004; 32(12):1728-1743.

167. Mooney DJ, Mikos AG. Growing new organs. *Scientific American* 1999; 280(4):60-65.

168. Salgado AJ, Coutinho OP, Reis RL. Bone tissue engineering: State of the art and future trends. *Macromolecular Bioscience* 2004; 4(8):743-765.

169. Gallardo A, Abraham GA, Elvira C, Vázquez B, San Román J. Polymeric matrices for release of growth factors, hormones and other bioactive agents. In: Reis RL, Cohn D, editors. *Polymer based systems on tissue engineering, replacement and regeneration*. Dordrecht, The Netherlands: Kluwer Academic Publishers, 2002. p. 37-52.

170. Pillai O, Panchagnula R. Polymers in drug delivery. *Current Opinion in Chemical Biology* 2001; 5(4):447-451.

171. Baran ET, Tuzlakoglu K, Salgado AJ, Reis RL. Multichannel mould processing of 3D structures from microporous coralline hydroxyapatite granules and chitosan support materials for guided tissue regeneration/engineering. *Journal of Materials Science: Materials in Medicine* 2004; 15(2):161-165.

172. Correlo VM, Boesel LF, Bhattacharya M, Mano JF, Neves NM, Reis RL. Properties of melt processed chitosan and aliphatic polyester blends. *Materials Science and Engineering A* 2005; 403(1-2):57-68.

173. Correlo VM, Pinho ED, Pashkuleva I, Bhattacharya M, Neves NM, Reis RL. Water absorption and degradation characteristics of chitosan-based polyesters and hydroxyapatite composites. *Macromolecular Bioscience* 2007; 7(3):354-363.

174. Dhariwala B, Hunt E, Boland T. Rapid prototyping of tissue-engineering constructs, using photopolymerizable hydrogels and stereolithography. *Tissue Engineering* 2004; 10(9-10):1316-1322.

175. Gomes ME, Ribeiro AS, Malafaya PB, Reis RL, Cunha AM. A new approach based on injection moulding to produce biodegradable starch-based polymeric scaffolds: Morphology, mechanical and degradation behaviour. *Biomaterials* 2001; 22(9):883-889.

176. Gomes ME, Sikavitsas VI, Behravesh E, Reis RL, Mikos AG. Effect of flow perfusion on the osteogenic differentiation of bone marrow stromal cells cultured on starch-based three-dimensional scaffolds. *Journal of Biomedical Materials Research - Part A* 2003; 67(1):87-95.

177. Hutmacher DW, Schantz T, Zein I, Kee Woei N, Swee Hin T, Kim Cheng T. Mechanical properties and cell cultural response of polycaprolactone scaffolds designed and fabricated via fused deposition modeling. *Journal of Biomedical Materials Research* 2001; 55(2):203-216.

178. Landers R, Pfister A, Hübner U, John H, Schmelzeisen R, Mülhaupt R. Fabrication of soft tissue engineering scaffolds by means of rapid prototyping techniques. *Journal of Materials Science* 2002; 37(15):3107-3116.

179. Malafaya PB, Elvira C, Gallardo A, San Román J, Reis RL. Porous starch-based drug delivery systems processed by a microwave route. *Journal of Biomaterials Science - Polymer Edition* 2001; 12(11):1227-1241.

180. Mikos AG, Bao Y, Cima LG, Ingber DE, Vacanti JP, Langer R. Preparation of poly(glycolic acid) bonded fiber structures for cell attachment and transplantation. *Journal of Biomedical Materials Research* 1992; 27(2):183-189.

181. Murphy WL, Dennis RG, Kileny JL, Mooney DJ. Salt fusion: An approach to improve pore interconnectivity within tissue engineering scaffolds. *Tissue Engineering* 2002; 8(1):43-52.

182. Oliveira AL, Malafaya PB, Reis RL. Sodium silicate gel as a precursor for the in vitro nucleation and growth of a bone-like apatite coating in compact and porous polymeric structures. *Biomaterials* 2003; 24(15):2575-2584.

183. Pfister A, Landers R, Laib A, Hübner U, Schmelzeisen R, Mülhaupt R. Biofunctional Rapid Prototyping for Tissue-Engineering Applications: 3D Bioplotting versus 3D Printing. *Journal of Polymer Science, Part A: Polymer Chemistry* 2004;42(3):624-638.

184. Silva RM, Elvira C, Mano JF, San Román J, Reis RL. Influence of  $\beta$ -radiation sterilisation in properties of new chitosan/soybean protein isolate membranes for guided bone regeneration. *Journal of Materials Science: Materials in Medicine* 2004; 15(4):523-528.

185. Silva RM, Silva GA, Coutinho OP, Mano JF, Reis RL. Preparation and characterisation in simulated body conditions of glutaraldehyde crosslinked chitosan membranes. *Journal of Materials Science: Materials in Medicine* 2004; 15(10):1105-1112.

186. Sousa RA, Kalay G, Reis RL, Cunha AM, Bevis MJ. Injection molding of a starch/EVOH blend aimed as an alternative biomaterial for temporary applications. *Journal of Applied Polymer Science* 2000; 77(6):1303-1315.

187. Temenoff JS, Mikos AG. Injectable biodegradable materials for orthopedic tissue engineering. *Biomaterials* 2000; 21(23):2405-2412.

188. Vaz CM, van Doeveren PFNM, Reis RL, Cunha AM. Soy matrix drug delivery systems obtained by melt-processing techniques. *Biomacromolecules* 2003; 4(6):1520-1529.

189. Woodfield TBF, Malda J, De Wijn J, Peeters F, Riesle J, Van Blitterswijk CA. Design of porous scaffolds for cartilage tissue engineering using a three-dimensional fiber-deposition technique. *Biomaterials* 2004; 25(18):4149-4161.

190. Schreuder-Gibson H, Gibson P, Senecal K, Sennett M, Walker J, Yeomans W, *et al.* Protective textile materials based on electrospun nanofibers. *Journal of Advanced Materials* 2002; 34(3):44-55.

191. Gomes ME, Godinho JS, Tchalamov D, Cunha AM, Reis RL. Alternative tissue engineering scaffolds based on starch: Processing methodologies,

morphology, degradation and mechanical properties. *Materials Science and Engineering C* 2002; 20(1-2):19-26.

192. Laurencin CT, Ambrosio AMA, Borden MD, Cooper Jr JA. Tissue engineering: Orthopedic applications. *Annual Review of Biomedical Engineering* 1999; 1(1):19-46.

193. Shin H, Jo S, Mikos AG. Biomimetic materials for tissue engineering. *Biomaterials* 2003; 24(24):4353-4364.

194. Bolgen N, Menceloglu YZ, Acatay K, Vargel I, Piskin E. In vitro and in vivo degradation of non-woven materials made of poly( $\epsilon$ -caprolactone) nanofibers prepared by electrospinning under different conditions. *Journal of Biomaterials Science - Polymer Edition* 2005; 16(12):1537-1555.

195. Theron SA, Yarin AL, Zussman E, Kroll E. Multiple jets in electrospinning: Experiment and modeling. *Polymer* 2005; 46(9):2889-2899.

196. Dzenis Y. Spinning continuous fibers for nanotechnology. *Science* 2004; 304(5679):1917-1919.

197. Jayasinghe SN, Irvine S, McEwan JR. Cell electrospinning highly concentrated cellular suspensions containing primary living organisms into cell-bearing threads and scaffolds. *Nanomedicine* 2007; 2(4):555-567.

198. Townsend-Nicholson A, Jayasinghe SN. Cell electrospinning: a unique biotechnique for encapsulating living organisms for generating active biological microthreads/scaffolds. *Biomacromolecules* 2006; 7(12):3364-3369.

199. Lee S-W, Belcher AM. Virus-based fabrication of micro- and nanofibers using electrospinning. *Nano Letters* 2004; 4(3):387-390.

200. Salalha W, Kuhn J, Dror Y, Zussman E. Encapsulation of bacteria and viruses in electrospun nanofibres. *Nanotechnology* 2006; 17(18):4675-4681.

201. Stankus JJ, Guan J, Fujimoto K, Wagner WR. Microintegrating smooth muscle cells into a biodegradable, elastomeric fiber matrix. *Biomaterials* 2006; 27(5):735-744.

202. Stankus JJ, Soletti L, Fujimoto K, Hong Y, Vorp DA, Wagner WR. Fabrication of cell microintegrated blood vessel constructs through electrohydrodynamic atomization. *Biomaterials* 2007; 28(17):2738-2746.

203. Santos MI, Fuchs S, Gomes ME, Unger RE, Reis RL, Kirkpatrick CJ. Response of micro- and macrovascular endothelial cells to starch-based fiber meshes for bone tissue engineering. *Biomaterials* 2007; 28(2):240-248.

204. Santos MI, Tuzlakoglu K, Gomes ME, Fuchs S, Unger RE, Piskin E, *et al.* Nano- and micro-fiber combined scaffolds: An innovative design for improving endothelial cell migration in bone tissue engineering approaches. *Tissue Engineering* 2006; 12(4):986-987.

205. Nam J, Huang Y, Agarwal S, Lannutti J. Improved Cellular Infiltration in Electrospun Fiber via Engineered Porosity. *Tissue Engineering* 2007; 13(9):2249-57.

206. Kim G, Kim W. Highly porous 3D nanofiber scaffold using an electrospinning technique. *Journal of Biomedical Materials Research, Part B - Applied Biomaterials* 2007; 81(1):104-110.

207. Zhang YZ, Venugopal J, Huang ZM, Lim CT, Ramakrishna S. Characterization of the surface biocompatibility of the electrospun PCL-collagen nanofibers using fibroblasts. *Biomacromolecules* 2005; 6(5):2583-2589.

208. Chen F, Lee CN, Teoh SH. Nanofibrous modification on ultra-thin poly(epsilon-caprolactone) membrane via electrospinning. *Materials Science & Engineering C - Biomimetic and Supramolecular Systems* 2007; 27(2):325-332.

## **Section II**

### **DETAILED DESCRIPTION OF EXPERIMENTAL TESTING AND MATERIALS**



## Chapter 2

### Materials & Methods

The main aim of this chapter is to describe, in greater detail, the experimental work and protocols related to experiments performed and the obtained results. It will introduce the rationale of this PhD work, namely the aspects concerning the selection of the materials, the scaffolds processing methodologies and the physicochemical and biological characterization techniques.

## 2.2. Materials

### 2.2.1. Polycaprolactone

Polycaprolactone (PCL) is a biodegradable polyester whose chemical structure is shown in Figure 2.1. It is hydrophobic in its wettability and semicrystalline, with a melting point of around 60 °C and a glass transition temperature of about -60 °C. PCL is derived by chemical synthesis from crude oil and can be synthesized by a ring opening polymerization of a cyclic lactone monomer (i.e.  $\epsilon$ -caprolactone).

PCL is degraded by hydrolysis of its ester bonds in physiological conditions (such as in the human body) [4, 5]. Recently, PCL has stimulated significant research into its potential use as a biomaterial, mainly due to its good biocompatibility and exceptional ability to form compatible blends and copolymers with a wide range of other polymers, producing materials with unique elastomeric properties [6]. PCL is a Food and Drug Administration (FDA) approved material that is used in the human body as a drug delivery device, suture or adhesion preventing barrier [7-9].

The PCL used in this PhD work, commercially available as TONE™ polymer ( $M_w = 80000$  Da), was purchase from Union Carbide Chemicals and Plastics Division (Bound Brook, New Jersey).

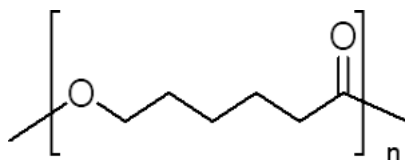


**Figure 2.1** - Chemical structure of polycaprolactone

### 2.2.2. Poly(ethylene Oxide)

Poly(ethylene oxide) (PEO) is a linear or branched polyether often terminated with hydroxyl groups that are derived from neutralization of the terminal ether repeated unit in the chain (Figure 2.2). PEO oligomers are most commonly synthesized via anionic ring-opening polymerization of ethylene oxide (EO) [10]. Typically, materials with  $M_w < 100000$  are usually called poly(ethylene glycol) (PEG), while higher molecular weight polymers are classified as PEO. PEO is clear, colorless, odorless, inert to many chemical agents, stable against hydrolysis, and nontoxic [10]. Biocompatibility and lack of immunogenicity make PEO an important polymer for biomedical applications. Another important property of PEO is its solubility in water, as well as in many organic solvents (e.g. methylene chloride, ethanol, toluene, acetone, and chloroform) depending on its molecular weight [11]. The used PEO (Aldrich, Germany) has a  $M_w \sim 100000$ , a glass transition temperature ( $T_g$ ) of  $-67\text{ }^\circ\text{C}$ , a melting point at  $65\text{ }^\circ\text{C}$ , a density of  $1.13\text{ g/ml}$  and a viscosity of  $12\text{-}50\text{ cP}$  (5% in  $\text{H}_2\text{O}$  at  $25\text{ }^\circ\text{C}$ ).

PEG is one of the most frequently used water-soluble polymers for biomedical applications because of its high water solubility and chain flexibility [11]. The high degree of hydration and flexibility confers it as protein resistant, biocompatible, and non-immunogenic. The PEG has been used to prolong the half-life of enzymes conjugated to the molecule thereby decreasing liver uptake. The PEGs have also been used in drug delivery to increase water-solubility of poorly soluble drugs such as paclitaxel. The long circulating property of PEG is used to improve tumor targeting and accumulation of monoclonal antibody fragments by the passive enhanced permeability and retention (EPR) mechanism. The PEG stabilized liposomal formulations of many drugs have similarly found application in drug delivery.

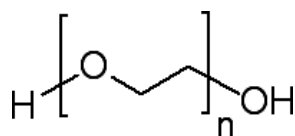


**Figure 2.2** – Chemical structure of poly(ethylene oxide)

### 2.2.3. Starch-Polycaprolactone blend

Starch is a polysaccharide carbohydrate consisting of a large number of glucose units joined together by glycosidic bonds. It consists of two types of molecules: the linear and helical amylose and the branched amylopectin (Figure 2.3). Amylose is a linear polymer of several thousand glucose residues linked mainly by  $\alpha(1\rightarrow4)$  bonds (Figure 2.3 A). Amylopectin is a polysaccharide and highly branched polymer of glucose units linked in a linear way with  $\alpha(1\rightarrow4)$  glycosidic bonds (Figure 2.3 B). Branching takes place at the  $\alpha(1\rightarrow6)$  bonds occurring every 24 to 30 glucose units.

Starch has been successfully incorporated in many synthetic polymeric systems to lower its cost and increase its biodegradability [12-15]. Additionally, the use of starch-based materials have attracted great attention in tissue engineering applications due to the advantages of being non-cytotoxic, having good mechanical properties and being processed by various methodologies, including by melt-based routes.

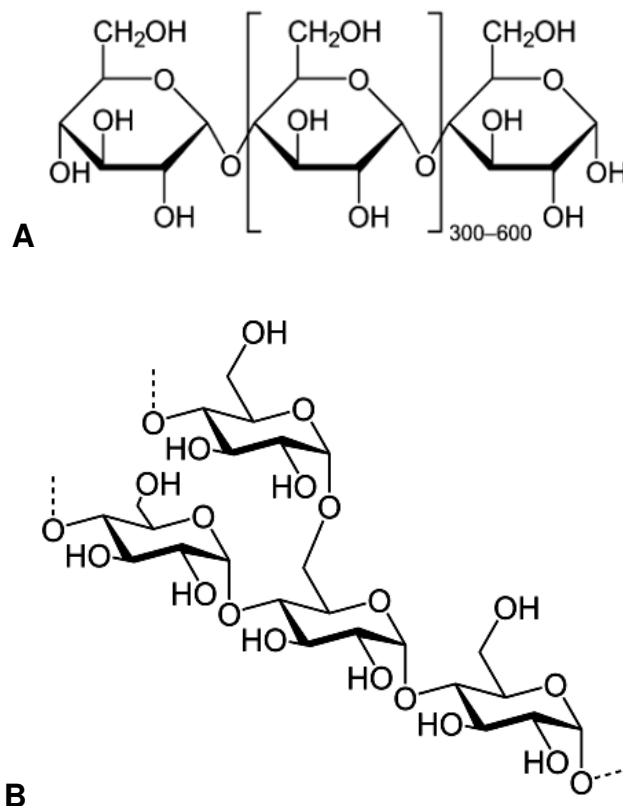


**Figure 2.3** - Chemical structures of the amylose (A) and amylopectin (B) molecules.

Starch-based scaffolds obtained from a blend of corn starch and polycaprolactone (SPCL) have been proposed as candidates for bone tissue engineering applications, as well as drug delivery systems, in multiple studies from our group [16-22]. Indeed, successful results were demonstrated in terms of cell viability, proliferation and maturation of osteoblastic cells or differentiation of bone marrow stromal cells. Additionally, *in vivo* studies also demonstrate that biodegradable starch-based materials did not induce a severe immune response [23]. Accordingly, the 30:70 (wt.%) SPCL blend was purchased to Novamont (Novara, Italy). The thermal and mechanical properties of the SPCL were previously reported [24-26]. Briefly, starch effectively increased the non-isothermal crystallisation rate of PCL, effectively reinforced PCL and enhanced its damping properties, as it might help in the dissipation of the mechanical energy generated by the patient movements.

#### 2.2.4. *Poly(butylene succinate)*

Poly(butylene succinate) (PBS) is an aliphatic polyester, sold under the trademark Bionolle [27]. It was obtained from Showa Highpolymer Co. Ltd. (Tokyo, Japan), with the reference 1050, a polybutylene succinate copolymer. Bionolle<sup>®</sup> has been shown to be biodegradable in a variety of natural environments, decomposing into water and carbon dioxide. It has been processed into films, sheets, filaments, nonwoven fabrics, laminates, molded foams and injection-molded products for diverse applications, namely in agriculture, fishery, forestry, civil engineering and for common household goods.

Pure PBS presents a hydrophobic behavior with low water uptake (~ 1.5 %) and displayed a decrease in the mechanical properties without any appreciable weight loss (~ 0.5 %), after 60 days of immersion in the isotonic saline solution [28]. This polymer presents a melting temperature ( $T_m$ ) of 104.3 °C and an enthalpy ( $\Delta H$ ) value of 60.8 J/g, comparing to the  $\Delta H_m$  of a 100 % crystalline PBS (110.3 J/g), determined by differential scanning calorimeter (DSC) [29]. Additionally, the material data sheet reported a density of 1260 g/L, a heat of combustion of 23.6 KJ/g and a glass transition temperature ( $T_g$ ) of -32 °C.

### 2.2.5. Chitosan

Chitosan ( $\alpha(1\rightarrow4)$ -2-amino-2-deoxy- $\beta$ -D-glucan) is the alkaline deacetylated product of chitin, which is the principal organic component of the exoskeleton of invertebrates such as crustaceans (crabs, shrimp, etc.), insects and spiders, being also found in the cell walls of fungi and many algae. It is a linear polysaccharide composed of randomly distributed  $\beta$ -(1 $\rightarrow$ 4)-linked *D*-glucosamine (deacetylated unit) and *N*-acetyl-*D*-glucosamine (acetylated unit) (Figure 2.4).

Important parameters affecting the characteristics of chitosan are its molecular weight ( $M_w$ ) and its degree of deacetylation (DD) [30]. The degree of deacetylation of chitosan refers to the ratio between the deacetylated and acetylated units. Chitosan is a semi-crystalline polymer and the degree of crystallinity depends on the degree of deacetylation.

Chitosan is one of the most appealing biomaterials for prospective applications in tissue engineering and drug delivery [31-34], due to its biological properties such as potential biocompatibility and immunological, antibacterial and wound-healing activity [32, 35, 36]. Additionally, chitosan shares structural characteristics with various glucosaminoglycans (GAGs) and hyaluronic acid (HA) present in various tissues, namely in articular cartilage [37, 38].

The chitosan herein used was purchased to France Chitine (Orange, France). Firstly, chitin was isolated from shrimp shells and squid bones by deproteinization and/or demineralization, respectively. The chitosan was further obtained by the removal of enough acetyl groups ( $\text{CH}_3\text{-CO}$ ) from the chitin molecule - deacetylation process -, releasing the amine groups ( $\text{NH}$ ) and giving the chitosan a cationic characteristic.

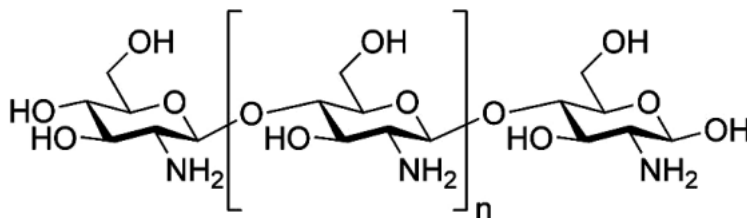


**Figure 2.4** - Chemical structure of chitosan

Considering the described procedure, chitosan raw-materials sometimes possess an insoluble fraction which could be remaining chitin or other type of impurities. For that reason, a purification procedure was carried out.

#### 2.2.5.1. Purification of chitosan

A determined amount of chitosan (~ 50 g) was dissolved in an aqueous acetic acid solution (1 %) at ~ 1 wt.%. The insoluble material was removed by filtration with Whatman<sup>®</sup> ashless filter paper (20-25 µm). The obtained clear solution was neutralized using a NaOH solution (final pH ~ 8). The obtained white gel was centrifuged to remove the exuded liquid and systematically rinsed with distilled water, until no changes in the pH were observed. The chitosan gel was further washed with ethanol, freeze-dried, ground to powder and dried at 60 °C overnight.

Since the purification process can affect the final physicochemical properties of this natural polymer, determination of the average viscosity molecular weight ( $M_v$ ) and the degree of deacetylation (DD) was performed.

#### 2.2.5.2. Determination of the viscosity average molecular weight

To evaluate the molecular weight of polymeric chains various methods can be used: widespread are viscometric and gel permeation chromatographic techniques. Viscosity is empirically related to molecular weight, because the measurement depends upon the hydrodynamic volume of the macromolecule, which is a function of the molecular weight, conformational properties and polymer-solvent interactions [39-41]. Measurements of solution viscosity are made by comparing the flow time  $t$  required for a specific volume of polymer solution to flow through a capillary tube with the correspondent flow time  $t_0$  for the solvent. Relative viscosity ( $\eta_r$ ) (equation 2.1) and specific viscosity ( $\eta_{sp}$ ) (equation 2.2) are calculated from  $t$  and  $t_0$ , according to the following equations:

$$\eta_r = \eta/\eta_0 \cong t/t_0 \quad (2.1)$$

$$\eta_{sp} = \eta_r - 1 \quad (2.2)$$

Several equations are available for determining the intrinsic viscosity  $[\eta]$  of a polymer. These equations are found to be valid at sufficiently low concentrations, assuring that the polymer chains are free to move individually in the solvent, i.e., the kinetic units are not aggregates but single polymer molecules. The equations derived by Huggins [40] (equation 2.3) and Kraemer [41] (equation 2.4) relate  $\eta_{sp}$  and  $\eta_r$ , respectively, with the polymer concentration in the solvent ( $c$  in g/dL or any other units proportional to this), according to the following expressions:

$$\eta_{sp}/c = [\eta] + k'[\eta]^2 c \quad (2.3)$$

$$\ln \eta_r/c = [\eta] - k''[\eta]^2 c \quad (2.4)$$

The Huggins ( $K_H$ ) and the Kraemer ( $K_K$ ) coefficients give information on the polymer-solvent interactions, being the  $K_H$  lower values (ranging from 0.25 to 0.5) and the  $K_K$  negative values related to a better solvation of the polymer chains [42]. Theoretically,  $K_H + K_K$  should be equal to 0.5. The intrinsic viscosity  $[\eta]$  is a theoretical value calculated at the limit of infinite dilution using those equations:

$$[\eta] = (\eta_{sp}/c)_{c=0} \quad (\text{Huggins}) \quad (2.5)$$

$$[\eta] = (\ln \eta_r/c)_{c=0} \quad (\text{Kraemer}) \quad (2.6)$$

The graphical extrapolation ( $c=0$ ) using both equations is expected to result approximately in the same values of  $[\eta]$  for a particular polymer-solvent system.

To allow performing that quantification, five chitosan fresh solutions with different concentrations were prepared, in the range that gives  $\eta_r$  between 1.1 and 1.9. The purified chitosan samples were dried in the oven overnight and accurately weighted in an analytical balance ( $\pm 0.1$  mg). The residual water was determined thermogravimetrically (TGA) and the concentration of the chitosan solutions corrected accordingly. First, the weighted chitosan powder was completely dissolved in acetic acid (AcOH) 0.5 M. A suitable amount of sodium acetate (AcONa) was added to give a final concentration of 0.2 M. A blank solution was prepared in the same way, but without chitosan. The flow time for each solution was obtained from five reproducible measurements, using an Ubbelohde viscometer at  $25.0 \pm 0.1$  °C. The intrinsic

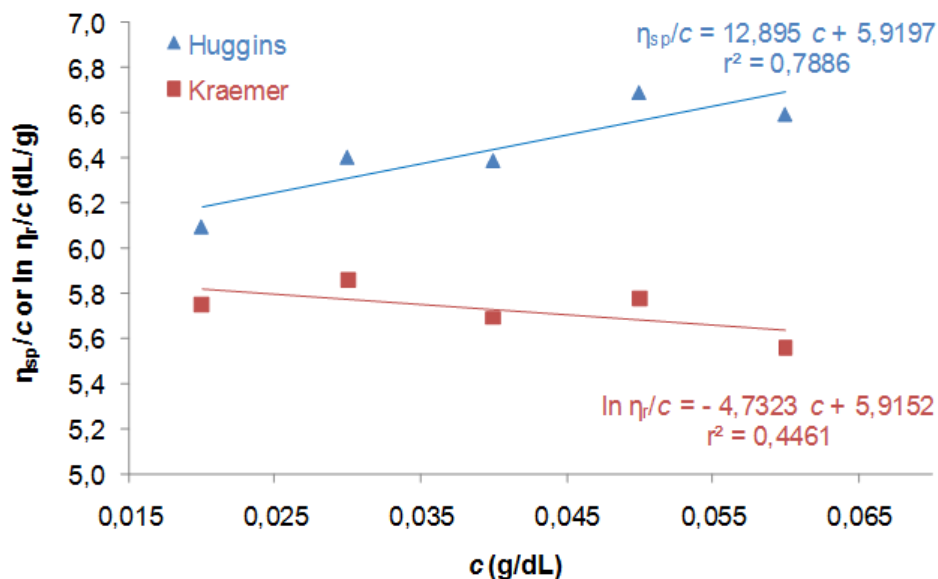


**Figure 2.5** - Linear regressions obtained by plotting  $\eta_{sp}/c$  or  $\ln \eta_r/c$  against  $c$ , according to the Huggins or Kraemer equations, respectively.

viscosity  $[\eta]$  was calculated by linear regression plotting  $\eta_{sp}/c$  and  $\ln \eta_r/c$  against  $c$  (Figure 2.5).

The viscosity average molecular weight ( $M_v$ ) is calculated based on the Mark-Houwink equation:

$$[\eta] = k(M_v)^a \quad (2.7)$$

being  $[\eta] = 5.91$  dL/g (previously determined),  $M_v$  in Da,  $k = 3.5 \times 10^{-4}$  and  $a = 0.76$  for 0.5 M AcOH/0.2 M NaOAc aqueous solution as solvent at 25 °C (independent of the DD at these conditions) [43]. Accordingly to the intrinsic viscosity calculated, the viscosity average molecular weight of the purified chitosan from France Chitine was 416 kDa.

### 2.2.5.3. Determination of the degree deacetylation

Although being apparently a simple analytical problem, the determination of the DD revealed to be not simple. A large number of methods were proposed in the literature, including Fourier transformed infrared spectroscopy (FTIR) [44-46],

potentiometric [47] and conductometric titration [48], ultraviolet (UV) spectrophotometry [49-51], ninhydrin assay [52], and nuclear magnetic resonance (NMR) spectroscopy [53, 54]. The great number of methods described in the literature may be regarded as an advantage, but these methods differ in reliability, robustness, precision and accuracy over the entire DD range. To overcome those considerations, three different methods were applied to ascertain about the DD of our chitosan batch, namely  $^1\text{H}$ -NMR, FTIR and UV spectrophotometry.

Nuclear magnetic resonance (NMR) spectroscopy is one of the most useful techniques for characterizing polymeric biomaterials [11]. The basic principle behind NMR involves the detection of absorption or emission of radiation resulting from the interaction of an applied EM radiation with nuclear spins of the polymeric molecules when the energy levels in the latter are split by an external magnetic field. The primary prerequisite of NMR is that the material contains atoms whose nuclei contain an unpaired proton or neutron that possess nuclear spin properties. Since most polymeric biomaterials possess high concentration of  $^1\text{H}$  they can be characterized by NMR. The early applications of  $^1\text{H}$  resonance high resolution NMR to polymers were at 60 or 100MHz (field strengths of 1.4 and 2.3 T respectively) and detailed information on the chain structure. Therefore, the  $^1\text{H}$ -NMR is commonly considered the reference method to determine the DD of chitosan [53]. To improve the solubility and to obtain high quality NMR spectra in solution state, chitosan samples were partially depolymerised and the spectra recorded at 60 °C. Making use of the signal from the chitosan  $^1\text{H}$ -NMR spectra peaks of acetyl group, namely  $I_c$  and  $I_e$  peaks (see Figure 2.6), the DD was calculated using the equation 2.8 [53].

$$DD(\%) = \left( 1 - \left( \frac{1}{3} I_e / \frac{1}{6} I_c \right) \right) \times 100 \quad (2.8)$$

Applying the equation 2.8, it was calculated a DD of  $87.7 \pm 0.4 \%$  for the purified chitosan from France Chitine.

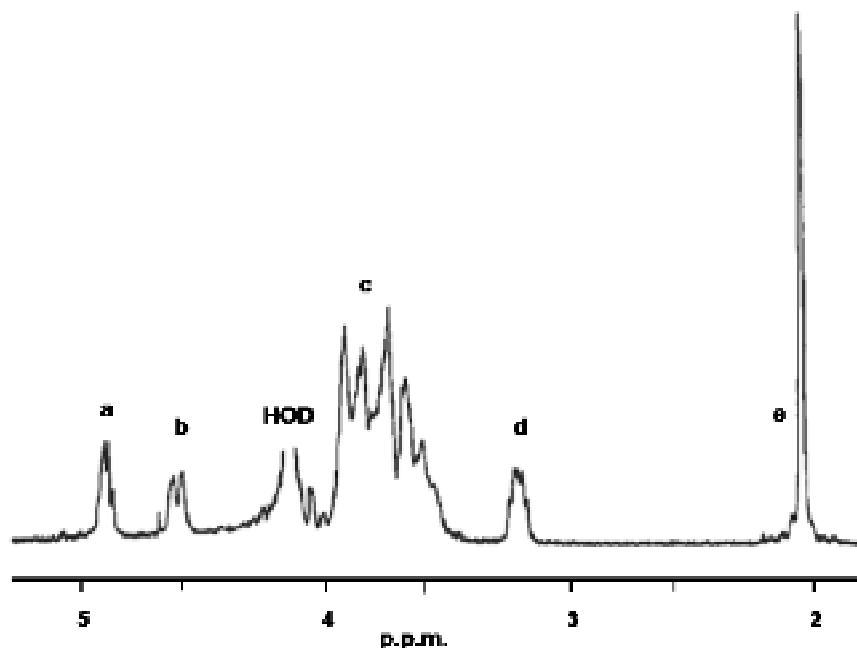


**Figure 2.6** - Identification of the chitosan  $^1\text{H-NMR}$  spectra peaks (*adapted from reference [1]*)

FTIR methods are widely used to determine the DD of chitosan and, since the determination is performed in the solid state, they are also suitable to determine the DD of insoluble chitin (DD < 40). FTIR has been often preferred because it is a quick and low-cost method. The method requires the construction of a specific calibration line for each particular sample and for each deacetylation procedure it is necessary to obtain reference values of DA [45]. Consequently, the FTIR methods involve the comparison between the absorbance of a band assigned exclusively to one of the monosaccharides and a suitable internal reference band to correct for film thickness or sample concentration (KBr disks). A considerable effort has been devoted to identify the right combination of bands and respective baselines, which led to a large number of proposed methods found in the literature [44-46, 55]. In our first attempt to determine the DD by FTIR we used the method proposed by Baxter *et al.* [55] and the bands proposed by Brugnerotto *et al.* [46] that are depicted in Table 2.1.

The values determined by means of FTIR using the  $3450\text{ cm}^{-1}$  band (assigned to the -NH and -OH stretching bands) are lower than the DD achieved by using the band at  $1420\text{ cm}^{-1}$  (method II). These differences could be due to the uptake of

**Table 2.1** - Calibration curves to determine the DD using the FTIR spectrum of chitosan that make use of different combinations of bands and baselines. The absorbance (*A*) is the height at the band maximum corrected by the intercepting with the respective baseline

<i>Method</i>	<i>Band</i> ( $\text{cm}^{-1}$ )	<i>Baseline</i> ( $\text{cm}^{-1}$ )	<i>Calibration curve</i>	<i>DD</i> (%)
I [52]	1655	1800 - 1600	$DD = 100 - (A_{1655}/A_{3450}) \times 115$	$72,0 \pm 1,0$
	3450	4000 - 2500		
II [42]	1320	1355 - 1270	$A_{1320}/A_{1420} = 0.3822 + 0.03133 (100 - DD)$	$88,4 \pm 0,9$
	1420	1495 - 1405		
III [42]	1320	1355 - 1270	$A_{1320}/A_{3450} = 0.03146 + 0.00226 (100 - DD)$	$73,7 \pm 2,9$
	3450	4000 - 2500		

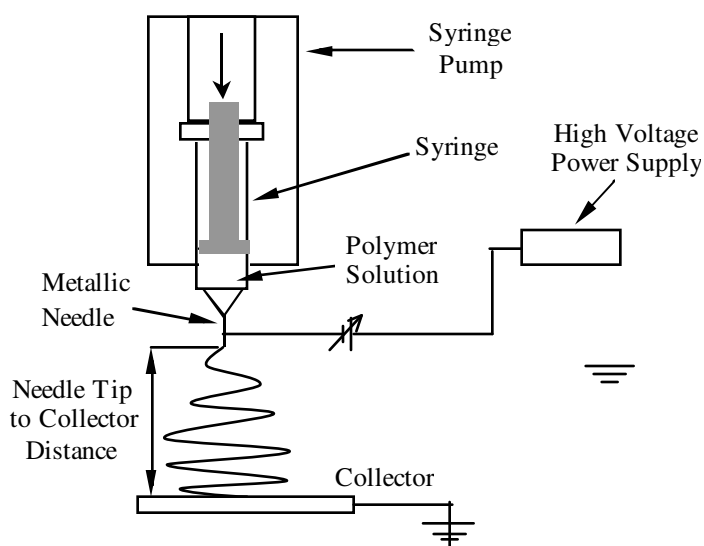
atmospheric moisture from the oven-dried chitosan samples. The water band at this region (-OH stretching) is superimposed with the chitosan concentration reference band ( $3450 \text{ cm}^{-1}$ ), and its intensity is possible to be overestimated. However, the better accuracy of the method II is confirmed in comparison with the results of *DD* determined by  $^1\text{H-NMR}$ , the reference method.

Muzzarelli and Rocchetti [49] firstly propose the use of the 1<sup>st</sup> derivative UV spectrophotometry as a simple and time saving, but accurate and precise method to determine the *DD* of chitosan samples. This method allows its determination for high deacetylated chitosans which can be hardly analyzed by techniques that record the signs of the *N*-acetyl group: when this group is removed by extensive deacetylation processes and the degree of acetylation (*DA*) becomes lower than 20 %, the errors associated with the reading become exceedingly large. Therefore, our group [56] derived a mathematical expression avoiding the use of empiric correction curves for highly deacetylated samples. In this case, the *DA* is determined directly from the mass concentration of chitosan solutions and the first derivative value of its UV spectra at 202 nm (the acetic acid solutions zero crossing point), over the entire range of the *DD* of chitosan. Applying this method, a *DD* of  $87.7 \pm 0.4$  % was determined, which is very similar to the *DD* of purified chitosan determined by means of both  $^1\text{H-NMR}$  and FTIR-method II.

## 2.3. Scaffolds Fabrication

### 2.3.1. Electrospinning

The elements of a basic electrospinning unit include a high voltage power supply (HVPS) with an electrode connected to the needle of a syringe reservoir, that contains the polymeric solution, and a ground metallic collector placed at a defined distance from the tip of the metallic needle (Scheme 2.1).



**Scheme 2.1** - Schematic representation of the electrospinning apparatus (*adapted from reference [3]*)

The electrospinning apparatus developed during the course of this PhD comprises: two semi-commercial HVPS, a syringe pump, a ground collector, a cuboid chamber with a 3D position system and an isolation transformer. The main electrical characteristics of the semi-commercial HVPS are: positive voltage (40 and 12 kV), continuously adjustable voltage, digital indication for the output voltage and current, preset of the output voltage, high voltage control switch and indicator, security interlock and indicator (Figure 2.7 A); a basic single syringe infusion pump (KDS100, KD Scientific) to control the polymeric solution feeding, with flow rates ranging from 0.1  $\mu\text{l/h}$  (when a 10  $\mu\text{l}$  syringe is used) to a maximum of 519 ml/h (when a 60 ml syringe was used) (Figure 2.7 B); and a metallic collector placed perpendicularly to



**Figure 2.7** - Photographs of the components of the electrospinning apparatus: the semi-commercial high voltage power supply (**A**); the single syringe infusion pump (**B**); and a grounded metallic collector located inside the cuboid acrylic structure, with a vertical position holder of the syringe pump(**C**).

the syringe main axis to create the electric field necessary for the electrospinning process to take place (Figure 2.7 C).

To prevent possible safety problems related to the use of solvents needed to dissolve some of the polymers used, the deposition system (needle coupled to a syringe and collector), operates inside a chemical hood to protect the users from the contact with the solvent vapours. Since the air flow generated by the exhaustion of the hood disturbs the normal deposition of the fibers, a “closed” cuboid structure had to be designed and built (Figure 2.7 C). This chamber was enclosed by two covers that allow the user to access the collector, attach or fixate the syringe and program the syringe pump. The covers leave a opening in the top when mounted that allows for solvent evaporation, as well as access to the syringe pump, and exhaustion air to circulate without disturbing the deposition process. The upper part of the chamber is also used as the support of a 3D position system, allowing the user to move it in the  $x$ ,  $y$ ,  $z$  directions, being  $z$  the direction normal to the plane of the collector (parallel to  $x$ ,  $y$ ). Another advantage of this transparent acrylic box is the possibility to couple laterally a system to produce cylindric samples by using a rotating cylinder as collector. The angular velocity of the cylinder is controlled by a small motor. Due to its dielectric properties, acrylic was used to construct the described chamber.

Since electrospinning involves high voltages applied to a metallic needle, an isolation transformer had to be added to the electrospinning setup in order to avoid damaging the electronic equipment. This metallic needle is normally associated to a

basic syringe infusion pump and, therefore, the main power network should be insulated from the HVPS. If the insulation is not effective, electric discharges are not be prevented, eventually, causing damage and/or malfunction of the equipment.

In the electrospinning processing, the polymer solution is placed in a 5 ml plastic syringe with a metallic blunted end needle coupled to it. The tip of the needle has a circular internal diameter of 0.8 mm. All the electrospinning experiments were performed at room temperature, as well as the subsequently drying of the electrospun nanofiber meshes. The main parameter controlling the topography of the nanofiber meshes produced by electrospinning is the architecture of the collector [57]. Considering this statement, different metallic collectors were tested, namely a flat aluminium sheet, a corrugated aluminium sheet, a metallic wire net and a rotating plate.

#### 2.3.1.1. Processing of polycaprolactone nanofiber meshes

To process polycaprolactone nanofiber meshes (PCL NFM), a polymeric solution of 17 % (w/v) PCL is prepared using an organic solvent mixture composed of Chloroform (Aldrich; Germany) and N,N-Dimethylformamide (Aldrich; Germany) (7:3 ratio). This solution was electrospun at 9-10 kV, establishing a needle tip to ground collector distance of 20 cm, a flow rate of 1.0 ml/h and collecting the random nanofiber mesh on a flat aluminium foil or the patterned nanofiber mesh on a metallic wire net. These are the optimized processing conditions of PCL nanofiber meshes, resulting from an optimization procedure where three variables/parameters were systematically studied: voltage, needle tip to ground collector distance and flow rate.

To produce dexamethasone-loaded PCL nanofiber meshes, different quantities (5, 10, 15 and 20 wt.% polymer) of dexamethasone (DEX; Sigma-Aldrich, Germany) were added to the polymeric solution previously prepared, and let to stir until complete dissolution (~ 20 min). The previously optimized processing conditions were also established in this experiment. After being produced, the nanofiber meshes were dried at room temperature during 1 day inside a chemical hood, to allow for complete evaporation of the solvent.

### 2.3.1.2. Processing of dual composition nanofiber meshes

To produce dual composition electrospun nanofiber meshes, a second polymeric solution needs to be prepared: a solution of PEO ( $M_w = 100$  kDa; Sigma-Aldrich, Germany) at the concentration of 25 wt.%, in a mixture of water and ethanol (ratio 6:4). The polymer concentration and the water/ethanol ratio were both defined after several optimization stages to obtain the most stable processing conditions and leading to the more convenient mesh morphology. To achieve the aimed result, a multi-syringe holding system was developed which allows for simultaneous electrospinning of more than one polymeric solution. Two independently controlled semi-commercial HVPS were used to generate electrical voltages ranging from 8 to 20 kV, with the lower values being applied to the PCL solution. In this experiment, the feeding rate was established at a constant value of 0.25 ml/h, by a second precision syringe pump (Aladdin-1000-220B, UK), for both solutions. A conducting plate, connected to the ground, and rotating at a speed of 15 r.p.m. was used as collector to obtain a homogeneous nanofiber mixture. A collector to needle tip distance of 12 cm was defined after an optimization procedure, and the syringes were placed at 9 cm distance to minimize the electrospun jet interference. The process was continued for at least 2 hours for the production of each dual composition nanofiber mesh. With the goal of increasing the porosity of the dual composition nanofibers meshes, the PEO nanofibers were selectively removed by dissolution in distilled water, for a period of 24 hours, at 37 °C. After the dissolution procedure the meshes were dried in an oven at 37 °C.

### 2.3.1.3. Processing of chitosan nanofiber meshes

The electrospinning of chitosan nanofiber meshes (Cht NFM) was successfully achieved by the use of a 6 wt.% chitosan solution prepared as presented in [58], with some modifications. Briefly, the powder purified chitosan was added to a solvents mixture of Trifluoroacetic acid (TFA; Sigma) and Dichloromethane (DC; Aldrich), in a volume ratio of 70:30, respectively. Before electrospinning, the solution was left under stirring overnight at room temperature. The processing of that polymeric solution was

carried out using a corrugated aluminium foil as ground collector. The capillary tip-to-collector distance and the flow rate were fixed in 12 cm and 0.8 ml/h, respectively. The applied voltage was in the range of 15-20 kV. These are the optimized processing conditions of Cht NFM, resulting from an optimization procedure where three variables/parameters were studied: tension, needle tip to ground collector distance and flow rate. Neutralization of the electrospun chitosan nanofibers meshes was carried out by immersing the meshes in either Methanol (Fluka) and Ammonia 7N (Aldrich) aqueous solution (50:50 wt.%) for 7 minutes at room conditions. After the immersion, the meshes were repeatedly washed with distilled water until neutral pH was obtained. The meshes were further let to dry at room temperature.

Before the *in vitro* studies, the random and patterned PCL nanofiber meshes, as well as the DEX-loaded nanofiber meshes, were cut in samples with areas of approximately 1 cm<sup>2</sup> and sterilized by UV irradiation during 1 hour on each side of the mesh. The morphology of the various electrospun nanofiber meshes could be observed at Figure 2.8.

### 2.3.2. Rapid Prototyping

Rapid prototyping has emerged as a set of powerful polymer processing techniques for the production of scaffolds in the tissue engineering area [59, 60]. The appealing characteristic of these techniques, when used for the production of scaffolds, is that a defined structure can be built with customized shapes linked with computer aided design (CAD) which provides more flexibility, versatility, and

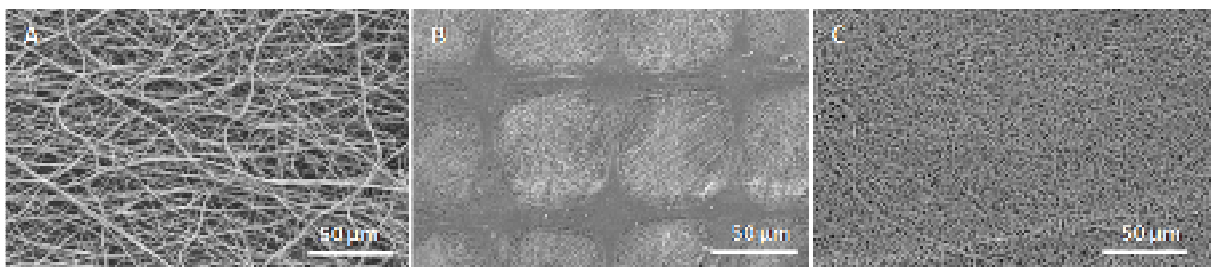


**Figure 2.8** - SEM micrographs showing the morphology of electrospun PCL random (A) and patterned (B) nanofiber meshes, and chitosan (C) nanofiber meshes.

reproducibility in creating scaffolds with precise control of its morphology [59, 61]. Models can be derived from computed tomography scans, magnetic resonance imaging scans or model data created from 3D object digitizing systems. Between the several rapid prototyping systems, based on laser, printing and extrusion technologies (i.e. selective laser sintering, stereolithography, 3D printing, fused deposition modeling (FDM), and 3D plotting), 3D printers and plotters are generally faster, more affordable and easier to use than the others [62]. Herein, a 3D plotting technique (Bio-plotter, EnvisionTec GmbH, Germany) was employed, consisting in the use of a temperature-controlled extruder to force out a thermoplastic filament material and deposit the semi-molten polymer onto a platform in a layer by layer process.

The three-dimensional (3D) rapid prototyping scaffolds (6RP) (Figure 2.9 A) were fabricated using the blend of starch and polycaprolactone (SPCL; Novamont, Italy) previously described. SPCL polymer powder was placed into a metal barrel and heated at 140 °C through a heated cartridge unit and further plotted through a nozzle by air pressure control. The nozzle comprises a stainless steel needle with internal diameter of 0.5 mm and length 6 mm. A metal piston plunger with a Teflon seal was used to apply pressure to the molten polymer. The machine was linked to a CAD software (PrimCam, Germany) which required inputs of dispensing and processing parameters (e.g. speed of the head, dispensing pressure and temperature) and the design parameters of the scaffold (e.g. scaffold dimensions, spacing between the polymer strands, and number of layers). The strand spacing was set to 1 mm, without offsets between the consecutive orthogonal layers. The orientation was changed by plotting the polymer with 90° angle steps between two successive layers. The production of hierarchical fibrous scaffolds (6RP+5NFM) (Figure 2.9 B) was achieved by intercalating PCL nanofiber meshes between every two consecutive layers of plotted microfibers.

The scaffolds (6RP and 6RP+5NFM scaffolds) were all cut into 5x5 mm cubic samples from the originally deposited bulk 20 x 20 mm plates (12 layers) and sterilized using ethylene oxide (EO) before being used for the cell culture assays.

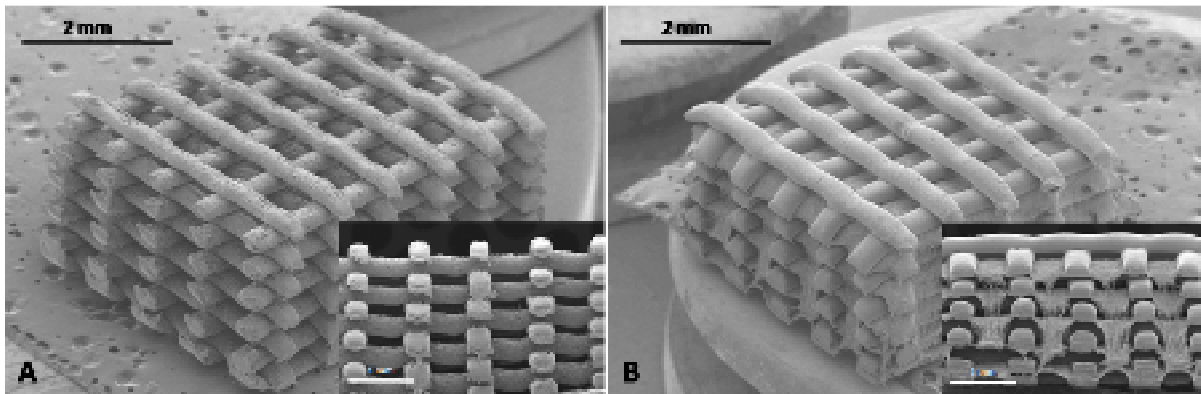


**Figure 2.9** – SEM micrographs of the starch-based rapid prototyped (6RP) (**A**) and hierarchical fibrous scaffolds (6RP+5NFM) (**B**).

### 2.3.3. Melt Fiber Extrusion – Fiber Bonding

The extrusion of a thermoplastic material in powder or in granules involves heating until molten and forced in a continuous flow through a die. The extruder allows melting, mixing and homogenize the melt and pump the material directly to the die, at a steady rate and constant temperature. This is achieved by using a rotating screw inside a barrel, electrically heated by heater bands or elements located around the barrel. The thermoplastic material is also mechanically heated by friction as the screw conveys the material along the barrel. Several commercial and laboratorial extrusion lines are available that enable manufacturing different cross-section extrudates, such as tubing, blown tubular films, monofilament and coating of electrical cables [2]. Even if those devices aim at mixing small amounts of material, they require the availability of tens grams to few kilograms of raw material to allow the production of a sufficient sample. During the development stage of innovative polymer systems with improved performance (e.g. nanocomposites, nanoclays, polymer blends, modified polymers and new compounds), it is desirable to process smaller quantities of some components, either as a result of the synthetic method or due to the high cost of some of the components. In the present work, it was used a vertical, in house-developed miniature extrusion line (Figure 2.10) with three main purposes: (i) possibility of mixing/processing a few grams of material; (ii) capability of producing continuously an extrudate, such as a fiber; (iii) creation of a thermo-mechanical

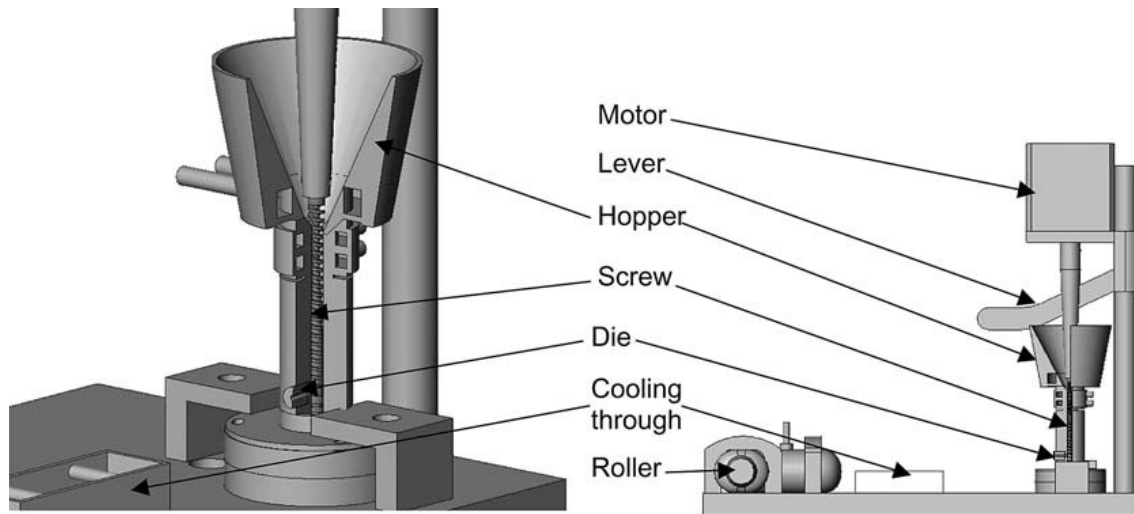


**Figure 2.10** - Design of the micro-extruder (*adapted from reference [2]*)

environment inside the extruder which is as similar as possible to that developed in commercial extruders [2].

The nanofiber reinforced microfibers were produced by melt extrusion of poly(butylene succinate) (PBS) or a particulate composite of PBS/Cht (50:50 wt), compounded with electrospun chitosan nanofiber meshes (0.05 wt.%). Previously, the PBS/Cht composite were compounded in a counter rotating twin-screw extruder (Carvex, Lisbon, Portugal) and milled into a powder using a Retsch mill. The Cht NFMs were added during a further composition step using the micro-extruder previously presented. The processing conditions of the nanofiber reinforced microfibers were: melt temperatures of 115 °C for the PBS-based fibers and 145 °C for the PBS/Cht, a screw rotation speed of 40 r.p.m. and a die diameter of 0.5 mm, as previously optimized and described elsewhere [63, 64]. PBS and PBS/Cht microfibers without nanofiber reinforcements were also processed according to the conditions previously described.

The production of microfibrinous scaffolds reinforced or not with electrospun chitosan nanofiber meshes was achieved by a fiber bonding technique. Basically, a predefined quantity of microfibers (PBS or PBS/Cht), reinforced or not with electrospun chitosan nanofiber meshes, were randomly arrayed in the custom-designed Teflon mold and heated at 120 °C (for PBS-based) or 150 °C (for PBS/Cht-

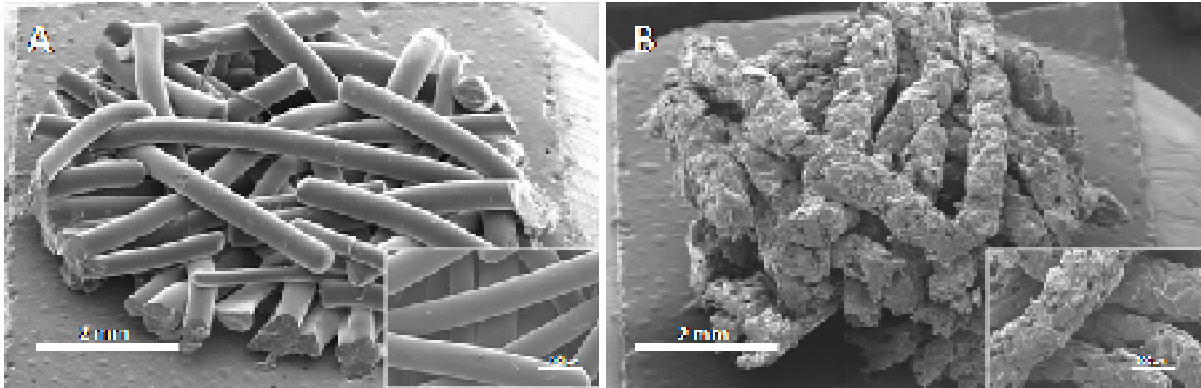


**Figure 2.11** – SEM micrographs of the PBS-based (A) and PBS/Cht-based microfibrous scaffolds (B).

based) during 10 minutes under compression. The morphology of those scaffolds is shown in Figure 2.11. This method helps retain the spatial random arrangement of the fibers so that, when the PBS begins to melt, the fiber structure does not collapse [65]. Besides, fibers at intersections are welded by the combined action of pressure and temperature. The highly porous mesh scaffold with interconnected pores produced by this method enable an efficient diffusion of nutrients and oxygen to the adhered cells. The scaffolds were cut into cylindrical samples (6 mm in diameter and 2 mm in thickness) and sterilized by ethylene oxide before *in vitro* biological assays.

#### 2.4. Modification of PCL Nanofiber Meshes Surface by Plasma Treatment

Modification of biomaterials surface is possible using a plasma treatment [66]. A plasma may be described as a partially ionized gas composed of free radicals, ions, photons and electrons, excited gas atoms and molecules. In general there are two classes of plasma: cold or low temperature plasma and hot or elevated temperature plasma. We will focus on low temperature plasma which is produced by electrical discharge in low-pressure defined gases. The chemical composition and physical characteristics of the plasmas are determined, in addition to the gas used (e.g. Oxygen, Argon, Nitrogen and Water), by the device parameters, such as chamber geometry, gas flow rate, frequency and the electric power applied [67]. This method is used to modify the morphology and chemistry of polymer surfaces to a depth of

several tens of microns, thus leaving the bulk properties practically intact. The mainly physical modification interpreted as etching are the consequence of ion bombardment, while chemical modifications were mainly due to the action of neutral species on the plasma-activated polymer surface. The main effects of the active species created from the gas on the polymer chain is mainly chain scission with new functional group creation and crosslinking. Thus, different surface chemistry or roughness may be obtained with impact in the hydrophilicity.

The PCL nanofiber meshes obtained by electrospinning were modified by plasma treatment. The treatment was performed in a PlasmaPrep 5 reactor (GaLa Instrumente, Germany) with a chamber size of 15 cm of diameter and 31 cm long (volume 5L) and with a fully automated process control. The samples were clamped between both electrodes and the chamber was evacuated. Two different gases (Oxygen or Argon) were used in this study and the chamber, in each case, was filled with the working gas five times prior to the treatment. A radio frequency (RF) source operating at 13.56 MHz was used and the power intensity (either 20 or 30 W) was applied during either 5 or 10 minutes. The pressure of the plasma chamber was kept at 0.2 mbar in all the conditions of the study by controlling the working gas flow. When the higher power level (30 W) and longer treatment time (10 min) were used as working conditions, it was observed an increase of the temperature inside the chamber (reaching a maximum temperature of 35 °C). Prior to the biological assays, the untreated and plasma-modified PCL NFMs were cut in samples with areas of approximately 1 cm<sup>2</sup> and further sterilized by ethylene oxide.

## **2.5. Dexamethasone Kinetic Release Studies**

DEX-loaded PCL nanofiber meshes (with 4 cm<sup>2</sup>) were weighted and suspended in 30 ml of phosphate buffer solution agitated at 60 rpm at 37 °C. Aliquots of 3 ml (10 %) were withdrawn in predetermined time intervals ( and the same volume of fresh medium was added to the suspension. The samples were analysed by UV-Vis spectrophotometry at 242 nm (Shimadzu UV 1601). The DEX concentration of each sample was calculated using a standard curve (concentrations ranging from 0.288 µg/ml to 72 µg/ml), relating the quantity of DEX with the absorbance intensity.

The results presented are an average of three measurements. Calculations of the amount of drug released took into account the replacement of aliquots with fresh medium. Control PCL nanofiber meshes (PCL NFMs) were considered as blanks in the performed quantification.

Ultraviolet-visible spectroscopy or ultraviolet-visible spectrophotometry (UV-Vis or UV/Vis) involves the spectroscopy of photons in the UV-visible region. This means it uses light in the visible and adjacent regions near ultraviolet (UV) and near infrared (NIR) ranges. The absorption in the visible ranges directly affects the colour of the chemicals involved. The method is routinely used in a quantitative way to determine concentrations of an absorbing species in solution, using the Beer-Lambert law. This law states that the absorbance of a solution is directly proportional to the concentration of the absorbing species in the solution and the path length. This can be taken from references (tables of molar extinction coefficients) or, more accurately, determined from a calibration curve.

## **2.6. Scaffolds Characterization**

When a new polymeric structure is developed or a known polymeric structure is physically and/or chemically modified, the surface morphology/topography, architecture and surface chemistry of those structures must be studied. Various techniques are available for those studies, being described the ones that we consider the most effective and extensively used for surface characterization.

### *2.6.1. Physical Characterization*

#### 2.6.1.1. Scanning Electron Microscopy

Scanning electron microscopy (SEM) is a microscopic method extremely valuable in studying the morphology of polymeric materials and structures, along with many other research areas [67]. Its main attributes are that it reveals the 3D topography of the specimen examined at large magnifications and also the details of the structure up to the sub-micron level. For polymeric structures, the highest

magnifications are generally not possible because of the intensity of the electron beams damaging the thin polymeric samples which generally leads to deformation and even melting of the specimen. To overcome this problem, polymeric samples are usually coated with conductive materials such as gold or carbon by sputtering.

The different scaffolds developed during this PhD program were sputter-coated with gold (Fisons Instruments, model SC502; England) for 2 minutes at 15 mA. The samples were further analyzed by Scanning Electron Microscopy (Leica Cambridge, model S360; England). Micrographs were recorded at 15 kV with magnifications ranging from 100 to 5000 times.

The fiber diameter was measured from SEM micrographs with the software *ImageJ* (version 1.38X, Wayne Rasband Nacional Institutes of Health, USA). For each sample, at least 10 micrographs were used (at a 5000X magnification) and, in each micrograph, 15 different fibers were randomly selected. Pore size was also evaluated from SEM micrographs using the *ImageJ* software. The pore size values were obtained from SEM micrographs (magnification of 5000X), in a total of 60 measurements for each of the conditions. The pore size values were obtained by converting the contour of the pore area into a circumference of equivalent perimeter and determined from the circumference an equivalent diameter [68].

#### 2.6.1.2. Interferometric Optical Profilometry

Surface texture is of paramount importance in engineering especially for applications where surfaces come into contact with each other [69]. Most surface texture measurements are made using stylus-based devices in direct contact with the surface where the movement of a probe is monitored as it travels through the surface, scanning it. These instruments are not adequate for measuring the texture of soft materials, as they tend to damage the surface. Non-contacting instruments that rely on optical measurements or current flow are more appropriated methods for obtaining data from these materials, since they do not directly interfere with the surface. Between the different non-contacting methods available, optical profilers are especially useful for assessing the surface roughness of soft materials [69]. Basically, the vertical scanning white light interferometer (WLI) uses a broadband light source

and measures the degree of modulation contrast as a function of path difference, i.e. the height variations across a surface can be determined. Vertical scanning WLI is very versatile and can be used to characterize the surfaces of materials ranging from low reflectivity plastics to high reflectivity mirrors.

The surface topography of the plasma-treated electrospun PCL nanofiber meshes, random and patterned PCL nanofiber meshes was assessed by noncontact profilometry using an interferometer profiler (Wyko-Veeco, model NT1100; USA), in Vertical Scanning Interferometry (VSI) mode, with a vertical resolution of 3 nm. Topographic roughness parameters  $R_a$  (Roughness Average) and  $R_q$  (Root Mean Square (RMS) Roughness) were automatically determined by the WycoVision<sup>®</sup> 32 analytical software, for each sample. These parameters give information regarding the smoothness of a surface and the deviations of the peak heights and the valley depths from the midline, respectively. Each sample was evaluated, at least, at three randomly selected and representative specimen locations.

#### 2.6.1.3. Micro-computed tomography

Microtomography (or micro-computed tomography, micro-computer tomography, X-ray tomographic microscopy, high resolution X-ray tomography), like computed tomography (CT), makes use of a X-ray source to create shadow cross-section images/projections of a 3D object that later can be used to recreate a virtual model without destroying the original object [70]. The term micro is used to indicate that the pixel sizes of the cross-sections are in the micrometer range. In general, there are two types of scanner setups. In one setup, the X-ray source and detector are typically stationary during the scan while the sample/animal rotates, which is the case of the micro-CT used in the present work. The second setup, much more like a clinical CT scanner, is mainly based stationary in space animal/specimen while the X-ray tube and detector rotate around collecting the data. These micro-CT scanners are typically used for imaging small animals (e.g. bone, lung, cardiovascular, tumors or soft tissue), human samples (e.g. skin and bone biopsies), electronic pieces and microdevices, plastic foams and composite materials, wood and paper, microfossils and diamonds, and other studies for which detailed morphology data is desired [71].

Scaffold architecture was analyzed using a desktop micro-CT scanner (SkyScan 1072; Aartselaar, Belgium). Each scaffold type was scanned in high-resolution mode using a pixel size of 12  $\mu\text{m}$  and an integration time of 2 ms. The X-ray source was set at 80 keV of energy and a current of 248  $\mu\text{A}$ . Representative data sets of 150 slices, covering the height of 1.5 x 4 mm, were transformed into binary using a dynamic threshold of 60-255 (gray values) to distinguish between polymer material and the void space. Those operating parameters were maintained for all the samples. For morphometric analysis, including porosity and mean pore size quantification, the sliced 2D tomographic raw images were reconstructed using CT Analyzer software from the micro-CT scanner supplier. 3D virtual models of representative regions in the bulk of the scaffolds was also created, visualized and registered using the image processing software supplied by the manufacture.

#### 2.6.1.4. Differential Scanning Calorimetry

Thermal analysis techniques such as differential scanning calorimetry (DSC) or differential thermal analysis (DTA) allow characterizing the thermal properties of a material and allow calculation of the enthalpy ( $\Delta H$ ) or entropy ( $\Delta S$ ) changes when phase transitions take place [11]. In normal DSC analysis it is assumed that the heat capacity is thermodynamically reversible. However, for a number of transitions such as the glass transition temperature ( $T_g$ ) measurements, the heat capacity may be irreversible. This results in different DSC traces of the same sample obtained by subsequent cooling and reheating. The glass transition temperature ( $T_g$ ) or the temperature of transition of a polymer from the glassy state into the rubbery phase is one important property of amorphous polymers that is measured using the DSC technique. Measurements of melting temperature ( $T_m$ ) and other phase transitions are also conveniently made by this thermal analysis technique. A melting temperature range is observed in all semicrystalline polymers, because of variations in the sizes and perfection of crystallites [72]. The value of  $T_m$  is usually taken as the temperature at which the larger melting crystallites disappear. This parameter depends on the thermal history of the sample since more perfect and larger crystallites are produced by slower crystallization processes in which more time is provided for the

conformational changes needed to fit macromolecular segments into the appropriate crystal pattern and to reach the lower energy states.

Differential Scanning Calorimetry (DSC) experiments were carried out using a DSC Q100 equipment (TA Instruments – ELNOR). The experiments were conducted, under a nitrogen atmosphere, on samples (5-10 mg) packed in aluminum pans. The samples were heated at a constant heating rate of 10 °C/min from room temperature up to 300 °C.

### *2.6.2. Chemical Characterization*

The surface chemistry of a polymeric structure intended for biomedical applications can be searched by a number of methods, mostly based on spectroscopy and surface energetics. In the following section, information about some used techniques is provided.

#### *2.6.2.1. Fourier Transform Infra-red Spectroscopy*

Before the advent of other powerful techniques, the simplest and reliable method for polymer surface chemistry studies was infra-red spectroscopy (with or without attenuated total reflectance (ATR)). This method requires samples with flat or easily deformable surfaces and typically gives the characteristic absorption bands of functional groups with a depth of analysis of 0.1-10  $\mu\text{m}$  into the material [67]. In recent years, the analysis sensitivity of Fourier transform infra-red (FTIR) spectroscopy has been improved, but even then FTIR can neither match the sensitivity of electron spectroscopy for chemical analysis (ESCA) nor can it be so focused on the surface. In the systems with variable composition, the two methods could be applied to complement each other effectively.

FTIR analysis was performed to the DEX-loaded electrospun PCL nanofiber meshes. The samples were powdered, mixed with KBr, and processed into pellets. Spectra were recorded at 48 scans with a resolution of 2  $\text{cm}^{-1}$  (Shimadzu – IR Prestige 21).

### 2.6.2.2. X-ray Photoelectron Spectroscopy

X-ray Photoelectron Spectroscopy (XPS), also called ESCA, is a technique for studying the energy distribution of electrons ejected from a material that has been irradiated with a source of ionized radiation such as X-rays [67]. Although the X-ray beam may penetrate deeply into the sample to produce photoelectrons, most of these electrons lose its energy in numerous inelastic collisions; only the atoms residing in the top few monolayers give rise to undistorted spectra. Therefore, the typical analysis depth in XPS is about 10-200 Å, constituting a surface-sensitive analytical technique. This powerful technique not only provides quantitative information about basic properties such as binding energy, charge, and valence state of the present elements, but also about their oxidation state and chemical identities. The impact of XPS in polymeric surface chemistry characterization has been twofold: it can analyze relatively intractable materials without the need for special sample preparation and it is a surface sensitive technique. Of all the presently available instrumental techniques for surface analysis, XPS is generally regarded as being the most quantitative, the most readily interpretable, and the most informative with regard to chemical information [73].

Analysis of the untreated and plasma modified electrospun nanofiber meshes was performed using an VG Escalab 250 iXL ESCA instrument (VG Scientific; UK), equipped with aluminum Ka<sub>1,2</sub> monochromatized radiation at 1486.92 eV in the X-ray source. Due to the non conductive nature of the samples, it was necessary to use an electron flood gun to minimize the surface charging accumulation. The neutralization of the surface charge was performed by using both a low energy flood gun (electrons in the range of 0 to 14 eV) and an electrically grounded stainless steel screen was placed directly over the sample surface.

The XPS measurements were carried out using monochromatic Al-K $\alpha$  radiation ( $h\nu=1486.92$  eV). Photoelectrons were collected from a takeoff angle of 90° relative to the sample surface. The measurement was performed in a Constant Analyzer Energy mode (CAE) with pass energy of 100 eV for the screening stage and 20 eV pass energy to obtain high resolution spectra.

Charge referencing was carried out by setting the lower binding energy C1s hydrocarbon (CH<sub>x</sub>) peak at 285 eV. The spectra fitting is based on a “Chi-squared” algorithm used to determine the effectiveness of the peak fit. Surface elemental composition was determined using the standard Scofield photoemission cross section.

### 2.6.2.3. Contact Angle measurements

The investigation of surface wettability by means of contact angle determination is of special interest in the characterization of the polymeric surfaces [67]. Contact angle may be geometrically defined as the angle formed by the intersection of two planes at a tangent to the liquid and solid surface at the perimeter of contact between the two phases and the third surrounding phase, typically air or vapor. Contact angle measurements are carried out in various ways of widely differing sensitivity. Typically they are made with a goniometry and a syringe with a flat-tipped needle that is used to apply the solvent droplet on the surface.

The static contact angles were measured at room temperature with a Contact Angle Equipment (DataPhysics Instruments, model OCA 15plus; Germany). The values were obtained by the sessile drop method. The used liquids (water and glycerol, HPLC grade, 3 $\mu$ L) were applied by a motor driven syringe at different zones of each sample and the measurement time was extended until 5 minutes. At least five measurements were carried out for each sample and the presented data are averaged values for those measurements.

## 2.7. Biological assays

### 2.7.1. Cell Lines

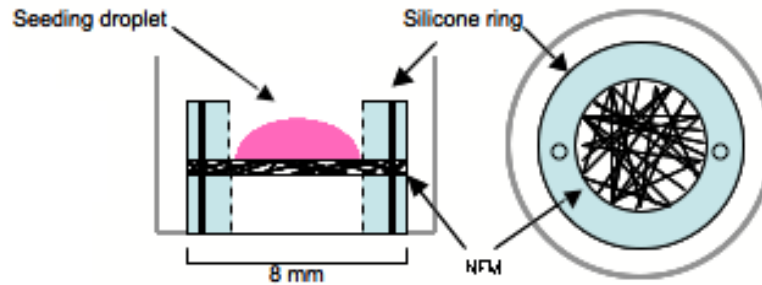
A continuously growing cell line generally is easier to maintain in commercially available media, with low serum dependence, increased growth rate in monolayer or suspension (population doubling time of 12-24 h). The cell lines present a reduced or absent density limitation of proliferation, and produce a higher cell yield per flask

[74]. Those cells are typically immortalized, then presenting the altered on growth control, but with the absence of virus susceptibility and differentiation capacity. Their disadvantages include greater chromosomal instability, divergence from the donor phenotype, and loss of tissue-specific markers. Continuous cell lines have escaped from senescence control, so the generation number becomes less important, as well as the number of passages. In addition, because of the increased cell proliferation rate and saturation density, split ratios become much greater (1:20-1:100). For the maintenance of a stable phenotype it is essential the standardization of culture conditions. Consequently, the maintenance regime (i.e. medium formulation, periodic medium change and subculture) should remain consistent throughout all the period of the cell line culture.

Due to the advantages previously described, three types of cell lines were chosen to verify the efficacy of the plasma modifications performed to the PCL nanofiber meshes: L929, a mouse lung fibroblastic cell line; Saos-2, a human primary osteosarcoma cell line; and ATDC5, a mouse chondrocyte teratocarcinoma-derived cell line, all supplied by the European Collection of Cell Cultures (ECACC; UK). L929 and Saos-2 cells were maintained in Dulbecco's Modified Eagle's Medium (DMEM; Sigma-Aldrich, Germany) supplemented with 10 % heat-inactivated fetal bovine serum (Biochrom AG, Germany) and 1 % antibiotic-antimycotic solution (penicillin 100 units/ml and streptomycin 100 µg/ml) (Gibco, GB). ATDC5 cells were cultured in DMEM-F12 Medium (Gibco, GB) supplemented with 10 % heat-inactivated fetal bovine serum (Biochrom AG; Germany) and 2 mM L-Glutamine (Sigma-Aldrich, Germany). All cell types were cultured in a humidified incubator at 37 °C, in 5 % CO<sub>2</sub> atmosphere. The various media were routinely renewed every 2-3 days.

### *2.7.2. Seeding and Culture of the Cell Lines on the Electrospun Nanofiber Meshes*

The sterile samples of plasma-treated NFMs and controls, PCL solvent-cast membranes, and TCPS coverslips, were placed in 24-well cell culture plates (Costar<sup>®</sup>, Corning; NY). A 50 µl cell suspension containing 1x10<sup>5</sup> cells was added per cm<sup>2</sup> of surface area of each sample and controls. The biological parameters, described below, were assessed at different culture periods: 1, 3, 7, and 14 days.



**Scheme 2.2** - Schematic representation (lateral and top view) of the fixing system used in the biologic assay.

In order to demonstrate the enhanced cellular infiltration into the nanofiber meshes, it was developed a system to clamp the mesh. This system consists of two silicone rings (with 8 mm outside and 5 mm inside diameters), held together with the sample in two points by a nylon stitch (Scheme 2.2). When clamped between the rings, the samples have no direct contact with the surface of the well. This clamping system was sterilized by ethylene oxide, with the meshes already mounted between the rings. The clamping systems containing the dual composition electrospun nanofiber meshes were placed in a 48 well-plate with 1 mL of ultra pure water to dissolve the PEO nanofibers. The well-plate was placed in an incubator at 37 °C for a period of 24 hours. The seeding of Saos-2 cells was performed with 50  $\mu$ L cell suspension ( $1 \times 10^5$  cells/mL) over the top surface of each scaffold. The developed nanofiber mesh fixing system confined the seeding area, avoiding cell adhesion to other surfaces of the culture well.

### 2.7.3. Primary Cultures of Human Bone Marrow Mesenchymal Stem Cells

Mesenchymal stem cells (MSC) are an interesting candidate for cell-based therapeutics and regenerative medicine [75, 76]. While several tissues remain an important source of therapeutic relevant differentiated cells, stem cells have emerged as a strong alternative due to their potential of expansion - self-renewal potential - and the fact that they can be obtained from autologous sources. In fact, the generation of autologous grafts *in vitro*, avoiding the harvest of autologous tissue in a second anatomic location, is one of the goals in tissue engineering. Additionally,

MSCs can be differentiated into a variety of connective tissues, including bone, cartilage, fat, muscle and tendon, when cultured with appropriated supplemented culture media and specific environments [77-79].

Human bone marrow aspirates were obtained during routine surgical procedures involving knee arthroplasties, as approved by the Ethical Committee of the São Marcos Hospital, Braga, under the Cooperation Agreement established between the 3B's Research Group-UM and that Hospital. A detailed Informed Consent (IC) was signed by each patient/donor. Bone marrow contains at least two distinct populations of stem cells, one hematopoietic and the other non-hematopoietic mesenchymal [80]. Hematopoietic stem cells in the adult give rise to all components of the immune and blood system, whereas MSCs can differentiate into bone, cartilage or adipose tissue, among others. Due to feasibility purposes, human bone marrow mesenchymal stem cells (hBMSCs) kindly supplied by Biopredic International (France) were also used in the work. Both populations of hBMSCs were isolated and characterized according to the method established by Delorme and Charbord [81]. Briefly, plastic adherent fractions of marrow cells characterized by a spindle-shape morphology and colony-forming unit (CFU) capacity; expression of surface antigens like CD 29, 73, 90 and 105, while negatives for hematopoietic markers such as CD 34 and 45 (assessed by flow cytometry); and by their differentiation potential into the osteogenic, chondrogenic and adipogenic lineages.

#### *2.7.4. hBMSCs Culture, Seeding and Differentiation into the Osteogenic Lineage*

To reach the needed amount of undifferentiated hBMSCs, they were expanded in 'basal medium' consisting of Dulbecco's modified Eagle's medium (DMEM; Sigma-Aldrich, Germany) supplemented with 10 % heat-inactivated fetal bovine serum (FBS; Biochrom AG, Germany) and 1 % antibiotic/antimycotic solution (Gibco; GB). Cells were cultured at 37 °C in a atmosphere of 5 % CO<sub>2</sub>.

Confluent hBMSCs at passages 4-5 were harvested for static seeding onto the random PCL nanofiber meshes, patterned nanofiber meshes and DEX-loaded nanofiber meshes at a density of  $1.5 \times 10^5$  cells/scaffold, and on nanofiber reinforced or not microfibrinous composite scaffolds at a density of  $5.0 \times 10^5$  cells/scaffold. The

constructs were cultured under static conditions, in standard 'osteogenic differentiation medium' (basal medium supplemented with 50 µg/mL ascorbic acid, 10 mM β-glycerophosphate and 10<sup>-7</sup> M dexamethasone). The constructs were retrieved at different culture times: 7, 14 and 21 days. In the case of DEX-loaded PCL NFMs-hBMSCs constructs, they were cultured under static conditions, in dexamethasone-absent 'osteogenic differentiation medium' (basal medium supplemented with 50 µg/mL ascorbic acid and 10 mM β-glycerophosphate).

The differentiation of MSCs towards the osteogenic lineage is a highly programmed process that is best described *in vitro*. Typically it requires the supplementation of culture media with dexamethasone, β-glycerophosphate and ascorbic acid [75, 82]. Dexamethasone (DEX) is routinely added in assays of osteoprogenitor cells, having both inhibitory and stimulatory effects over skeletal cells. An emerging view is that this reflects opposite effects on precursors versus mature cells in the lineages. It has also been suggested that even a transient exposure of stem cells to DEX may be effective in inducing and maintaining the osteoblastic phenotype [82]. Glycerophosphate is the organic phosphate source, playing an important role in the mineralization process and modulation of osteoblast activities, namely on the alkaline phosphatase (ALP) activity and osteocalcin production. Ascorbic acid (AA, vitamin C) increases cell viability and is a cofactor in the hydroxylation of proline and lysine residues and is therefore necessary for the production of collagen [80]. AA has also been demonstrated to increase ALP activity. Together with β-glycerophosphate, AA was found to be a prerequisite for the formation and mineralization of the extracellular matrix.

#### 2.7.5. Evaluation of Cell Morphology and Distribution

To analyse the level of cell attachment and its morphology, and distribution on the surface of the scaffolds it was used SEM. To achieve those goals it is required the use of methods of fixation or stabilization of the cells on the scaffolds to obtain biological samples in their natural state. Additionally, due to the non-electric conductivity of those samples it is also needed to coat the samples with a conductive material such as gold or carbon. To overcome the limitation in the level of vacuum

required for biological samples and/or the charging of non-conducting samples, a so-called environmental SEM (E-SEM) was developed [83]. This technique requires a higher partial pressure of, e.g. water, keeps the biological structure almost in the native state, making this method a valuable tool for imaging. Accordingly to these statements and the available SEM, the constructs (scaffolds-cells) were fixed with 2.5 % Glutaraldehyde (Sigma, USA) in Phosphate Buffer Saline (Sigma, USA) solution, during 1h at 4 °C. Then, they were dehydrated through graded series of ethanol and let to dry overnight at room temperature. Finally, they were gold or carbon sputter coated (Fisons Instruments, model SC502; England) during 2 minutes at 15 mA, and analyzed by SEM (Leica Cambridge, model S360; England) equipped with an energy dispersive spectrometer (EDS; link-eXL-II).

In parallel to this indirect observation, the constructs were also analyzed by fluorescence microscopy. In this technique, the biological molecules are labeled with a fluorescent marker and detected visually, usually by selecting an appropriated wavelength [83]. One advantage of the fluorescence microscopy is the fact that some dyes quench the fluorescence of another dye by the so-called Förster energy transfer. Another advantage is that the fluorescence wavelength is influenced by the environment; this can also be used to get more insight into the structural properties of a biomolecule. In other fluorescence-based microscopy, specifically in confocal microscopy, a laser beam is split and refocused just on the plane of interest [83]. This reduces one problem of normal fluorescence microscopy where the entire sample is illuminated and both in-focus and out-of-focus points contribute equally to the signal. The resolution reaches 200 nm in the *xy*-plane and 500 nm in the *z*-plane. The greatest advantage is the possibility of making three-dimensional maps of the samples to within a depth of around 100-200  $\mu\text{m}$ . This is particularly relevant to demonstrate the penetration of cells into the thickness of PCL-PEO NFM. For that, PCL-PEO NFM-osteoblastic cells hybrid constructs, as well as the patterned nanofiber meshes-hBMSCs, were firstly fixed in 10 % formalin solution neutral buffer (Sigma-Aldrich, Germany) for 30 min and maintained in phosphate buffer saline (PBS) until further use. The nucleus and the cytoskeleton actin filaments of the cells were fluorescently labelled with 4,6-diamidino-2-phenylindole, diacetate (DAPI; Sigma,

USA; dilution 1:1000) and phalloidintetramethylrhodamine B isothiocyanate (Sigma, USA; dilution 1:100), respectively. Patterned nanofiber meshes-hBMSCs constructs were analyzed using a fluorescence microscope (Zeiss, Germany), whereas the PCL-PEO NFM-osteoblastic cells constructs were observed by laser scanning confocal microscopy (Fluoview 1000, Olympus, Germany). The former samples were excited simultaneously at 345 nm for DAPI and 540/545 nm for Phalloidin. Emission at 458 nm was mapped to the blue channel and 570/573 nm to the red channel. PCL nanofibers were observed in DIC black ground levelling mode.

Alternatively to the previous histological procedure, formalin-fixed nanofiber reinforced or not microfibrinous composite scaffolds-hBMSCs constructs were embedded in Teknovit resin to allow their sectioning (10  $\mu$ m each section). Hematoxylin-Eosin staining was performed to observe the cell morphology and its distribution into the nanofiber reinforced microfibrinous composite scaffolds. Basically, the constructs were stained with Harris Hematoxylin (Merck, Germany) during a suitable time (1-3 minutes), until reaching a desired staining intensity. They were washed in running tap water and afterwards a blue stain enhancement was performed by an immersion in 0.5 % ammonia (Aldrich, Germany), for 5–10 seconds. The constructs were washed again in running tap water, followed by an immersion in alcohol 96 %, and stained in Shandon Eosin-Y (Thermo Scientific, UK) for 30 seconds. They were again washed in alcohol 96 % and dehydrated through two immersions in alcohol 100 %. Before permanent mounting in Histomount™ (National Diagnostics, UK), the stained constructs were immersed in a clearing agent, Histo-Clear® (National Diagnostics, UK) for 1-2 min. Stained sections were observed under an optical microscope (BX61, Olympus Corporation, Germany) and images captured with a digital camera (DP70, Olympus Corporation, Germany).

#### *2.7.6. Cell Viability Assay*

Viability assays were used to measure the proportion of viable cells after a potentially traumatic procedure, such as primary disaggregation, cell separation, or cryostorage [84]. The net increase in the number of cells (i.e., the growth yield) is

labor intensive and time consuming to set up and analyze, particularly when a large number of samples is involved, and the duration of each experiment may be anywhere from 2 to 4 weeks. Instead, a number of alternatives have been devised for assaying cells at higher densities, e.g. in microtitration plates. Indirect measurements of viability are mainly based on its metabolic activity. Indeed, the increase in the number of cells is proportional to the increase in the total amount of protein or DNA, or continued metabolic activity. In these cases, the survival is defined as the retention of metabolic or proliferative ability by the cell population as a whole, some time after removal of the toxic influence.

At each defined culture period, metabolic activity and, consequently, cell viability was determined by a colorimetric assay named CellTiter 96<sup>®</sup> AQueous One Solution Cell Proliferation Assay (Promega; USA). Briefly, this assay is based on the bioreduction of a tetrazolium compound [3-(4,5-dimethylthiazol-2-yl)-5-(3-carboxymethoxyphenyl)-2-(4-sulfofenyl)-2H-tetrazolium, inner salt (MTS)] into a brown formazan product that is soluble in culture medium [85]. This conversion is accomplished by the production of nicotinamide adenine dinucleotide phosphate (NADPH) or nicotinamide adenine dinucleotide (NADH) by the dehydrogenase enzymes existing in the metabolically active cells. The quantity of formazan product bioreduced is directly proportional to the number of living cells in culture, as measured by the amount of 490nm absorbance in a microplate reader (Bio-Tek, model Synergie HT; USA), after 3h of incubation at 37 °C. Three specimens per condition and per time point were characterized.

#### *2.7.7. Cell Proliferation Assay*

Measurements of DNA synthesis are frequently taken to be representative of the amount of cell proliferation [84]. Cell proliferation rate determination is often used to determine the response of cells to a particular stimulus, i.e. physical (e.g. topography of a substrate) or chemical (i.e. toxin or growth/differentiation factor). The most commonly used technique for measuring nucleic acid concentration is the determination of absorbance at 260 nm ( $A_{260}$ ). The major disadvantages of the absorbance method are the large relative contribution of RNA and single-stranded

DNA to the signal, the interference caused by contaminants commonly found in nucleic acid preparations, the inability to distinguish between DNA and RNA, and the relative insensitivity of the assay (an  $A_{260}$  of 0.1 corresponds to a 5  $\mu\text{g/mL}$  double-stranded DNA solution). Alternatively, DNA content may be assayed by several fluorescence methods, including reaction with DAPI, PicoGreen or Hoechst 33258. The fluorescence emission of Hoechst 33258 at 458 nm is increased by interaction of the dye with DNA at pH 7.4 and in high salt to dissociate the chromatin protein [86]. This method gives a sensitivity of 10 ng/mL, but requires intact double-stranded DNA.

In the present work, cell proliferation was quantified by the total amount of double-stranded DNA (dsDNA) using an ultrasensitive fluorescent nucleic acid stain [87], during the culturing periods. To reach that aim, Quant-iT™ PicoGreen® dsDNA reagent was selected since it enables to quantify as little as 25 pg/mL of dsDNA (50 pg dsDNA in a 2 mL assay volume) with a standard spectrofluorometer and fluorescein excitation and emission wavelengths. Additionally, dsDNA can be quantified in the presence of equimolar concentrations of ssDNA and RNA with minimal effect on the quantitative results obtained. The Quant-iT™ PicoGreen dsDNA Assay Kit (Invitrogen™, Molecular Probes™; Oregon, USA) was used according to the manufacturer's instructions. Briefly, cells in the construct were lysed by osmotic and thermal shock and the supernatant used for the DNA quantification assay. A fluorescent dye, PicoGreen, was used because of its high sensitivity and specificity to double-stranded DNA. The fluorescence of the dye was measured at an excitation wavelength of 485/20 nm and at an emission wavelength of 528/20 nm, in a microplate reader (Synergie HT, Bio-Tek; USA). Triplicates were made for each sample and per culturing time. The DNA concentration for each sample was calculated using a standard curve (DNA concentration ranging from 0.0 to 1.5  $\mu\text{g/mL}$ ) relating quantity of DNA and fluorescence intensity.

#### *2.7.8. Alkaline Phosphatase Quantification*

A detailed analysis of the mineralization and of the progression of differentiation can be obtained by biochemical assays. Routine assessments involve the quantification of total calcium content and the activity of alkaline phosphatase

(ALP), a cell surface protein bound to the plasma membrane through phosphatidylinositol phospholipid complexes [80]. High ALP activity is associated with the active formation of mineralized matrix, and highest levels are found in the mineralization front of the bone healing process.

The concentration of ALP was determined for all time culture periods, using the same samples used for DNA quantification. Briefly, the activity of ALP was assessed using the *p*-nitrophenol assay. Nitrophenyl phosphate disodium salt (pnPP; Fluka BioChemika, Austria), which is colourless, is hydrolysed by the alkaline phosphatase produced by the cells at pH 10.5 and temperature of 37 °C, to form free *p*-nitrophenol, which is yellow. The reaction was stopped by the addition of 2M NaOH (Panreac Quimica, Spain) and the absorbance read at 405 nm in a microplate reader (Bio-Tek, Synergie HT; USA). Standards were prepared with 10 µmol/ml *p*-nitrophenol (pNP; Sigma, USA) solution, to obtain a standard curve ranging from 0 to 0.25 µmol/ml). Triplicates of each sample and standard were made, and the ALP concentrations read off directly from the standard curve.

#### *2.7.9. Alizarin Red Staining*

Von Kossa and Alizarin Red are the most used stainings to detect the mineralization process in osteoblasts culture. Both stainings are used to detect the mineralization, but the reactions that generate a positive staining are different. In fact the Von Kossa staining is based on a reaction of the silver nitrate that allows to visualize phosphate and carbonate anions that stain with a black colour, while alizarin red S reacts with calcium and other cations staining red [88]. Von Kossa staining can also react with other type of phosphate or carbonate salts, such as sodium phosphate staining black and generating false positives. Therefore, the Von Kossa stain is not specific for calcium, while alizarin red S reacts specifically with calcium and therefore can be considered a more reliable stain to detect the level of mineralization.

The DEX-loaded nanofiber meshes-hBMSCs constructs were fixed in 10 % formalin solution neutral buffer (Sigma-Aldrich, Germany) for 30 min and maintained in phosphate buffer saline (PBS) until further use. The constructs were then stained with a 2 % Alizarin Red solution (Merk, Germany) in distilled water for 5 min, and

finally washed with distilled water. Stained constructs were observed under an optical microscope (BX61, Olympus Corporation, Germany) and images captured by a digital camera (DP70, Olympus Corporation, Germany).

#### 2.7.10. *Immunodetection of Bone-specific Proteins*

Particularly important in defining the phenotype of the differentiating stem cells is an understanding of bone tissue development in relation to the gene expression of the cells [80]. Consequently, the osteogenic phenotype of hBMSCs seeded onto the random and patterned, and also in dexamethasone-loaded PCL nanofiber meshes was also assessed by the immunodetection of bone-specific proteins. Osteopontin is one of the most abundant noncollagenous proteins in bone; it binds to various extracellular molecules, including type I collagen, fibronectin and osteocalcin, and may add physical strength to the extracellular matrix. Osteocalcin comprises 10-20 % of the noncollagenous proteins in bone, depending on the age and species. Levels of osteocalcin are low at early stages and increase with increasing age. The function of osteocalcin may be to inhibit calcification until the appropriate temporal and spatial conditions are met. Bone sialoprotein (BSP) has been proposed as the main nucleator of hydroxyapatite crystal formation and correlates with the initial phase of matrix deposition [80]. Accordingly, immunocytochemistry was performed following the streptavidin-biotin-peroxidase complex approach (R.T.U. Vectastain<sup>®</sup> Universal Elite<sup>®</sup> ABC kit; Vector Laboratories Inc., Burlingame, CA), using a rabbit polyclonal antibody against osteopontin (Abcam Ltd., Cambridge, UK; dilution 1:1500), a mouse monoclonal antibody against osteocalcin (clone OC4-30, Abcam Ltd., Cambridge, UK; dilution 1:100) and a rabbit polyclonal antibody against bone sialoprotein II (Chemicon<sup>®</sup> International Inc., Germany; dilution 1:2500).

Prior to the immunocytochemistry procedure, constructs were fixed in 10 % formalin solution neutral buffer (Sigma-Aldrich, Germany) for 30 min and maintained in phosphate buffer saline (PBS) until further use. The constructs were firstly treated with 0.3 % hydrogen peroxide in methanol during 30 min to inactivate the endogenous peroxidases. After washing with PBS, the constructs were blocked with 2.5 % normal horse serum for 20 min at room temperature to avoid unspecific

reactions. Primary antibodies were incubated overnight at 4 °C. Negative controls were set in the absence of primary antibodies incubation. After washing in PBS, the samples were incubated for 30 min with biotinylated secondary antibody anti-rabbit/mouse IgG, followed by incubation with streptavidin-peroxidase complex (Elite ABC Reagent). The immune reaction was visualized using DAB as a chromogen (DAB Substrate Reagent from Peroxidase Substrate Kit; Vector Laboratories Inc, Burlingame, CA). The constructs were observed under an optical microscope (BX61, Olympus Corporation, Germany) and images captured by a digital camera (DP70, Olympus Corporation, Germany).

#### 2.7.11. RNA isolation and Real-Time Quantitative Polymerase Chain Reaction

Total RNA from the constructs was extracted using the Trizol<sup>®</sup> (Invitrogen, Life Technologies Inc., UK) method according to the manufacturer's protocol. Briefly, at each culturing time the constructs were washed with PBS, immersed in Trizol and stored at -80 °C until further use. Proteins were removed with chloroform extraction, and the RNA pellets were washed once with isopropyl alcohol and once with 70 % ethanol. The total RNA pellets were reconstituted in Rnase free water (Gibco, Invitrogen, UK). Determination of the RNA concentration for each scaffold replica (triplicates of each scaffold per time point) was performed by microspectrophotometry (NanoDrop ND-1000, USA).

The mRNA expression of the genes encoding important proteins during osteogenic differentiation of hMSCs *in vitro* were not systematically investigated, and results from different studies are frequently contradictory [80]. Besides those genes, two major transcription factors involved in the osteogenic differentiation, namely the core binding factor  $\alpha$  1/runt-related gene (*Cbfa1/Runx2*) and the zinc finger-containing transcription factor *Osterix* (*Osx*), were also investigated in this work. *Cbfa1/Runx2* has been shown to preferentially initiate two steps of the differentiation process, stem cells into preosteoblasts and preosteoblasts into osteoblasts, whereas *Osterix* acts only during the last preosteoblast/osteoblast stage [76, 89]. Recently established real-time quantitative RT-PCR technology has made mRNA analysis more reproducible, precise, and sensitive than conventional RT-PCR, because it allows: (i) measurement

**Table 2.2** - List of primer sets for bone-specific genes

<i>Gene</i>		<i>Primer sequences (5'-3')</i>	<i>T<sub>m</sub> [°C]</i>
<i>ALP</i>	sense	CTCCTCGGAAGACACTCTG	60,0
	antisense	AGACTGCGCCTGGTAGTTG	
<i>OP</i>	sense	GGGGACA AACTGGAGTGAAAA	58,4
	antisense	CCCACAGACCCTTCCAAGTA	
<i>BSP</i>	sense	CAACAGCACAGAGGCAGAAAAC	59,9
	antisense	CCTCGTATTCAACGGTGGTG	
<i>OC</i>	sense	CTGAGAGGAGCAGAACTGG	61,4
	antisense	GGCAGCGAGGTAGTGAAGAG	
<i>Runx2</i>	sense	TTCCAGACCAGCAGCACTC	58,1
	antisense	CAGCGTCAACACCATCATTC	
<i>Osterix</i>	sense	CCCTTTACAAGCACTAATGG	57,1
	antisense	ACACTGGGCAGACAGTCAG	
<i>GAPDH</i>	sense	ACAGTCAGCCGCATCTTCTT	58,4
	antisense	GACAAGCTTCCCGTTCTCAG	

of the amount of amplified product with a quantitative laser-based method and (ii) data collection in the early exponential phase of the PCR reaction, when none of the reagents is rate-limiting.

Reverse transcriptase (RT)-PCR was performed according to the protocol from iScript™ cDNA synthesis kit (BioRad, Hercules, CA, USA). Briefly, a reaction mixture consisting of 1X iScript Reaction Mix, 1 µl iScript Reverse Transcriptase, RNA template (1 µg total RNA from random and patterned nanofiber meshes; 300 ng total RNA from DEX-loaded nanofiber meshes; 150 ng total RNA from *PBS-R* and *PBS* scaffolds, and 1 µg total RNA from *PBS/Cht-R* and *PBS/Cht* scaffolds) and nuclease-free water was prepared, in 20 µl of total volume. The single-strand cDNA synthesis occurred by incubating the complete reaction mixture 5 min at 25 °C, followed by 30 min at 42 °C and terminated by an incubation at 85 °C for 5 min.

Amplification of the target cDNA for real-time PCR quantification were performed according to manufacturer, using 2 µl RT cDNA products, 1 µM each primer (bone-specific primer sets listed in Table 2.2), 1X iQ SYBR Green Supemix (BioRad, Hercules, CA, USA) and nuclease-free water, in a final volume of 25 µL. Forty-four cycles of denaturation (95 °C, 10 s), annealing (temperature dependent on the gene, 30 s) and extension (72 °C, 30 s) were carried out in the gradient thermocycler MiniOpticon real-time PCR detection system (BioRad, Hercules, CA,

USA) for all genes. The transcripts expression data were normalized to the housekeeping gene glyceraldehydes-3-phosphate-dehydrogenase (*GAPDH*) and the relative quantification calculated by the  $\Delta C_T$  method.

## 2.8. Statistical Analysis

Statistical Analysis was performed using the SPSS statistic software (Release 15.0.0 for Windows). Firstly, a Shapiro-Wilk test was used to ascertain about the data normality [90]. The normality is strongly rejected, as observed by the very small  $p$ -value ( $p < 0.001$ ). Therefore, nonparametric tests should be used in further comparisons. A Mann-Whitney  $U$  test was applied to compare two independent samples on one variable [91]. This test was performed to analyze the effect of random and patterned electrospun nanofibrous structures on the hBMSCs'-derived phenotype (i.e. cellular proliferation and ALP quantification) and osteogenic genotype (i.e. relative gene expression) (Chapter 4). Mann-Whitney  $U$  test was also performed to compare the effect of hierarchical fibrous scaffold architecture over cell performance (i.e. cell viability and proliferation, and ALP quantification) (Chapter 5). In another study, to find differences in terms of cell viability and proliferation among PCL NFM and PCL-PEO NFM after PEO dissolution, the Mann-Whitney  $U$  test was also performed (Chapter 7).  $P$  values lower than 0.01 were considered statistically significant in the analysis of the results.

When more than two independent groups of samples are being compared for one variable, a Kruskal-Wallis test [92] was performed. When the Kruskal-Wallis test indicated significant differences between the independent groups, different multiple comparison tests could be performed to find which one or how many are different. The Dunnett's test is a specialized multiple comparison test that allows to compare a single control group (e.g. TCPS or untreated PCL NFM) to all other sample groups [93]. Therefore, those tests were applied to analyze the effect of the various plasma treatments performed on the material hydrophilicity and cellular performance (Chapter 3). Other multiple comparison test, the Tukey test, was applied to find which pairs of nanofibrous-based structures exhibited significant differences [94]. The Tukey multiple comparison procedure is also known as the "honestly significant difference

test" or HSD test. Those tests (i.e. Kruskal-Wallis test followed by the Tukey's HSD test) were performed to compare the morphological properties (i.e. fiber diameter, pore size, roughness parameters and water contact angle) of the PCL NFM, the PCL-PEO NFM and the PCL-PEO NFM after PEO dissolution (Chapter 7); and in studies on the effect of the electrospun nanofibers-reinforced microfibrinous scaffolds (Chapter 6) or the dexamethasone-loaded nanofiber meshes (Chapter 8) over the cell viability, proliferation and differentiation of hBMSCs. *P* values lower than 0.01 were considered statistically significant in all the analysis.

## 2.9. References

1. Varum KM, Anthonsen MW, Grasdalen H, Smidsrod O. Determination of the degree of N-acetylation and the distribution of N-acetyl groups in partially N-deacetylated chitins (chitosans) by high-field n.m.r. spectroscopy. *Carbohydrate Research* 1991; 211(1):17-23.
2. Covas JA, Costa P. A miniature extrusion line for small scale processing studies. *Polymer Testing* 2004; 23(7):763-773.
3. Neves NM, Campos R, Pedro A, Cunha J, Macedo F, Reis RL. Patterning of polymer nanofiber meshes by electrospinning for biomedical applications. *International Journal of Nanomedicine* 2007; 2(3):1-16.
4. Pitt CG, Gratzl MM, Kimmel GL. Aliphatic polyesters II. The degradation of poly (DL-lactide), poly ( $\epsilon$ -caprolactone), and their copolymers in vivo. *Biomaterials* 1981; 2(4):215-220.
5. Tsuji H, Ikada Y. Blends of aliphatic polyesters. II. Hydrolysis of solution-cast blends from poly(L-lactide) and poly ( $\epsilon$ -caprolactone) in phosphate-buffered solution. *Journal of Applied Polymer Science* 1998; 67(3):405-415.
6. Tsuji H, Ikada Y. Blends of aliphatic polyesters. I. Physical properties and morphologies of solution-cast blends from poly(DL-lactide) and poly( $\epsilon$ -caprolactone). *Journal of Applied Polymer Science* 1996;60(13):2367-2375.
7. Bezwada RS, Jamiolkowski DD, Lee IY, Agarwal V, Persivale J, Trenka-Benthin S, *et al.* Monocryl<sup>®</sup> suture, a new ultra-pliable absorbable monofilament suture. *Biomaterials* 1995; 16(15):1141-1148.

8. Darney PD, Monroe SE, Klaisle CM, Alvarado A. Clinical evaluation of the Capronor contraceptive implant: Preliminary report. *American Journal of Obstetrics and Gynecology* 1989; 160(5 II):1292-1295.

9. Allen C, Han J, Yu Y, Maysinger D, Eisenberg A. Polycaprolactone-b-poly(ethylene oxide) copolymer micelles as a delivery vehicle for dihydrotestosterone. *Journal of Controlled Release* 2000; 63(3):275-286.

10. Thompson MS, Vadala TP, Vadala ML, Lin Y, Riffle JS. Synthesis and applications of heterobifunctional poly(ethylene oxide) oligomers. *Polymer* 2008; 49(2):345-373.

11. Nan A, Ghandehari H. Structure, Properties, and Characterization of Polymeric Biomaterials. In: Mahato RI, editor. *Biomaterials for Delivery and Targeting of Proteins and Nucleic Acids*. Boca Raton, Florida: CRC Press, 2005. p. 1-45.

12. Bastioli C, Cerutti A, Guanella I, Romano GC, Tosin M. Physical state and biodegradation behavior of starch-polycaprolactone systems. *Journal of Environmental Polymer Degradation* 1995; 3(2):81-95.

13. Koenig MF, Huang SJ. Biodegradable blends and composites of polycaprolactone and starch derivatives. *Polymer* 1995; 36(9):1877-1882.

14. Vikman M, Hulleman SHD, Van Der Zee M, Myllärinen P, Feil H. Morphology and enzymatic degradation of thermoplastic starch-polycaprolactone blends. *Journal of Applied Polymer Science* 1999; 74(11):2594-2604.

15. Yavuz H, Babaç C. Preparation and Biodegradation of Starch/Polycaprolactone Films. *Journal of Polymers and the Environment* 2003; 11(3):107-113.

16. Gomes ME, Azevedo HS, Moreira AR, Ella V, Kellomaki M, Reis RL. Starch-poly(epsilon-caprolactone) and starch-poly(lactic acid) fibre-mesh scaffolds for bone tissue engineering applications: structure, mechanical properties and degradation behaviour. *Journal of Tissue Engineering and Regenerative Medicine* 2008; 2(5):243-252.

17. Gomes ME, Reis RL, Cunha AM, Blitterswijk CA, de Bruijn JD. Cytocompatibility and response of osteoblastic-like cells to starch-based polymers:

effect of several additives and processing conditions. *Biomaterials* 2001; 22(13):1911-1917.

18. Gomes ME, Sikavitsas VI, Behravesh E, Reis RL, Mikos AG. Effect of flow perfusion on the osteogenic differentiation of bone marrow stromal cells cultured on starch-based three-dimensional scaffolds. *Journal of Biomedical Materials Research A* 2003; 67(1):87-95.

19. Salgado AJ, Coutinho OP, Reis RL. Novel starch-based scaffolds for bone tissue engineering: cytotoxicity, cell culture, and protein expression. *Tissue Engineering* 2004; 10(3-4):465-474.

20. Salgado AJ, Coutinho OP, Reis RL, Davies JE. In vivo response to starch-based scaffolds designed for bone tissue engineering applications. *Journal of Biomedical Materials Research A* 2007; 80(4):983-989.

21. Elvira C, Mano JF, San Román J, Reis RL. Starch-based biodegradable hydrogels with potential biomedical applications as drug delivery systems. *Biomaterials* 2002; 23(9):1955-1966.

22. Balmayor ER, Tuzlakoglu K, Marques AP, Azevedo HS, Reis RL. A novel enzymatically-mediated drug delivery carrier for bone tissue engineering applications: Combining biodegradable starch-based microparticles and differentiation agents. *Journal of Materials Science: Materials in Medicine* 2008; 19(4):1617-1623.

23. Marques AP, Reis RL, Hunt JA. An in vivo study of the host response to starch-based polymers and composites subcutaneously implanted in rats. *Macromolecular Bioscience* 2005; 5(8):775-785.

24. Mano JF, Koniarova D, Reis RL. Thermal properties of thermoplastic starch/synthetic polymer blends with potential biomedical applicability. *Journal of Materials Science: Materials in Medicine* 2003; 14(2):127-135.

25. Wang Y, Rodriguez-Perez MA, Reis RL, Mano JF. Thermal and thermomechanical behaviour of polycaprolactone and starch/polycaprolactone blends for biomedical applications. *Macromolecular Materials and Engineering* 2005; 290(8):792-801.

26. Alves NM, Saiz-Arroyo C, Rodriguez-Perez MA, Reis RL, Mano JF. Microhardness of starch based biomaterials in simulated physiological conditions. *Acta Biomaterialia* 2007; 3(1):69-76.
27. Fujimaki T. Processability and properties of aliphatic polyesters, 'BIONOLLE', synthesized by polycondensation reaction. *Polymer Degradation and Stability* 1998; 59(1-3):209-214.
28. Correlo VM, Pinho ED, Pashkuleva I, Bhattacharya M, Neves NM, Reis RL. Water absorption and degradation characteristics of chitosan-based polyesters and hydroxyapatite composites. *Macromolecular Bioscience* 2007; 7(3):354-363.
29. Correlo VM, Boesel LF, Pinho E, Costa-Pinto AR, Alves Da Silva ML, Bhattacharya M, *et al.* Melt-based compression-molded scaffolds from chitosan-polyester blends and composites: Morphology and mechanical properties. *Journal of Biomedical Materials Research - Part A* 2009; 91(2):489-504.
30. Rinaudo M. Chitin and chitosan: Properties and applications. *Progress in Polymer Science* 2006; 31(7):603-632.
31. Prabakaran M, Mano JF. Chitosan-based particles as controlled drug delivery systems. *Drug Delivery: Journal of Delivery and Targeting of Therapeutic Agents* 2005; 12(1):41-57.
32. Kumar MNVR, Muzzarelli RAA, Muzzarelli C, Sashiwa H, Domb AJ. Chitosan chemistry and pharmaceutical perspectives. *Chemical Reviews* 2004; 104(12):6017-6084.
33. Janes KA, Calvo P, Alonso MJ. Polysaccharide colloidal particles as delivery systems for macromolecules. *Advanced Drug Delivery Reviews* 2001; 47(1):83-97.
34. Felt O, Buri P, Gurny R. Chitosan: A unique polysaccharide for drug delivery. *Drug Development and Industrial Pharmacy* 1998; 24(11):979-993.
35. Muzzarelli RAA. Chitins and chitosans for the repair of wounded skin, nerve, cartilage and bone. *Carbohydrate Polymers* 2009; 76(2):167-182.
36. Muzzarelli RAA, Muzzarelli C. Chitosan chemistry: Relevance to the biomedical sciences. *Advances in Polymer Science*, 2005; 186:151-209.

37. Francis Suh JK, Matthew HWT. Application of chitosan-based polysaccharide biomaterials in cartilage tissue engineering: A review. *Biomaterials* 2000; 21(24):2589-2598.

38. Di Martino A, Sittinger M, Risbud MV. Chitosan: A versatile biopolymer for orthopaedic tissue-engineering. *Biomaterials* 2005; 26(30):5983-5990.

39. Roberts GAF, Domszy JG. Determination of the viscometric constants for chitosan. *International Journal of Biological Macromolecules* 1982; 4(6):374-377.

40. Huggins ML. The viscosity of dilute solutions of long-chain molecules. IV. Dependence on concentration. *Journal of the American Chemical Society* 1942; 64(11):2716-2718.

41. Kraemer EO, Lansing WD. The molecular weights of cellulose and cellulose derivatives. *Journal of Physical Chemistry* 1935; 39(1):153-168.

42. Delpach MC, Oliveira CMF. Viscometric study of poly(methyl methacrylate-g-propylene oxide) and respective homopolymers. *Polymer Testing* 2005; 24(3):381-386.

43. Terbojevich M, Cosani A, Muzzarelli RAA. Molecular parameters of chitosans depolymerized with the aid of papain. *Carbohydrate Polymers* 1996; 29(1):63-68.

44. Van De Velde K, Kiekens P. Structure analysis and degree of substitution of chitin, chitosan and dibutylchitin by FT-IR spectroscopy and solid state  $^{13}\text{C}$ -NMR. *Carbohydrate Polymers* 2004; 58(4):409-416.

45. Duarte ML, Ferreira MC, Marvalhoo MR, Rocha J. An optimised method to determine the degree of acetylation of chitin and chitosan by FTIR spectroscopy. *International Journal of Biological Macromolecules* 2002; 31(1-3):1-8.

46. Brugnerotto J, Lizardi J, Goycoolea FM, Argaelles-Monal W, Desbriares J, Rinaudo M. An infrared investigation in relation with chitin and chitosan characterization. *Polymer* 2001; 42(8):3569-3580.

47. Jiang X, Chen L, Zhong W. A new linear potentiometric titration method for the determination of deacetylation degree of chitosan. *Carbohydrate Polymers* 2003; 54(4):457-463.

48. Raymond L, Morin FG, Marchessault RH. Degree of deacetylation of chitosan using conductometric titration and solid-state NMR. *Carbohydrate Research* 1993; 246:331-336.
49. Muzzarelli RAA, Rocchetti R. Determination of the degree of acetylation of chitosans by first derivative ultraviolet spectrophotometry. *Carbohydrate Polymers* 1985; 5(6):461-472.
50. Liu D, Wei Y, Yao P, Jiang L. Determination of the degree of acetylation of chitosan by UV spectrophotometry using dual standards. *Carbohydrate Research* 2006; 341(6):782-785.
51. Tan SC, Khor E, Tan TK, Wong SM. The degree of deacetylation of chitosan: Advocating the first derivative UV-spectrophotometry method of determination. *Talanta* 1998; 45(4):713-719.
52. Prochazkova S, Varum KM, Ostgaard K. Quantitative determination of chitosans by ninhydrin. *Carbohydrate Polymers* 1999; 38(2):115-122.
53. Hirai A, Odani H, Nakajima A. Determination of degree of deacetylation of chitosan by  $^1\text{H}$  NMR spectroscopy. *Polymer Bulletin* 1991; 26(1):87-94.
54. Lavertu M, Xia Z, Serreji AN, Berrada M, Rodrigues A, Wang D, *et al.* A validated  $^1\text{H}$  NMR method for the determination of the degree of deacetylation of chitosan. *Journal of Pharmaceutical and Biomedical Analysis* 2003; 32(6):1149-1158.
55. Baxter A, Dillon M, Taylor KDA, Roberts GAF. Improved method for i.r. determination of the degree of N-acetylation of chitosan. *International Journal of Biological Macromolecules* 1992; 14(3):166-169.
56. Da Silva RMP, Mano JF, Reis RL. Straightforward determination of the degree of N-acetylation of chitosan by means of first-derivative UV spectrophotometry. *Macromolecular Chemistry and Physics* 2008; 209(14):1463-1473.
57. Li D, Wang YL, Xia YN. Electrospinning of polymeric and ceramic nanofibers as uniaxially aligned arrays. *Nano Lett* 2003; 3(8):1167-1171.
58. Ohkawa K, Cha DI, Kim H, Nishida A, Yamamoto H. Electrospinning of chitosan. *Macromol Rapid Comm* 2004; 25(18):1600-1605.

59. Peltola SM, Melchels FP, Grijpma DW, Kellomaki M. A review of rapid prototyping techniques for tissue engineering purposes. *Annals of Medicine* 2008; 40(4):268-280.

60. Yeong WY, Chua CK, Leong KF, Chandrasekaran M. Rapid prototyping in tissue engineering: challenges and potential. *Trends in Biotechnology* 2004; 22(12):643-652.

61. Landers R, Pfister A, Hubner U, John H, Schmelzeisen R, Mulhaupt R. Fabrication of soft tissue engineering scaffolds by means of rapid prototyping techniques. *Journal of Materials Science* 2002; 37(15):3107-3116.

62. Pfister A, Landers R, Laib A, Hubner U, Schmelzeisen R, Mulhaupt R. Biofunctional rapid prototyping for tissue-engineering applications: 3D bioplotting versus 3D printing. *Journal of Polymer Science, Part A: Polymer Chemistry* 2004; 42(3):624-638.

63. Pinho ED, Martins A, Araujo JV, Reis RL, Neves NM. Degradable particulate composite reinforced with nanofibres for biomedical applications. *Acta Biomaterialia* 2009; 5:1104-1114.

64. Pinho ED, Martins A, Araujo JV, Reis RL, Neves NM. Size also matters in biodegradable composite microfibre reinforced by chitosan nanofibres. Submitted, 2009.

65. Mikos AG, Temenoff JS. Formation of highly porous biodegradable scaffolds for tissue engineering. *Electronic Journal of Biotechnology* 2000; 3(2):114-119.

66. Tavakoli M. Surface modification of polymers to enhance biocompatibility. In: Vadgama P, editor. *Surface and interfaces for biomaterials*. Cambridge and Boca Raton: Woodhead Publishing Limited and CRC Press LLC, 2005. p. 723-725.

67. Hasirci V, Hasirci N. Control of polymeric biomaterial surfaces. In: Vadgama P, editor. *Surface and interfaces for biomaterials*. Cambridge and Boca Raton: Woodhead Publishing Limited and CRC Press LLC, 2005. p. 29-59.

68. She FH, Tung, K. L., Kong, L. X. Calculation of Effective Pore Diameters in Porous Filtration Membranes with Image Analysis. *Robotics and Computer-Integrated Manufacturing* 2008; 24:427-434.

69. Tomlins PE, Leach R, Vadgama P, Mikhalovsky S, James S. On the topographical characterisation of biomaterial surfaces. In: Vadgama P, editor. Surface and interfaces for biomaterials. Cambridge and Boca Raton: Woodhead Publishing Limited and CRC Press LLC, 2005. p. 693-716.

70. Ho ST, Hutmacher DW. A comparison of micro CT with other techniques used in the characterization of scaffolds. *Biomaterials* 2006; 27(8):1362-1376.

71. Ritman EL. Micro-computed tomography - Current status and developments. *Annual Review of Biomedical Engineering*, 2004. p. 185-208.

72. Rudin A. Mechanical Properties of Polymer Solids and Liquids. In: Rudin A, editor. *Elements of Polymer Science and Engineering*: Elsevier Science & Technology Book, 1998. p. 377-443.

73. Iwasaki Y, Nakabayashi N. Interaction between biomaterials and cell tissues. In: Vadgama P, editor. Surface and interfaces for biomaterials. Cambridge and Boca Raton: Woodhead Publishing Limited and CRC Press LLC, 2005. p. 389-413.

74. Freshney RI. Subculture and Cell Lines. In: Freshney RI, editor. *Culture of Animal Cells: A Manual of Basic Technique*. Fifth ed: John Wiley & Sons, Inc., 2005. p. 199-216.

75. Salgado AJ, Oliveira JT, Pedro AJ, Reis RL. Adult stem cells in bone and cartilage tissue engineering. *Current Stem Cells Research & Therapy* 2006; 1(3):345-364.

76. Satija NK, Gurudutta GU, Sharma S, Afrin F, Gupta P, Verma YK, *et al.* Mesenchymal stem cells: molecular targets for tissue engineering. *Stem Cells and Development* 2007; 16(1):7-23.

77. Jiang YH, Jahagirdar BN, Reinhardt RL, Schwartz RE, Keene CD, Ortiz-Gonzalez XR, *et al.* Pluripotency of mesenchymal stem cells derived from adult marrow. *Nature* 2002; 418(6893):41-49.

78. Bianco P, Riminucci M, Gronthos S, Robey PG. Bone marrow stromal stem cells: Nature, biology, and potential applications. *Stem Cells* 2001; 19(3):180-192.

79. Pittenger MF, Mackay AM, Beck SC, Jaiswal RK, Douglas R, Mosca JD, *et al.* Multilineage potential of adult human mesenchymal stem cells. *Science* 1999; 284(5411):143-147.

80. Hofmann S, Kaplan D, Vunjak-Novakovic G, Meinel L. Tissue Engineering of Bone. In: Vunjak-Novakovic G, Freshney RI, editors. *Culture of Cells for Tissue Engineering*. New Jersey: John Wiley & Sons, Inc., 2006. p. 323-373.

81. Delome B, Charbord P. Culture and characterization of human bone marrow mesenchymal stem cells. *Methods in Molecular Medicine* 2007; 140:67-81.

82. Jaiswal N, Haynesworth SE, Caplan AI, Bruder SP. Osteogenic differentiation of purified, culture-expanded human mesenchymal stem cells in vitro. *Journal of Cellular Biochemistry* 1997; 64(2):295-312.

83. Ziegler C. Surface microscopies. In: Vadgama P, editor. *Surface and interfaces for biomaterials*. Cambridge and Boca Raton: Woodhead Publishing Limited and CRC Press LLC, 2005. p. 200-224.

84. Freshney RI. Cytotoxicity. In: Freshney RI, editor. *Culture of Animal Cells: A Manual of Basic Technique*. Fifth ed: John Wiley & Sons, Inc., 2005. p. 359-373.

85. Cory AH, Owen TC, Barltrop JA, Cory JG. Use of an aqueous soluble tetrazolium/formazan assay for cell growth assays in culture. *Cancer Communications* 1991; 3(7):207-212.

86. Labarca C, Paigen K. A simple, rapid, and sensitive DNA assay procedure. *Analytical Biochemistry* 1980; 102(2):344-352.

87. Chadwick RB, Conrad MP, McGinnis MD, Johnston-Dow L, Spurgeon SL, Kronick MN. Heterozygote and mutation detection by direct automated fluorescent DNA sequencing using a mutant Taq DNA polymerase. *BioTechniques* 1996; 20(4):676-683.

88. Puchtler H, Meloan SN, Terry MS. On the history and mechanism of alizarin and alizarin red S stains for calcium. *Journal of Histochemistry and Cytochemistry* 1969; 17(2):110-124.

89. Nakashima K, de Crombrughe B. Transcriptional mechanisms in osteoblast differentiation and bone formation. *Trends in Genetics* 2003; 19(8):458-466.

90. Shapiro SS, Wilk MB. An analysis of variance test for normality (complete samples). *Biometrika* 1965; 52(3-4):591-611.

91. Mann HB, Whitney DR. On a test of whether one of two random variables is stochastically larger than the other. *Annals of Mathematical Statistics* 1947; 18:50–60.

92. Kruskal WH, Wallis WA. Use of ranks on one-criterion variance analysis. *Journal of the American Statistical Association* 1952; 47:583–621.

93. Dunnett CW. New tables for multiple comparisons with a control. *Biometrics* 1964; 20:482–491.

94. Tukey JW. The problem of multiple comparisons. Unpublished manuscript. In: *The Collected Works of John W. Tukey VIII. Multiple Comparisons: 1948-1983*. New York: Chapman and Hall, 1953. p. 1-300

## **Section III**

### **ENHANCING THE FUNCTIONALITY OF ELECTROSPUN NANOFIBER MESHES**



## Chapter 3

### Surface Modification of Electrospun Polycaprolactone Nanofiber Meshes by Plasma Treatment to Enhance Biological Performance

This chapter is based on the following publication: Martins A, Pinho ED, Faria S, Pashkuleva I, Marques AP, Reis RL, Neves NM. *Surface Modification of Electrospun Polycaprolactone Nanofiber Meshes by Plasma Treatment to Enhance Biological Performance*. Small 2009; 5(10):1195-1206.

### **3.1. Abstract**

A critical aspect in the development of biomaterials is the optimization of their surface properties to achieve an adequate cell response. In the present work, electrospun polycaprolactone nanofiber meshes (NFMs) are treated by radio-frequency (RF) plasma using different gases (Ar or O<sub>2</sub>), power (20 or 30 W) and exposure time (5 or 10 min). Morphological and roughness analyses showed topographical changes on the plasma-treated NFMs. X-ray Photoelectron Spectroscopy (XPS) results indicate an increment of the oxygen-containing groups, mainly -OH and -C=O, at the plasma-treated surfaces. Accordingly, the glycerol contact angle results demonstrate a decrease in the hydrophobicity of plasma-treated meshes, particularly in the O<sub>2</sub>-treated ones.

Three model cell lines (fibroblasts, chondrocytes and osteoblasts) are used to study the effect of plasma treatments over the morphology, cell adhesion and proliferation. A plasma treatment with O<sub>2</sub> and one with Ar are found to be the most successful for all the studied cell types. The influence of hydrophilicity and roughness of those NFMs on their biological performance is discussed. Despite the often claimed morphological similarity of NFMs to natural extracellular matrixes, their surface properties contribute substantially to the cellular performance and therefore those should be optimized.

### **3.2. Introduction**

Biomaterials can be used to tailor the biophysical and biochemical milieus that direct cellular behavior and function into the desired regeneration of tissues [1]. Thus, they may play a significant role in the modern strategies of regenerative medicine and tissue engineering. A number of naturally derived polymers, such as collagen, gelatine, albumin, chitosan and starch have already shown to have properties relevant to many biomedical applications [2]. However, biodegradable polymers belonging to the aliphatic polyester family currently represent the most attractive group of polymers that meet various medical and physical demands for safe clinical

applications [3]. This is mainly due to their biocompatibility, acceptable degradation rates and versatility regarding physical and chemical properties [4]. Undoubtedly, three of the most significant members of the aliphatic polyester family are the polyglycolide (PGA), polylactide (PLA) and the poly- $\epsilon$ -caprolactone (PCL). Among them, PCL is the most hydrophobic and degrades by hydrolysis of its ester bonds under physiological conditions at a much slower rate than PGA and PLA [5]. It has been shown that PCL is biocompatible for some applications [4, 6-8] and it has exceptional ability to form compatible blends and copolymers with a wide range of other polymers, resulting in materials with unique ranges of properties [5, 9].

Much attention has been also devoted to the electrospinning technique as an innovative processing method for biodegradable polymers [10-13]. It is a versatile technique allowing for the production of polymeric ultrafine fibers with diameters ranging from few microns down to tens of nanometers [13, 14]. Besides the dimensional reduction to the nano-level, the ability of this technique to shape materials with morphology mimicking the extracellular matrix (ECM) of many tissues in the body, is relevant to control cell affinity and adhesion [12, 15, 16]. The cell behavior on nano-structured surface materials has been extensively studied [15-22]. Indeed, an enhanced cell attachment and proliferation was observed on nano-structured surfaces in comparison to the micro-structured surfaces [23].

An ideal biomaterial should have adequate bulk properties, while the surface should have enhanced affinity with cells. As it is very difficult to design biomaterials combining bulk properties and surface properties, a common approach is to produce biomaterials with adequate bulk properties followed by a surface modification to enhance the surface properties. The surface modification of a biomaterial can be achieved by various techniques, including treatments by flame, corona discharge, plasma, photons, electron beam, ion beam, X-ray, and  $\gamma$ -ray [24, 25]. In the present study, plasma treatment was the selected process to modify the surfaces of electrospun PCL nanofiber meshes (NFMs). Plasma treatment is a versatile and effective method for modifying the surface properties or introducing desired chemical groups at the surface of a material without affecting its bulk properties [24, 26-28]. The most apparent effects of plasma treatment are surface cleaning, microetching

and surface activation (attachment of chemical groups, modification of surface charge, increased the surface free energy) [27, 28]. A common application of this technique is to improve the surface hydrophilicity by forming oxygen-containing groups at the surface of the materials [29-31]. In recent years, plasma surface modifications have been used very intensively in the field of biomedical materials research [24, 26-28]. Typical examples of plasma-modified polymers used for cell culture experiments are Primaria® and tissue culture polystyrene (TCPS). Both types of polymer surfaces induce good cell adhesion in vitro, but are not able to fulfill the requirements for a prosthetic implant material [32].

The aim of the present study was to produce electrospun PCL NFMs and modify their surface in order to improve the adhesion and proliferation of cells. Untreated and plasma modified NFMs were characterized using various surface-sensitive techniques, namely scanning electron microscopy (SEM), interferometric optical profilometry, contact angle measurement and X-ray photoelectron spectroscopy (XPS). These techniques enable the evaluation of changes in surface topography, hydrophilicity, and surface chemistry, as a result of the treatment. Different assays were used to characterize the effects of the plasma treatments over fibroblast, chondrocyte, and osteoblastic cell lines when seeded on the plasma-treated and untreated PCL NFMs. The biological relevance of each plasma treatment was assessed, analyzing the cell attachment, morphology, viability, and proliferation. To the best of our knowledge, this is the first systematic study where different plasma treatment conditions for electrospun biodegradable NFM modification was reported with respect to the performance of different cell types, and aiming at the regeneration of different tissues.

### **3.3. Materials & Methods**

#### *3.3.1. Electrospinning process*

A polymeric solution of 17 % w/v PCL (TONE™, Union Carbide Chemicals and Plastics Division; New Jersey) was prepared using an organic solvent mixture composed of Chloroform (Aldrich; Germany) and N,N-Dimethylformamide (Aldrich)

(7:3 ratio). The solution was electrospun at 9-10 kV, a needle-to-ground collector distance of 20 cm, and a flow rate of 1.0 ml/h. The nonwoven fibrous meshes were collected on a flat aluminium foil and the solvent evaporation was performed at room temperature during at least 2 days.

### *3.3.2. Surface Modification by Plasma Treatment*

The PCL NFMs obtained by electrospinning were modified by plasma treatment. The treatment was performed in a PlasmaPrep 5 reactor (GaLa Instrumente, Germany) with a chamber size of 15 cm diameter and 31 cm length (volume 5 L) and with fully automated process control. The samples were clamped between both electrodes and the chamber was evacuated. Two different gases (O<sub>2</sub> or Ar) were used and the chamber was filled with the working gas five times prior to the treatment. A radio frequency (RF) source operating at 13.56 MHz was used and the power intensity (20 or 30 W) was applied for either 5 or 10 min. The pressure of the plasma chamber was kept at 0.2 mbar in all conditions by controlling the working gas flow. When the higher power level (30 W) and longer treatment time (10 min) were used as working conditions, an increase of the temperature inside the chamber ( $\approx 35$  °C).

### *3.3.3. Surface Characterization of Untreated and Plasma-Treated PCL Nanofiber Meshes*

#### *3.3.3.1. Scanning Electron Microscopy*

Untreated and plasma-treated electrospun PCL NFMs were sputter-coated with gold (Fisons Instruments, model SC502; England) for 2 min at 15 mA. The samples were further analyzed by SEM (Leica Cambridge, model S360; England).

#### *3.3.3.2. Interferometric Optical Profilometry*

The surface topography of the untreated and plasma-treated electrospun PCL NFMs was assessed by noncontact profilometry using an interferometer profiler

(Wyko-Veeco, model NT1100; USA) equipped with the WycoVision<sup>®</sup> 32 analytical software. Topographic roughness parameters average roughness ( $R_a$ ) and root mean square (RMS) roughness ( $R_q$ ) were both determined for each sample. Each sample was evaluated, at least, at two randomly selected and representative specimen locations.

### 3.3.3.3. Contact Angle Measurements

The static contact angles were measured at room temperature with a Contact Angle Equipment (DataPhysics Instruments, model OCA 15plus; Germany). The values were obtained by the sessile drop method. The used liquids (water and glycerol, HPLC grade, 3 $\mu$ L) were applied by a motor driven syringe at different zones of each sample and the measurement time was extended until 5 min. At least five measurements were carried out for each sample and the presented data are averaged values for those measurements.

### 3.3.3.4. X-ray Photoelectron Spectroscopy

Analysis of the untreated and plasma-modified electrospun NFMs was performed using an VG Escalab 250 iXL ESCA instrument (VG Scientific; UK), equipped with Al-K $\alpha$  1,2 monochromatized radiation at 1486.92 eV in the X-ray source. Due to the non conductive nature of the samples, it was necessary to use an electron flood gun to minimize the surface charging accumulation. The neutralization of the surface charge was performed by using both a low energy flood gun (electrons in the range of 0.00-14.00 eV) and an electrically grounded stainless steel screen was placed directly at the sample surface.

The XPS measurements were carried out using monochromatic Al-K $\alpha$  radiation ( $h\nu=1486.92$  eV). Photoelectrons were collected from a takeoff angle of 90 $^\circ$  relative to the sample surface. The measurement was performed in a constant analyzer energy mode (CAE) with 100.00 eV pass energy for the screening stage and 20.00 eV pass energy to obtain high resolution spectra.

Charge referencing was carried out by setting the lower binding energy C1s hydrocarbon (CH<sub>x</sub>) peak at 285.00 eV. The spectra fitting is based on a  $\chi$ -squared algorithm used to determine the effectiveness of the peak fit. Surface elemental composition was determined using the standard Scofield photoemission cross section.

### 3.3.4. *Biological Assays*

#### 3.3.4.1. Cell Lines

Three types of cell lines were used: L929, a mouse lung fibroblastic cell line; the Saos-2, a Human primary osteosarcoma cell line; and the ATDC5, a mouse chondrocyte teratocarcinoma-derived cell line, all supplied by European Collection of Cell Cultures (ECACC; UK). L929 and Saos-2 cells were maintained in Dulbecco's Modified Eagle's Medium (DMEM) (Sigma-Aldrich; Germany) supplemented with 10 % heat-inactivated fetal bovine serum (Biochrom AG; Germany) and 1 % antibiotic-antimycotic solution (Gibco; GB). ATDC5 cells were cultured in DMEM-F12 (Gibco; GB) supplemented with 10 % heat-inactivated fetal bovine serum (Biochrom AG; Germany) and 2 mM L-Glutamine (Sigma-Aldrich). All cell types were cultured in a humidified incubator at 37 °C, in 5 % CO<sub>2</sub> atmosphere. The media were routinely replaced every 2-3 days.

#### 3.3.4.2. Cell Seeding

Prior to the biological assays, the untreated and plasma-modified PCL NFMs were sterilized by ethylene oxide. The sterile samples of NFMs and controls, PCL solvent-cast membranes, and TCPS coverslips, were placed in 24-well cell culture plates (Costar<sup>®</sup>, Coming; NY). A 50  $\mu$ L cell suspension containing  $1 \times 10^5$  cells was added to each cm<sup>2</sup> of each sample and controls. The biological parameters were assessed at different culture periods: 1, 3, 7 and 14 days.

#### 3.3.4.3. Evaluation of Cell Morphology

To evaluate the cell adhesion and morphology, the constructs (cells-NFMs) were fixed with 2.5 % glutaraldehyde (Sigma; USA) in phosphate buffer saline (Sigma; USA) solution, for 1 h at 4 °C. The samples were further dehydrated through a graded series of ethanol and coated in a gold sputter coating equipment (Fisons Instruments, model SC502; England) for 2 min at 15 mA, and analyzed by SEM (Leica Cambridge, model S360; England).

#### 3.3.4.4. Metabolic Activity Analysis (MTS Assay)

At each defined culture period, cell viability and proliferation was determined using the CellTiter 96<sup>®</sup> AQ<sub>ueous</sub> One Solution Cell Proliferation Assay (Promega; USA). Briefly, this assay is based on the bioreduction of a tetrazolium compound, 3-(4,5-dimethylthiazol-2-yl)-5-(3-carboxymethoxyphenyl)-2-(4-sulfophenyl)-2H-tetrazolium (MTS), into a brown formazan product that is soluble in water. This conversion is accomplished by the production of nicotinamide adenine dinucleotide phosphate (NADPH) or nicotinamide adenine dinucleotide (NADH) by the dehydrogenase enzymes existing in metabolically active cells. The absorbance relative to the quantity of formazan product is directly proportional to the number of living cells in culture, and was measured at 490 nm in a microplate reader (Bio-Tek, model Synergie HT; USA). Three specimens per condition and per time point were characterized.

#### 3.3.5. Statistical Analysis

Statistical analysis was performed using the SPSS statistic software (Release 8.0.0 for Windows). Firstly, a Shapiro-Wilk test was used to ascertain about the normality of the data and the results showed that the data was not following a normal distribution. For this reason, a Kruskal-Wallis test followed by Dunnett's test for multiple comparisons was performed to analyze the effect of the various plasma treatments performed on material the hydrophilicity and cellular performance. The *p*-

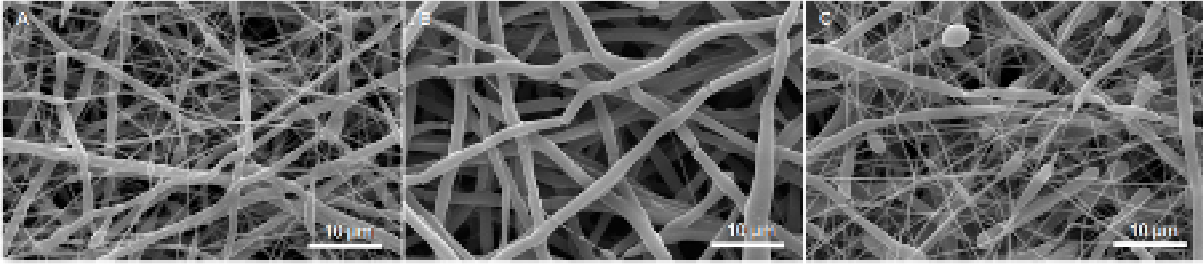


**Figure 3.1** - SEM micrographs of untreated and plasma-treated PCL nanofiber meshes. **A** – untreated PCL nanofiber mesh; **B** – O<sub>2</sub> 30W 10min; **C** – Ar 30W 10min.

values lower than 0.01 were considered statistically significant in the analysis of the results.

### 3.4. Results

#### 3.4.1. Morphological Characterization of Plasma-Treated Electrospun Nanofibers

The SEM photomicrographs of the untreated and plasma-treated electrospun PCL NFMs are shown in Figure 3.1. The O<sub>2</sub>-plasma treatments analyzed by SEM revealed that the 10 min treatment with 30 W power induced melting of the thinner nanofibers (Figure 3.1 A). This effect creates more open space between the fibers still present in the mesh (Figure 3.1 B). When the exposure time or the power were reduced, fibers with irregular morphology and non-uniform diameter and spherical terminated ends were observed. The melting of thinner fibers was also observed when the working atmosphere was changed to Ar. The exception was the treatment at 30 W power and 10 min exposure in which the nanofibers appear with blunted ends (Figure 3.1 C).

The surface roughness parameters of the untreated and plasma-treated electrospun NFMs are shown in Table 3.1. The average surface roughness,  $R_a$ , of untreated NFM was 2.01  $\mu\text{m}$  and its surface profile obtained in interferometric optical profilometry is presented in Figure 3.2 A. Generally, for the conditions involving higher power and longer exposure time, the surface of PCL NFM becomes smoother with an average roughness of 1.40  $\mu\text{m}$  for O<sub>2</sub>-plasma (Figure 3.2 B) and 1.86  $\mu\text{m}$  for Ar-plasma. Conversely, the lower power and shorter exposure time resulted in a rougher

**Table 3.1** - Surface roughness parameters ( $\mu\text{m}$ ) of some plasma-treated and untreated electrospun PCL nanofiber meshes.  $R_a$  - Roughness Average;  $R_q$  - Root Mean Square (RMS) Roughness.

Roughness Parameters	Untreated	O <sub>2</sub> 30W, 10 min.	O <sub>2</sub> 30W, 5 min.	O <sub>2</sub> 20W, 10 min.	O <sub>2</sub> 20W, 5 min.	Ar 30W, 10 min.	Ar 30W, 5 min.	Ar 20W, 10 min.	Ar 20W, 5 min.
$R_a$	2.01	1.40	2.26	2.65	2.51	1.86	1.97	2.05	4.72
$R_q$	2.49	1.95	2.81	3.30	3.31	2.41	2.51	2.63	6.55

surface, with a  $R_a$  value of 2.51  $\mu\text{m}$  in the O<sub>2</sub>-plasma treatment and 4.72  $\mu\text{m}$  in the Ar-plasma treatment (Figure 3.2 C).

### 3.4.2. Hydrophilicity of Plasma-Treated Electrospun Nanofibers

Contact angle measurements for the untreated and plasma-treated electrospun PCL NFMs were performed to determine the effect of treatments on the surface hydrophilicity. The measurements were carried out at different time periods: the initial time points are the most important because they reflect the moment when the materials come into contact with body fluids. Measurements for longer times were intended to evaluate the equilibrium surface wettability. A direct comparison between each couple – modified vs. untreated-PCL NFMs was performed. A Kruskal-Wallis statistical analysis test was performed for each couple and time period, and statistically significant differences were obtained ( $p < 0.00001$ ). Dunnett's test for multiple comparisons was used to determine the plasma treatments that led to statistically significant differences when compared with untreated NFMs.

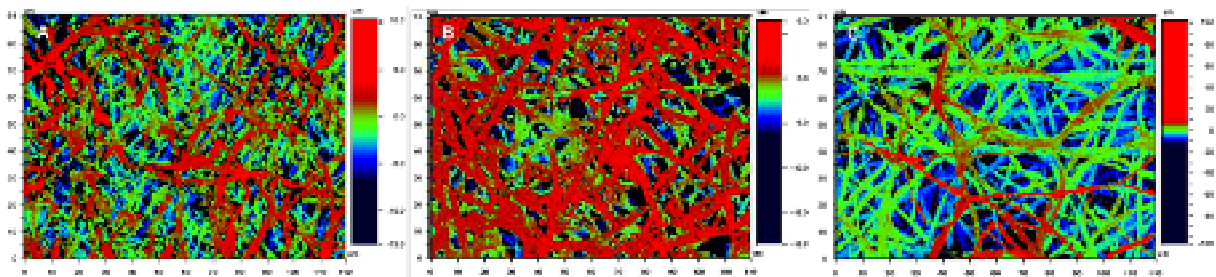


**Figure 3.2** - Optical profilometry images of the untreated PCL nanofiber meshes (A), Oxygen-treated at 30W during 10 minutes (B) and Argon-treated at 20W during 5 minutes (C).

Initially, the contact angle measurements were performed using water. Untreated PCL NFMs demonstrated a water contact angle of  $130^\circ$  (data not shown), and this value was shown to be stable during the studied time periods. Considering the water contact angle of Ar-treated samples, a decrease of  $20^\circ$  was observed (data not shown), that is, the surfaces became less hydrophobic. Oxygen-treated NFMs presented water contact angles below  $20^\circ$ , which could not be detected by the high speed camera. To overcome this difficulty, a highly viscous polar liquid, glycerol, was used instead of water to characterize the differences in contact angle of the surface-modified NFMs.

As can be observed in Figure 3.3,  $O_2$ -plasma treated NFMs presented significantly smaller contact angles than untreated NFMs ( $p < 0.01$ ). The only exception was the treatment with  $O_2$  at 20 W for 5 min. Conversely, the Ar-treated NFM at 30 W for 10 min also presented significantly lower values of contact angle ( $p < 0.01$ ) when compared to untreated PCL NFMs. The combined effect of power and exposure time on the surface hydrophilicity should be highlighted: 30 W and 10 min exposure resulted in the most hydrophilic surface, while 20 W and 5 min did not show any significant difference in hydrophilicity. Additionally, the drop spreading profile

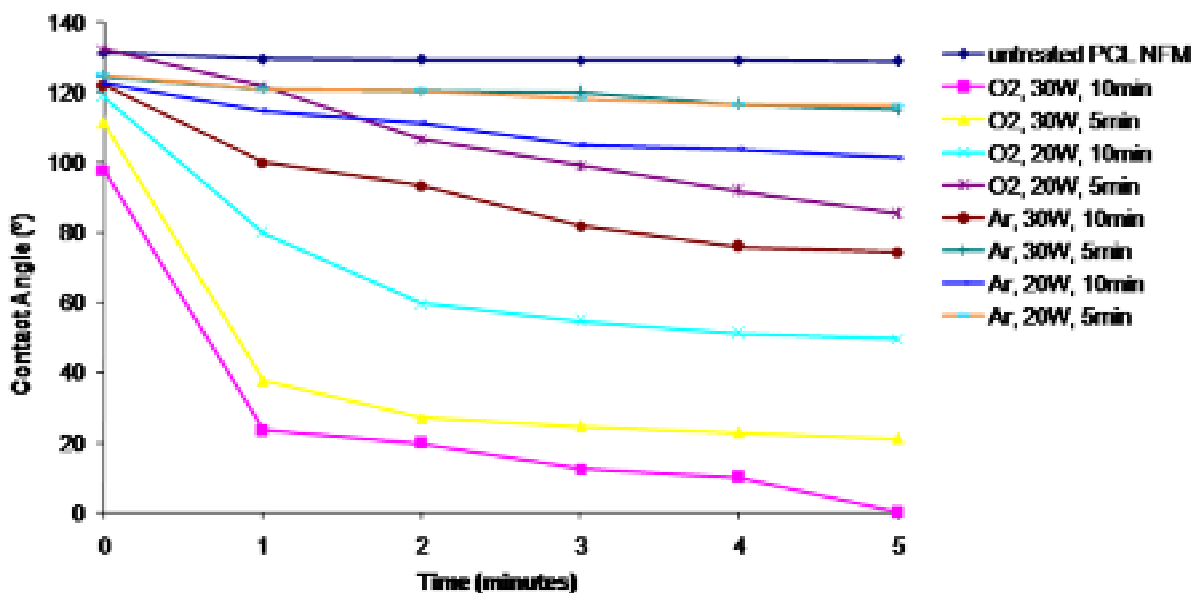


**Figure 3.3** - Glycerol Contact Angle values of untreated and plasma modified PCL nanofiber meshes as function of the time.

**Table 3.2** - Elemental composition of some plasma-treated and untreated electrospun PCL nanofiber meshes. C – Carbon; O – Oxygen.

Elements	Untreated	O <sub>2</sub> 30W, 10 min.	O <sub>2</sub> 30W, 5 min.	O <sub>2</sub> 20W, 10 min.	O <sub>2</sub> 20W, 5 min.	Ar 30W, 10 min.	Ar 30W, 5 min.	Ar 20W, 10 min	Ar 20W, 5 min
C	80.5	75.3	70.7	77.0	79.0	82.2	82.6	73.1	72.2
O	19.0	23.9	27.7	22.9	19.9	16.7	16.5	23.3	22.7
C/O ratio	4.24	3.15	2.55	3.36	3.96	4.92	5.00	3.13	3.18

before. Thus, it becomes clear that the different surface treatments have significant effects on the hydrophilicity of the NFMs.

### 3.4.3. Chemical Composition of Plasma-Treated Electrospun Nanofibers

XPS was used to analyze the surface chemistry of electrospun PCL NFMs before and after plasma treatment. As expected and according to the chemical structure of PCL, the XPS analysis of the untreated NFM indicated that the surface was dominated by carbon (80.5 %) and oxygen (19.0 %) species (Table 3.2). Generally, the elemental composition analysis of the plasma-treated samples showed a decrease of carbon content, probably due to the melting process. The oxygen content increases because of the surface oxidation. The exceptions were the PCL NFMs treated with Ar atmosphere at 30 W for 10 and 5 min, where the carbon content was enhanced. The melting process was more pronounced in the NFMs treated with Ar at lower power, as well as with O<sub>2</sub> at 30 W for 10 and 5 min. The increment of oxygen, depending on the plasma treatment, oscillates between 19.9 %, for the O<sub>2</sub>- plasma treatment at 20 W for 5 min, and 27.7 % for the O<sub>2</sub> treatment at 30W for 5 min. The C/O ratio decreases in all conditions of plasma treatment with the exceptions already mentioned.

High-resolution peak analysis of carbon 1s (C1s) at the surface was performed for both untreated and plasma-treated PCL NFMs to determine the chemical functional groups present at the surface. All studied materials exhibited three components of C1s core level peak, which correspond to the aliphatic carbon bonds (–C–C– or –C–H), carbon single bonded to oxygen (–C–OH or –C–O–) and carbonyl functional groups (–C=O) located at approximately 285, 287, and 289 eV, respectively (Figure 3.4). As was expected, considerable differences were detected in

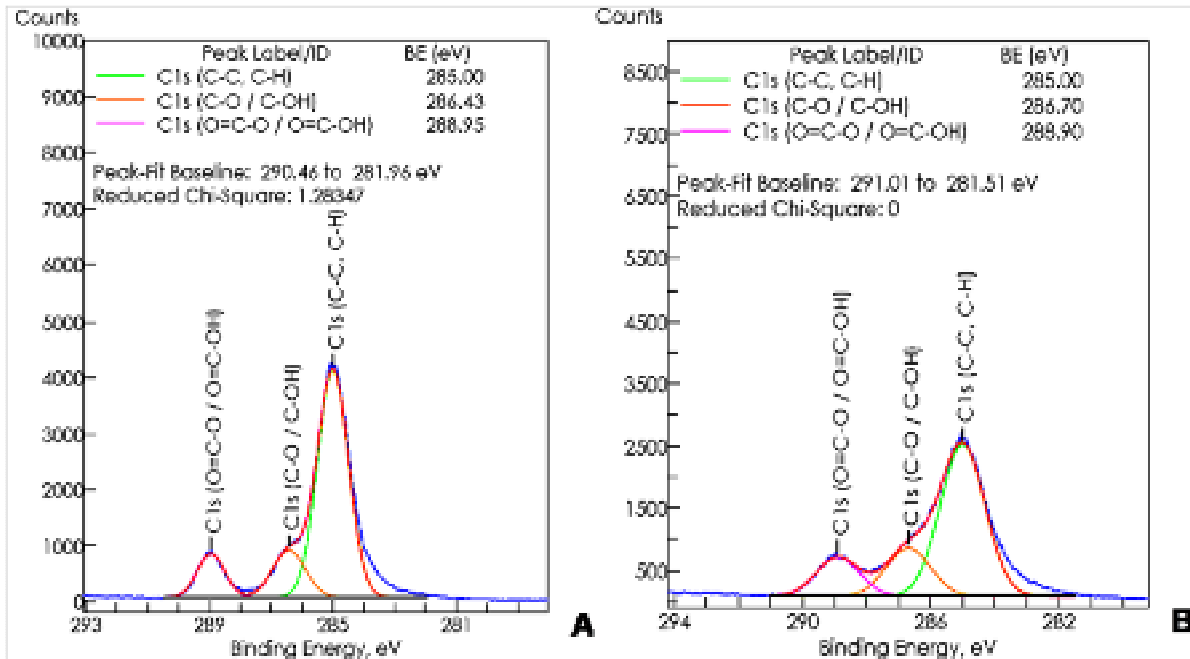


**Figure 3.4** - High resolution C1s core level signals of untreated (A) and Oxygen-treated electrospun PCL nanofiber meshes at 30W during 5 minutes (B).

the intensity of these peaks for the untreated and plasma-treated electrospun PCL NFMs (e.g., O<sub>2</sub> treatment at 30 W for 5 min). Thus, the XPS analyses confirmed that the plasma treatments lead to different surface chemistry, which in turn affects the wettability and, consequently, the cell attachment.

#### 3.4.4. Cellular Performance over Plasma-Treated Electrospun Nanofibers

The morphology of the cells cultured on untreated and plasma-treated electrospun PCL NFMs was examined by SEM. For comparative purposes, biological studies were also performed in TCPS coverslips as an optimized substrate for 2D cell culture. These observations were conducted in the first day after cell culture, because the alterations of the surface induced by the plasma treatments have a major influence at the beginning of the cell adhesion process. SEM micrographs of the direct contact assay with fibroblast-like cells showed a typical spindle-shape morphology of cells cultured on Ar-treated PCL NFMs at 30 W for 5 min and at 20 W for 10 min (Figure 3.5 I and J). Cells were observed to be dispersed and stretched at the surface of the both plasma-treated and untreated mesh-like fibrous structure. The

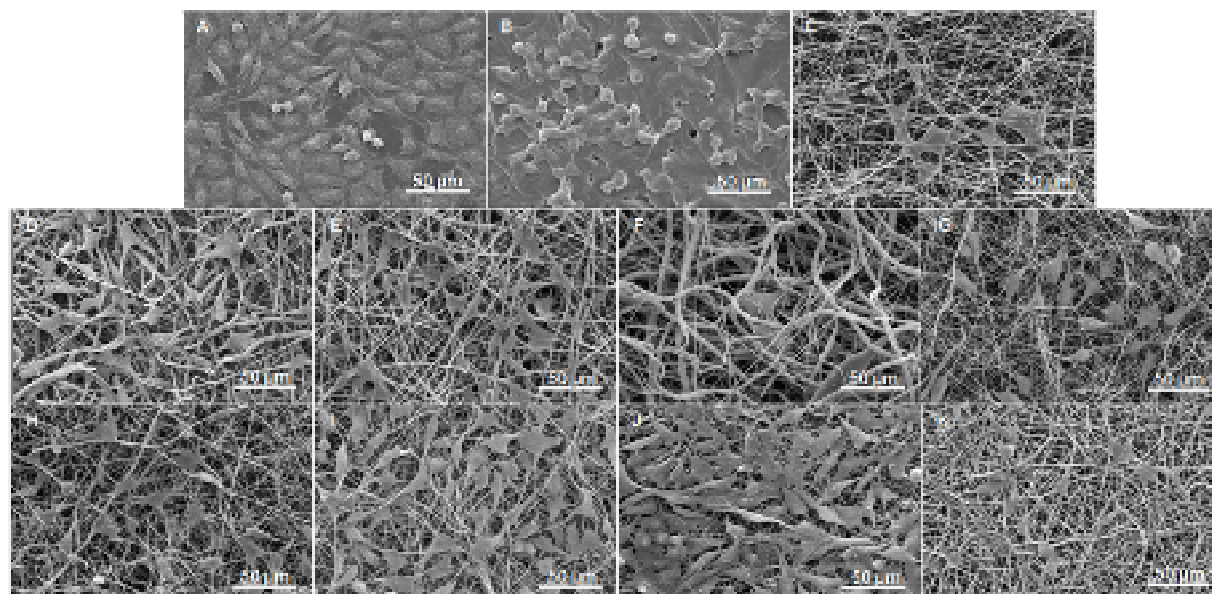


**Figure 3.5** - SEM micrographs of L929 cells growing onto plasma-treated and untreated PCL nanofiber meshes, after 1 day of culture. **A** – TCPS; **B** - PCL solvent-casted membrane; **C** – untreated PCL nanofiber mesh; **D** – O<sub>2</sub> 30W 10min; **E** – O<sub>2</sub> 30W 5min; **F** – O<sub>2</sub> 20W 10min; **G** – O<sub>2</sub> 20W 5min; **H** – Ar 30W 10min; **I** – Ar 30W 5min; **J** – Ar 20W 10min; **K** – Ar 20W 5min.

round shape of the chondrocyte-like cells was only kept on untreated PCL NFMs (Figure 3.6 C).

Poor chondrocyte attachment was observed on PCL NFMs subjected to plasma-treatment with O<sub>2</sub> at 30 W for 10 min and Ar at 30 W for 10 min (Figure 3.6 D and H), which is understandable since those cells tend to prefer hypoxic environments. On the O<sub>2</sub>-treated NFMs at 20 W for 10 min, Ar-treated at 30 W for 5 min and at 20 W for 10 min, the cells presented a flatten morphology, covering almost all the available surface of the meshes. SEM micrographs from the assays with osteoblast-like cells demonstrated that the 2D PCL solvent-cast membrane induces the maintenance of the cell morphology (i.e. cuboid shape) (Figure 3.7 B), as well as on the TCPS surface (Figure 3.7 A). The largest amount of cells was observed on the NFMs treated with O<sub>2</sub> at 20 W for 10 min, Ar at 30 W for 5 min and Ar at 20 W for 10 min, forming a continuous layer of spread cells. For all the other plasma-treated

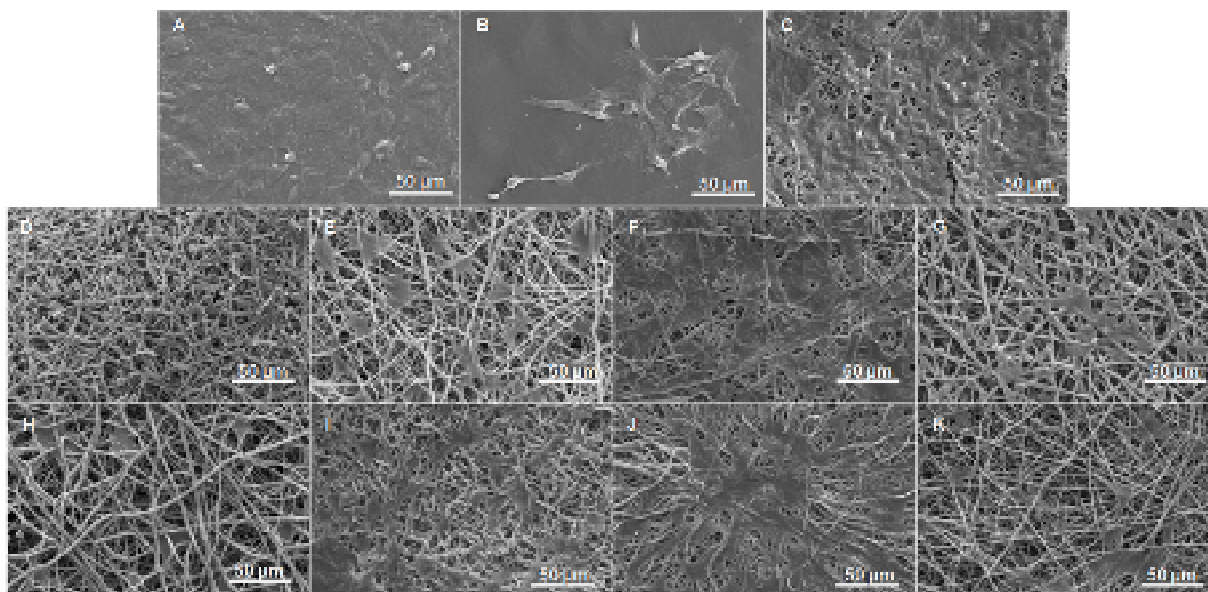


**Figure 3.6** - SEM micrographs of ATDC5 cells growing onto plasma-treated and untreated PCL nanofiber meshes, after 1 day of culture. **A** – Tissue Culture Polystyrene; **B** - PCL solvent-casted membrane; **C** – untreated PCL nanofiber mesh; **D** – O<sub>2</sub> 30W 10min; **E** – O<sub>2</sub> 30W 5min; **F** – O<sub>2</sub> 20W 10min; **G** – O<sub>2</sub> 20W 5min; **H** – Ar 30W 10min; **I** – Ar 30W 5min; **J** – Ar 20W 10min; **K** – Ar 20W 5min.

samples, the cells adhered and interacted with the nanofibrous structure, spreading over the surface.

A metabolic activity-based (MTS) assay was used to determine cell viability of the three cell types along the testing periods on the different studied surfaces. For these assays, standard TCPS surface was used as a control. For each cell type and culture period, the Kruskal-Wallis test was carried out in order to evaluate significant differences ( $p < 0.00001$ ) between the studied surfaces in terms of cell activity. Additionally, a Dunnett's test for multiple comparisons was performed to determine which plasma treatment has significant influence on the cell behavior when compared to standard TCPS. The results are shown in Figures 3.8-3.10.

In the case of the fibroblastic cell type, the statistical analysis demonstrated that PCL NFMs modified by O<sub>2</sub>-plasma at 30 W for 10 min and at 20 W for 10 min are not appropriate substrates for cell adhesion ( $p < 0.01$ ) considering their values of cell

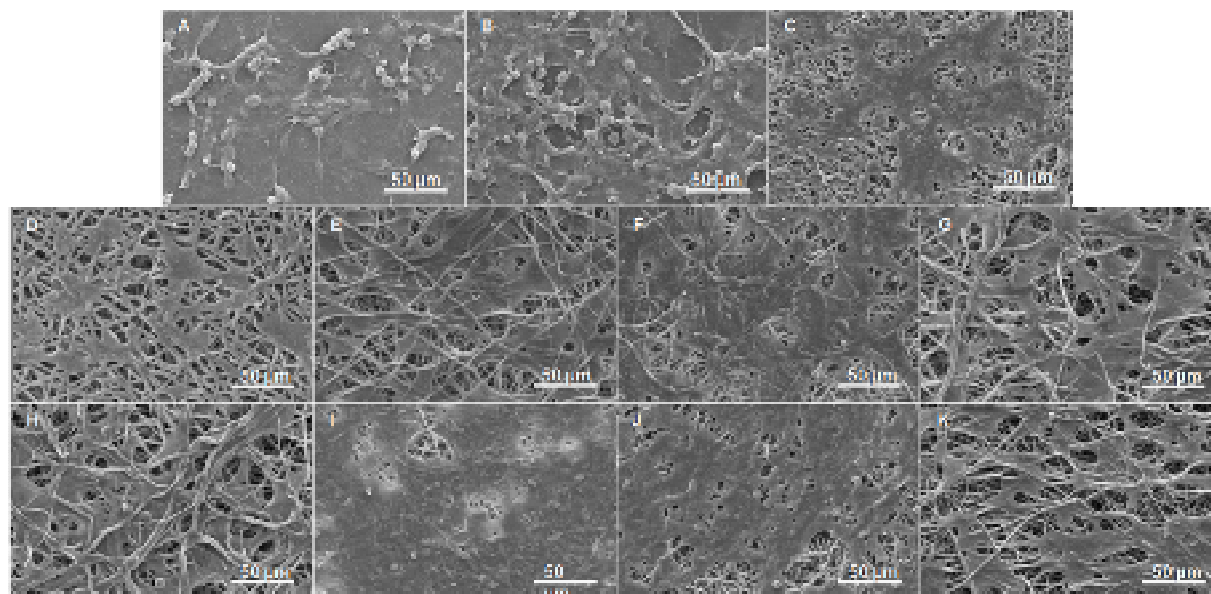


**Figure 3.7** - SEM micrographs of Saos-2 cells growing onto plasma-treated and untreated PCL nanofiber meshes, after 1 day of culture. **A** – TCPS; **B** - PCL solvent-casted membrane; **C** – untreated PCL nanofiber mesh; **D** – O<sub>2</sub> 30W 10min; **E** – O<sub>2</sub> 30W 5min; **F** – O<sub>2</sub> 20W 10min; **G** – O<sub>2</sub> 20W 5min; **H** – Ar 30W 10min; **I** – Ar 30W 5min; **J** – Ar 20W 10min; **K** – Ar 20W 5min.

viability after 1 day of culture (Figure 3.8). The other plasma treatments did not present statistically significant difference when compared with the untreated PCL NFMs or the TCPS.

After 3 days of culture, the NFMs treated with O<sub>2</sub> at 30 W for 5 min, or Ar atmosphere at 20 W for 10 and 5 min presented statistically significant higher values of cell viability ( $p < 0.01$ ) when compared to those observed for the untreated samples. However, those values were very similar to that observed for the TCPS. At 7 days of fibroblast culture, all Ar-treated samples presented significantly higher values of cell viability than untreated PCL NFMs ( $p < 0.01$ ). When those values were compared with ones obtained for TCPS, only the Ar-plasma treatments at 20 W revealed significant difference ( $p < 0.01$ ). At this period of culture, the O<sub>2</sub>-treated NFMs at 30 W for 10 and 5 min also presented significantly higher values than untreated PCL NFMs ( $p < 0.01$ ), but they did not differ from the TCPS. For longer

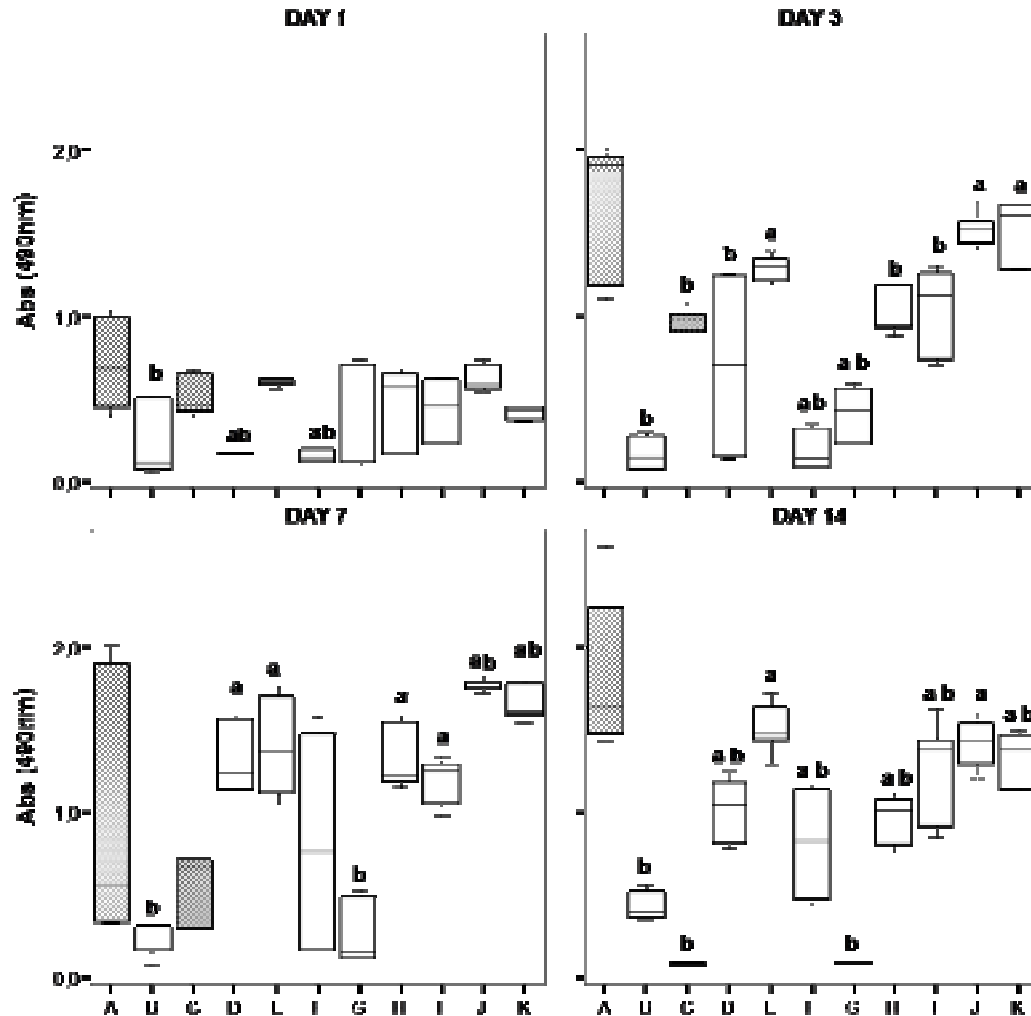


**Figure 3.8** - Box plot of MTS assay results for fibroblasts (L929 cell line) cultured on untreated and plasma treated PCL nanofiber meshes during 1, 3, 7 and 14 days. **A** – TCPS; **B** - PCL solvent-casted membrane; **C** – untreated PCL nanofiber mesh; **D** – O<sub>2</sub> 30W 10min; **E** – O<sub>2</sub> 30W 5min; **F** – O<sub>2</sub> 20W 10min; **G** – O<sub>2</sub> 20W 5min; **H** – Ar 30W 10min; **I** – Ar 30W 5min; **J** – Ar 20W 10min; **K** – Ar 20W 5min. Data were analyzed by nonparametric way of a Kruskal-Wallis test followed by Dunnett's test for multiple comparisons. **a**,  $p < 0.01$  vs untreated PCL nanofiber mesh. **b**,  $p < 0.01$  vs TCPS.

culture periods (14 days), the O<sub>2</sub>- plasma treatment at 30 W for 5 min and the Ar treatment at 20 W for 10 min, presented similar fibroblast viability to standard TCPS. All the other plasma treatments resulted in lower viability than TCPS ( $p < 0.01$ ). However, a significantly higher cell viability was measured when compared to untreated PCL NFMs. Overall, the plasma-modified NFM with O<sub>2</sub> at 30 W for 5min

with Ar at 20 W for 10 and 5 min are the best substrates for fibroblastic proliferation for shorter (3 days) culture times, with cellular activity similar to standard TCPS. After 7 days of culture, the samples treated with O<sub>2</sub> at 30 W for 10 min and with Ar at 30 W for 10 and 5 min are the ones that performed better in terms of cellular proliferation.

Regarding the influence of the different plasma treatments over chondrocytic cells (ATDC5 cell line) behavior, the surfaces modified by O<sub>2</sub> plasma at 30 W for 5 min and at 20 W for 10 min, as well as the Argon-treated nanofiber meshes at 20W during 10 and 5 minutes, presented significantly higher values of cell viability in the first day of culture ( $p < 0.01$ ), when compared to the viability of ATDC5 observed for untreated PCL nanofiber meshes (Figure 3.9). However, only the treatments by O<sub>2</sub> presented significantly higher cellular activity than TCPS ( $p < 0.01$ ). This tendency was kept for longer culture time (3 days) with only the exception Ar-treated NFMs at 20 W for 5 min. Moreover, the NFMs treated in Ar atmosphere at 30 W for 10 min also presented higher cellular viability than untreated NFMs ( $p < 0.01$ ). In comparison with TCPS, only the O<sub>2</sub>-treated at 20 W for 10 min NFMs presented higher cellular activity ( $p < 0.01$ ). O<sub>2</sub>-treated NFMs for a shorter time period (5 min) showed significantly lower values of cellular activity ( $p < 0.01$ ). The Dunnett's test performed in data obtained after 7 days of culture revealed that the untreated PCL NFMs as well as the ones treated with O<sub>2</sub> at 30 W and 20 W for 10 min, with Ar at 30 W for 5 min and at 20 W for 5 min show higher values of cell viability than standard polystyrene ( $p < 0.01$ ), which is a remarkable result. After 14 days of culture, only the plasma treatment with O<sub>2</sub> at 30 W for 5 min and with Ar at 20 W for 5 min presented higher values of cell viability than untreated PCL NFMs ( $p < 0.01$ ). The treatments with O<sub>2</sub> also presented higher cellular activity than TCPS ( $p < 0.01$ ). Taken as a whole, the O<sub>2</sub>-treated NFMs at 30 W for 5 min always show a better performance in cell adhesion and proliferation than untreated PCL NFMs, for shorter culture periods (up to 3 days). For longer culture periods (> 7 days), the Ar-treated NFMs at 20 W for 5 min demonstrated the support of higher cellular activity.

Concerning the influence of plasma-treatment over the activity of osteoblast-like cells after 1 day of culture, the plasma treatments with O<sub>2</sub> at 30 W for 5 min and Ar at 30 W for 10 min induced significantly higher cellular viability than untreated PCL

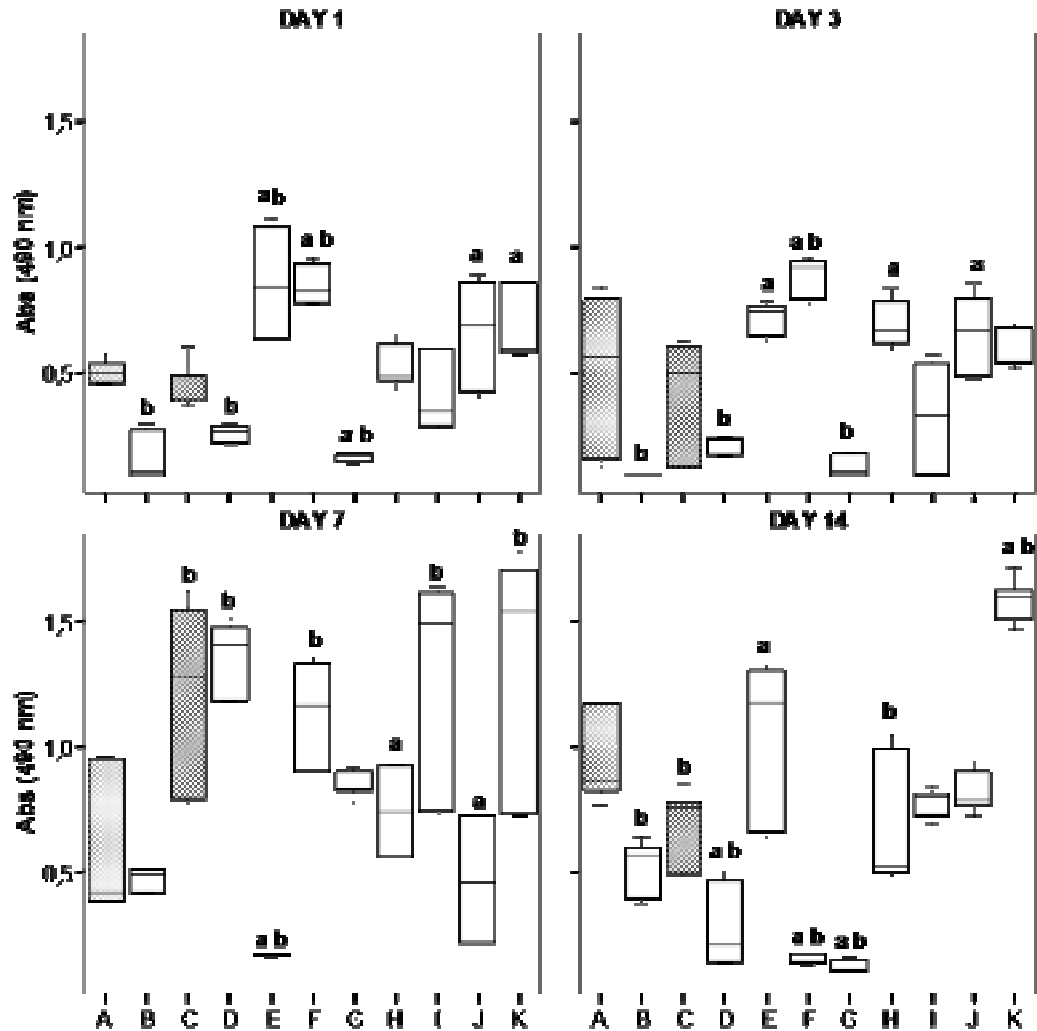


**Figure 3.9** - Box plot of MTS assay results for chondrocytes (ATDC5 cell line) cultured on untreated and plasma treated PCL nanofiber meshes during 1, 3, 7 and 14 days. **A** – TCPS; **B** - PCL solvent-casted membrane; **C** – untreated PCL nanofiber mesh; **D**– O<sub>2</sub> 30W 10min; **E**– O<sub>2</sub> 30W 5min; **F**– O<sub>2</sub> 20W 10min; **G**– O<sub>2</sub> 20W 5min; **H** – Ar 30W 10min; **I** – Ar 30W 5min; **J** – Ar 20W 10min; **K** – Ar 20W 5min. Data were analyzed by nonparametric way of a Kruskal-Wallis test followed by Dunnett's test for multiple comparisons. **a**,  $p < 0.01$  vs untreated PCL nanofiber mesh. **b**,  $p < 0.01$  vs TCPS.

NFMs ( $p < 0.01$ ), but similar to the performance observed for TCPS (Figure 3.10). After 3 days of culture, the NFMs treated with O<sub>2</sub> at 30 W for 5 min and 20 W for 10 min, and Ar at 30 W for 10 min and 20 W for 5 min presented significantly higher

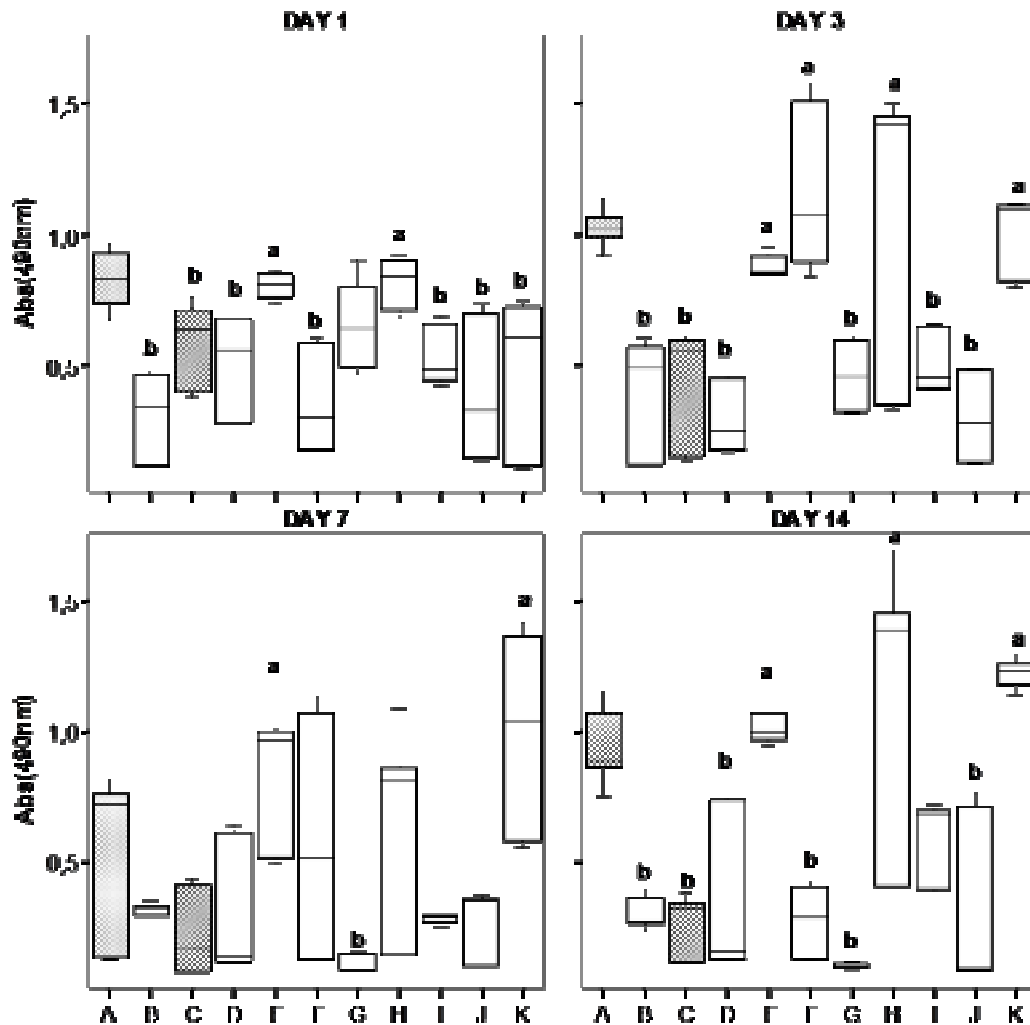


**Figure 3.10** - Box plot of MTS assay results for osteoblasts (Saos-2 cell line) cultured on plasma treated and untreated PCL nanofiber meshes during 1, 3, 7 and 14 days. **A** – TCPS; **B** - PCL solvent-casted membrane; **C** – untreated PCL nanofiber mesh; **D** – O<sub>2</sub> 30W 10min; **E** – O<sub>2</sub> 30W 5min; **F** – O<sub>2</sub> 20W 10min; **G** – O<sub>2</sub> 20W 5min; **H** – Ar 30W 10min; **I** – Ar 30W 5min; **J** – Ar 20W 10min; **K** – Ar 20W 5min. Data were analyzed by nonparametric way of a Kruskal-Wallis test followed by Dunnett’s test for multiple comparisons. **a**,  $p < 0.01$  vs untreated PCL nanofiber mesh. **b**,  $p < 0.01$  vs TCPS.

values of cell viability ( $p < 0.01$ ) when compared to untreated NFMs. Those values are well in the range of those observed for standard polystyrene. After 7 days of culture, only the O<sub>2</sub>-treated NFMs at 30 W for 5 min and Ar-treated at 20 W for 5 min present comparable cell activity to TCPS, as revealed by the Dunnett’s test. Those

conditions together with the Ar-plasma treatment at 30 W for 10 min also presented significantly higher cellular performance than untreated NFMs ( $p < 0.01$ ) for longer time culture periods (14 days). In fact, these plasma treatment conditions presented similar cellular viability than TCPS, demonstrating its suitability for longer cell culturing periods. It could also be observed that the O<sub>2</sub>-treated NFMs at 30 W for 5 min were consistently the most effective in all the culturing periods and the NFMs treated with Ar at 20 W for 5 min was also very effective after 3 days of cell culture.

### 3.5. Discussion

The engineering of nanoscale surfaces allows tailoring the material surface characteristics, which can lead to significant effects upon the cellular behavior. The main advantage of this engineering approach is the ability to design the materials surfaces to provide microenvironments closer to the native ECM and thus facilitate cell activity [33]. Theoretically, an optimal substrate for cells should emulate as near as possible the topographical and biochemical nature of the native tissue. In the present study, nanostructured materials with morphologies similar to the native ECM were produced by electrospinning. Electrospun-processed materials have the potential to generate scaffolds capable of providing ECM-like surfaces, facilitating cell-matrix and cell-cell interactions, and therefore being very useful for tissue engineering strategies. However, cells recognize not only topographical clues on the surfaces, but also the surface chemistry, which can significantly influence their behavior. Surface functionalization of biodegradable synthetic polymers has been successfully achieved by plasma treatments, thus decreasing their intrinsic hydrophobicity [25]. However, only recently has the plasma surface modification of 3D polymer-based structures been considered as an alternative route to enhance their biological performance. The difficulties in the surface modification of scaffolds by plasma are raised by the requirement for highly porous and interconnected samples (the pores must be wider than the mean free path of the electrons and the Debye length [34]). Thus, this technique is suitable to modify electrospun structures because of its inherent interconnectivity. Moreover, unlike other physical and chemical surface modification techniques, the plasma action is limited to 10 nm below the surface and

does not affect the bulk properties of the material [24, 26-28, 35]. The selection of appropriate treatment conditions is very important since the nanosized structure of NFMs should not be compromised, and nor should its cellular performance. Depending on the treatment conditions used, such as the type of gas, pressure, temperature, time of exposure, and intensity (or power), both chemical and some physical characteristics of the surface may be tailored to develop optimal interactions with cells and tissues [36].

The electrospun NFMs subjected to different plasma treatments were morphologically characterized by SEM. This analysis showed that thinner nanofibers were not present in some plasma conditions probably because of polymer melting that could be due to an undesired increment of the reaction chamber temperature or by the electric power used. Other works reported significant morphological alterations by plasma surface modification [37]. The analysis of the morphological alterations was also performed by the characterization of the surface roughness. This analysis may be performed by various techniques such as atomic force microscopy (AFM) or interferometric optical profilometry. The latest was selected in this study because of its ability to scan a larger area than by AFM. Some works in literature [38, 39] confirmed an increase in surface roughness after the plasma treatment, due to polymer melting at the surface. This effect increases directly with the duration of the treatment. Recently, Wei *et al.* [40] modified the surface of electrospun polyamide 6 nanofibers by cold gas plasma treatment and observed that the surface roughness of the fiber was greatly increased when compared to the surface of the untreated fiber. The results obtained in the present study with plasma treatments at low power and exposure time confirm those previous observations. However, for longer treatment times and higher power, a smoothing of the surface nanofibers was observed, which may have been due to the partial polymer melting during the plasma treatment.

The contact angle analysis is a highly-sensitive technique for the determination of the surface wettability. Moreover, the surface energy can be quantified using standard polar and non-polar liquids and some well-established models. However, this test is also dependent on the surface roughness. In fact, the NFMs present a quite rough surface and the data herein reported is particularly valid for comparative

purposes. The untreated electrospun PCL NFMs is highly hydrophobic (with a measured water contact angle of  $\approx 130^\circ$ ). A decrease of the contact angle due to the plasma treatments was observed mainly after the  $O_2$  treatments. These results demonstrated that plasma treatment is an effective method to increase the surface hydrophilicity of polyester NFMs. Recently, Lai *et al.* [30] showed that the polyethylene terephthalate (PET) smoother surfaces at the microscale led to smaller contact angles. Generally [29, 31], plasma-induced polar chemical groups such as oxygen-containing groups tend to increase the surface energy of the polymers and thus enhance their hydrophilic behavior.  $O_2$ -plasma treatment is commonly used to introduce those functional groups at the nanofiber surface [29]. It has been shown already that much of the oxidation is caused by radical reactions between the polymer chain backbone and the atomic oxygen in the plasma, leading to various functionalities such as hydroperoxides, carbonyls, carboxylic acids, and peracids [41]. Higher content of oxygen-containing groups (namely, -O-H and -C=O) were detected by XPS in our plasma-treated electrospun PCL NFMs. As previously stated, these changes result in a significant increase in the hydrophilicity of the surfaces. Indeed, Lai *et al.* [30] stated that the C=O bond is the main factor controlling the hydrophilicity of polymer surfaces. Although Ar is an inert gas, plasma-treatment with this gas can also introduce oxygen-containing functionality at the surface [30]. This effect is caused by reaction between the free radicals at the surface created during the treatment and the oxygen existing in the air.

As previously mentioned, the main purpose of this work was to define conditions of the treatment that result in surfaces favorable for cell growth. We have used different cell types (i.e. fibroblasts, chondrocytes and osteoblasts) to validate the efficacy of a defined plasma-treatment. Among the plasma-treated electrospun NFMs, the ones modified in an  $O_2$  atmosphere at 30 W for 5 min and with Ar at 20 W for 5 min can be classified as optimal substrates for the cell adhesion and proliferation. The NFMs treated at those conditions shown similar cell viability as the one observed for TCPS. In the case of  $O_2$ -modified NFM at 30 W for 5 min, we believe that the observed cellular activity is mainly due to the increased hydrophilic character of the NFM (glycerol contact angle  $\approx 30^\circ$ ). Similar results were observed for human skin

fibroblasts whose spreading increased along chemically characterized gradient surfaces going from the most hydrophobic towards the hydrophilic end [42]. Among the hydrophilic surfaces, differences in charge and wettability significantly influence cell attachment but not spreading or cytoskeleton organization. Surface hydrophilicity (20–40° water contact angle) is the major parameter promoting high levels of cell attachment [43]. However, another study demonstrated that the maximum adhesion and growth of various cell types (ovary, fibroblast, and endothelial cells) on polymer surfaces with a wettability gradient appeared around water contact angles of 55° [44]. Therefore, the optimum value of contact angle for optimal cell adhesion is somewhat inconclusive in the literature, varying between 20° and 70°.

The samples treated at these conditions also presented the highest oxygen content (XPS analysis), indicating the importance of the surface chemistry for cell adhesion. The oxygen atoms at the surface may be part of carbonyl, carboxyl, ester, or hydroxyl groups [45]. However, it is not clear which of these groups is the most effective in influencing the cell-biomaterial interaction. It has been suggested [46] that the oxygen from the carboxyl group is more effective in promoting this interaction, while the oxygen derived from the ester and hydroxyl groups are less effective. However, authors suggested that the presence of hydroxyl groups was beneficial for cell adhesion [47]. Furthermore, a selective blocking of the hydroxyl groups was shown to result in the inhibition of the adhesion of baby hamster kidney cells or leukocytes, while blocking the carboxyl groups did not affect cell adhesion [48].

The NFMs treated in an Ar atmosphere at 20 W for 5 min presented a more hydrophobic character (glycerol contact angle  $\approx 110^\circ$ ), most probably because of the surface roughness observed for this treated NFM. It was stated previously that surface topography is a key factor affecting cellular morphology, proliferation and differentiation [33]. Our experimental results also confirm many reports describing an increased proliferation of osteoblastic cells on rough substrata [49-53]. However, it is also possible to find reports where it is demonstrated that the surface roughness negatively affects the adhesion, proliferation and differentiation of different cell types, namely osteoblasts and chondrocytes [54-58]. Furthermore, SEM micrographs of bone cells on biomaterials with different surface roughnesses generally demonstrate

that the cell spreading and monolayer formation was more effective on smoother surfaces [59]. In the case of fibroblastic cells, there are many studies demonstrating the slower cell proliferation on rough substrates compared to smooth surfaces [39, 51, 60, 61]. Thus, we may say that the effect or influence of the surface roughness on the cell adhesion and proliferation is not a consensual in the literature.

Many authors write that the NFMs are morphologically similar with the ECM of many tissues and this similarity must enhance the cell behavior at the surface of those structures. Herein, we showed that the surface chemistry has, at least, as strong of an effect over cell activity as the structural morphology of the NFMs. Thus, we propose that the performance of NFMs also requires chemical surface optimization.

### **3.6. Conclusions**

Electrospun PCL NFMs were submitted to different plasma-treatments including the gas used ( $O_2$  and Ar), the electrical power, and the exposure time. The goal was to obtain enhanced cellular response at the surface of NFMs by adjusting the treatment conditions. SEM micrographs and surface roughness analysis demonstrated the induction of topographical alterations by the plasma-treatments. The contact angle analysis revealed that the electrospun NFMs became generally more hydrophilic after the applied modifications. The most significant changes in the wettability were observed for  $O_2$ -treated NFMs. XPS results indicated higher oxygen-contents at the surface of plasma-treated NFMs, including hydroxyl (C-O-) and carbonyl (C=O) functionalities. However, the relative content of these functional groups was dependent on the specific conditions used.

Different cell types, namely fibroblasts (L929 cell line), chondrocytes (ATDC5 cell line) and osteoblast-like (Saos-2 cells), adhered and proliferated at the surface of plasma-treated nanofibrous structures. It was possible to define treatment conditions leading to enhanced cell adhesion and faster proliferation, namely  $O_2$  at 30 W for 5 min and Ar at 20 W for 5 min. Using those conditions, both the hydrophilic behavior and the roughness of the NFM surfaces were affected. Therefore, both those plasma

treatment conditions could be further applied in the development of biomaterials with enhanced biological performance independently of the tissue to be regenerated.

It was shown that one treatment with O<sub>2</sub> and one with Ar outperform significantly the other treatment conditions and also the untreated NFMs. Our results show that the biological performance of NFMs can be improved by the careful control of its surface properties without compromising significantly the overall morphology of the nanofibers.

### 3.7. References

1. Hubbell JA. Biomaterials in tissue engineering. *Nature Biotechnology* 1995; 13(6):565-576.

2. Mano JF, Silva GA, Azevedo HS, Malafaya PB, Sousa RA, Silva SS, *et al.* Natural origin biodegradable systems in tissue engineering and regenerative medicine: Present status and some moving trends. *Journal of the Royal Society Interface* 2007; 4(17):999-1030.

3. Agrawal CM, Ray RB. Biodegradable polymeric scaffolds for musculoskeletal tissue engineering. *Journal of Biomedical Materials Research* 2001;55(2):141-150.

4. Pitt CG, Gratzl MM, Kimmel GL, Surles J, Schindler A. Aliphatic polyesters II. The degradation of poly (DL-lactide), poly (epsilon-caprolactone), and their copolymers in vivo. *Biomaterials* 1981; 2(4):215-220.

5. Tsuji H, Ikada Y. Blends of aliphatic polyesters. II. Hydrolysis of solution-cast blends from poly(L-lactide) and poly (ε-caprolactone) in phosphate-buffered solution. *Journal of Applied Polymer Science* 1998; 67(3):405-415.

6. Ciapetti G, Ambrosio L, Savarino L, Granchi D, Cenni E, Baldini N, *et al.* Osteoblast growth and function in porous poly epsilon -caprolactone matrices for bone repair: a preliminary study. *Biomaterials* 2003; 24(21):3815-3824.

7. Hutmacher DW, Ng KW, Kaps C, Sittinger M, Klaring S. Elastic cartilage engineering using novel scaffold architectures in combination with a biomimetic cell carrier. *Biomaterials* 2003; 24(24):4445-4458.

8. Shao XX, Hutmacher DW, Ho ST, Goh JC, Lee EH. Evaluation of a hybrid scaffold/cell construct in repair of high-load-bearing osteochondral defects in rabbits. *Biomaterials* 2006; 27(7):1071-1080.
9. Tsuji H, Ikada Y. Blends of aliphatic polyesters. I. Physical properties and morphologies of solution-cast blends from poly(DL-lactide) and poly( $\epsilon$ -caprolactone). *Journal of Applied Polymer Science* 1996; 60(13):2367-2375.
10. Dersch R, Steinhart M, Boudriot U, Greiner A, Wendorff JH. Nanoprocessing of polymers: Applications in medicine, sensors, catalysis, photonics. *Polymers for Advanced Technologies* 2005; 16(2-3):276-282.
11. Huang ZM, Zhang YZ, Kotaki M, Ramakrishna S. A review on polymer nanofibers by electrospinning and their applications in nanocomposites. *Composites Science and Technology* 2003; 63(15):2223-2253.
12. Martins A, Araujo JV, Reis RL, Neves NM. Electrospun nanostructured scaffolds for tissue engineering applications. *Nanomedicine* 2007; 2(6):929-942.
13. Zeng J, Chen X, Xu X, Liang Q, Bian X, Yang L, *et al.* Ultrafine fibers electrospun from biodegradable polymers. *Journal of Applied Polymer Science* 2003; 89(4):1085-1092.
14. Reneker DH, Chun I. Nanometre diameter fibres of polymer, produced by electrospinning. *Nanotechnology* 1996; 7(3):216-223.
15. Ma Z, Kotaki M, Inai R, Ramakrishna S. Potential of nanofiber matrix as tissue-engineering scaffolds. *Tissue Engineering* 2005; 11(1-2):101-109.
16. Smith LA, Ma PX. Nano-fibrous scaffolds for tissue engineering. *Colloid Surface and Biointerface* 2005; 39(3):125-131.
17. Fujihara K, Kotaki M, Ramakrishna S. Guided bone regeneration membrane made of polycaprolactone/calcium carbonate composite nano-fibers. *Biomaterials* 2005; 26(19):4139-4147.
18. Li WJ, Danielson KG, Alexander PG, Tuan RS. Biological response of chondrocytes cultured in three-dimensional nanofibrous poly( $\epsilon$ -caprolactone) scaffolds. *Journal of Biomedical Materials Research* 2003; 67(4):1105-1114.

19. Li WJ, Tuli R, Huang X, Laquerriere P, Tuan RS. Multilineage differentiation of human mesenchymal stem cells in a three-dimensional nanofibrous scaffold. *Biomaterials* 2005; 26(25):5158-5166.
20. Min BM, Lee G, Kim SH, Nam YS, Lee TS, Park WH. Electrospinning of silk fibroin nanofibers and its effect on the adhesion and spreading of normal human keratinocytes and fibroblasts in vitro. *Biomaterials* 2004; 25(7-8):1289-1297.
21. Xu C, Inai R, Kotaki M, Ramakrishna S. Electrospun nanofiber fabrication as synthetic extracellular matrix and its potential for vascular tissue engineering. *Tissue Engineering* 2004; 10(7-8):1160-1168.
22. Yang F, Xu CY, Kotaki M, Wang S, Ramakrishna S. Characterization of neural stem cells on electrospun poly(L-lactic acid) nanofibrous scaffold. *Journal of Biomaterials Science* 2004; 15(12):1483-1497.
23. Tuzlakoglu K, Bolgen N, Salgado AJ, Gomes ME, Piskin E, Reis RL. Nano- and micro-fiber combined scaffolds: a new architecture for bone tissue engineering. *Journal of Materials Science: Materials in Medicine* 2005; 16(12):1099-1104.
24. Chan CM, Ko TM, Hiraoka H. Polymer surface modification by plasmas and photons. *Surface Science Reports* 1996; 24(1-2):1-54.
25. Wang S, Cui W, Bei J. Bulk and surface modifications of polylactide. *Analytical and bioanalytical chemistry* 2005; 381(3):547-556.
26. Chu PK, Chen JY, Wang LP, Huang N. Plasma-surface modification of biomaterials. *Materials Science and Engineering: R: Reports* 2002; 36(5-6).
27. Ibnabddjalil M, Loh IH, Chu CC, Blumenthal N, Alexander H, Turner D. Effect of surface plasma treatment on the chemical, physical, morphological, and mechanical properties of totally absorbable bone internal fixation devices. *Journal of Biomedical Materials Research* 1994; 28(3):289-301.
28. Loh IH, Lin HL, Chu CC. Plasma surface modification of synthetic absorbable sutures. *Journal of Applied Biomaterials* 1992 Summer;3(2):131-146.
29. Cui NY, Brown NMD. Modification of the surface properties of a polypropylene (PP) film using an air dielectric barrier discharge plasma. *Applied Surface Science* 2002; 189(1-2):31-38.

30. Lai J, Sunderland B, Xue J, Yan S, Zhao W, Folkard M, *et al.* Study on hydrophilicity of polymer surfaces improved by plasma treatment. *Applied Surface Science* 2006; 252(10):3375-3379.
31. Liston EM, Martinu L, Wertheimer MR. Plasma surface modification of polymers for improved adhesion: a critical review. *Journal of Adhesion Science and Technology* 1993; 7(10):1091-1127.
32. Briem D, Strametz S, Schroder K, Meenen NM, Lehmann W, Linhart W, *et al.* Response of primary fibroblasts and osteoblasts to plasma treated polyetheretherketone (PEEK) surfaces. *Journal of Materials Science: Materials in Medicine* 2005; 16(7):671-677.
33. Flemming RG, Murphy CJ, Abrams GA, Goodman SL, Nealey PF. Effects of synthetic micro- and nano-structured surfaces on cell behavior. *Biomaterials* 1999; 20(6):573-588.
34. Holländer A. Surface oxidation inside of macroscopic porous polymeric materials. *Surface and Coatings Technology* 2005; 200(1-4 SPEC. ISS.):561-564.
35. Baker SC, Atkin N, Gunning PA, Granville N, Wilson K, Wilson D, *et al.* Characterisation of electrospun polystyrene scaffolds for three-dimensional in vitro biological studies. *Biomaterials* 2006; 27(16):3136-3146.
36. Gugala Z, Gogolewski S. Attachment, growth, and activity of rat osteoblasts on polylactide membranes treated with various low-temperature radiofrequency plasmas. *Journal of Biomedical Materials Research* 2006; 76(2):288-299.
37. Park K, Ju YM, Son JS, Ahn KD, Han DK. Surface modification of biodegradable electrospun nanofiber scaffolds and their interaction with fibroblasts. *Journal of Biomaterials Science* 2007; 18(4):369-382.
38. Wan Y, Qu X, Lu J, Zhu C, Wan L, Yang J, *et al.* Characterization of surface property of poly(lactide-co-glycolide) after oxygen plasma treatment. *Biomaterials* 2004; 25(19):4777-4783.
39. Yang J, Bei J, Wang S. Enhanced cell affinity of poly (D,L-lactide) by combining plasma treatment with collagen anchorage. *Biomaterials* 2002; 23(12):2607-2614.

40. Wei QF, Gao WD, Hou DY, Wang XQ. Surface modification of polymer nanofibres by plasma treatment. *Applied Surface Science* 2005; 245(1-4):16-20.
41. Lianos L, Quet C, Duc TM. Surface structural studies of polyethylene, polypropylene and their copolymers with ToF SIMS. *Surface and Interface Analysis* 1994 ;21(1):14-22.
42. Groth T, Altankov G. Studies on cell-biomaterial interaction: role of tyrosine phosphorylation during fibroblast spreading on surfaces varying in wettability. *Biomaterials* 1996; 17(12):1227-1234.
43. Webb K, Hlady V, Tresco PA. Relative importance of surface wettability and charged functional groups on NIH 3T3 fibroblast attachment, spreading, and cytoskeletal organization. *Journal of Biomedical Materials Research* 1998; 41(3):422-430.
44. Lee JH, Khang G, Lee JW, Lee HB. Interaction of Different Types of Cells on Polymer Surfaces with Wettability Gradient. *Journal of Colloidal Interface Science* 1998; 205(2):323-330.
45. Haiber S, Ai X, Bubert H, Heintze M, Bruser V, Brandl W, *et al.* Analysis of functional groups on the surface of plasma-treated carbon nanofibers. *Analytical and bioanalytical chemistry* 2003; 375(7):875-883.
46. Vogler EA, Bussian RW. Short-term cell-attachment rates: a surface-sensitive test of cell-substrate compatibility. *Journal of Biomedical Materials Research* 1987; 21(10):1197-1211.
47. Lee JH, Lee HB. A wettability gradient as a tool to study protein adsorption and cell adhesion on polymer surfaces. *Journal of Biomaterials Science* 1993; 4(5):467-481.
48. Curtis AS, Forrester JV, McInnes C, Lawrie F. Adhesion of cells to polystyrene surfaces. *The Journal of Cell Biology* 1983; 97(5 Pt 1):1500-1506.
49. Degasne I, Basle MF, Demais V, Hure G, Lesourd M, Grolleau B, *et al.* Effects of roughness, fibronectin and vitronectin on attachment, spreading, and proliferation of human osteoblast-like cells (Saos-2) on titanium surfaces. *Calcified tissue international* 1999; 64(6):499-507.

50. Hatano K, Inoue H, Kojo T, Matsunaga T, Tsujisawa T, Uchiyama C, *et al.* Effect of surface roughness on proliferation and alkaline phosphatase expression of rat calvarial cells cultured on polystyrene. *Bone* 1999; 25(4):439-445.
51. Kunzler TP, Drobek T, Schuler M, Spencer ND. Systematic study of osteoblast and fibroblast response to roughness by means of surface-morphology gradients. *Biomaterials* 2007; 28(13):2175-2182.
52. Lincks J, Boyan BD, Blanchard CR, Lohmann CH, Liu Y, Cochran DL, *et al.* Response of MG63 osteoblast-like cells to titanium and titanium alloy is dependent on surface roughness and composition. *Biomaterials* 1998 Dec;19(23):2219-2232.
53. Zinger O, Zhao G, Schwartz Z, Simpson J, Wieland M, Landolt D, *et al.* Differential regulation of osteoblasts by substrate microstructural features. *Biomaterials* 2005; 26(14):1837-1847.
54. Anselme K, Bigerelle M, Noel B, Dufresne E, Judas D, Iost A, *et al.* Qualitative and quantitative study of human osteoblast adhesion on materials with various surface roughnesses. *Journal of Biomedical Materials Research* 2000; 49(2):155-166.
55. Anselme K, Linez P, Bigerelle M, Le Maguer D, Le Maguer A, Hardouin P, *et al.* The relative influence of the topography and chemistry of TiAl6V4 surfaces on osteoblastic cell behaviour. *Biomaterials* 2000; 21(15):1567-1577.
56. Boyan BD, Lincks J, Lohmann CH, Sylvia VL, Cochran DL, Blanchard CR, *et al.* Effect of surface roughness and composition on costochondral chondrocytes is dependent on cell maturation state. *Journal of Orthopedical Research* 1999; 17(3):446-457.
57. Martin JY, Schwartz Z, Hummert TW, Schraub DM, Simpson J, Lankford J, Jr., *et al.* Effect of titanium surface roughness on proliferation, differentiation, and protein synthesis of human osteoblast-like cells (MG63). *Journal of Biomedical Materials Research* 1995; 29(3):389-401.
58. Schwartz Z, Martin JY, Dean DD, Simpson J, Cochran DL, Boyan BD. Effect of titanium surface roughness on chondrocyte proliferation, matrix production, and differentiation depends on the state of cell maturation. *Journal of Biomedical Materials Research* 1996; 30(2):145-155.

59. Anselme K, Bigerelle M. Statistical demonstration of the relative effect of surface chemistry and roughness on human osteoblast short-term adhesion. *Journal of Materials Science: Materials in Medicine* 2006; 17(5):471-479.

60. Grossner-Schreiber B, Herzog M, Hedderich J, Duck A, Hannig M, Griepentrog M. Focal adhesion contact formation by fibroblasts cultured on surface-modified dental implants: an in vitro study. *Clinical Oral Implants Research* 2006; 17(6):736-745.

61. Kononen M, Homia M, Kivilahti J, Hautaniemi J, Thesleff I. Effect of surface processing on the attachment, orientation, and proliferation of human gingival fibroblasts on titanium. *Journal of Biomedical Materials Research* 1992; 26(10):1325-1341.

## **Section IV**

### COMPLEX ORDERED FIBROUS STRUCTURES



## Chapter 4

### Differentiated Human Bone Marrow Stem Cells are Sensitive to Patterned Nanofiber Meshes?

This chapter is based on the following publication: Martins A, Alves da Silva ML, Faria S, Marques AP, Reis RL, Neves NM. *Differentiated Human Bone Marrow Stem Cells are Sensitive to Patterned Nanofiber Meshes?* Submitted.

## **4.1 Abstract**

Electrospinning has emerged as a promising polymer processing technique, enabling the production of synthetic nanofibrous structures with topographical properties similar to those found in the natural extracellular matrix of many tissues. Typically, those structures are based on randomly distributed fibers, although fiber meshes with preferential directions of alignment can be produced using specific collectors. A special-designed electroconductive collector enabled the production of a polycaprolactone (PCL) nanofiber mesh, comprising areas of fibers parallel/uniaxially aligned and areas of random/orthogonal nanofibers distribution, herein referred as patterned nanofiber meshes (P-NFM). Human bone marrow mesenchymal stem cells (hBMSCs) were seeded on those nanofibrous structures and induced to differentiate into the osteogenic lineage. Scanning electron microscopy and fluorescence microscopy analysis of cultured hBMSCs showed that the cell phenotype was sensitive to the topography of the meshes, at the earliest time points. A progressive increment on the cellular proliferation and alkaline phosphatase concentration was observed, demonstrating the onset of the hBMSCs' osteoblastic differentiation at the surface of P-NFM. Immunocytochemistry against osteopontin, bone sialoprotein and osteocalcin confirmed the osteoblastic phenotype of hBMSCs cultured on the P-NFM. Additionally, the expression of early and late genotypic markers of osteoblastic cells was higher in the P-NFM than in the typical random nanofiber meshes. It is concluded that the patterned nanofiber meshes sustain the differentiation of hBMSCs towards osteogenic lineage, associated with cell-deposition of mineralized extracellular matrix.

## **4.2 Introduction**

In the Tissue Engineering field, electrospinning has received considerable interest and research effort as a polymeric nanofibrous scaffolds production technique [1-5]. The obtained mesh-like structures are typically characterized by a random distribution of fibers with diameters in the nanometer/sub-micrometer range and, thus, by a high specific surface area. The topography and surface morphology of this

nanofibrous scaffold resembling the fibrous structure of the natural extracellular matrix (ECM) of many living tissues has been considered as a major benefit of these structures [4]. High microporosity and improved mechanical properties are also important properties of the electrospun nanofiber meshes, allowing mass transport across the structure without compromising its structural integrity. In particular these properties seem to be beneficial in the adhesion, viability, proliferation, and maturation or differentiation of different cell types, namely keratinocytes and fibroblasts [6], smooth muscle and endothelial cells [7], chondrocytes [8, 9], osteoblasts [10, 11], cardiomyocytes [12], mesenchymal stem cells [13], and neural stem cells [14]. Indeed, such fiber meshes offer specific properties, as previously referred, for inducing tissue regeneration, once cells can bridge the scaffold pores and fibers, allowing a faster and more homogeneous tissue growth.

Functional and structural engineering of musculoskeletal tissue may involve the use of appropriated cells cultured with specific growth factors in biomaterial scaffolds [15-17]. While several tissues remain an important source of therapeutic relevant differentiated cells, stem cells have emerged as a strong alternative due to their expansion potential and the fact that they can be obtained from autologous sources [18]. Additionally, advances in stem cell biology have shown that mesenchymal stem cells (MSCs) can differentiate into a variety of connective tissues, including bone, cartilage, fat, muscle and tendon, when cultured with appropriated supplemented culture media and specific environments [19]. Moreover, the successful differentiation of MSCs along these distinct lineages on electrospun nanofibrous scaffolds has been also demonstrated [13, 20-22].

In the electrospinning technique, a high voltage potential is applied to a polymeric solution held in a syringe and coupled to a pump for flow control. A jet is driven from the needle in the direction of the grounded collector. The larger diameter reduction from a millimeter fluid jet to a nanoscale solid fiber is due to an instability, where the jet is stretched by fast whipping and bending, in the way towards the collector, also involving solvent evaporation [23]. Thus, the polymeric solution properties (i.e. concentration, viscosity, surface tension, conductivity and type of solvent), the processing parameters (i.e. electric field, needle tip-to-collector distance

and polymeric flow rate) and the environmental conditions are all determinant factors for a successful electrospinning process [24, 25]. Among them, the type of collector may play an important role in the production of nanofiber meshes with different topographies. Typically, electrospun nanofibers are collected randomly in a mesh-like structure due to the bending instability associated with the electrified polymeric jets. The main topographical achievement reported in literature was the production of parallel alignment of nanofibers in meshes [24, 26]. These meshes could be produced using rotating cylinder or plate collectors, conductive metallic strips with geometrical distribution and sharp metallic pieces positioned oppositely. However, the production of electrospun nanofiber meshes with complex ordered topographies and patterns remains a challenge [27]. Recently, our group and others [28-31] described the possibility to electrospun nanofiber meshes comprising both types of topographies (random and parallel alignment of nanofibers in the same mesh), designated as patterning of polymer nanofiber meshes.

We report wherein the production of patterned nanofiber meshes by electrospinning using a specially-designed electroconductive collector, aimed at obtaining a chess-like geometry. These nanofibrous structures are characterized by areas of random/orthogonal alignment and areas of parallel/uniaxial alignment of fibers in the same mesh. Therefore, we aim at going a step forward in the nanofabrication of structures mimicking the complex ordered structure of the natural extracellular matrix. Although the processing parameters controlling the deposition and arrangement of fibers on the patterned architectures are well documented [23], the potential of patterned nanofiber meshes on the biomedical field was not explored. To test the potential of those structures for bone tissue engineering, human bone marrow mesenchymal stem cells (hBMSCs) were seeded on and induced to differentiate towards the osteogenic lineage. This cellular performance (i.e. adhesion, morphology, viability, proliferation and differentiation) was assessed at different time points to understand the influence of patterned nanofiber meshes, compared to the typical random nanofibrous structures produced by electrospinning.

## 4.3 Materials & Methods

### 4.3.1 Production of Patterned Nanofiber Meshes

A polymeric solution of poly( $\epsilon$ -caprolactone) (PCL) (TONE™, Union Carbide Chemicals and Plastics Division; New Jersey) 17 % (w/v) was prepared using a mixture of chloroform and dimethylformamide (7:3), as described elsewhere [28, 29]. A voltage of 10 kV, a current of 0,05  $\mu$ A and a needle tip-to-ground collector distance of 20 cm were selected as processing conditions after optimization. An electroconductive chess-like wire net with 1.0 mm spacing between two consecutive wires was used as collector.

### 4.3.2 Characterization of Patterned Nanofiber Meshes

Patterned electrospun PCL nanofiber meshes were gold sputter-coated (model SC502, Fisons Instruments; England) for 2 min at 15 mA. Samples were analyzed using a Scanning Electron Microscope (model S360, Leica Cambridge; England). Micrographs were recorded at 15 kV with magnifications ranging from 100 to 5000 times.

The surface topography of the patterned electrospun PCL nanofiber meshes was assessed from the noncontact profilometry using an interferometer profiler (model NT1100, Wyko-Veeco; Tucson, AZ) equipped with WycoVision® 32 analytical software. Topographic roughness parameters Ra (Roughness Average) and Rq (Root Mean Square (RMS) Roughness) were determined for each sample. Each sample was evaluated at three randomly selected and representative specimen locations.

### 4.3.3 Expansion, Seeding and Osteogenic Differentiation of Human Bone Marrow Mesenchymal Stem Cells

Human bone marrow mesenchymal stem cells (hBMSCs) (Biopredic International, France) were isolated and characterized according to the method established by Delorme and Charbord [32]. hBMSCs were expanded in basal medium consisting of Dulbecco's modified Eagle's medium (DMEM; Sigma-Aldrich, Germany)

supplemented with 10 % heat-inactivated fetal bovine serum (FBS; Biochrom AG, Germany) and 1 % antibiotic/antimycotic solution (final concentration of penicillin 100 units/ml and streptomycin 100 µg/ml; Gibco, GB). Cells were cultured in a 5 % CO<sub>2</sub> incubator at 37 °C.

Before the *in vitro* studies, the random and patterned PCL nanofiber meshes were cut in samples with areas of approximately 1 cm<sup>2</sup> and sterilized by UV irradiation during 1 h on each side of the mesh. Confluent hBMSCs at passage 2 were harvested for seeding onto the patterned PCL nanofiber meshes at a density of 1.5x10<sup>5</sup> cells/cm<sup>2</sup> of the nanofiber mesh. Random PCL nanofiber meshes were used as controls in the study. The nanofiber mesh/hBMSCs constructs were left for 48h under agitation (orbital shaker), allowing cells to arbitrarily colonize the entire surface of the mesh. After the seeding was completed, the constructs were cultured during 7, 14 and 21 days under static conditions, in standard osteogenic differentiation medium (basal medium supplemented with 50 µg/ml ascorbic acid, 10 mM β-glycerophosphate and 10<sup>-7</sup> M dexamethasone).

#### *4.3.4 Cell Morphology and Distribution*

After each culture period the constructs for fluorescence microscopy analysis were fixed in 10 % formalin solution neutral buffer (Sigma-Aldrich, Germany) for 30 min and maintained in phosphate buffer saline (PBS) until further use. The nucleus and the cytoskeleton actin filaments of the cells were fluorescently labelled with 4,6-diamidino-2-phenylindole, dilactate (DAPI; Sigma, USA; dilution 1:1000) and phalloidin-tetramethylrhodamine B isothiocyanate (Sigma, USA; dilution 1:100), respectively and the constructs analyzed using a fluorescence microscope (Zeiss, Germany).

For scanning electron microscopy (SEM) evaluation, the samples were previously fixed with 2.5 % Glutaraldehyde (Sigma; USA) in a Phosphate Buffer Saline solution (Sigma; USA) during 1h at 4 °C, and then dehydrated through an increasing series of ethanol concentrations and let to dry overnight. Finally, they were gold sputter coated (sputter coater model SC502, Fisons Instruments; England) and analysed by SEM (model S360, Leica Cambridge; England).

#### 4.3.5 Cell Viability and Proliferation (MTS assay and DNA content)

Cell viability for each culturing time was determined using the CellTiter 96<sup>®</sup> AQueous One Solution Cell Proliferation Assay (Promega; USA). This assay is based on the bioreduction of a tetrazolium compound, 3-(4,5-dimethylthiazol-2-yl)-5-(3-carboxymethoxyphenyl)-2-(4-sulfofenyl)-2H-tetrazolium [MTS], into a water soluble brown formazan product. This conversion is accomplished by NADPH or NADH production by the dehydrogenase enzymes in metabolically active cells. The absorbance was measured at 490 nm in a microplate reader (Synergie HT, Bio-Tek; USA), being related with the quantity of formazan product and directly proportional to the number of living cells in the constructs. Three samples of each nanofiber mesh, per time point, were characterized.

Cell proliferation was quantified by the total amount of double-stranded DNA, along the culturing time. Quantification was performed using the Quant-iT<sup>™</sup> PicoGreen dsDNA Assay Kit (Invitrogen<sup>™</sup>, Molecular Probes<sup>™</sup>; Oregon, USA), according to the instructions of the manufacturer. Briefly, cells in the construct were lysed by osmotic and thermal shock and the supernatant used for the DNA quantification assay. A fluorescent dye, PicoGreen, was used because of its high sensitivity and specificity to double-stranded DNA. The fluorescence of the dye was measured at an excitation wavelength of 485/20 nm and at an emission wavelength of 528/20 nm, in a microplate reader (Synergie HT, Bio-Tek; USA). Triplicates were made for each sample and per culturing time. The DNA concentration for each sample was calculated using a standard curve (DNA concentration ranging from 0.0 to 1.5 µg/ml) relating quantity of DNA and fluorescence intensity.

#### 4.3.6 Alkaline Phosphatase quantification and Immunodetection of Bone-specific Proteins

The concentration of alkaline phosphatase (ALP) was determined for all time culture periods, using the same samples used for DNA quantification. Briefly, the activity of ALP was assessed using the p-nitrophenol assay. Nitrophenyl phosphate disodium salt (pnPP; Fluka BioChemika, Austria), which is colourless, is hydrolysed

by alkaline phosphatase at pH 10.5 and temperature of 37 °C to form free *p*-nitrophenol, which is yellow. The reaction was stopped by addition of 2M NaOH (Panreac Quimica, Spain) and the absorbance read at 405 nm in a microplate reader (Bio-Tek, Synergie HT; USA). Standards were prepared with 10 µmol/ml *p*-nitrophenol (pNP; Sigma, USA) solution, to obtain a standard curve ranging from 0.0 to 0.3 µmol/ml. Triplicates of each sample and standard were made, and the ALP concentrations read off from the standard curve.

The osteogenic phenotype of hBMSCs seeded onto the patterned PCL nanofiber meshes was also assessed by the immunodetection of bone-specific proteins. Immunocytochemistry was performed following the streptavidin-biotin-peroxidase complex approach (R.T.U. Vectastain<sup>®</sup> Universal Elite<sup>®</sup> ABC kit; Vector Laboratories Inc., Burlingame, CA), using a rabbit polyclonal antibody against osteopontin (Abcam Ltd., Cambridge, UK; dilution 1:1500), a mouse monoclonal antibody against osteocalcin (clone OC4-30, Abcam Ltd., Cambridge, UK; dilution 1:100) and a rabbit polyclonal antibody against bone sialoprotein II (Chemicon<sup>®</sup> International Inc., Germany; dilution 1:2500). Prior to the immunocytochemistry procedure, constructs were fixed in 10 % formalin solution neutral buffer (Sigma-Aldrich, Germany) for 30 min and maintained in phosphate buffer saline (PBS) until further use. The constructs were treated with 0.3 % hydrogen peroxide in methanol during 30 min to inactivate the endogenous peroxidases. After washing with PBS, the constructs were blocked with 2.5 % normal horse serum for 20 min at room temperature to avoid unspecific reactions. Primary antibodies were incubated overnight at 4 °C. Negative controls were set in the absence of primary antibodies incubation. After washing in PBS, the samples were incubated for 30 min with biotinylated secondary antibody anti-rabbit/mouse IgG, followed by incubation with streptavidin-peroxidase complex (Elite ABC Reagent). The immune reaction was visualized using DAB as a chromogen (DAB Substrate Reagent from Peroxidase Substract Kit; Vector Laboratories Inc, Burlingame, CA).

**Table 4.1** - Primers list of osteogenic markers.

<b>Gene</b>		<b>Primer sequences (5'-3')</b>	<b>T<sub>m</sub> [°C]</b>
<i>ALP</i>	sense	CTCCTCGGAAGACACTCTG	60,0
	antisense	AGACTGCGCCTGGTAGTTG	
<i>OP</i>	sense	GGGGACA AACTGGAGTGAAAA	58,4
	antisense	CCCACAGACCCTTCCAAGTA	
<i>BSP</i>	sense	CAACAGCACAGAGGCAGAAAAC	59,9
	antisense	CCTCGTATTCAACGGTGGTG	
<i>OC</i>	sense	CTGAGAGGAGCAGAACTGG	61,4
	antisense	GGCAGCGAGGTAGTGAAGAG	
<i>Runx2</i>	sense	TTCCAGACCAGCAGCACTC	58,1
	antisense	CAGCGTCAACACCATCATTC	
<i>Osterix</i>	sense	CCCTTTACAAGCACTAATGG	57,1
	antisense	ACACTGGGCAGACAGTCAG	
<i>GAPDH</i>	sense	ACAGTCAGCCGCATCTTCTT	58,4
	antisense	GACAAGCTTCCCGTTCTCAG	

#### 4.3.7 RNA isolation and Real-Time Quantitative Polymerase Chain Reaction

Total RNA from the constructs was extracted using the Trizol<sup>®</sup> (Invitrogen, Life Technologies Inc., UK) method according to the manufacturer's directions. Briefly, at each culturing time the constructs were washed with PBS, immersed in Trizol and storage at -80 °C until further use. Proteins were removed with chloroform extraction, and the RNA pellets were washed once with isopropyl alcohol and once with 70 % ethanol. The total RNA pellets were reconstituted in Rnase free water (Gibco, Invitrogen, UK).

Reverse transcriptase (RT)-PCR was performed according to the protocol from iScript<sup>™</sup> cDNA synthesis kit (BioRad, Hercules, CA, USA). Briefly, a reaction mixture consisting of 1X iScript Reaction Mix, 1 µl iScript Reverse Transcriptase, RNA template (up to 1 µg total RNA) and nuclease-free water was prepared, in 20 µl of total volume. The single-strand cDNA synthesis occurred by incubating the complete reaction mixture 5 min at 25 °C, followed by 30 min at 42 °C and terminated by an incubation at 85 °C for 5 min.

Amplification of the target cDNA for real-time PCR quantification were performed according to manufacturer, using 2 µl RT cDNA products, 1 µM each primer (bone-specific primer sets listed in Table 4.1), 1X iQ SYBR Green Supemix (BioRad,

Hercules, CA, USA) and nuclease-free water, in a final volume of 25  $\mu$ L. Forty-four cycles of denaturation (95  $^{\circ}$ C, 10 s), annealing (temperature dependent on the gene, 30 s) and extension (72  $^{\circ}$ C, 30 s) were carried out in the gradient thermocycler MiniOpticon real-time PCR detection system (BioRad, Hercules, CA, USA) for all genes. The transcripts expression data were normalized to the housekeeping gene glyceraldehydes-3-phosphate-dehydrogenase (*GAPDH*) and the relative quantification calculated by the  $\Delta C_T$  method.

#### 4.3.8 Statistical Analysis

Statistical Analysis was performed using the SPSS statistic software (Release 15.0.0 for Windows). Firstly, a Shapiro-Wilk test was used to ascertain about the data normality. The results indicated that nonparametric tests should be used for all comparisons. A Mann-Whitney U test was performed to analyze the effect of the random and patterned electrospun nanofibrous structures on the hBMSCs'-derived phenotype (cellular proliferation and ALP quantification) and osteogenic genotype. *P* values lower than 0.01 were considered statistically significant.

### 4.4 Results and Discussion

#### 4.4.1 Morphological Characterization of Patterned Nanofiber Meshes

Typically, a random distribution of nanofibers is obtained in a static flat collector, caused by the chaotic motion of polymeric solution during the electrospinning process (Figure 4.1 A). However, when a metallic conducting wire net was used as collector, two distinct areas of nanofiber deposition (Figure 4.1 B), reproducing the architecture of the collector used, were obtained [29, 30]. The fibers appear aligned and collapsed on the electroconductive wires of the collector and, consequently, where the electric field is more intense (Figure 4.1 C). This area is characterized by significantly larger fiber densities, due to the preferential deposition and fiber agglomeration, which is believed to be caused by the excess of residual solvent during the deposition process. Consequently, in this area of parallel/uniaxial

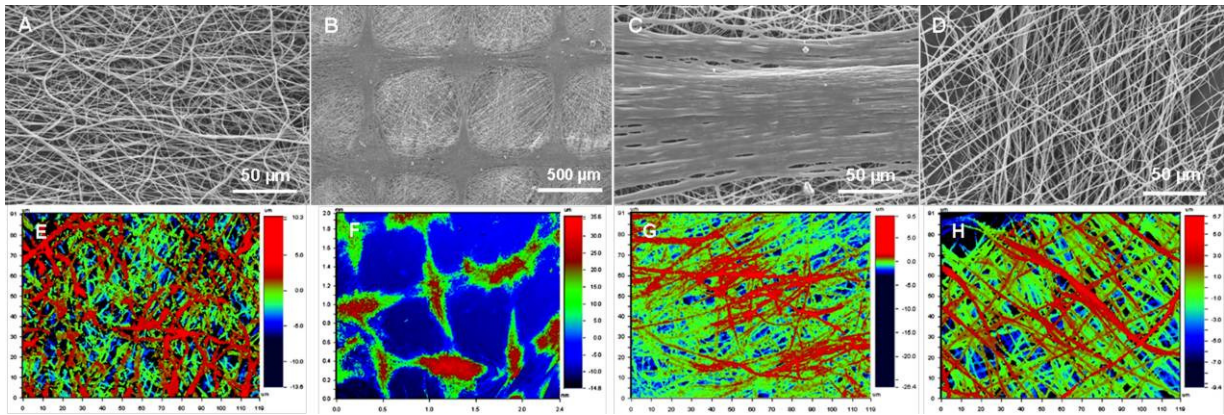


**Figure 4.1** - SEM micrographs (A-D) and optical profilometric images (E-H) of the typical random (A and E) and patterned (B and F) nanofiber meshes (P-NFM). P-NFM comprise areas of parallel/uniaxial (C and G) and orthogonal (D and H) alignment of the fibers.

alignment, the average roughness, determined by interferometric optical profilometry is significantly smaller ( $R_a = 789,68 \text{ nm}$ ) (Figure 4.1 G), when compared to the random nanofiber meshes (PCL NFM) ( $R_a = 1,93 \mu\text{m}$ ) (Figure 4.1 E). In the spacing between the wires, the nanofibers deposition followed an orthogonally aligned pattern and a lower density (Figure 4.1 D). The roughness parameter analysis revealed a smooth surface in the orthogonal alignment area ( $R_a = 1,79 \mu\text{m}$ ) (Figure 4.1 H), when compared with the typical random nanofiber meshes (Figure 4.1 E).

It is well known that materials with ordered microstructures and patterns may possess specific interest functions useful in numerous applications, such as microelectronic, photonic, and biomedical applications [33]. As previously mentioned and herein described [28, 29], our group has the possibility to electrospinning nanofiber meshes with controlled microstructure and pattern structures, demonstrating their potential for biomedical applications. In fact, those patterned structures were initially developed in an attempt to control the morphological and, consequently, the mechanical properties of the nanofiber meshes. It was demonstrated that P-NFM present a tensile modulus of  $2.0 \pm 0.2 \text{ MPa}$ , what was lower than expected due to the high degree of fiber alignment [29]. However, the orthogonal fiber alignment in the mesh associated with uniaxial fiber alignment, transversal to the testing of the main tensile test direction, explain the observed value of the modulus.

Those transversely aligned fibers could control the strain in the tensile test, causing a more compliant behaviour of the P-NFM. Even so, the semi-crystalline property of PCL is likely to have a beneficial effect on the structural integrity of the scaffold, maintaining the size and the shape of the original P-NFM, without observable macroscopic shrinkage.

#### 4.4.2 *Phenotypic Characterization of Differentiated hBMSCs on Patterned Nanofiber Meshes*

Various studies demonstrated that electrospun PCL scaffolds exhibited optimal structural integrity and supported desirable cellular proliferation and differentiation (MSCs differentiated into osteoblastic- and chondrocytic-like cells) *in vitro* [9, 20, 21, 34, 35]. In addition, 3-D porous networks, composed of PCL and collagen (COL) (1:1), produced by multilayered organization of electrospun nanofiber membranes appeared to support hBMSCs attachment [36]. Subcutaneous implantation of the cultured construct into nude mice demonstrated good integration with the surrounding tissues and neovascularisation. Electrospun PCL scaffolds seeded with autologous mesenchymal stem cells (MSCs) were studied as bone grafts for the regeneration of the omenta of rats [37]. The cell/scaffold constructs were cultured under osteogenic supplementation, in a rotating bioreactor, before implantation. Those studies show the interest of electrospun nanofibrous scaffolds as bone grafts.

The search for surfaces and structures having strong, well-defined, beneficial influence on cell growth is an active subject of contemporary research [3, 38]. In fact, it was demonstrated that cells are sensitive to the topography of the supporting surface, although the exact reasons for this observation are unclear. In our previous studies with patterned nanofiber meshes, direct contact tests with human osteoblast-like cells demonstrated a preferential cell adhesion to regions of random/orthogonal fiber alignment, although some cells were aligned with the regions of parallel orientation [28, 29]. Initially, in the present study, hBMSCs were seeded on random and patterned PCL nanofiber meshes (P-NFM) to verify the influence of nanofiber mesh topography on cell morphology and distribution. SEM micrographs

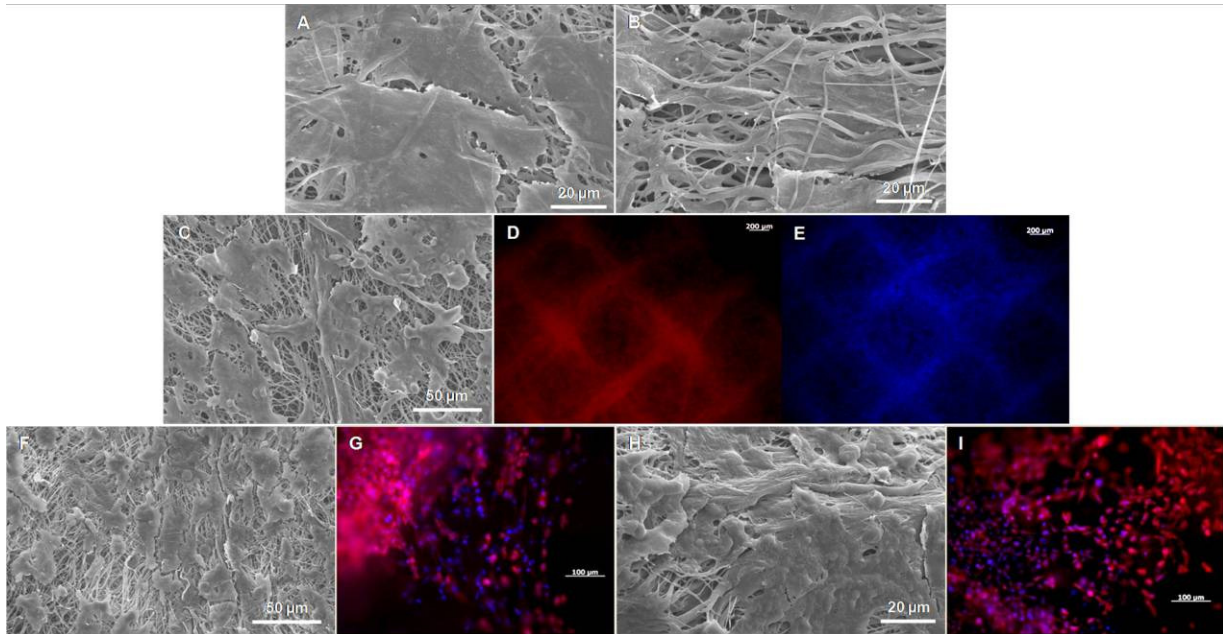


**Figure 4.2** - SEM micrographs of undifferentiated hBMSCs cultured on patterned nanofiber meshes, at the random/orthogonal area of alignment (**A**) and at the parallel/uniaxial fibers (**B**). SEM micrographs (**C**, **F** and **H**) and fluorescence images (**D**, **E**, **G** and **I**) of hBMSCS induced to differentiate into the osteogenic lineage at days 7 (**C-E**), 14 (**F-G**) and 21 (**H-I**) of culture.

demonstrated that undifferentiated cells respond differently to the areas of P-NFM (Figure 4.2). In orthogonally distributed nanofibers, cells presented the typical fibroblastic morphology of undifferentiated hBMSCs (Figure 4.2 A). In the area of parallel/uniaxial alignment, hBMSCs attached and spread along the aligned nanofibers of the patterned fiber meshes (Figure 4.2 B). Thus, the patterned nanofibrous scaffolds created in this study were found to dictate cellular morphology, with cell polarity following the established fiber direction. These observations are supported by a recent study showing that hMSCs maintained their phenotypic shape when seeded on randomly oriented scaffolds, and a guided growth with actin organization dictated by the prevailing nanofiber orientation of aligned nanofiber meshes [39]. Overall, the results in literature demonstrate that the highly oriented electrospun PCL nanofibers are capable of supporting cell attachment and proliferation of hMSCs.

Considering the previous findings, hBMSCs were induced to differentiate into the osteogenic lineage, aiming to understand the influence of the P-NFM on the osteogenic differentiation of hBMSCs, when compared with the typical PCL NFM. SEM and fluorescence microscopy characterization of cell adhesion and morphology showed cell response to the topography of the P-NFM, being spread in the area of nanofibers parallel/uniaxial alignment (Figure 4.2 C-E). This tendency is very clear in the earliest time culture period (7 days) due to the amount of dispersed cells onto the nanofiber mesh and the morphology of undifferentiated hBMSCs. For longer time culture periods, the cell numbers increase progressively and only in the outer regions of the mesh, where lower density of cells is present, was possible to observed cell alignment by the nanofibers (Figure 4.2 F-I). Furthermore, at those later culturing times, hBMSCs start to differentiate into the osteoblastic lineage and the cells tend to

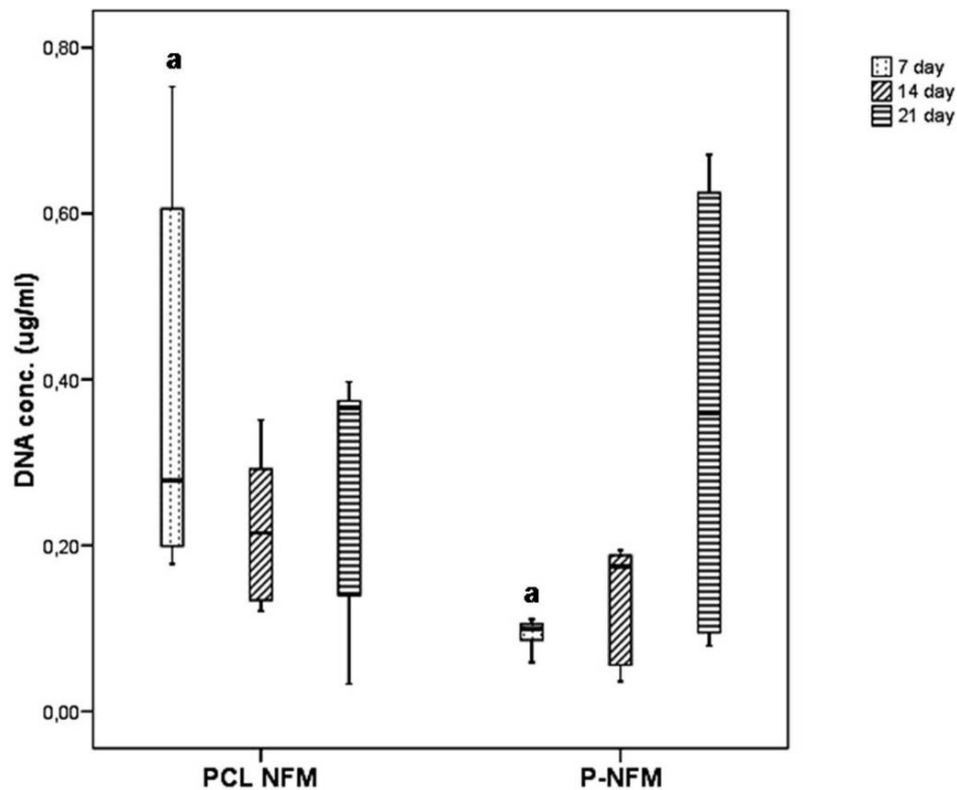


**Figure 4.3** – Box plot of DNA content of hBMSCS induced to differentiate into the osteogenic lineage during 21 days, cultured on random and patterned nanofiber meshes. Data were analysed by the non-parametric method of Mann-Whitney U test. **a**,  $p < 0.01$

show a more polygonal shape. This increment on the cell numbers was confirmed by the cellular proliferation assay, by quantification of the double strand DNA content (Figure 4.3). DNA content of hBMSCs, induced to differentiate into the osteogenic lineage, increases progressively with culture time on P-NFM. In fact, it was only found a highly significant difference ( $p < 0.00001$ ) between the PCL NFM and P-NFM for 7 days of culture in terms of DNA concentration.

Osteoblastic differentiation of hBMSCs was pursued on P-NFM by the quantification of the alkaline phosphatase (ALP). Indeed, ALP production is a distinctive biochemical indicator of the presence of osteoblasts, since MSCs produce negligible amounts of this enzyme. It can be observed in Figure 4.4 that, the ALP concentration values increases progressively along time in culture of hBMSCs, when seeded on the patterned nanofiber meshes, reaching a median maximum value at 14

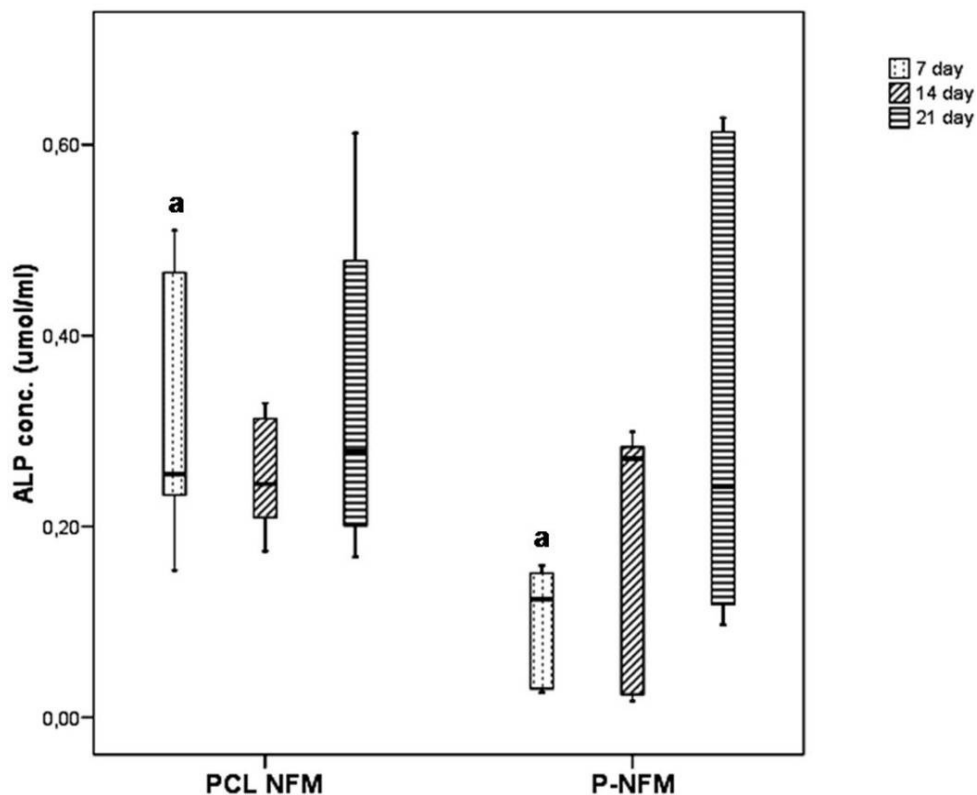


**Figure 4.4** – Box plot of ALP quantification from hBMSCS induced to differentiate into the osteogenic lineage during 21 days, cultured on random and patterned nanofiber meshes. Data were analysed by the non-parametric method of Mann-Whitney U test. **a**,  $p < 0.01$

days of culture under osteogenic differentiation conditions. The corresponding values of the ALP concentration, for PCL NFM, maintain a constant value along time. Additionally, it was only found a highly significant difference ( $p < 0.00001$ ) between the PCL NFM and P-NFM for 7 days of culture, in terms of ALP concentration. Immunocytochemistry against some bone-specific proteins, namely osteopontin, osteocalcin and bone sialoprotein, was performed to confirm the osteogenic phenotype of hBMSCs seeded onto the P-NFM. Photomicrographs showed a

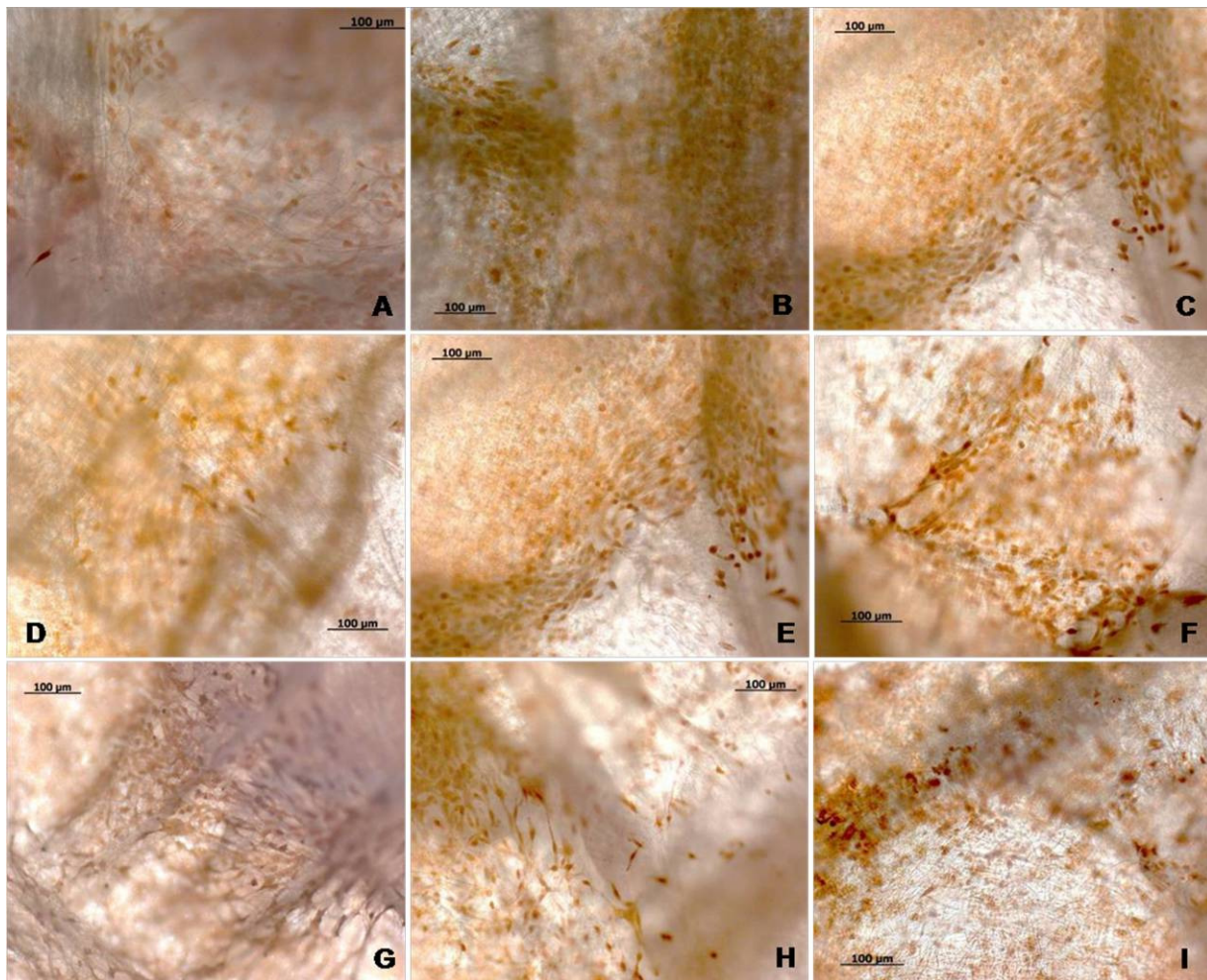


**Figure 4.5** - Optical images of immunodetected osteogenic markers, namely osteopontin (**A-C**), bone sialoprotein (**D-F**) and osteocalcin (**G-I**), expressed by hBMSCs, induced to differentiate into the osteogenic lineage and cultured on patterned nanofiber meshes during 7 (**A, D and G**), 14 (**B, E and H**) and 21 (**C, F and I**) days.

progressive expression of specific osteoblastic glycoproteins (i.e. osteopontin and bone sialoprotein) on hBMSCs/patterned nanofiber meshes constructs along the culturing period (Figure 4.5), indicating their capability to deposit mineralized extracellular matrix (ECM) mainly in the areas of parallel/uniaxial alignment of the nanofibers. In fact, these phosphorylated glycoproteins are also present in the ECM of bone. The deposition of mineralized ECM was also confirmed by the immunodetection of osteocalcin protein, which binds strongly to apatite and calcium. In addition, the increased concentration of the enzyme alkaline phosphatase (ALP) until 14 days of hBMSCs culture also confirm the osteoblastic differentiation and mineralization of hBMSCs on patterned nanofiber meshes; because this enzyme catalyses the splicing of phosphate from non-phosphoric esters, constituting an early biochemical marker of osteogenesis and deposition of mineralized ECM. These observations are corroborated by a study where hybrid random nanofibrous scaffolds, consisting of PCL, poly(vinyl alcohol) (PVA) and chitosan, were used to culture MSCs and successfully sustained the induced differentiation into osteoblasts [40].

#### 4.4.3 Genotypic Characterization of Differentiated hBMSCs on Patterned Nanofiber Meshes

Complementary to previous biological data, the differentiation level of seeded hBMSCs on P-NFM was assessed by quantitative PCR of mRNA transcripts of some bone-specific genes. The relative expression of those genes was normalized against the housekeeping gene *GAPDH* and compared to hBMSCs cultured and differentiated on PCL NFM. From the analysis of Figure 4.6, it was observed that some transcript levels, namely *Alkaline Phosphatase*, *Runx2* and *Osterix*, shown the tendency to be increasingly expressed on P-NFM, during the 21 days of culture. The remaining transcripts, specifically the *Bone Sialoprotein* and the *Osteocalcin*, were expressed at stable levels during the period in culture, with the exception of *Osteopontin* which presented the highest expression at 14 days. Recently, it was reported the expression pattern of osteoblastic markers during the differentiation of embryonic stem (ES) cells [41]. Three periods were defined: a proliferative phase,

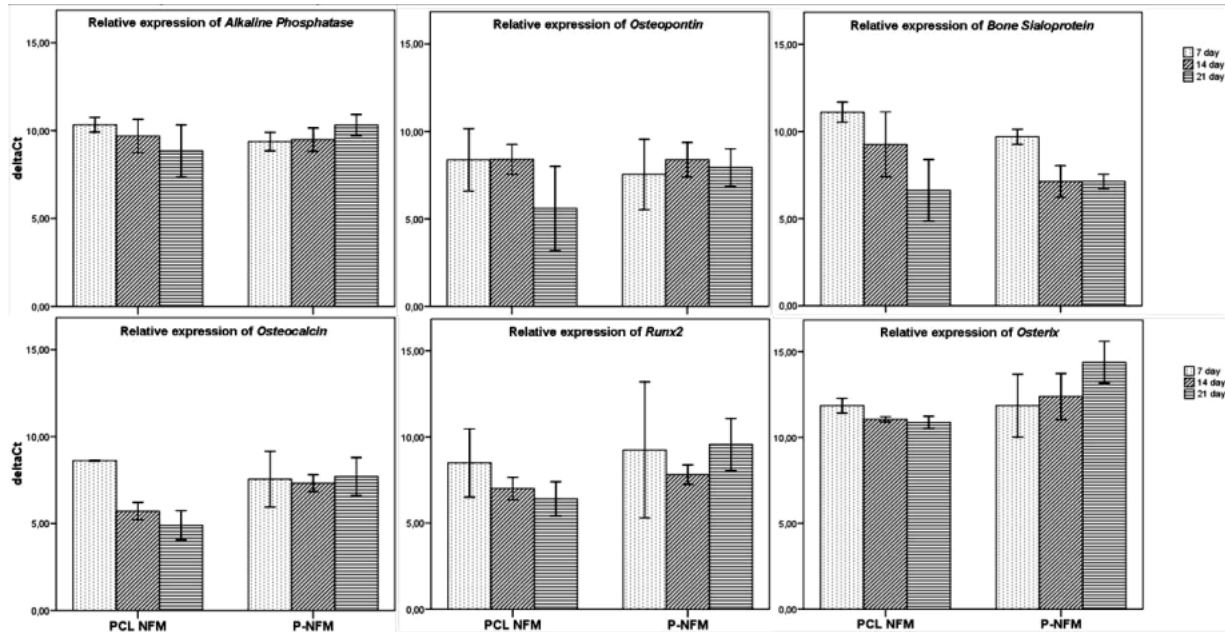


**Figure 4.6** – Relative expression of bone-specific transcripts, namely *Alkaline Phosphatase*, *Osteopontin*, *Bone Sialoprotein*, *Osteocalcin*, *Runx2* and *Osterix*, by hBMSCs induced to differentiate into the osteogenic lineage during 21 days, cultured on random and patterned nanofiber meshes. The expression of these genes was normalized against the housekeeping gene *GAPDH* and calculated by the  $\Delta C_T$  method.

followed by the period of matrix deposition and the mineralization phase. At the end of the matrix deposition phase and the beginning of the mineralization phase, *Osteopontin* mRNA is expressed. *Bone Sialoprotein* is expressed during the mineralization phase, corresponding to the presence of mature osteoblasts. Finally, *Osteocalcin* mRNA is expressed at very high level and so is designed as the essential marker of the mineralization phase. Thus, considering our results and the differences in the cell type used, the most important genes involved in the mineralization process (i.e. *Osteopontin*, *Bone Sialoprotein* and *Osteocalcin* genes) were constitutively expressed, confirming the matrix deposition and mineralization by hBMSCs cultured and differentiated on P-NFM. The main specific transcription factors involved in the osteogenesis were also quantified by qPCR, namely the core binding factor  $\alpha$  1/runt-related gene (*Cbfa1/Runx2*) and *Osterix* (*Osx*). *Cbfa1/Runx2* has been shown to preferentially initiate two steps of the differentiation process, stem cells into

preosteoblasts and preosteoblasts into osteoblasts, whereas *Osterix* acts only during the last preosteoblast/osteoblast stage [42, 43]. Our results showed that *Osterix* was the bone-specific transcript with the highest expression relative to the housekeeping gene (*GAPDH*), accompanied by the progressive expression of *Runx2*, corroborating the successful osteogenic differentiation of hBMSCs on P-NFM.

Altogether, the results from phenotypic and genotypic characterization demonstrated the effectiveness of P-NFM on the differentiation of hBMSCs into osteoblastic cells and, consequently, in the deposition of mineralized ECM. Furthermore, this specific substrate topography could promote a favorable biological response, such as cell guidance and proliferation. Recently, a study demonstrated that ligament fibroblasts cultured on aligned nanofibrous meshes produce more collagen than random meshes [44]. Indeed, material structures with parallel orientation or patterns of different ordering may have specific biological performance on tissue engineering [38, 44, 45]. Therefore, it is hypothesized that by creating an initial synthetic ECM architecture - scaffold - , cell-formed ECM will be deposited along the predefined fiber direction in greater amounts in these patterned nanofibrous scaffolds, facilitating the formation of a neo-tissue with enhanced functional characteristics.

#### **4.5 Conclusions**

The phenotype of hBMSCs was sensitive to the unique microtopography of P-NFM, inducing cell orientation along the uniaxially aligned fibers, mainly at earlier culturing periods under basal and osteogenic differentiation conditions. The unique topography of the patterned scaffold sustains the deposition of mineralized extracellular matrix, as observed by the immunodetection of osteoblast-specific glycoproteins (i.e. osteopontin and bone sialoprotein), as well as of osteocalcin protein, associated with an increased ALP concentration. Additionally, the progressive expression of bone-specific transcripts confirmed the osteogenic genotype of cultured hBMSCs on P-NFM. Our observations indicate that the presence of ordered microstructures and patterns support the development of bony-like engineered

substitutes. The application of those P-NFM for complex ordered tissues involving more than one cell communities may provide helpful cues enabling its self-assembling.

#### 4.6 References

1. Pham QP, Sharma U, Mikos AG. Electrospinning of polymeric nanofibers for tissue engineering applications: a review. *Tissue Engineering* 2006; 12(5):1197-1211.

2. Ashammakhi N, Ndreu A, Piras AM, Nikkola L, Sindelar T, Ylikauppila H, *et al.* Biodegradable nanomats produced by electrospinning: Expanding multifunctionality and potential for tissue engineering. *Journal of Nanoscience and Nanotechnology* 2007; 7(3):862-882.

3. Lannutti J, Reneker D, Ma T, Tomasko D, Farson D. Electrospinning for tissue engineering scaffolds. *Materials Science and Engineering C - Biomimetic Supramolecular Systems* 2007; 27(3):504-509.

4. Martins A, Araujo JV, Reis RL, Neves NM. Electrospun nanostructured scaffolds for tissue engineering applications. *Nanomedicine* 2007; 2(6):929-942.

5. Martins A, Reis RL, Neves NM. Electrospinning: Processing technique for tissue engineering scaffolding. *International Materials Reviews* 2008; 53(5):257-274.

6. Min BM, Lee G, Kim SH, Nam YS, Lee TS, Park WH. Electrospinning of silk fibroin nanofibers and its effect on the adhesion and spreading of normal human keratinocytes and fibroblasts in vitro. *Biomaterials* 2004; 25(7-8):1289-1297.

7. Xu CY, Inai R, Kotaki M, Ramakrishna S. Electrospun nanofiber fabrication as synthetic extracellular matrix and its potential for vascular tissue engineering. *Tissue Engineering* 2004; 10(7-8):1160-1168.

8. Li WJ, Danielson KG, Alexander PG, Tuan RS. Biological response of chondrocytes cultured in three-dimensional nanofibrous poly( $\epsilon$ -caprolactone) scaffolds. *Journal of Biomedical Materials Research - Part A* 2003; 67A(4):1105-1114.

9. Alves da Silva MA, Crawford A, Mundy J, Martins A, Araújo JV, Hatton PV, *et al.* Evaluation of extracellular matrix formation in PCL and SPCL nanofiber meshes

when seeded with bovine articular chondrocytes. *Tissue Engineering, Part A* 2009; 15:377-385.

10. Fujihara K, Kotaki M, Ramakrishna S. Guided bone regeneration membrane made of polycaprolactone/calcium carbonate composite nano-fibers. *Biomaterials* 2005; 26(19):4139-4147.

11. Araujo JV, Martins A, Leonor IB, Pinho ED, Reis RL, Neves NM. Surface controlled biomimetic coating of polycaprolactone nanofiber meshes to be used as bone extracellular matrix analogues. *Journal of Biomaterials Science - Polymer Edition* 2008; 19(10):1261-1278.

12. Shin M, Ishii O, Sueda T, Vacanti JP. Contractile cardiac grafts using a novel nanofibrous mesh. *Biomaterials* 2004; 25(17):3717-3723.

13. Li WJ, Tuli R, Huang XX, Laquerriere P, Tuan RS. Multilineage differentiation of human mesenchymal stem cells in a three-dimensional nanofibrous scaffold. *Biomaterials* 2005; 26(25):5158-5166.

14. Yang F, Xu CY, Kotaki M, Wang S, Ramakrishna S. Characterization of neural stem cells on electrospun poly(L-lactic acid) nanofibrous scaffold. *Journal of Biomaterials Science - Polymer Edition* 2004; 15(12):1483-1497.

15. Gomes ME, Reis RL. Biodegradable polymers and composites in biomedical applications: From catgut to tissue engineering Part 1 Available systems and their properties. *International Materials Reviews* 2004; 49(5):261-273.

16. Hutmacher DW. Scaffolds in tissue engineering bone and cartilage. *Biomaterials* 2000; 21(24):2529-2543.

17. Salgado AJ, Coutinho OP, Reis RL. Bone tissue engineering: State of the art and future trends. *Macromolecular Bioscience* 2004; 4(8):743-765.

18. Bajada S, Mazakova I, Richardson JB, Ashammakhi N. Updates on stem cells and their applications in regenerative medicine. *Journal of Tissue Engineering and Regenerative Medicine* 2008; 2(4):169-183.

19. Pittenger MF, Mackay AM, Beck SC, Jaiswal RK, Douglas R, Mosca JD, *et al.* Multilineage potential of adult human mesenchymal stem cells. *Science* 1999; 284(5411):143-147.

20. Li WJ, Tuli R, Okafor C, Derfoul A, Danielson KG, Hall DJ, *et al.* A three-dimensional nanofibrous scaffold for cartilage tissue engineering using human mesenchymal stem cells. *Biomaterials* 2005; 26(6):599-609.

21. Yoshimoto H, Shin YM, Terai H, Vacanti JP. A biodegradable nanofiber scaffold by electrospinning and its potential for bone tissue engineering. *Biomaterials* 2003; 24(12):2077-2082.

22. Xin XJ, Hussain M, Mao JJ. Continuing differentiation of human mesenchymal stem cells and induced chondrogenic and osteogenic lineages in electrospun PLGA nanofiber scaffold. *Biomaterials* 2007; 28(2):316-325.

23. Doshi J, Reneker DH. Electrospinning process and applications of electrospun fibers. *Journal of Electrostatic* 1995; 35(2-3):151-160.

24. Li D, Xia YN. Electrospinning of nanofibers: Reinventing the wheel? *Advanced Materials* 2004; 16(14):1151-1170.

25. Rutledge GC, Fridrikh SV. Formation of fibers by electrospinning. *Advanced Drug Delivery Reviews* 2007; 59(14):1384-1391.

26. Murugan R, Ramakrishna S. Design Strategies of Tissue Engineering Scaffolds with Controlled Fiber Orientation. *Tissue Engineering* 2007; 13:1845-1866.

27. Martins A, Chung S, Pedro AJ, Sousa RA, Marques AP, Reis RL, *et al.* Hierarchical starch-based fibrous scaffold for bone tissue engineering applications. *Journal of Tissue Engineering and Regenerative Medicine* 2009; 3(1):37-42.

28. Martins A, Cunha J, Macedo F, Reis RL, Neves NM. Improvement of polycaprolactone nanofibers topographies: Testing the influence in osteoblastic proliferation. *NSTI Nanotech 2006 Technical Proceedings*; Boston, MA; 2006. p. 148-151.

29. Neves NM, Campos R, Pedro A, Cunha J, Macedo F, Reis RL. Patterning of polymer nanofiber meshes by electrospinning for biomedical applications. *International Journal of Nanomedicine* 2007; 2(3):1-16.

30. Zhang D, Chang J. Patterning of electrospun fibers using electroconductive templates. *Advanced Materials* 2007; 19(21):3662-3667.

31. Zhang D, Chang J. Electrospinning of three-dimensional nanofibrous tubes with controllable architectures. *Nano letters* 2008; 8(10):3283-3287.

32. Delome B, Charbord P. Culture and characterization of human bone marrow mesenchymal stem cells. *Methods in Molecular Medicine* 2007; 140:67-81.
33. Whitesides GM. The 'right' size in nanobiotechnology. *Nature Biotechnology*; 21(10):1161-1165.
34. Li WJ, Cooper JA, Jr., Mauck RL, Tuan RS. Fabrication and characterization of six electrospun poly(alpha-hydroxy ester)-based fibrous scaffolds for tissue engineering applications. *Acta Biomaterialia* 2006; 2(4):377-385.
35. Martins A, Pinho ED, Faria S, I. P, Marques AP, Reis RL, *et al.* Surface Modification of Electrospun Polycaprolactone Nanofiber Meshes by Plasma Treatment to Enhance its Biological Performance. *Small* 2009; 5(10):1195-1206.
36. Srouji S, Kizhner T, Suss-Tobi E, Livne E, Zussman E. 3-D Nanofibrous electrospun multilayered construct is an alternative ECM mimicking scaffold. *Journal of Materials Science* 2008; 19(3):1249-1255.
37. Shin M, Yoshimoto H, Vacanti JP. In vivo bone tissue engineering using mesenchymal stem cells on a novel electrospun nanofibrous scaffold. *Tissue Engineering* 2004; 10(1-2):33-41.
38. Dalby MJ, Gadegaard N, Tare R, Andar A, Riehle MO, Herzyk P, *et al.* The control of human mesenchymal cell differentiation using nanoscale symmetry and disorder. *Nature Materials* 2007; 6(12):997-1003.
39. Li WJ, Mauck RL, Cooper JA, Yuan X, Tuan RS. Engineering controllable anisotropy in electrospun biodegradable nanofibrous scaffolds for musculoskeletal tissue engineering. *Journal of Biomechanics* 2007; 40(8):1686-1693.
40. Mohammadi Y, Soleimani M, Fallahi-Sichani M, Gazme A, Haddadi-Asl V, Arefian E, *et al.* Nanofibrous poly(epsilon-caprolactone)/poly(vinyl alcohol)/chitosan hybrid scaffolds for bone tissue engineering using mesenchymal stem cells. *The International Journal of Artificial Organs* 2007; 30(3):204-211.
41. zur Nieden NI, Kempka G, Ahr HJ. In vitro differentiation of embryonic stem cells into mineralized osteoblasts. *Differentiation* 2003; 71(1):18-27.
42. Ryoo HM, Lee MH, Kim YJ. Critical molecular switches involved in BMP-2-induced osteogenic differentiation of mesenchymal cells. *Gene* 2006; 366(1):51-57.

43. Satija NK, Gurudutta GU, Sharma S, Afrin F, Gupta P, Verma YK, *et al.* Mesenchymal stem cells: molecular targets for tissue engineering. *Stem Cells and Development* 2007; 16(1):7-23.

44. Lee CH, Shin HJ, Cho IH, Kang YM, Kim IA, Park KD, *et al.* Nanofiber alignment and direction of mechanical strain affect the ECM production of human ACL fibroblast. *Biomaterials* 2005; 26(11):1261-1270.

45. Zong X, Bien H, Chung CY, Yin L, Fang D, Hsiao BS, *et al.* Electrospun fine-textured scaffolds for heart tissue constructs. *Biomaterials* 2005; 26(26):5330-5338.

## Chapter 5

### Hierarchical Starch-based Fibrous Scaffold for Bone Tissue Engineering Applications

This chapter is based on the following publication: Martins A, Chung S, Pedro AJ, Sousa RA, Marques AP, Reis RL, Neves NM. *Hierarchical starch-based fibrous scaffolds for bone tissue engineering applications*. Journal of Tissue Engineering and Regenerative Medicine 2009; 3(1):37-42.

## 5.1. Abstract

Fibrous structures mimicking the morphology of the natural extracellular matrix are considered promising scaffolds for tissue engineering. This work aims to develop a novel hierarchical starch-based scaffold. Such scaffolds were obtained by a combination of starch-polycaprolactone micro- and polycaprolactone nano-motifs, respectively produced by rapid prototyping (RP) and electrospinning techniques. Scanning electron microscopy (SEM) and micro-computed tomography analysis showed the successful fabrication of a multilayer scaffold composed of parallel aligned microfibers in a grid-like arrangement, intercalated by a mesh-like structure with randomly distributed nanofibers (NFM). Human osteoblast-like cells were dynamically seeded on the scaffolds, using spinner flasks, and cultured during 7 days under static conditions. SEM analysis showed predominant cell attachment and spreading on the nanofiber meshes, which enhanced cell retention at the bulk of the composed/hierarchical scaffolds. A significant increment in cell proliferation and osteoblastic activity, assessed by alkaline phosphatase quantification, was observed on the hierarchical fibrous scaffolds. These results support our hypothesis that the integration of nanoscale fibers into 3D rapid prototype scaffolds substantially improves their biological performance in bone tissue engineering strategies.

## 5.2. Introduction

Biodegradable scaffolds are generally recognized as indispensable element in tissue engineering and regenerative medicine strategies. They are used as temporary templates for cell seeding, migration, proliferation and differentiation prior to the regeneration of biologically functional tissue or natural extracellular matrix (ECM) [1, 2]. Ideally, to create a tissue-engineered construct capable of regenerating a fully functional tissue, it should mimic both the fibrous form and the complex function of the native ECM [3]. Like natural ECM, a range of topographic features at the macro-, micro- and even nano-scale levels must lead cell response [4]. A multi-scale network

structure can be developed by integrating microfibrillar structures, produced by wet-spinning or rapid prototyping, with electrospun nanofibers [5-7].

Electrospun fibers typically have dimensions varying from the nano- to the micro-scale, although fiber diameters in the sub-micrometer range are mainly observed [8]. These mesh-like scaffold are characterized by high porosity, high surface:volume ratio and, most importantly, they can closely mimic the morphology of native ECM of many tissues. Such physical cues enhance cell adhesion, proliferation and differentiation, and consequently neo-tissue formation on nanofibrillar meshes of both natural and synthetic polymers [9, 10].

Rapid prototyping has emerged as a powerful polymer processing technique for the production of scaffolds in the area of tissue engineering [11-17]. The main advantage of this technique is the possibility of creating structures with customized shapes linked with computer aided design (CAD), thus providing more flexibility, versatility and reproducibility in creating scaffolds [11, 18-20]. However, the typical pore size of RP scaffold constitutes a limitation in cell seeding efficiency [15], once it is relatively large as compared to cell dimensions.

Therefore, the aim of this study was to characterize a novel hierarchical starch-based fibrous scaffold obtained by the combination of starch-polycaprolactone (SPCL) micro- and polycaprolactone (PCL) nano-motifs, respectively produced by rapid prototyping (RP) and electrospinning. The defined strategy aimed at overcoming the high number of cells needed to attain sufficient adherent cells to the RP scaffolds [7], which can be accomplished by alternately integrating electrospun nanofiber meshes every two consecutive layers of plotted microfibers. In this way these nanofiber meshes will act as cell entrapment systems, increasing cell attachment, cell proliferation and tissue regeneration. Ultimately, this integration will enhance the potential application of such three dimensional (3D) fibrous structures in bone tissue engineering strategies. This work reports the results of a set of experiments where human osteoblast-like cells were dynamically seeded and statically cultured for 7 days on the micro-nano fiber polymeric scaffolds designed to validate this hypothesis.

### **5.3. Materials & Methods**

#### *5.3.1. Scaffold Fabrication*

Three-dimensional (3D) rapid prototyping scaffolds (6RP) were fabricated using a 3D plotting technique (Bio-plotter, EnvisionTec GmbH, Germany), using a 30:70 (wt.%) blend of starch and polycaprolactone (SPCL; Novamont, Italy). SPCL polymer powder was placed into a metal barrel and heated at 140 °C through a heated cartridge unit, then plotted through a nozzle by air pressure control. The nozzle comprises a stainless steel needle with internal diameter of 0.5 mm and length of 6 mm. A metal piston plunger with a Teflon seal was used to apply pressure to the molten polymer. The machine was linked to a CAD software (PrimCam, Germany) which required inputs of dispensing and processing parameters (e.g. speed of the head, dispensing pressure and temperature) and the design parameters of the scaffold (e.g. scaffold dimensions, spacing between the polymer strands, and number of layers). The strand spacing was set to 1mm, without offsets between the consecutive equivalent layers. The orientation was changed by plotting the polymer with 90° angle steps between two successive layers. The production of hierarchical fibrous scaffolds (6RP+5NFM) was achieved by integrating nanofiber meshes (NFM) every two consecutive layers of plotted microfibers. The nanofiber meshes were previously produced by electrospinning, as described elsewhere [21]. Briefly, a polymeric solution of 17 % (w/v) PCL, dissolved in an organic solvent mixture of chloroform/dimethylformamide (7:3 ratio), was electrospun by establishing a electric tension of 9.5 kV, a needle tip-to-ground collector distance of 200 mm and a flow rate of 1 ml/h. The scaffolds (6RP and 6RP+5NFM scaffolds) were all cut into 5x5 mm cubical samples from the originally deposited bulk 20x20 mm cube (12 layers), and sterilized by ethylene oxide (EO) before the cell culture assays.

#### *5.3.2. Scaffold Characterization*

Scaffold architecture was analyzed using micro-computed tomography ( $\mu$ -CT) with a desktop micro CT scanner (SkyScan 1072, Aartselaar, Belgium). The scanner

was set to a voltage of 40 kV and a current of 248  $\mu\text{A}$ , and the samples were scanned at 8.71  $\mu\text{m}$  pixel resolutions by approximately 350 slices covering the sample height of 2.5 mm. For imaging, the sliced 2D tomographic raw images were reconstructed using CT Analyzer software, and the threshold levels of the grey scale images were equally adjusted for all the samples to allow the measurement of the volume of pores providing the data for scaffold porosity. 3D modelling was also used to analyze the scaffold structure in a non-destructive manner using imaging software. The morphology of the scaffold was also analysed using scanning electron microscopy (SEM; Leica Cambridge, Model S360; UK). All samples were previously sputter-coated with gold (Sputter Coater, Model SC502, Fisons Instruments, UK).

### 5.3.3. Cell Seeding and Culture

Human osteosarcoma-derived cells [Saos-2 cell line, European Collection of Cell Cultures (ECACC), UK], were maintained in Dulbecco's modified Eagle's medium (DMEM, Sigma-Aldrich, Germany) supplemented with 10 % heat-inactivated fetal bovine serum (Biochrom AG, Germany) and 1 % antibiotic-antimycotic solution (Gibco, UK). Cells were cultured in a humidified incubator at 37  $^{\circ}\text{C}$  in 5 %  $\text{CO}_2$  atmosphere, and the medium was routinely replaced every 3-4 days.

Confluent osteoblastic-like cells were harvested and dynamically seeded onto the polymeric scaffolds, as follows. The combined and the RP (controls) scaffolding structures were placed between stainless steel holding wires in spinner flasks (12 scaffolds/spinner flask) containing a suspension of osteoblast-like cells with a concentration of  $0.5 \times 10^6$  cells/ml in a total volume of 35 ml. The stirrer was set at 80 r.p.m. and the spinner flasks left for 72h to allow the cells to colonize the entire scaffold. After the seeding was completed, the osteoblasts/scaffold constructs were transferred to 24-well cell culture plates (Costar<sup>®</sup>; Corning, NY, USA) and statically cultured during 1 and 7 days, under the cultured conditions previously described for maintenance of the cell line.

#### *5.3.4. Evaluation of Cell Adhesion, Morphology and Distribution*

To evaluate the cell morphology, the cells-scaffold constructs were fixed with 2.5 % Glutaraldehyde (Sigma, USA) in Phosphate Buffer Saline (PBS; Sigma, USA) solution, FOR 1h at 4 °C. Then, the samples were dehydrated through a graded series of ethanol and let to dry overnight. Finally, they were sputter-coated with gold (Model SC502, Fisons Instruments, UK) and observed in a scanning electron microscope (Model S360, Leica Cambridge, UK).

#### *5.3.5. Cell Viability Assay*

At each defined time culture period, the cell viability was determined using CellTiter 96<sup>®</sup> Aqueous One Solution Cell Proliferation Assay (Promega, USA). This assay is based on the bioreduction of a tetrazolium compound, 3-(4,5-dimethylthiazol-2-yl)-5-(3-carboxymethoxyphenyl)-2-(4-sulfophenyl)-2H-tetrazolium (MTS), into a water-soluble brown formazan product. This conversion is accomplished by NADPH or NADH production by the dehydrogenase enzymes in metabolically active cells. The absorbance, measured at 490nm in a microplate reader (Bio-Tek, Synergie HT, USA), being related to the quantity of formazan product and directly proportional to the number of living cells in the constructs. Three samples per type of scaffold and per time point were characterized.

#### *5.3.6. DNA Quantification*

Cell proliferation was evaluated by quantifying the total amount of double-stranded DNA throughout the culturing time. Quantification was performed using the Quant-iT<sup>™</sup> PicoGreen dsDNA Assay Kit (Invitrogen, Molecular Probe; OR, USA), according to the manufacturer's instructions, and after the cells in the construct were lysed by osmotic and thermal shock. The intensity of fluorescence proportional of the amount of double-strand DNA, was measured at an excitation wavelength of 485/20 nm and at an emission wavelength of 528/20 nm, in a microplate reader (Bio-Tek, Synergie HT, USA). Triplicates of each sample, allowed for a statistical analysis. The

DNA concentration for each sample was calculated using a standard curve relating quantity of DNA and fluorescence intensity.

#### *5.3.7. Alkaline Phosphatase (ALP) Quantification*

To assess the osteogenic activity of cells seeded into the 3D scaffolds (6RP and 6RP + 5NFM), the expression of ALP was determined for both culture time periods, in the same samples for DNA quantification. In each well of a 96-well plate (Costar<sup>®</sup>; Corning, NY, USA), 20  $\mu$ l of each sample were mixed with 60  $\mu$ l substrate solution and 0.2 % wt/v *p*-nitrophenyl phosphate (Sigma, USA), in a substrate buffer of 1 M diethanolamine HCl (Merck, Germany) at pH 9.8. The plate was then incubated in the dark for 45 minutes at 37 °C. After the incubation period, 80  $\mu$ l stop solution, 2 M NaOH (Panreac, Barcelona, Spain) plus 0.2 mM EDTA (Sigma, USA), was added to each well. Standards were prepared with 10  $\mu$ mol/ml *p*-nitrophenol (pNP, Sigma, USA) solution, to obtain a standard curve ranging from 0.0 to 0.3  $\mu$ mol/ml. Triplicates of each sample and standard were made. Absorbance was read at 405 nm in a microplate reader (Bio-Tek, Synergie HT, USA) and sample concentrations were read off from the standard curve. These ALP concentrations were normalized against the DNA concentrations of the same samples to determine the ALP activity.

#### *5.3.8. Statistical analysis*

Statistical analysis was performed using the SPSS statistic software (Release 8.0.0 for Windows). First, a Shapiro-Wilk test was used to ascertain about data normality. Once biological results did not follow a normal distribution, Mann-Whitney *U* test was performed to compare the effect of scaffold architecture over cell performance. In the analysis of the results,  $p < 0.01$  were considered statistically significant.

## 5.4. Results & Discussion

A novel hierarchical fibrous scaffold was developed, combining starch-polycaprolactone micro- and polycaprolactone nano-motifs, respectively produced by rapid prototyping (RP) and electrospinning (ES). These scaffolds were characterized by a 3D structure of parallel aligned rapid prototyped microfibers (average fiber diameter, 300  $\mu\text{m}$ ), periodically intercalated by randomly distributed electrospun nanofibers (fiber diameters in the range 400 nm -1.4  $\mu\text{m}$ ) (Figure 5.1B). When nanofiber meshes were integrated within the 3D scaffold, no delamination between consecutive layers of RP fibers was observed, resulting in a stable scaffold. Additionally, this micro-nano scaffold architecture comprises a high-throughput scaffold process methodology, with regular control over RP-produced structure and nanofibers distribution within the scaffold. The integration of these nano-motifs results in a decrease of scaffold porosity of around 11 % (from 79.4 % on 6RP scaffolds to

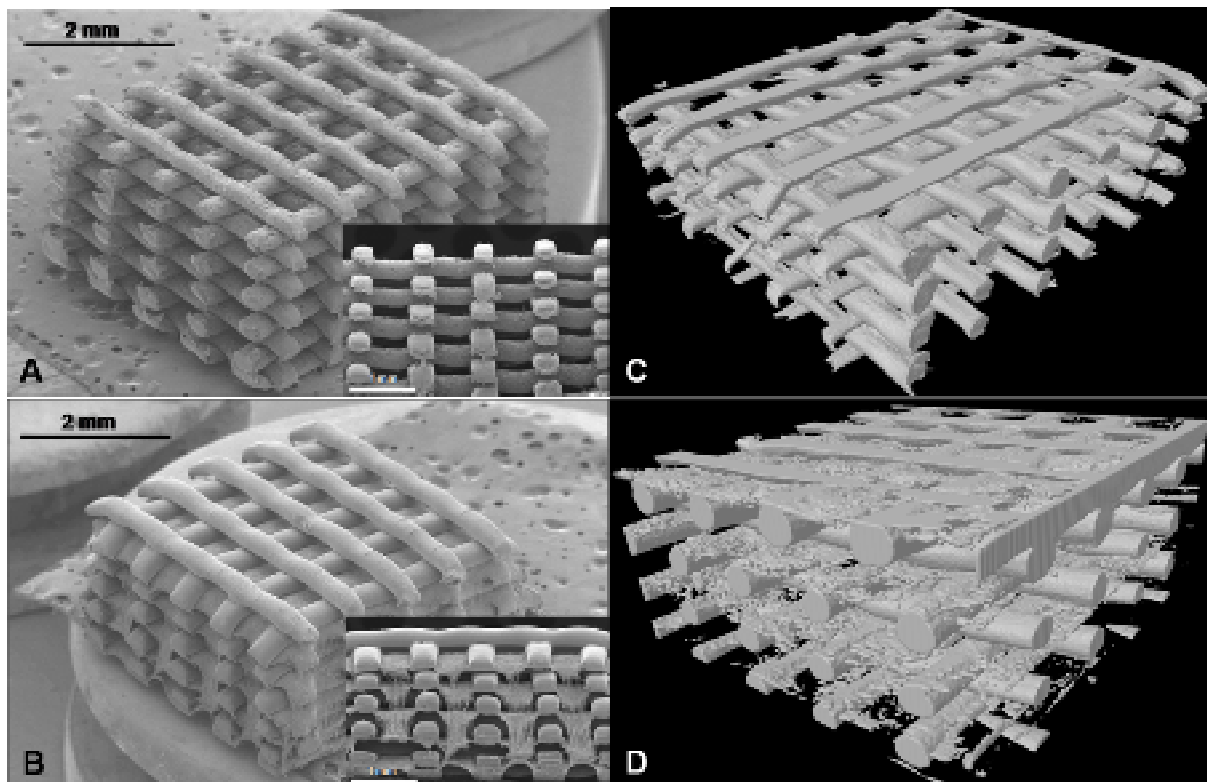


**Figure 5.1** - SEM and  $\mu\text{-CT}$  micrographs of the starch-based rapid prototyped, 6RP (A and C), and hierarchical fibrous scaffolds, 6RP+5NFM (B and D).

68.3 % on 6RP + 5NFM scaffolds), as determined by  $\mu$ -CT analysis (Figure 5.1 C and D). Despite a decrease in porosity, a fully interconnected porous structure was observed, allowing gas, nutrient and waste transport through the 3D structure.

Starch-based scaffolds have been proposed as candidates for bone tissue engineering strategies in multiple studies [5, 22-28], supporting the choice of SPCL to develop the structures proposed in this study. Indeed, successful results in terms of cell viability, proliferation and maturation of osteoblastic cells or differentiation of bone marrow stromal cells. Moreover, other starch-based blends (corn starch, dextran and gelatine, 50:30:20 wt.%) have already been used to produce different scaffold designs by 3D printing (3DP) [29]. Although showing suitable physicochemical properties for tissue-engineering applications, the biocompatibility of those 3DP geometric scaffolds, with a highly interconnected porous network, remains to be tested. The hierarchical starch-based fibrous scaffolds developed in the present study were seeded with human osteoblast-like cells to observe how the scaffold architecture affects their behaviour. Cells were initially allowed to attach to the scaffold using a dynamic system; this spinner flask bioreactor allows the cells to efficiently penetrate into the inner regions of the scaffolds, avoiding in a certain extent the preferential colonization of the outer outer most parts of the scaffolds [30]. Consequently, a homogeneous distribution of cells throughout the entire scaffold was observed. However, SEM micrographs demonstrated that osteoblastic cells preferentially adhered to the nanofibrous meshes (Figure 5.2 B, D, G and H). This phenomena of cellular preference was previously described by our group and others [5, 31, 32], when different cell types (osteoblastic, endothelial and neural stem cells) were seeded in micro- and nano-fiber-based scaffolds. Additionally, the integration of nanofiber meshes into the 3D rapid prototyped scaffolds seemed to act as a cell entrapment system within the RP scaffold. It was reported by others [15] that cells go through the pores of rapid prototyped scaffolds and accumulate at the bottom of the well plate during the seeding process, without attaching the scaffold, and thus reducing the seeding efficiency typically down to values of 25-35 %. Thus, the integration of nanofiber meshes constitutes an innovative strategy to enhance cell seeding efficiency into 3D RP scaffolds.

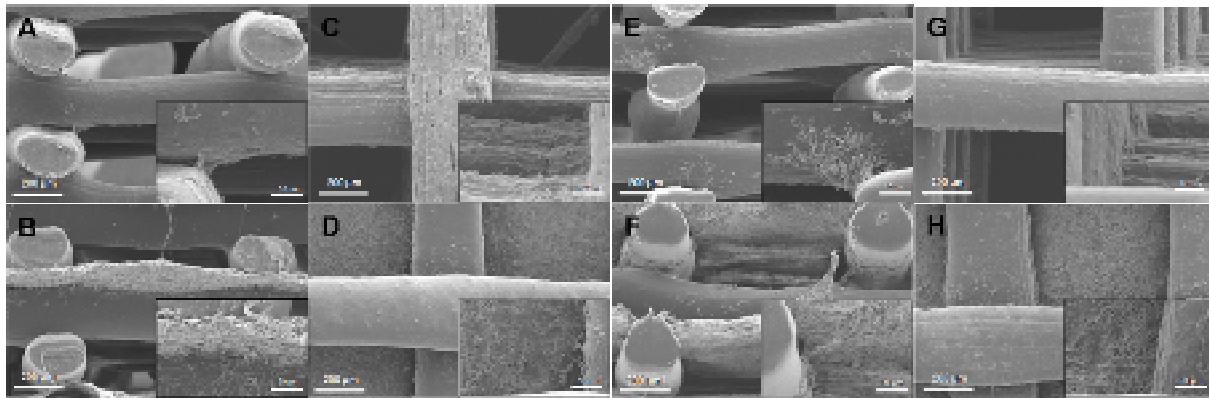


**Figure 5.2** – SEM micrographs of rapid prototyped (A, C, E and G) and hierarchical fibrous (B, D, F and H) scaffolds cultured with human osteoblast-like cells (Saos-2 cell line) during 1 (A -D) and 7 days (E-H). Cross-sections (A, B, E and F) and top view (C, D, G and H) of the constructs. Higher magnifications enclosed.

The quantification of cell viability and metabolic activity of human osteoblast-like cells seeded into the combined electrospun fiber meshes and RP scaffolds was evaluated by MTS assay (Figure 5.3). The results revealed a steadily increasing trend, with culture time, although there was no significant difference on the effect of the type of

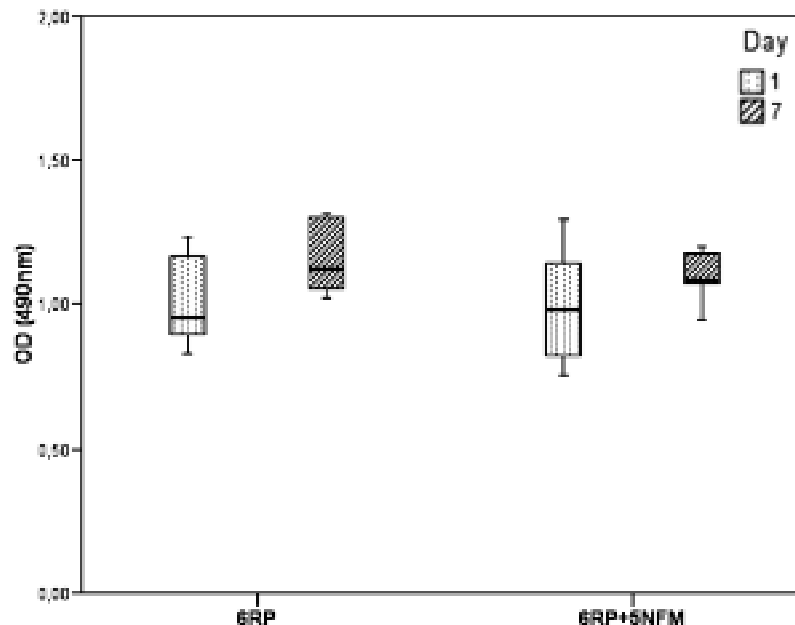


**Figure 5.3** - Box plot of cell viability results of human osteoblastic cells cultured on rapid prototyped (6RP) and hierarchical fibrous (6RP+5NFM) scaffolds, during 1 and 7 days. Data were analyzed by nonparametric way of a Mann–Whitney *U* test.

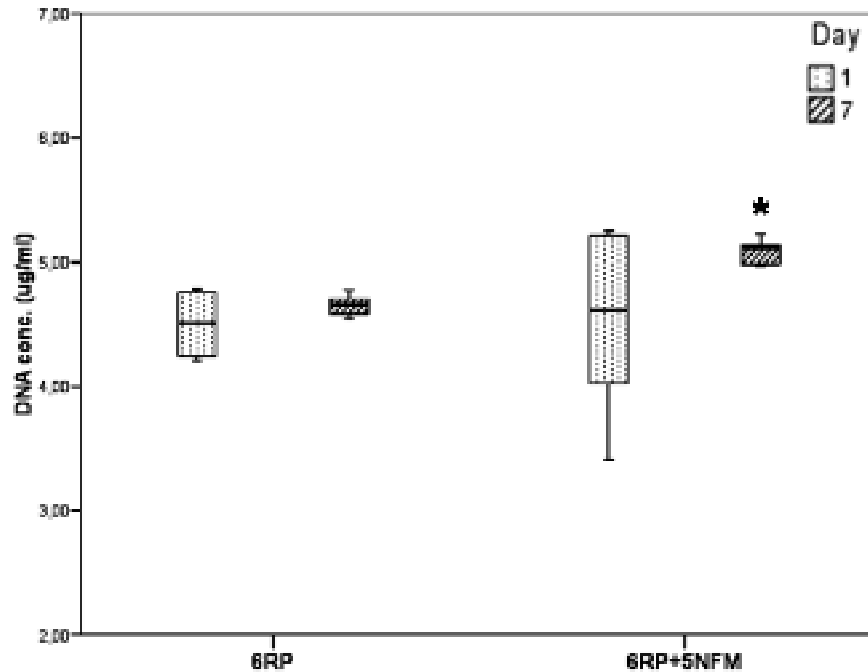


**Figure 5.4** - Box plot of DNA content of osteoblast-like cells cultured on rapid prototyped (6RP) and hierarchical fibrous (6RP+5NFM) scaffolds, during 1 and 7 days. Data were analyzed by nonparametric way of a Mann-Whitney  $U$  test; \*  $p < 0.01$ .

scaffold architectures ( $p > 0.01$ ). From the morphological evaluation of the constructs, it seems that the integrated nanofiber meshes into the 3D rapid prototyped structure also acted as a cell entrapment system within the scaffold. Consequently, a significant increment of cell proliferation and maturation, respectively assessed by DNA and ALP activity quantification, along the culture time, was observed on the hierarchical fibrous scaffolds (Figures 5.4 and 5.5) in comparison to the rapid prototyped scaffolds ( $p < 0.01$ ), especially for longer culture periods. However, for the RP scaffolds, the osteoblastic activity was not maintained throughout the experiment, as observed by a decrease in ALP concentration from day 1 to day 7 of culture. It was already reported by Schantz *et al.* [33] that rabbit calvarial osteoblasts, seeded onto PCL scaffolds fabricated via fused deposition modelling (FDM) and embedded into a fibrin matrix (Tisseel, Baxter Hyland Immuno), showed no significant differences in their ALP concentration along time. These results are in accordance with those of our study.

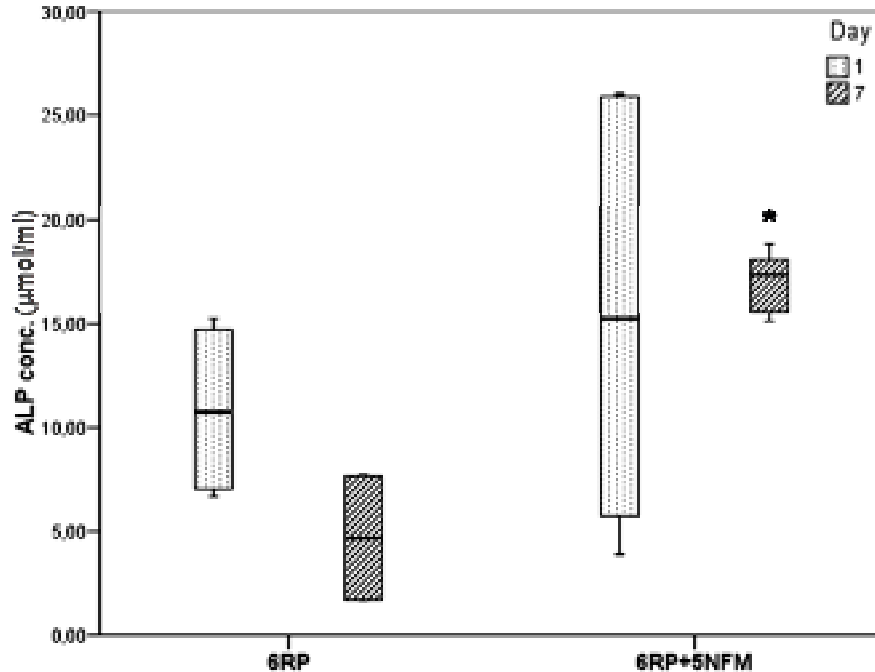


**Figure 5.5** - Box plot of ALP from osteoblastic cells (Saos-2 cell line) cultured on rapid prototyped (6RP) and hierarchical fibrous (6RP+5NFM) scaffolds, during 1 and 7 days. Data were analyzed by nonparametric way of a Mann-Whitney  $U$  test; \*  $p < 0.01$ .

## 5.5. Conclusions

A novel hierarchical fibrous scaffold was developed, combining starch-polycaprolactone micro- and polycaprolactone nano-motifs, respectively produced by rapid prototyping and electrospinning. It is evident that the nanofiber meshes demonstrate that the integration of nanofiber meshes supply topological cues at the ECM level, whereas the micro 3D fibrous structure provide the required mechanical stability. We here demonstrated that the integration of these two hierarchical structures lead to improved biological performance. Indeed, human osteoblast-like cells presented significantly higher proliferation and maturation when seeded on these hierarquical starch-based fibrous scaffolds. Overall, the results corroborate our hypothesis that the hierarchical structure of the scaffolds, mimicking the hierarchical structure of the native ECM, is favourable for bone tissue-engineering strategies.

## 5.6. References

1. Lutolf MP, Hubbell JA. Synthetic biomaterials as instructive extracellular microenvironments for morphogenesis in tissue engineering. *Nature Biotechnology* 2005; 23(1):47-55.
2. Hutmacher DW, Schantz JT, Lam CX, Tan KC, Lim TC. State of the art and future directions of scaffold-based bone engineering from a biomaterials perspective. *Journal of Tissue Engineering and Regenerative Medicine* 2007; 1(4):245-260.
3. Agrawal CM, Ray RB. Biodegradable polymeric scaffolds for musculoskeletal tissue engineering. *Journal of Biomedical Materials Research* 2001; 55(2):141-150.
4. Norman JJ, Desai TA. Methods for fabrication of nanoscale topography for tissue engineering scaffolds. *Annals of Biomedical Engineering* 2006; 34(1):89-101.
5. Tuzlakoglu K, Bolgen N, Salgado AJ, Gomes ME, Piskin E, Reis RL. Nano- and micro-fiber combined scaffolds: A new architecture for bone tissue engineering. *Journal of Materials Science: Materials in Medicine* 2005; 16(12):1099-1104.
6. Santos MI, Fuchs S, Gomes ME, Unger RE, Reis RL, Kirkpatrick CJ. Response of micro- and macrovascular endothelial cells to starch-based fiber meshes for bone tissue engineering. *Biomaterials* 2007; 28(2):240-248.
7. Moroni L, Schotel R, Hamann D, de Wijn JR, van Blitterswijk CA. 3D fiber-deposited electrospun integrated scaffolds enhance cartilage tissue formation. *Advanced Functional Materials* 2008; 18:53-60.
8. Huang ZM, Zhang YZ, Kotaki M, Ramakrishna S. A review on polymer nanofibers by electrospinning and their applications in nanocomposites. *Composites Science and Technology* 2003; 63(15):2223-2253.
9. Zhang YZ, Lim CT, Ramakrishna S, Huang ZM. Recent development of polymer nanofibers for biomedical and biotechnological applications. *Journal of Materials Science: Materials in Medicine* 2005; 16(10):933-946.
10. Martins A, Araujo JV, Reis RL, Neves NM. Electrospun nanostructured scaffolds for tissue engineering applications. *Nanomedicine* 2007; 2(6):929-942.

11. Hutmacher DW, Sittinger M, Risbud MV. Scaffold-based tissue engineering: rationale for computer-aided design and solid free-form fabrication systems. *Trends in Biotechnology* 2004; 22(7):354-362.
12. Leong KF, Cheah CM, Chua CK. Solid freeform fabrication of three-dimensional scaffolds for engineering replacement tissues and organs. *Biomaterials* 2003; 24(13):2363-2378.
13. Mironov V, Boland T, Trusk T, Forgacs G, Markwald RR. Organ printing: computer-aided jet-based 3D tissue engineering. *Trends in Biotechnology* 2003; 21(4):157-161.
14. Peltola SM, Melchels FP, Grijpma DW, Kellomaki M. A review of rapid prototyping techniques for tissue engineering purposes. *Annals of Medicine* 2008; 40(4):268-280.
15. Pfister A, Landers R, Laib A, Hubner U, Schmelzeisen R, Mulhaupt R. Biofunctional rapid prototyping for tissue-engineering applications: 3D biplotting versus 3D printing. *Journal of Polymer Science, Part A - Polymer Chemistry* 2004; 42(3):624-638.
16. Yang S, Leong KF, Du Z, Chua CK. The design of scaffolds for use in tissue engineering. Part II. Rapid prototyping techniques. *Tissue Engineering* 2002; 8(1):1-11.
17. Yeong WY, Chua CK, Leong KF, Chandrasekaran M. Rapid prototyping in tissue engineering: challenges and potential. *Trends in Biotechnology* 2004; 22(12):643-652.
18. Moroni L, de Wijn JR, van Blitterswijk CA. Three-dimensional fiber-deposited PEOT/PBT copolymer scaffolds for tissue engineering: influence of porosity, molecular network mesh size, and swelling in aqueous media on dynamic mechanical properties. *Journal of Biomedical Materials Research* 2005; 75(4):957-965.
19. Moroni L, de Wijn JR, van Blitterswijk CA. 3D fiber-deposited scaffolds for tissue engineering: influence of pores geometry and architecture on dynamic mechanical properties. *Biomaterials* 2006; 27(7):974-985.

20. Capes JS, Ando HY, Cameron RE. Fabrication of polymeric scaffolds with a controlled distribution of pores. *Journal of Materials Science: Materials in Medicine* 2005; 16(12):1069-1075.

21. Araujo JV, Martins A, Leonor IB, Pinho ED, Reis RL, Neves NM. Surface Controlled Biomimetic Coating of Polycaprolactone Nanofiber Meshes to Be Used as Bone Extracellular Matrix Analogues. *Journal of Biomaterials Science - Polymer Edition* 2008; 19(10): 1261-1278.

22. Gomes ME, Holtorf HL, Reis RL, Mikos AG. Influence of the porosity of starch-based fiber mesh scaffolds on the proliferation and osteogenic differentiation of bone marrow stromal cells cultured in a flow perfusion bioreactor. *Tissue Engineering* 2006; 12(4):801-809.

23. Gomes ME, Reis RL, Cunha AM, Blitterswijk CA, de Bruijn JD. Cytocompatibility and response of osteoblastic-like cells to starch-based polymers: effect of several additives and processing conditions. *Biomaterials* 2001 Jul;22(13):1911-1917.

24. Gomes ME, Sikavitsas VI, Behravesh E, Reis RL, Mikos AG. Effect of flow perfusion on the osteogenic differentiation of bone marrow stromal cells cultured on starch-based three-dimensional scaffolds. *Journal of Biomedical Materials Research* 2003; 67(1):87-95.

25. Salgado AJ, Coutinho OP, Reis RL. Novel starch-based scaffolds for bone tissue engineering: cytotoxicity, cell culture, and protein expression. *Tissue Engineering* 2004; 10(3-4):465-474.

26. Salgado AJ, Coutinho OP, Reis RL, Davies JE. In vivo response to starch-based scaffolds designed for bone tissue engineering applications. *Journal of Biomedical Materials Research* 2007; 80(4):983-989.

27. Salgado AJ, Figueiredo JE, Coutinho OP, Reis RL. Biological response to pre-mineralized starch based scaffolds for bone tissue engineering. *Journal of Materials Science: Materials in Medicine* 2005; 16(3):267-275.

28. Gomes ME, Azevedo HS, Moreira AR, Ella V, Kellomaki M, Reis RL. Starch-poly(epsilon-caprolactone) and starch-poly(lactic acid) fibre-mesh scaffolds for bone tissue engineering applications: structure, mechanical properties and

degradation behaviour. *Journal of Tissue Engineering and Regenerative Medicine* 2008; 2(5):243-252.

29. Lam CXF, Mo XM, Teoh SH, Hutmacher DW. Scaffold development using 3D printing with a starch-based polymer. *Materials Science and Engineering C* 2002; 20(1-2):49-56.

30. Oliveira JT, Crawford A, Mundy JM, Moreira AR, Gomes ME, Hatton PV, *et al.* A cartilage tissue engineering approach combining starch-polycaprolactone fibre mesh scaffolds with bovine articular chondrocytes. *Journal of Materials Science: Materials in Medicine* 2007; 18(2):295-302.

31. Kwon IK, Kidoaki S, Matsuda T. Electrospun nano- to microfiber fabrics made of biodegradable copolyesters: structural characteristics, mechanical properties and cell adhesion potential. *Biomaterials* 2005; 26(18):3929-3939.

32. Yang F, Murugan R, Wang S, Ramakrishna S. Electrospinning of nano/micro scale poly(L-lactic acid) aligned fibers and their potential in neural tissue engineering. *Biomaterials* 2005; 26(15):2603-2610.

33. Schantz JT, Teoh SH, Lim TC, Endres M, Lam CX, Hutmacher DW. Repair of calvarial defects with customized tissue-engineered bone grafts I. Evaluation of osteogenesis in a three-dimensional culture system. *Tissue Engineering* 2003; 9 (Suppl 1):S113-126.

## Chapter 6

# Biodegradable Nanofiber-Reinforced Microfibrous Composite Scaffolds for Bone Tissue Engineering Applications

This chapter is based on the following publication: Martins A, Pinho ED, Correlo VM, Faria S, Marques AP, Reis RL, Neves NM. *Biodegradable Nanofiber-Reinforced Microfibrous Composite Scaffolds for Bone Tissue Engineering Applications*. Submitted.

## 6.1. Abstract

Native bone extracellular matrix (ECM) is a complex hierarchical fibrous composite structure, resulting from the assembling of collagen fibrils at several length scales, ranging from the macro to the nanoscale. The combination of nanofibers within microfibers following conventional reinforcement methodologies seems to be a feasible solution to the rational design of highly functional synthetic ECM substitutes. The present work aims at the development of bone ECM inspired structures, conjugating electrospun chitosan (Cht) nanofibers within biodegradable polymeric microfibers (poly(butylene succinate) - *PBS* and *PBS/Cht*), assembled in a fiber mesh structure. The nanofiber-reinforced composite fiber mesh scaffolds were seeded with human bone marrow mesenchymal stem cells (hBMSCs) and cultured under osteogenic differentiation conditions. These nanofiber-reinforced composite scaffolds sustained ECM deposition and mineralization, mainly in the *PBS/Cht*-based fiber meshes, as depicted by the increased amount of calcium phosphates produced by the osteogenic differentiated hBMSCs. The osteogenic genotype of the cultured hBMSCs was confirmed by the expression of osteoblastic genes, namely *Alkaline Phosphatase*, *Osteopontin*, *Bone Sialoprotein* and *Osteocalcin*, and the transcription factors *Runx2* and *Osterix*, all involved in different stages of the osteogenesis. These data represent the first report on the biological functionality of nanofiber-reinforced composite scaffolds, envisaging the applicability of the developed structures for bone tissue engineering.

## 6.2. Introduction

The native extracellular matrix (ECM) is a dynamic and hierarchically organized fibrous nanocomposite. It provides mechanical support for the embedded cells and also interacts with cells regulating various cellular functions such as adhesion, migration, proliferation, differentiation and tissue morphogenesis [1]. The ECM of connective tissues is a complex interconnected nano- or micro-ranged fibrous network of polysaccharides (such as glycosaminoglycans or cellulose) and proteins

(such as collagen and proteoglycans) secreted by the adjacent cells. The nano-scaled fibrils are further assembled into larger collagen bundles. Thus hierarchically organized structure stands from the molecular level up to the macroscopic scale. In the case of bone, collagen assemblies and its organization ensure its multiple functions [2]. Besides the outstanding hierarchically organized structure, native bone nanofibers are also covered by hydroxyapatite nano-crystals with their *c*-axis aligned with the longitudinal axis of the fibers. Although the basic organization and composition of the bone is known, replicating its structure and properties has been very challenging [3].

In the context of tissue engineering, three-dimensional synthetic ECM are developed not only to provide the initial structural integrity for cells to adhere, but also to direct cell proliferation and differentiation, ultimately leading to the assembly of functional tissue-like substitutes [4, 5]. The understanding that the natural ECM is a multifunctional nanocomposite motivated researchers to rationally design synthetic ECM substitutes-scaffolds. Nanocomposites that emulate the structural, compositional and biological characteristics of natural bone, are certainly major candidates to be used in bone tissue engineering applications [6]. Current attempts to replicate the complexity and hierarchical organization of natural ECM are mostly restricted to dispensing nanofibers in existing implants and biomedical devices or used as random nanofibrous meshes [3]. In fact, nature modulates the mechanical properties of biological tissues by subtle adjustments of its local composition with a perceivable alteration of its nano-scale organization.

To follow nature assembly, a processing method that is able to fabricate nanofibers from a variety of materials and mixtures is a prerequisite. The control of the nanofiber arrangement is also necessary to optimize the hierarchically organized multifunctional nanocomposites [3, 7-9]. Electrospinning allows the production of ECM-mimetics that exhibit a physical structure similar to that of the fibrous proteins in the native ECM, albeit their completely different chemical composition [10, 11]. Submicron electrospun polymer fibers are good candidates as reinforcing agents in the development of advanced nanocomposites due to their continuity, orientation, inherent flexibility, and potential high compatibility with polymer matrices. However,

only a limited number of composites reinforced with electrospun nanofibers have been developed, and mainly for providing some outstanding physical characteristics, namely optical transparency and mechanical properties [12-20]. The pioneer work on electrospun nanofiber-reinforced composite materials was developed by Kim and Reneker [21], reporting improvement on the mechanical properties (i.e. fracture toughness and the modulus) of a poly-benzimidazole (PBI)-reinforced epoxy resin composite and of a nanofiber-reinforced styrene-butadiene rubber (i.e. Young's modulus and tear strength). In the same year, Bergshoef and Vancso [12] described the incorporation of electrospun nylon-4,6 nanofibers with 30 to 200 nm diameter in phenolic epoxy films prepared by curing, with a thickness of 100  $\mu\text{m}$ . The composite films obtained by fiber reinforcement exhibited a characteristic transparency, due to the fiber sizes smaller than the wavelength of visible light. Fong *et al.* [13, 22] used electrospun nanofibers to improve the flexural strength, elastic modulus and work of fracture of Bis-GMA/TEGDMA dental restorative resin, using relatively small mass fractions (from 1-5 %) of electrospun nylon 6 nanofibers impregnation. Sihn *et al.* [23] used non-woven meshes, either of poly(2,6-dimethyl-1,4-phenylene oxide)/carbon nanotubes or polystyrene/carbon nanotubes composite nanofiber, as a nano-interfacial layer in laminated composites. With this nano-interfacial layer, the stress required for the onset of delamination and micro-crack formation was increased resulting in an increment of the ultimate strength of the composite. Although a prospective physical characterization of the nanofiber-reinforced composites was pursued, their biological functionality remains to be explored.

Like natural ECM, a range of topographic features at the macro-, micro- and even nano-scale levels may lead cell response [24]. A combination of nanofibers with conventional reinforcement at the micron scale may capture interesting features of the native ECM [25]. Recently, our group and others [26-31] developed multi-scale network structures by integrating electrospun nanofibers within the microfibrillar structures, produced by wet spinning or rapid prototyping techniques. Biological data demonstrated that the hierarchical fibrous structure of those scaffolds is favourable for bone tissue-engineering strategies. Considering the above referred background, the present work aims at producing bone ECM inspired structures, conjugating

electrospun chitosan (Cht) nanofibers with biodegradable polymeric microfibers (poly(butylene succinate) - *PBS* and *PBS/Cht*). Despite the recent increment of works on electrospun nanofiber-reinforced dental restorative composites resins [13, 16, 17, 19, 20, 22], this is the first work, from the best of our knowledge, reporting the biological functionality of nanofiber-reinforced composite scaffolds.

Functional and structural engineering of musculoskeletal tissue may involve the use of appropriated cells cultured with specific growth factors in biomaterial scaffolds. While several tissues remain an important source of therapeutic relevant differentiated cells, stem cells have emerged as a strong alternative due to their expansion potential - self-renewal potential - and the fact that they can be obtained from autologous sources [32]. Additionally, advances in stem cell biology have shown that mesenchymal stem cells (MSCs) can differentiate into a variety of connective tissues, including bone, cartilage, fat, muscle and tendon, when cultured with appropriated supplemented culture media and specific environments [33]. Herein, human bone marrow mesenchymal stem cells (hBMSCs) were cultured on those hierarchical nanocomposite structures, under osteogenic differentiation inductive conditions, to validate the applicability of the developed structures for bone tissue engineering. A phenotypic and genotypic characterization of osteoblastic markers was performed to quantitatively evaluate the formation of bone-like tissue.

### **6.3. Materials & Methods**

#### *6.3.1. Production of the Nanofiber-Reinforced Microfibrous Composite Scaffolds*

The processing of chitosan (Cht) nanofiber meshes by electrospinning and their subsequent neutralization process were detailed elsewhere [14]. The nanofiber-reinforced microfibers were produced by melt extruding poly(butylene succinate) (PBS) or a blend of PBS/Cht (50:50 wt.%), compounded with electrospun chitosan nanofiber meshes (0.05 wt.%). The processing conditions of the nanofiber-reinforced microfibers, as well as the *PBS* and *PBS/Cht* microfibers without nanofiber reinforcement, used as controls, were described elsewhere [14, 15]. Briefly, the processing conditions of those microfibers were: melt temperatures of 115 °C for the

PBS-based fibers and 145 °C for the PBS/Cht, a screw rotation speed of 40 r.p.m. and a die diameter of 0.5 mm.

The assembling of the microfibrinous scaffolds, reinforced or not with electrospun chitosan nanofiber meshes, was achieved by fiber bonding. Basically, a predefined quantity of microfibers (*PBS* or *PBS/Cht*), reinforced or not with electrospun chitosan nanofiber meshes, was randomly arrayed in the custom-designed Teflon mold and heated at 120 °C (for PBS-based) or 150 °C (for PBS/Cht-based) during 10 minutes under compression. Cylindrical samples of 6 mm in diameter and 2 mm in thickness were cut and sterilized by ethylene oxide before the *in vitro* biological assays.

### *6.3.2. Characterization of the Nanofiber-reinforced Microfibrinous Composite Scaffolds*

Nanofiber-reinforced microfibrinous composite scaffolds were gold sputter-coated (model SC502, Fisons Instruments; England) for 2 min at 15 mA and analyzed with a Scanning Electron Microscope (model S360, Leica Cambridge; England). Micrographs were recorded at 15 kV with magnifications ranging from 100 to 5000 times.

To better visualize and quantify the 3D internal structure of prepared scaffold, micro-computed tomography ( $\mu$ -CT) analyses were conducted using a desktop micro CT scanner (SkyScan 1072, Aartselaar, Belgium). Each scaffold type was scanned in high-resolution mode using a pixel size of 8.79  $\mu$ m and an exposure time of 2.2 ms. The X-ray source was set at 40 keV of energy and a current of 248  $\mu$ A. From the resulting voxel data, a cylindrical volume of interest with a diameter of 4 mm and 1.3 mm thick (corresponding to 150 slices) was selected in order to eliminate side effects that could be induced by the irregularity of the sample. The grey-scale images were transformed into binary data using a dynamic threshold of 60-255 (gray values) to distinguish between polymer material and the void space. Those operating parameters were maintained for all the samples. For morphometric analysis, including porosity and mean pore size quantification, the sliced 2D tomographic raw images were reconstructed using a CT Analyzer software from the micro CT scanner supplier. 3D virtual models of representative regions in the bulk of the scaffolds were

also created, visualized and processed using the image analysis software supplied by the manufacturer.

### *6.3.3. Expansion, Seeding and Osteogenic Differentiation of Human Bone Marrow Mesenchymal Stem Cells*

Human bone marrow aspirates were obtained, after Informed Consent (IC), during routine surgical procedures involving knee arthroplasties, as approved by the Ethical Committee of the São Marcos Hospital, Braga and under the Cooperation Agreement established between the 3B's Research Group-UM and that Hospital. Human bone marrow mesenchymal stem cells (hBMSCs) were isolated and characterized according to the method established by Delome and Charbord [34]. hBMSCs were expanded in basal medium consisting of MEM alpha medium ( $\alpha$ -MEM; Gibco, GB) supplemented with 10 % heat-inactivated fetal bovine serum (FBS; Biochrom AG, Germany) and 1 % antibiotic/antimycotic solution (final concentration of penicillin 100 units/ml and streptomycin 100  $\mu$ g/ml; Gibco, GB). Cells were cultured in a 5 % CO<sub>2</sub> incubator at 37 °C.

Confluent hBMSCs at passages 4-5 were harvested for seeding onto the nanofiber-reinforced microfibrous composite scaffolds at a density of  $5.0 \times 10^5$  cells/scaffold. Unreinforced microfibrous scaffolds (*PBS* and *PBS/Chit*) were used as controls. The constructs were cultured in standard osteogenic differentiation medium (basal medium supplemented with 50  $\mu$ g/mL ascorbic acid, 10 mM  $\beta$ -glicerophosphate and  $10^{-7}$  M dexamethasone) for 7, 14 and 21 days.

### *6.3.4. Analysis of Cell Morphology and Distribution, and ECM Mineralization*

For scanning electron microscopy (SEM) analysis, the constructs were fixed with 2.5 % Glutaraldehyde (Sigma; USA) in a Phosphate Buffer Saline solution (Sigma; USA) during 1h at 4 °C. The constructs were further dehydrated through an increasing series of ethanol concentrations and let to dry overnight. Before being analyzed by SEM (model S360, Leica Cambridge; England) equipped with an energy

dispersive spectrometer (EDS; link-eXL-II), the samples were gold or carbon sputter coated (sputter coater model SC502, Fisons Instruments; England).

Formalin-fixed constructs were embedded in Teknovit resin and sectioned (10  $\mu\text{m}$  each section) for histological purposes. Hematoxylin-Eosin stain was performed to analyse cell distribution within the microfibrillar composite scaffolds. Stained sections were observed under an optical microscope (BX61, Olympus Corporation, Germany) and images captured by a digital camera (DP70, Olympus Corporation, Germany).

### *6.3.5. Cell Viability and Proliferation Assessment*

Cell viability for each culturing time was determined using the CellTiter 96<sup>®</sup> AQueous One Solution Cell Proliferation Assay (Promega; USA), following manufacturer instructions. The absorbance of three different samples per type of scaffold and time point was measured at 490 nm in a microplate reader (Synergie HT, Bio-Tek; USA) and related with the number of living cells in the constructs.

Cell proliferation was quantified by the total amount of double-stranded DNA, along the culturing time. Quantification was performed using the Quant-iT<sup>™</sup> PicoGreen dsDNA Assay Kit (Invitrogen<sup>™</sup>, Molecular Probes<sup>™</sup>; Oregon, USA), according to the instructions of the manufacturer. Briefly, cells in the construct were lysed by osmotic and thermal shock and the supernatant used for the DNA quantification assay. The fluorescence was measured at an excitation wavelength of 485/20 nm and at an emission wavelength of 528/20 nm, in a microplate reader (Synergie HT, Bio-Tek; USA). Triplicates were made for each sample and per culturing time. The DNA concentration for each sample was calculated using a standard curve relating DNA concentration (ranging from 0.0 to 1.5  $\mu\text{g}/\text{mL}$ ) and fluorescence intensity.

### *6.3.6. Alkaline Phosphatase Quantification*

The concentration of alkaline phosphatase (ALP) was determined for all time culture periods, using the lysates used for DNA quantification. Briefly, the activity of ALP was assessed using the *p*-nitrophenol assay [35]. The reaction was stopped by

adding 2M NaOH (Panreac Quimica, Spain) and the absorbance read at 405 nm in a microplate reader (Bio-Tek, Synergie HT; USA). Standards were prepared with a 10  $\mu\text{mol/ml}$  p-nitrophenol (pNP; Sigma, USA) solution, to obtain a standard curve ranging from 0 to 250  $\mu\text{M}$ . Triplicates of each sample and standard were made, and the ALP concentrations read off from the standard curve.

### 6.3.7. RNA isolation and Real-Time Quantitative Polymerase Chain Reaction

Total RNA from the constructs was extracted using the Trizol<sup>®</sup> (Invitrogen, Life Technologies Inc., UK) method according to the manufacturer protocol. Briefly, at each culturing time the constructs were washed with PBS, immersed in Trizol and stored at -80 °C until further use. Proteins were removed with chloroform extraction, and the RNA pellets were washed once with isopropyl alcohol and once with 70 % ethanol. The total RNA pellets were reconstituted in Rnase free water (Gibco, Invitrogen, UK). Determination of the RNA concentration for each scaffold replica (triplicates of each scaffold per time point) was performed by microspectrophotometry (NanoDrop ND-1000, USA).

Reverse transcriptase (RT)-PCR was performed according to the protocol from iScript<sup>™</sup> cDNA synthesis kit (BioRad, Hercules, CA, USA). Briefly, a reaction mixture consisting of 1X iScript Reaction Mix, 1  $\mu\text{l}$  iScript Reverse Transcriptase, RNA template (150 ng total RNA for *PBS-R* and *PBS* scaffolds, and 1  $\mu\text{g}$  total RNA for *PBS/Cht-R* and *PBS/Cht*scaffolds) and nuclease-free water was prepared, in 20  $\mu\text{l}$  of total volume. The single-strand cDNA synthesis occurred by incubating the complete reaction mixture 5 min at 25 °C, followed by 30 min at 42 °C and terminated by an incubation at 85 °C for 5 min.

Amplification of the target cDNA for real-time PCR quantification were performed according to the manufacturer protocol, using 2  $\mu\text{l}$  RT cDNA products, 1  $\mu\text{M}$  each primer (osteoblastic genes primer sets listed in Table 6.1), 1X iQ SYBR Green Supermix (BioRad, Hercules, CA, USA) and nuclease-free water, in a final volume of 25  $\mu\text{L}$ . Forty-four cycles of denaturation (95 °C, 10 s), annealing (temperature dependent on the gene, 30 s) and extension (72 °C, 30 s) were carried out in the gradient thermocycler MiniOpticon real-time PCR detection system

**Table 6.1** - Primers list of osteogenic markers.

<b>Gene</b>		<b>Primer sequences (5'-3')</b>	<b>Tm [°C]</b>
<i>ALP</i>	sense	CTCCTCGGAAGACACTCTG	60,0
	antisense	AGACTGCGCCTGGTAGTTG	
<i>OP</i>	sense	GGGGACA AACTGGAGTGAAAA	58,4
	antisense	CCCACAGACCCTTCCAAGTA	
<i>BSP</i>	sense	CAACAGCAC AGAGGCAGAAAAC	59,9
	antisense	CCTCGTATTCAACGGTGGTG	
<i>OC</i>	sense	CTGAGAGGAGCAGAACTGG	61,4
	antisense	GGCAGCGAGGTAGTGAAGAG	
<i>Runx2</i>	sense	TTCCAGACCAGCAGCACTC	58,1
	antisense	CAGCGTCAACACCATCATTC	
<i>Osterix</i>	sense	CCCTTTAC AAGCACTAATGG	57,1
	antisense	ACACTGGGCAGACAGTCAG	
<i>GAPDH</i>	sense	ACAGTCAGCCGCATCTTCTT	58,4
	antisense	GACAAGCTTCCCGTTCTCAG	

(BioRad, Hercules, CA, USA) for all genes. The transcripts expression data were normalized to the housekeeping gene glyceraldehyde-3-phosphate-dehydrogenase (*GAPDH*) and the relative quantification calculated by the  $\Delta C_T$  method.

#### 6.3.8. Statistical Analysis

Statistical Analysis was performed using the SPSS statistic software package (Release 15.0.0 for Windows). Firstly, a Shapiro-Wilk test was used to ascertain about the data normality. The results indicated that nonparametric tests should be used for all comparisons. *P* values lower than 0.01 were considered statistically significant.

Firstly, a Kruskal-Wallis test was performed to analyze the effect of the electrospun nanofibers-reinforced microfibrinous composite scaffolds over hBMSCs viability and proliferation, ALP quantification, and osteogenic genotype. When this test indicated significant differences among scaffolds, a multiple comparison procedure, Tukey's HSD test, was performed to find where the differences occur.

## 6.4. Results

### 6.4.1. Morphology of the Nanofibers Reinforced Microfibrous Composite Scaffolds

PBS and PBS/Cht microfibers reinforced (i.e. *PBS-R* and *PBS/Ch-R*) or not (i.e. *PBS* and *PBS/Cht*) by electrospun chitosan nanofiber were processed by melt extrusion. The production of the fibrous scaffolds was achieved by fiber bonding, obtaining a random mesh-like structure. Their morphology and architecture are shown in the Figure 6.1. From the analysis of SEM micrographs it is possible to notice that *PBS* and *PBS-R* fibers have a very regular and smooth surface (Figure 6.1 A and B). Conversely, *PBS/Cht* and *PBS/Cht-R* fibers presented very irregular and rough surfaces (Figure 6.1 C and D) due to the presence of the chitosan microparticules (50 wt.%) within the PBS matrix (50 wt.%).

The  $\mu$ -CT analysis allows obtaining a representative volumetric region of the different porous fibrous scaffolds (Figure 6.1 E-H). These 3D images corroborate the observations previously stated by the SEM morphological analysis paragraph. The reconstructed 3D models also provide a quantitative morphometric analysis of the microfibrous scaffolds reinforced or not by electrospun chitosan nanofibers.

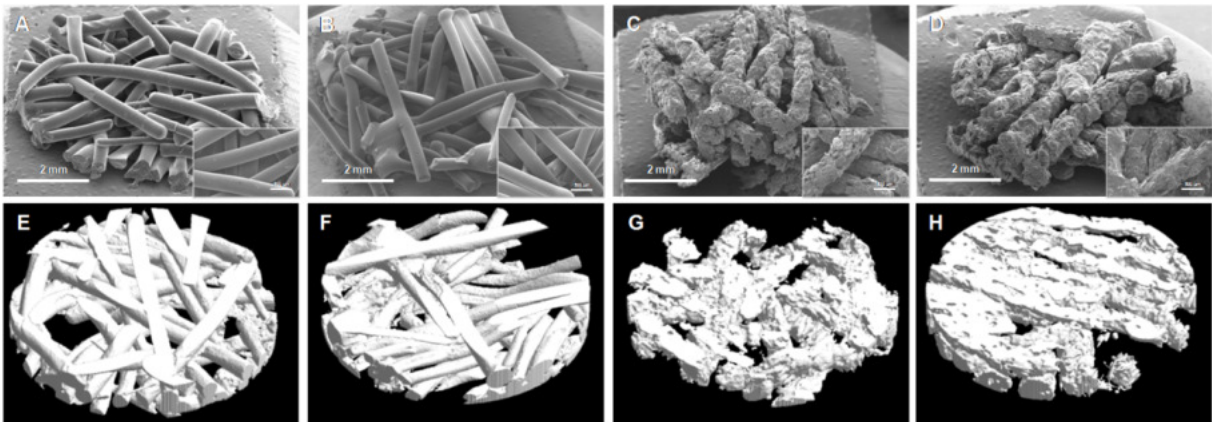


**Figure 6.1** - Morphology and architecture of the electrospun chitosan nanofibers reinforced (**A, C, E** and **G**) and non-reinforced (**B, D, F** and **H**) microfibrous scaffolds on photomicrographs from scanning electron microscopy (**A-D**) and 3D models from micro-computed tomography (**E-H**). **A** and **E** – *PBS-R*; **B** and **F** – *PBS*; **C** and **G** - *PBS/Cht-R*; **D** and **H** – *PBS/Cht*.

Accordingly, the porosity and mean pore size parameters for each type of fibrous scaffold were, respectively: 53.6 % and 333.9  $\mu\text{m}$  for *PBS-R* scaffolds; 60.4 % and 414.2  $\mu\text{m}$  for *PBS* scaffolds; 62.9 % and 303.6  $\mu\text{m}$  for *PBS/Cht-R* scaffolds; 53.4 % and 303.6  $\mu\text{m}$  for *PBS/Cht* scaffolds.

#### 6.4.2. Morphology, Viability and Proliferation of Human Bone Marrow Mesenchymal Stem Cells on Nanofiber-reinforced Microfibrous Composite Scaffolds

hBMSCs were cultured under osteogenic differentiation conditions on the

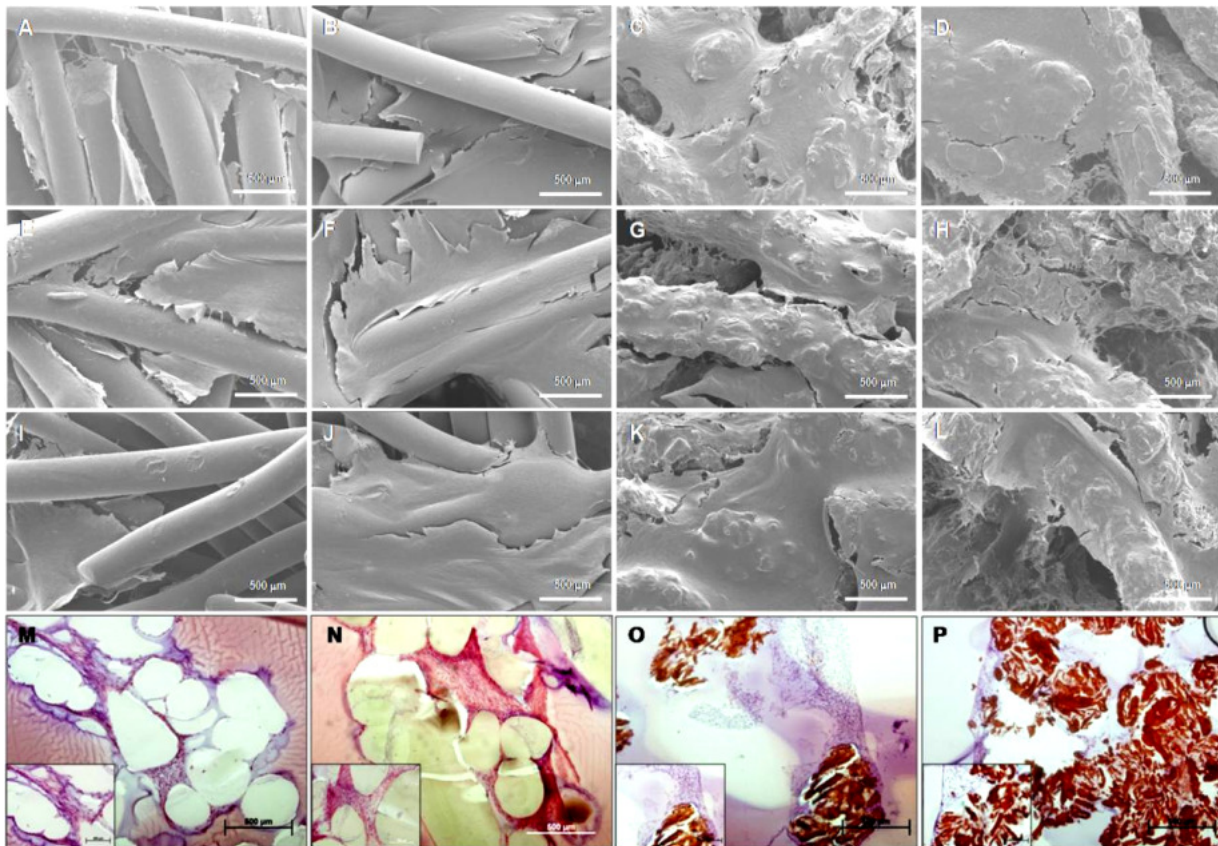


**Figure 6.2** - SEM photomicrographs of nanofibers reinforced (**A, C, E, G, I and K**) and non-reinforced (**B, D, F, H, J and L**) microfibrous scaffolds cultured with hBMSCs during 7 (**A-D**), 14 (**E-H**) and 21 days (**I-L**), under osteogenic conditions. **A, E and I** – *PBS-R*; **B, F and J** – *PBS*; **C, G and K** – *PBS/Cht-R*; **D, H and L** – *PBS/Cht*. Optical photographs from cross-sections of *PBS-R* (**M**), *PBS* (**N**), *PBS/Cht-R* (**O**) and *PBS/Cht* (**P**) constructs after 21 days of culture.

different microfibrous scaffolds, reinforced or not by electrospun nanofiber meshes, to validate the bone tissue engineering applicability of the developed structures. From the SEM micrographs was possible to observe dense sheets of hBMSCs crossing adjacent fibers of *PBS* or *PBS-R*, mainly for the longer culture periods (Figure 6.2 I and J). Cells covering the fibers surface, eventually embedded in a matrix, were also observed in the HE stained cross-section of these scaffolds (Figure 6.2 M and N). In the case of the composite fibrous scaffolds *PBS/Cht* or *PBS/Cht-R*, the hBMSCs not only adhere to the rough fibrous surface but also colonize the inner pores/regions of the scaffold (Figure 6.2 K and L). Furthermore, occlusion of those pores was not observed, allowing the exchanging of oxygen and nutrients for and metabolites from the proliferating cells. Those remarks were also possible to observe in the HE stained cross-section of these scaffolds (Figure 6.2 O and P).

By energy dispersive spectrometry (EDS) it was possible to obtain the spectra for the *PBS/Cht-R* (Figure 6.3 A) and for the *PBS/Cht* (Figure 6.3 B) scaffolds cultured with hBMSCs under osteogenic conditions. The analysis of the EDS spectra allows to detect an increment of the Calcium (Ca) and Phosphorus (P) elements from the day 14 to the day 21 of culture, corresponding to the deposition of a mineralized

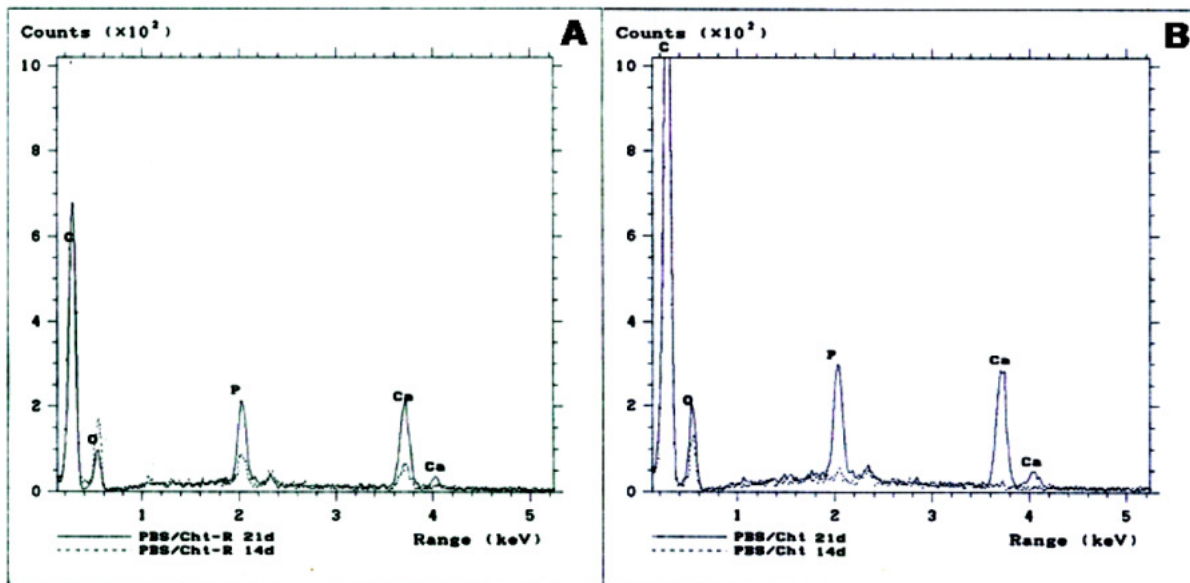


**Figure 6.3** - EDS spectra for electrospun nanofibers reinforced (i.e. *PBS/Cht-R*) (A) and non-reinforced *PBS/Cht* (B) scaffolds seeded with hBMSCs and cultured under osteogenic conditions, after 14 and 21 days.

matrix by the cells. These two chemical elements, characteristic of the inorganic phase of the native bone, were not found in the PBS-based constructs (*PBS-R* and *PBS* fibrous scaffolds) seeded and cultured with hBMSCs under the same conditions. The viability of the hBMSCs cultured on the nanofiber-reinforced microfibrinous composite scaffolds was followed along the 21 days of the experiment using the MTS assay. As depicted in Figure 6.4, all the studied fiber mesh scaffolds (nanofiber-reinforced and non-reinforced microfibrinous scaffolds) presented progressively increasing values of cell viability over the period of culture. At 7 days of culture, no significant differences were observed between all the fiber mesh scaffolds (Kruskal-Wallis test,  $p = 0.259$ ). At day 14, the hBMSCs cultured on non-reinforced *PBS* scaffolds presented a significantly higher viability than *PBS-R* ( $p = 0.002$ ), *PBS/Cht-R* ( $p < 0.001$ ) and *PBS/Cht* ( $p = 0.003$ ). At this culture time, *PBS/Cht* scaffolds also exhibited significantly higher cell viability than *PBS/Cht-R* ( $p < 0.001$ ). On the 21 day

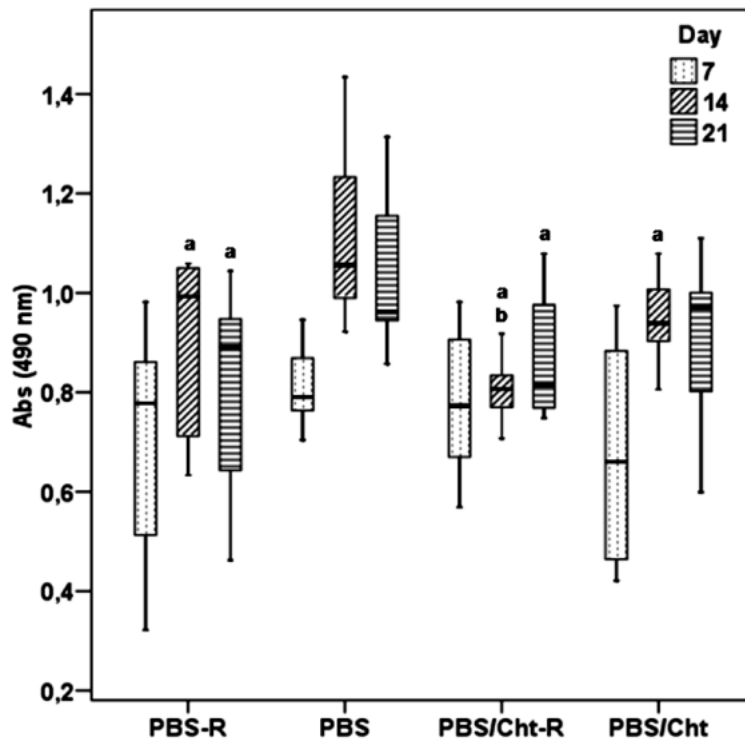


**Figure 6.4** - Box plot of the hBMSCs viability cultured in *PBS-R*, *PBS*, *PBS/Cht-R* and *PBS/Cht*, under osteogenic conditions. Data were analyzed by nonparametric way of a Kruskal-Wallis test followed by Tukey's HSD test: **a** denotes significant differences compared to *PBS*; **b** denotes significant differences compared to *PBS/Cht*.

of culture, *PBS* scaffolds showed significantly higher values of cell viability than *PBS-R* and *PBS/Cht-R* ( $p = 0.001$ ).

Considering the proliferation of hBMSCs seeded onto the studied structures (Figure 6.5), *PBS-R* scaffolds presented significantly higher DNA concentration than the other three types of scaffolds ( $p < 0.001$ ), for the 7 days of culture. Moreover, *PBS* scaffolds also presented a significantly higher proliferation than *PBS/Cht-R* and *PBS/Cht* ( $p < 0.001$ ). At the day 14, hBMSCs cultured on *PBS/Cht* exhibited significant lower DNA concentration than the other three scaffolds ( $p < 0.001$ ), while *PBS-R* scaffolds showed a significantly higher cell number than *PBS/Cht-R* ( $p < 0.001$ ). After 21 days of culture, *PBS-R* and *PBS* scaffolds presented significant higher DNA quantity than the *PBS/Cht-R* and *PBS/Cht* ( $p < 0.001$ ).

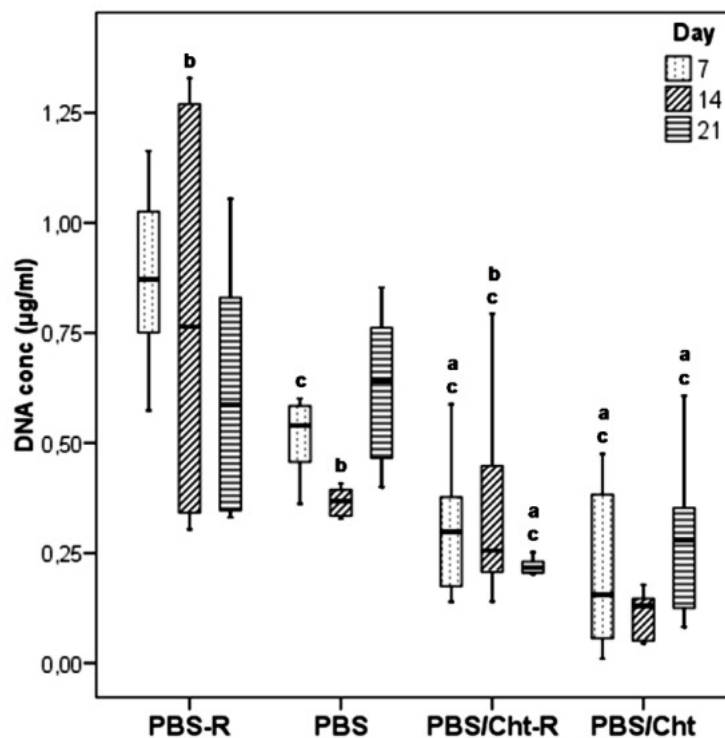


**Figure 6.5** - Box plot of the hBMSCs proliferation, cultured on *PBS-R*, *PBS*, *PBS/Cht-R* and *PBS/Cht* scaffolds under osteogenic conditions. Data were analyzed by nonparametric way of a Kruskal-Wallis test followed by Tukey's HSD test: **a** denotes significant differences compared to *PBS*; **b** denotes significant differences compared to *PBS/Cht*; **c** denotes significant differences compared to *PBS-R*.

### 6.4.3. Osteogenic Differentiation of Human Bone Marrow Mesenchymal Stem Cells on Nanofiber-Reinforced Microfibrous Composite Scaffolds

To ascertain about the osteogenic phenotype of the hBMSCs cultured on the nanofiber-reinforced microfibrous composite scaffolds and the control fiber mesh scaffolds, quantification of an enzyme involved in the onset of the mineralization process - alkaline phosphatase (ALP) - was performed (Figure 6.6). No significant differences were found between the fibrous scaffolds at the 7<sup>th</sup> day of cultured under osteogenic differentiation conditions. A significantly higher quantity of this enzyme was produced by hBMSCs cultured on non-reinforced *PBS* fiber meshes for the 14 and 21 days ( $p < 0.001$ ). Additionally, hBMSCs cultured on the other fibrous scaffolds (reinforced or not), under osteogenic differentiation conditions, present lower but constant values of ALP during the course of the experiment.

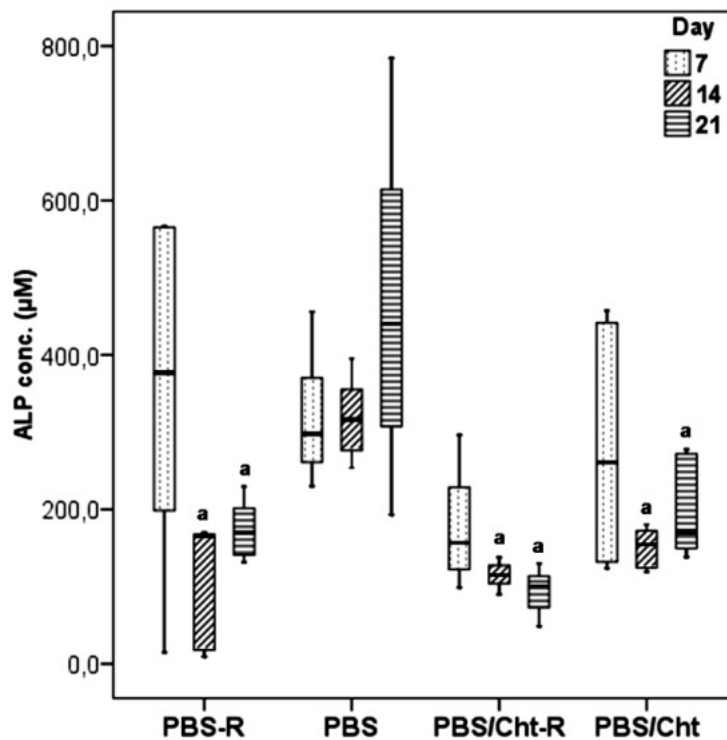


**Figure 6.6** - Box plot of the alkaline phosphatase (ALP) from hBMSCs cultured on *PBS-R*, *PBS*, *PBS/Cht-R* and *PBS/Cht* scaffolds under osteogenic conditions. Data were analyzed by nonparametric way of a Kruskal-Wallis test followed by Tukey's HSD test: **a** denotes significant differences compared to *PBS*.

The osteogenic genotype of the hBMSCs cultured on nanofiber-reinforced microfibrous composite scaffolds was assessed by quantitative PCR. The expression of the osteoblastic transcripts was normalized against the expression of a housekeeping gene, which expression is constitutive along the experimental course, without being influenced by the osteogenic differentiation culture conditions. From the analysis of the Figure 6.7 we could notice similar expression patterns of the osteoblastic genes between the nanofiber-reinforced microfibrous composite scaffolds (*PBS-R* and *PBS/Cht-R*) and the non-reinforced microfibrous scaffolds (*PBS* and *PBS/Cht*). No significant differences were found between the expression patterns of hBMSCs cultured on the *PBS/Cht-R* and *PBS/Cht*, excepting their significantly

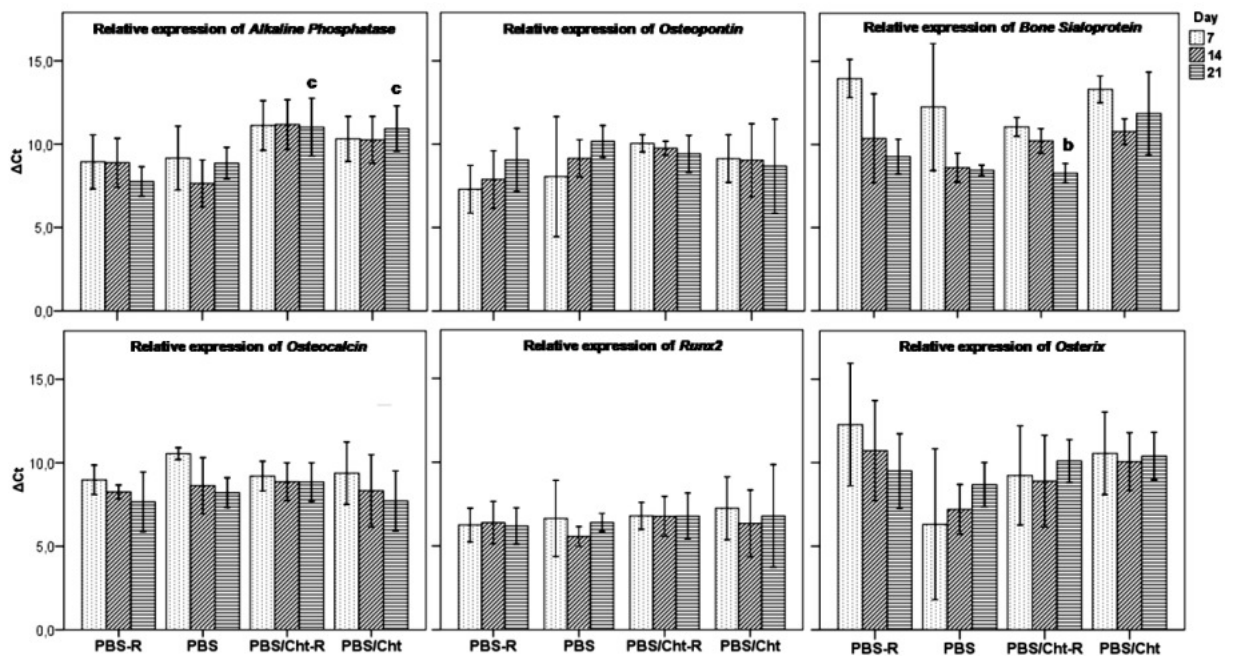


**Figure 6.7** - Relative expression of osteoblastic transcripts, namely *Alkaline Phosphatase*, *Osteopontin*, *Bone Sialoprotein*, *Osteocalcin*, *Runx2* and *Osterix*, by hBMSCs cultured on *PBS-R*, *PBS*, *PBS/Cht-R* and *PBS/Cht* scaffolds under osteogenic conditions. The expression of these genes was normalized against the housekeeping gene *GAPDH* and calculated by the  $\Delta CT$  method. Data were analyzed by nonparametric way of a Kruskal-Wallis test followed by Tukey's HSD test: **b** denotes significant differences compared to *PBS/Cht*; **c** denotes significant differences compared to *PBS-R*.

higher expression of *Alkaline Phosphatase* than hBMSCs cultured on *PBS-R*, after 21 days of culture ( $p = 0.004$  and  $p = 0.002$ , respectively). Inversely, the expression of *Bone Sialoprotein* was significant lower on the *PBS/Cht-R* than in the non-reinforced *PBS/Cht* fiber mesh scaffolds ( $p = 0.007$ ).

## 6.5. Discussion

By definition, polymer nanocomposites are two-phase systems consisting of polymers loaded with high-surface-area reinforcing fillers [36]. In addition, nanocomposites are compatible with conventional polymer processing, thus avoiding the costly layup required for the fabrication of conventional fiber-reinforced composites. The polymer-based nanocomposites are much less investigated than nanocomposites based on ceramics and metals matrices, and their studies are mostly limited to layered and particulate systems [25]. The emergence of functionalized nanoscale reinforcements having large surface area has enabled the design of novel nanocomposites with new and complex structures [3].

It is well-known that advanced composites possessing outstanding mechanical properties for structural applications are usually compounded with reinforcing of strong fibers dispersed in a continuous matrix material [21, 25]. The most important requirements of a nanofiber-reinforced composite are: adequate interface properties between the reinforcing phase and polymeric matrix [13]; the reinforcing phase should be homogeneously distributed/dispersed as isolated nanofibers and individually coated with the polymer matrix [37]. Nevertheless, even without taking into account the interfacial phenomena, the hierarchical nano-/micro-composite reinforced with a mixture of nano- and microfibers exhibit extreme properties [25]. We recently developed novel biodegradable reinforced fiber-based composites that combines electrospun chitosan nanofibers with polymeric microfibers, showing improved mechanical (i.e. tensile modulus) and degradation properties (i.e. water uptake) [14, 15]. It was also speculated that the mechanical properties of electrospun nanofibers reinforced composites could be substantially improved by forming a scaffold-like, highly interpenetrated and porous framework [20]. This hypothesis was the leading

force of the present work: the development of chitosan nanofiber-reinforced composite fiber mesh scaffolds.

Biodegradable synthetic polymers, such as polycaprolactone (PCL), poly(lactic acid) (PLA), poly(glycolic acid) (PGA), polyethylene glycol (PEG), polyvinyl alcohol (PVA) and polyurethane (PU) have been thoroughly explored as biomaterials in the field of tissue engineering [4, 38, 39]. Poly(butylene succinate) (PBS), an aliphatic thermoplastic polyester initially developed by Showa HighPolymer and proposed for environmentally driven applications under the trade name Bionolle® [40, 41], have been recently proposed as a novel biodegradable synthetic polymer for biomedical applications due to its interesting physical and biological properties [42-47]. Herein, the influence of electrospun chitosan nanofiber reinforcement on the biological performance of PBS microfibrous scaffolds was assessed; being the first report on the biological functionality of nanofiber-reinforced composite scaffolds. The main discriminatory results were observed at the phenotypic level: the higher proliferation potential of hBMSCs culture on nanofiber-reinforced PBS scaffolds (*PBS-R*) and the significant higher concentration of the enzyme ALP produced by hBMSCs cultured under osteogenic conditions on non-reinforced *PBS* scaffolds, also accompanied by significantly higher cell viability. At the genotypic level, no significant differences were observed between the nanofiber-reinforced (*PBS-R*) and non-reinforced (*PBS*) fiber mesh scaffolds. Anyway, the constitutive expression of the most important genes involved in the osteogenic differentiation process could confirm the matrix deposition and mineralization by hBMSCs cultured and differentiated on nanofibers reinforced composite scaffolds. Those observations could be justified by the location of the small amount of electrospun nanofibers (0.05 wt.%) within the bulk PBS microfibers matrix. Therefore, although electrospun nanofibers present high specific surface area, which could increase the cell-synthetic ECM interaction, this characteristic of the composite microfibers was not sensed by the adjacent cultured cells.

Considering the requirements of synthetic ECMs or scaffolds for tissue engineering applications, blends/compositions made of synthetic and natural biodegradable polymers can be designed and tailored to obtain a wide range of

desirable properties in exquisite combinations (i.e. mechanical properties, degradation, hydrophilicity and biocompatibility). It is possible to combine the processing freedom offered by synthetic polymers, with the biocompatibility and excellent biological interface of natural polymers with cells [42, 48]. Indeed, some natural-origin polymers may offer the advantage of being similar to native ECM macromolecules. In the present case, chitosan is a polysaccharide structurally similar to the glycosaminoglycans of the native ECM found in different human tissues. Moreover, natural polymers present the attractive characteristic of being degraded by naturally occurring enzymes and, eventually, metabolized by physiological mechanisms. The aliphatic polyester PBS previously described presents a hydrophobic character. Inversely, the chitosan molecule is rich in polar groups (i.e. –OH and –NH<sub>2</sub>) and thus very hydrophilic. Therefore, the presence of chitosan in the composite enhances the hydrophilic properties, thus resulting in enhanced degradation properties associated with a loss of tensile modulus [47]. The incorporation of electrospun nanofibers into the composite not only provides additional elastic modulus, but also enhances the surface area of the chitosan phase, facilitating the water uptake capability [14].

The composite microfibers of *PBS/Cht* reinforced by electrospun nanofibers, assemble in a fiber mesh structure, were also seeded with human bone marrow mesenchymal stem cells and cultured during 21 days under osteogenic differentiation conditions. No substantial differences were observed in the biological data (phenotypic and genotypic results) between nanofiber-reinforced (*PBS/Cht-R*) and non-reinforced (*PBS/Cht*) fiber mesh scaffolds. The constitutive expression of the transcripts involved in the osteogenesis, corroborate the successful differentiation of hBMSCs into osteoblasts on nanofiber-reinforced composite scaffolds. On those composite scaffolds, the electrospun nanofibers and also the chitosan microparticles are covered by a thin PBS rich layer [42, 43], preventing a close interaction of cells with the chitosan domains. However, the presence of the chitosan microparticles seems to have an important role in the deposition of mineralized ECM, as suggested by the increased amount of calcium phosphates produced by the osteogenic differentiated hBMSCs. This remarkable result was not observed in the PBS-based

microfibers, indicating that the natural origin material used in the composites (i.e. chitosan) plays an important role in the cell mediated mineralization process. Therefore, while a detailed mechanism is beyond the scope of this work (i.e. nanofiber reinforcement), the biological performance of the biodegradable nanofibrous reinforced microfibrous scaffolds is mainly a function of the physicochemical (e.g. roughness and chemical composition) surface properties.

## 6.6. Conclusions

Novel complex hierarchical fibrous composite scaffolds were developed based on biodegradable polymeric microfibers (*PBS* or *PBS/Chit*) reinforced by electrospun chitosan nanofibers. The osteogenic potential of these nanofiber-reinforced composite fiber mesh scaffolds was assessed by seeding and culturing human bone marrow mesenchymal stem cells (hBMSCs). Data demonstrated that the electrospun chitosan nanofibers used to reinforce the microfibers, although improving the mechanical and degradation properties of the composite fibers, still preserve the excellent *in vitro* biological performance already described for *PBS/Chit* fiber mesh scaffolds. Among the developed fiber meshes, the *PBS/Chit*-based scaffolds sustained an ECM deposition and mineralization by the osteogenic differentiated hBMSCs. This is the first biological work reporting the potentiality of nanofiber-reinforced microfibrous scaffolds for bone tissue engineering approaches.

## 6.7. References

1. Alberts B, Johnson A, Lewis J, Raff M, Roberts K, Walter P. Molecular Biology of the Cell. Fourth Edition ed. London, UK: Garland Science, 2002.
2. Weiner S, Wagner HD. The material bone: Structure-mechanical function relations. Annual Review of Materials Science 1998; 28(1):271-298.
3. Teo WE, Ramakrishna S. Electrospun nanofibers as a platform for multifunctional, hierarchically organized nanocomposite. Composites Science and Technology 2009; 69(11-12):1804-1817.

4. Lutolf MP, Hubbell JA. Synthetic biomaterials as instructive extracellular microenvironments for morphogenesis in tissue engineering. *Nature Biotechnology* 2005; 23(1):47-55.
5. Hutmacher DW, Schantz JT, Lam CX, Tan KC, Lim TC. State of the art and future directions of scaffold-based bone engineering from a biomaterials perspective. *Journal of Tissue Engineering and Regenerative Medicine* 2007; 1(4):245-260.
6. Goldberg M, Langer R, Jia XQ. Nanostructured materials for applications in drug delivery and tissue engineering. *Journal of Biomaterials Science - Polymer Edition* 2007; 18(3):241-268.
7. Neves NM, Campos R, Pedro A, Cunha J, Macedo F, Reis RL. Patterning of polymer nanofiber meshes by electrospinning for biomedical applications. *International Journal of Nanomedicine* 2007; 2(3):1-16.
8. Martins A, da Silva MA, Faria S, Marques AP, Reis RL, Neves NM. Differentiated Stem Cells are Sensitive to Patterned Nanofiber Meshes? Submitted 2009.
9. Zhang D, Chang J. Patterning of electrospun fibers using electroconductive templates. *Advanced Materials* 2007; 19(21):3662-3667.
10. Martins A, Araujo JV, Reis RL, Neves NM. Electrospun nanostructured scaffolds for tissue engineering applications. *Nanomedicine* 2007; 2(6):929-942.
11. Martins A, Pinho ED, Faria S, Pashkuleva I, Marques AP, Reis RL, *et al.* Surface modification of electrospun polycaprolactone nanofiber meshes by plasma treatment to enhance biological performance. *Small* 2009; 5(10):1195-1206.
12. Bergshoeff MM, Vancso GJ. Transparent nanocomposites with ultrathin, electrospun nylon-4,6 fiber reinforcement. *Advanced Materials* 1999; 11(16):1362-1365.
13. Fong H. Electrospun nylon 6 nanofiber reinforced BIS-GMA/TEGDMA dental restorative composite resins. *Polymer* 2004; 45(7):2427-2432.
14. Pinho ED, Martins A, Araujo JV, Reis RL, Neves NM. Degradable particulate composite reinforced with nanofibres for biomedical applications. *Acta Biomaterialia* 2009; 5:1104-1114.

15. Pinho ED, Martins A, Araujo JV, Reis RL, Neves NM. Size also matters in biodegradable composite microfiber reinforced by chitosan nanofibers. Submitted 2009.
16. Tian M, Gao Y, Liu Y, Liao Y, Xu R, Hedin NE, *et al.* Bis-GMA/TEGDMA dental composites reinforced with electrospun nylon 6 nanocomposite nanofibers containing highly aligned fibrillar silicate single crystals. *Polymer* 2007; 48(9):2720-2728.
17. Gao Y, Sagi S, Zhang L, Liao Y, Cowles DM, Sun Y, *et al.* Electrospun nano-scaled glass fiber reinforcement of bis-GMA/TEGDMA dental composites. *Journal of Applied Polymer Science* 2008; 110(4):2063-2070.
18. Chen G, Liu H. Electrospun cellulose nanofiber reinforced soybean protein isolate composite film. *Journal of Applied Polymer Science* 2008; 110(2):641-646.
19. Dodiuk-Kenig H, Lizenboim K, Roth S, Zalsman B, McHale WA, Jaffe M, *et al.* Performance enhancement of dental composites using electrospun nanofibers. *Journal of Nanomaterials* 2008; (6 pages).
20. Lin S, Cai Q, Ji J, Sui G, Yu Y, Yang X, *et al.* Electrospun nanofiber reinforced and toughened composites through in situ nano-interface formation. *Composites Science and Technology* 2008; 68(15-16):3322-3329.
21. Kim JS, Reneker DH. Mechanical properties of composites using ultrafine electrospun fibers. *Polymer Composites* 1999; 20(1):124-131.
22. Tian M, Gao Y, Liu Y, Liao Y, Hedin NE, Fong H. Fabrication and evaluation of Bis-GMA/TEGDMA dental resins/composites containing nano fibrillar silicate. *Dental Materials* 2008; 24(2):235-243.
23. Sihn S, Kim RY, Huh W, Lee KH, Roy AK. Improvement of damage resistance in laminated composites with electrospun nano-interlayers. *Composites Science and Technology* 2008; 68(3-4):673-683.
24. Norman JJ, Desai TA. Methods for fabrication of nanoscale topography for tissue engineering scaffolds. *Annals of Biomedical Engineering* 2006; 34(1):89-101.
25. Dzenis YA. Hierarchical nano-/micromaterials based on electrospun polymer fibers: Predictive models for thermomechanical behavior. *Journal of Computer-Aided Materials Design* 1996; 3(1-3):403-408.

26. Park SH, Kim TG, Kim HC, Yang DY, Park TG. Development of dual scale scaffolds via direct polymer melt deposition and electrospinning for applications in tissue regeneration. *Acta Biomaterialia* 2008; 4(5):1198-1207.
27. Santos MI, Fuchs S, Gomes ME, Unger RE, Reis RL, Kirkpatrick CJ. Response of micro- and macrovascular endothelial cells to starch-based fiber meshes for bone tissue engineering. *Biomaterials* 2007; 28(2):240-248.
28. Santos MI, Tuzlakoglu K, Fuchs S, Gomes ME, Peters K, Unger RE, *et al.* Endothelial cell colonization and angiogenic potential of combined nano- and micro-fibrous scaffolds for bone tissue engineering. *Biomaterials* 2008; 29(32):4306-4313.
29. Tuzlakoglu K, Bolgen N, Salgado AJ, Gomes ME, Piskin E, Reis RL. Nano- and micro-fiber combined scaffolds: a new architecture for bone tissue engineering. *Journal of Materials Science: Materials in Medicine* 2005; 16(12):1099-1104.
30. Martins A, Chung S, Pedro AJ, Sousa RA, Marques AP, Reis RL, *et al.* Hierarchical starch-based fibrous scaffold for bone tissue engineering applications. *Journal of Tissue Engineering and Regenerative Medicine* 2009; 3(1):37-42.
31. Moroni L, Schotel R, Hamann D, De Wijn JR, Van Blitterswijk CA. 3D fiber-deposited electrospun integrated scaffolds enhance cartilage tissue formation. *Advanced Functional Materials* 2008; 18(1):53-60.
32. Bajada S, Mazakova I, Richardson JB, Ashammakhi N. Updates on stem cells and their applications in regenerative medicine. *Journal of Tissue Engineering and Regenerative Medicine* 2008; 2(4):169-183.
33. Pittenger MF, Mackay AM, Beck SC, Jaiswal RK, Douglas R, Mosca JD, *et al.* Multilineage potential of adult human mesenchymal stem cells. *Science* 1999; 284(5411):143-147.
34. Delorme B, Charbord P. Culture and characterization of human bone marrow mesenchymal stem cells. *Methods in Molecular Medicine* 2007; 140:67-81.
35. Hofmann S, Kaplan D, Vunjak-Novakovic G, Meinel L. Tissue Engineering of Bone. In: Vunjak-Novakovic G, Freshney RI, editors. *Culture of Cells for Tissue Engineering*. New Jersey: John Wiley & Sons, Inc., 2006. p. 323-373.
36. Schaefer DW, Justice RS. How nano are nanocomposites? *Macromolecules* 2007; 40(24):8501-8517.

37. Coleman JN, Khan U, Gun'ko YK. Mechanical reinforcement of polymers using carbon nanotubes. *Advanced Materials* 2006; 18(6):689-706.
38. Agrawal CM, Ray RB. Biodegradable polymeric scaffolds for musculoskeletal tissue engineering. *Journal of Biomedical Materials Research, Part A* 2001; 55(2):141-150.
39. Gomes ME, Reis RL. Biodegradable polymers and composites in biomedical applications: From catgut to tissue engineering Part 1 Available systems and their properties. *International Materials Reviews* 2004; 49(5):261-273.
40. Gan Z, Abe H, Kurokawa H, Doi Y. Solid-state microstructures, thermal properties, and crystallization of biodegradable poly(butylene succinate) (PBS) and its copolyesters. *Biomacromolecules* 2001; 2(2):605-613.
41. Ray SS, Okamoto K, Maiti P, Okamoto M. New poly(butylene succinate)/layered silicate nanocomposites: preparation and mechanical properties. *Journal of Nanoscience and Nanotechnology* 2002; 2(2):171-176.
42. Correlo VM, Boesel LF, Bhattacharya M, Mano JF, Neves NM, Reis RL. Properties of melt processed chitosan and aliphatic polyester blends. *Materials Science and Engineering A* 2005; 403(1-2):57-68.
43. Correlo VM, Boesel LF, Pinho E, Costa-Pinto AR, Alves da Silva ML, Bhattacharya M, *et al.* Melt-based compression-molded scaffolds from chitosan-polyester blends and composites: Morphology and mechanical properties. *Journal of Biomedical Materials Research, Part A* 2009; 91(2):489-504.
44. Costa-Pinto AR, Salgado AJ, Correlo VM, Sol P, Bhattacharya M, Charbord P, *et al.* Adhesion, proliferation, and osteogenic differentiation of a mouse mesenchymal stem cell line (BMC9) seeded on novel melt-based chitosan/polyester 3D porous scaffolds. *Tissue Engineering, Part A* 2008; 14(6):1049-1057.
45. Coutinho DF, Pashkuleva IH, Alves CM, Marques AP, Neves NM, Reis RL. The effect of chitosan on the in vitro biological performance of chitosan-poly(butylene succinate) blends. *Biomacromolecules* 2008; 9(4):1139-1145.
46. Oliveira JT, Correlo VM, Sol PC, Costa-Pinto AR, Malafaya PB, Salgado AJ, *et al.* Assessment of the suitability of chitosan/polybutylene succinate scaffolds

seeded with mouse mesenchymal progenitor cells for a cartilage tissue engineering approach. *Tissue Engineering, Part A* 2008; 14(10):1651-1661.

47. Correlo VM, Pinho ED, Pashkuleva I, Bhattacharya M, Neves NM, Reis RL. Water absorption and degradation characteristics of chitosan-based polyesters and hydroxyapatite composites. *Macromolecular Biosciences* 2007; 7(3):354-363.

48. Sarasam A, Madihally SV. Characterization of chitosan-polycaprolactone blends for tissue engineering applications. *Biomaterials* 2005; 26(27):5500-5508.

## **Section V**

### **2<sup>ND</sup> GENERATION ELECTROSPUN SCAFFOLDS**



## Chapter 7

### Solving Cell Infiltration Limitations of Electrospun Nanofiber Meshes for Tissue Engineering Applications

This chapter is based on the following publication: Guimarães AC, Martins A, Pinho ED, Faria S, Reis RL, Neves NM. *Solving Cell Infiltration Limitations of Electrospun Nanofiber Meshes for Tissue Engineering Applications*. Submitted.

## **7.1. Abstract**

Electrospinning is a simple and versatile polymer processing technique, which applies electrostatic forces to a polymeric solution, generating ultrafine fibers. This technique has been gaining popularity, since it allows the production of non-woven meshes with high surface area-to-volume ratio and high micro-porosity. Additionally, these nanofiber meshes can mimic the morphology of the extracellular matrix of many human tissues and, therefore, have a specific interest as scaffolds for Tissue Engineering applications. However, electrospun nanofiber meshes present an important limitation to this type of application: the obtained pore size is typically too small to allow cell penetration into the inner regions of the nanofibrous scaffold. To overcome this problem, PCL and PEO solutions are electrospun simultaneously to obtain a dual composition nanofiber mesh. By the selective dissolution of the PEO nanofiber fraction, a mesh with higher pore size will be obtained. The electrospun nanofiber meshes, after the PEO dissolution show a statistically significant increased pore size, when compared with PCL nanofiber meshes with comparable quantity of material, and confirmed by interferometric optical profilometry. The biologic performance of these enhanced pore size nanofibrous structures is assessed with human osteoblast-like cells, using a specially designed fixing system that enables only cell infiltration across the thickness of the mesh. By scanning electron microscopy and laser scanning confocal microscopy it is observed that cells could penetrate into the nanofibrous structure and even migrate to the opposite side of the mesh. An electrospun mesh with sufficient pore size to allow cell infiltration into its structure was produced, enabling obtaining a fully populated construct appropriate for 3D Tissue Engineering applications.

## **7.2. Introduction**

Tissue Engineering is an emergent research area that offers the promise of tissue regeneration, relevant for many clinical conditions. The success of tissue engineering is highly dependent of a scaffold that will act as a temporary matrix for

cell proliferation and extracellular matrix deposition, with consequent tissue in-growth until the new tissue is totally regenerated [1]. So, an appropriate 3D scaffold (i.e. its biocompatibility, pore size, porosity and interconnectivity, biodegradability, and adequate surface chemistry and mechanical properties) is an essential component for a tissue engineering strategy [2, 3]. Polymers are believed to be the ideal material for tissue engineering applications. Both natural and synthetic origin polymers can be applied in this kind of strategy. Much of the current research is focused on natural materials by their improved biocompatibility (among others we can find, collagen [4-6], fibrinogen [7], chitosan [8-10], starch [11-13], hyaluronic acid [14, 15] and poly(hydroxybutyrate) [16]. Synthetic biodegradable polymers are the ones that are more commonly used within the biomedical engineering field. Their chemical versatility and processability varies according to their structure and nature.

Besides the choice of adequate materials, the macro and micro-structural properties of the materials are of utmost importance. It is very important that the scaffold can mimic, as much as possible, the physicochemical cues provided by extracellular matrix (ECM), to guide communities of cells to rebuild the native tissue structure [17-21]. In many tissues, cells are surrounded by an intricate network of protein fibrils and interwoven fibers within a hydrated network of glycosaminoglycan chains that determine the physical properties of the tissue [22]. Those components produce an interconnected nano- or micro-ranged fibrous network in the ECM. The ECM provides an appropriate microenvironment for cells, controls the tissue structure and regulate many cellular functions including the adhesion, migration and proliferation to maintain the tissue structure. ECM is also responsible for transmitting signals to cell membrane receptors, and to orchestrate the controlled release of growth factors and signaling molecules that control the structure and function of the tissue [22-24].

A series of processing techniques such as solvent casting [25], fiber bonding [26, 27], wet-spinning [28], melt based technologies [12, 29], high pressure-based methods [30, 31], freeze drying [32], and rapid prototyping technologies [33-35] were developed with the aim of producing scaffolds with adequate properties for tissue engineering. Electrospinning has attracted great attention in the field of Tissue

Engineering, since the produced structures are composed by nanoscale, or more correctly submicron, fibers with interconnected micro-pores and an high surface to volume ratio, which show features that are similar to the topographic characteristics of the ECM [17, 23, 36]. Additionally, electrospinning is a relatively versatile polymer processing technique, in the sense that several polymeric blends and compositions with other materials or additives (such as growth factors and other cell regulatory biomolecules) and even proteins [37] and living cells [38, 39] can be used to develop functionally active nanofibrous structures. The electrospinning process is based on the application of an electric field, generated by a high voltage power supply applied, between a polymeric solution and a metal ground collector. When the electric field reaches a critical value, the electrostatic force overcomes the surface tension of the polymeric solution and a charged polymer jet is ejected from the capillary tip of the needle. As the jet travels towards the grounded collector, undergoes a stretching process together with a fast solvent evaporation. This process results in the formation of a random non-woven mesh composed by solid and long nanofibers [40, 41]. The remaining solvent in the fibers allows for the establishment of links between successive layers of the fibers in the mesh.

Despite all the advantages of using electrospun scaffolds for Tissue Engineering applications, these meshes have a major limitation. The pores formed in the electrospun fibrous meshes typically do not allow cell infiltration into the inner regions of the structure. This is a major shortcoming of those structures that can compromise the otherwise interesting potential of electrospun nanofiber meshes in the tissue engineering and regenerative medicine [17]. Much research has been devoted focus in the on development of fibers with smaller diameters to maximize surface area. However, it was demonstrated that the mean pore radius varies directly with the fiber diameter, leading to smaller pore size [42]. Thus, the nanofiber mesh will essentially behave as a two dimensional sheet where the cells can only proliferate at the surface, instead of allowing a three-dimensional structure where cells are able to infiltrate. Some tissues may still benefit from such 2D structures but most tissues need 3D structuring. The use of porogen agents, such as salt particles [43, 44], chemical blowing agents [45] or post processing by laser machinery [46] are other

possible strategies that have been already described in literature, aiming at increasing pore size of electrospun meshes. In the referred salt leaching technique, salt particles are deposited layer by layer, which causes the final delamination of the nanofiber scaffold. The structures obtained have still limitations for cell infiltration that only takes place through the lateral side of the scaffold and not across the thickness of the nanofiber mesh [43]. By using a blowing agent pores are created in discrete points of the mesh, but cellular infiltration is not fully demonstrated [45]. Laser post-processing is also capable of producing localized cavities or channels in the nanofiber meshes. Biological assays were not yet reported to verify the extent of cell infiltration through those laser processed holes in the mesh structure [46].

In this work is presented a different strategy to increase the pore size of electrospun nanofiber meshes that consists in creating a dual composition (two types of polymer nanofibers produced simultaneously) non-woven nanofiber mesh. After the production of the mesh, one of these polymers was selectively removed, to increase the void volume and, consequently, the pore size. To test this concept, we combined an in-house developed dual-spinneret electrospinning setup with a rotating plate as collector, to obtain a homogenous mixture of the two polymeric nanofiber types. Other authors [47] described the use of a similar strategy applied to aligned nanofiber meshes, trying to overcome the dense fiber packing and reduced pore size. It is known however that the random distribution is the most typical morphology of electrospun meshes, thus being the morphology where the effective control of the pore size is much more challenging, imperative and also of wider application. We propose herein the production of composite meshes of polycaprolactone (PCL) and poly(ethylene oxide) (PEO) with the posterior selective removal of the PEO fraction to control the pore size.

To determine the success of our approach, the characterization of the produced electrospun nanofiber meshes was performed by scanning electron microscopy (SEM), interferometric optical profilometry and contact angle tests, characterizing some physical properties that may influence the cellular behavior. We also characterized the fiber diameter and pore size of the meshes by image analysis of SEM micrographs. Biologic assays were performed to show the efficacy of the

processing method, facilitating cell penetration into the nanofiber meshes with increased pore size. A novel clamping system was developed to undoubtedly prove the cellular penetration through all the thickness of the produced meshes. The cultured cells were analysed by SEM and laser scanning confocal microscopy. MTS and DNA assays were performed to conclude about the cell viability and proliferation, respectively. We conclude that the proposed method can be used to control the pore size without compromising the cell viability and proliferation.

### **7.3. Materials & Methods**

#### *7.3.1. Electrospinning processing*

Polycaprolactone (PCL), with a molecular weight of 80000 Da (TONE™, Union Carbide Chemicals and Plastics Division, New Jersey), was dissolved in an organic solvent mixture of chloroform (Sigma-Aldrich) and dimethylformamide (DMF) (Sigma-Aldrich) in a 7:3 ratio and at 17 % (w/v) concentration, as described elsewhere [48]. PEO (Sigma-Aldrich) with molecular weight of 100000 Da was dissolved at 25 % (w/v) in a mixture of water/ethanol (6:4 ratio). Both polymer concentrations and chloroform/DMF ratio were defined after several optimization stages to obtain the most stable processing and leading to the more convenient mesh morphology.

To produce the dual composition electrospun nanofiber meshes it was developed a system that allows the simultaneous electrospinning of more than one polymeric solutions. Two independently controllable high voltage power supplies (semi-commercial from UltraVolt and Bosh) were used to generate electrical voltages ranging from 8 kV to 20 kV, with the lower values being applied to the PCL solution. Each polymer solution was placed in a 10 ml syringe coupled to a needle of 21G with a blunt tip. The feeding rate was established at a constant value of 0.25 ml/h, by precision syringe pumps (Aladdin-1000-220B, UK), for both polymeric solutions.

A conducting and rotating plate, connected to the ground and with a rotating speed of 15 r.p.m., was used as collector to obtain a homogeneous nanofiber mixture. A collector to needle tip distance of 12 cm was defined after an optimization procedure, and the syringes were placed at 9 cm distance to minimize the

electrospun jet interference. The process was continued for at least 2 hours for the production of each dual composition nanofiber mesh with a final thickness of 50-60  $\mu\text{m}$ . The nanofiber meshes were further dried at room temperature for at least 1 day to remove all the remaining solvent.

With the goal of increasing the pore size of the dual composition nanofibers meshes, the PEO nanofibers were selectively removed by dissolution in distilled water, for a period of 24 hours, at 37  $^{\circ}\text{C}$ . After the dissolution procedure the meshes were dried in an oven at 37  $^{\circ}\text{C}$ .

### 7.3.2. Physical characterization

The morphology of the electrospun nanofiber meshes was assessed by scanning electron microscopy (SEM) (Leica Cambridge S360, England). The meshes were sputter coated with gold (sputter coater model SC502, Fisons Instruments, England) and then observed with an accelerating voltage of up to 15 kV. Samples were analyzed with the dual composition (PCL-PEO NFM) and after the selective PEO dissolution (PCL-PEO NFM, after PEO dissolution).

The fiber diameter was measured from SEM micrographs with the software *ImageJ* (version 1.38X, Wayne Rasband National Institutes of Health, USA). For each sample, at least 10 micrographs were used (at a 5000X magnification) and, in each micrograph, 15 different fibers were randomly selected. Pore size was also evaluated from SEM micrographs using the *ImageJ* software. The pore size values were obtained from SEM micrographs (magnification of 5000X), in a total of 60 measurements for each the condition. The pore size values were obtained by converting the contour of the pore area into a circumference of equivalent perimeter and determined from the circumference an equivalent diameter [49].

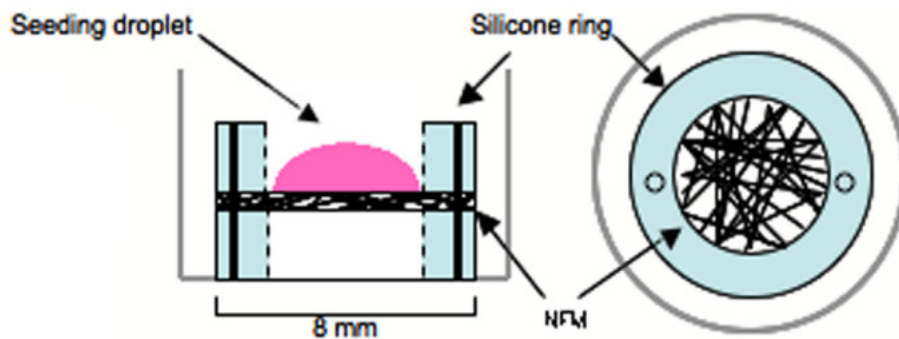
Interferometric Optical Profilometry was used to assess the topography of the samples. A surface profiler (DEKTA<sup>3</sup>ST, Veeco) in Vertical Scanning Interferometry (VSI) mode, with a vertical resolution of 3 nm, was used to measure the surface roughness. Five different regions (119  $\mu\text{m}$   $\times$  91  $\mu\text{m}$ ) for each sample were measured. The Average Roughness ( $R_a$ ) and root mean square (RMS) roughness ( $R_q$ ) values were automatically calculated by the equipment analytical software Wyco Vision<sup>®</sup> 32.

The wettability of the surfaces was assessed by contact angle measurements. Measurements of the static contact angle were carried out by the Sessile Drop method using contact angle equipment (model OCA 15plus, DataPhysics Instruments, Germany) with a high performance image processing system. The used standard polar liquid, water (2  $\mu$ l, HPLC grade) was added by a motor driven syringe, at different zones of each sample, and the measurement time was extended until 20 minutes at room temperature. At least three measurements were carried out for each sample (PCL NFM, PCL-PEO NFM and PCL-PEO NFM, after PEO dissolution).

### 7.3.3. Biological assays

The dual composition electrospun nanofiber meshes were cut into small disks with 8 mm diameter. In order to demonstrate the enhanced cellular infiltration into the nanofibers meshes, it was developed a system to clamp the mesh. This system consists in two silicone rings (with 8 mm and 5 mm of outside and inside diameter, respectively), held together with the sample in two points by a nylon stitch (Scheme 7.1). When clamped between the rings, the samples have no direct contact with the surface of the well. This fixing system was sterilized by ethylene oxide, with the meshes already clamped between the rings.

In this study, it was used a well established cell line of human primary osteosarcoma (SaOs-2 cell line; European Collection of Cell Cultures (ECACC), UK), cultered in Dulbecco's Modified Eagle Medium (DMEM) (Sigma-Aldrich, Germany)



**Scheme 7.1** - Schematic representation of the fixing system used in the biologic assay. Lateral and top views.

with 10 % fetal bovine serum (Biochrom AG, Berlin, Germany) and 1 % of antibiotic-antimycotic antimycotic mixture (Gibco, GB), and harvested by trypsinization before the scaffolds' seeding.

Before the seeding, the fixing systems containing the dual composition electrospun nanofiber meshes were placed in a 48 well-plate with 1 ml of ultra pure water to dissolve the PEO nanofibers. The well-plate was placed in a incubator at 37 °C for a period of 24 hours. The seeding was performed with 50 µL cell suspension ( $1 \times 10^5$  cells/ml) over each scaffold. The developed nanofiber mesh fixing system confined the seeding area, avoiding cell adhesion to other surfaces of the culture well. The cell-seeded scaffolds were incubated in a humidified atmosphere at 37 °C, containing 5 % CO<sub>2</sub>, during 4 hour and, then, it was added 1 ml of culture medium to each well. The culture medium was changed every 3 to 4 days. Triplicates were used for every time culture period (1, 3, 7 and 14 days).

To evaluate the cell morphology and their distribution in the nanofibrous scaffolds, the constructs were previously washed with phosphate buffer saline (Sigma, USA) and fixed with 2.5 % glutaraldehyde solution (Sigma, USA). Then, they were dehydrated by immersion in a series of ethanol solutions with increasing concentration, and air-dried overnight in a hood. The samples were sputter coated with gold (sputter coater model SC502, Fisons Instruments, England) and observed in the SEM (Leica Cambridge S360, England).

The penetration of the cells into the nanofiber mesh was evaluated by laser scanning confocal microscopy (Olympus, Fluoview 1000). The samples were fixed with formaline for 30 minutes at room temperature and then washed with PBS. The staining was made with 4,6-diamidino-2-phenylindole dilactate (DAPI) (Sigma, Germany) and phalloidin-tetramethylrhodamine B isothiocyanate (Sigma, Germany) for the nucleolus and actin filaments, respectively. The constructs was then mounted on glass microscope slides and observed. Samples were excited simultaneously at 345 nm for DAPI and 540/545 nm for phalloidin. Emission at 458 nm was mapped to the blue channel and 570/573 nm to the red channel. Nanofibers were observed in DIC black ground levelling mode. Representative images were taken as individual slices and the images are built from series of stacked images.

Cell viability was determined by the colorimetric MTS assay (CellTiter 96<sup>®</sup> AqQueous One Solution Cell Proliferation Assay, Promega, USA) on days 1, 3, 7 and 14 of culture. The constructs were immersed in phenol red- and FBS-free DMEM and MTS reagent was added in a proportion of 5 to 1, in a total of 600  $\mu$ L per well. The well-plate was incubated at 37 °C during 3 hours, according to the MTS reagent manufacturer instructions. Five replicas of 100  $\mu$ L were pipetted from each well and placed in a 96 Costar flat bottom well-plate and its absorbance read in a microplate reader (Synergie HT, Bio-Tek, USA) at a 490 nm.

Cell proliferation was assessed by the DNA quantification assay. This test determines the total amount of double-stranded DNA, corresponding to different culturing time. Quantification was performed using the Quant-iT<sup>™</sup> PicoGreen dsDNA Assay Kit (Invitrogen<sup>™</sup>, Molecular Probes<sup>™</sup>; Oregon, USA), according to the instructions of the manufacturer. Briefly, cells in the construct were lysed by osmotic and thermal shock and the supernatant used for the DNA quantification assay. A fluorescent dye, PicoGreen, was used because of its high sensitivity and specificity to double-stranded DNA. The fluorescence of the dye was measured at an excitation wavelength of 485/20 nm and at an emission wavelength of 528/20 nm, in a microplate reader (Synergie HT, Bio-Tek; USA), being the intensity of the signal proportional to the amount of DNA. Triplicates were made for each sample, allowing performing a statistical analysis. The DNA concentration of each sample was calculated using a standard curve relating quantity of DNA and fluorescence intensity.

#### *7.3.4. Statistical analysis*

Statistical analysis was performed using the SPSS statistic software (Release 8.0.0 for Windows). Firstly, a Shapiro-Wilk test was performed to ascertain about the data normality. This test showed that some results do not follow a normal distribution. In the analysis of the results, *p*-values lower than 0.01 were considered statistically significant.

To compare the morphological properties (i.e. fiber diameter, pore size, roughness parameters and water contact angle) of the produced NFMs, a Kruskal-

Wallis test was performed. When the analysis indicated significant differences among the produced NFMs, a Tukey's HSD test for multiple comparisons was performed to find where the differences occur. In the case of biological results, which also did not follow a normal distribution, a Mann-Whitney U-test was performed to determine the cell performance when cultured in those NFMs.

#### **7.4. Results**

Initially, PCL and PEO solutions were individually electrospun under several solution parameters (polymer and solvent concentration) and processing parameters (voltage, needle tip to collector distance and flow rate) to produce homogeneous fibers with uniform diameters in the absence of visible defects, namely bead-like morphology. Both polymers were electrospun with a needle tip to collector distance of 12 cm and voltages in the range of 9-15 kV for PCL solution and 13-19 kV for PEO solution. Due to the process instability, caused by the relative proximity of the two electrically driven polymer jets, forced us to vary the applied voltages for both polymers, being always required higher voltage for the PEO solution. Lower applied voltages were observed to result in fibers with visible defects and also regions of polymer aggregation (Figure 7.1 A1). Higher applied voltages produced less uniform fibers with larger diameter variations on the same fiber mesh (Figure 7.1 C1). Smooth, uniform fibers without bead-like structures were observed using intermediate voltages (Figure 7.1 B1). This sample was processed at 15 kV for PCL solution and 17 kV for PEO solution. The dual composition PCL-PEO nanofiber meshes (NFM) used afterwards were all processed using those optimal processing conditions.

To determine the ideal dissolution conditions for PEO nanofibers, several electrospun dual composition PCL-PEO NFM were immersed in distilled water without mechanical agitation. It was described in the literature that the PEO dissolution kinetics in water increases in the temperature range 20–40 °C [50]. Thus, a distilled water bath was heated at 37 °C to attain conditions promoting a faster and complete dissolution of the PEO fraction. After a dissolution period of 2 hours and 24 hours, the meshes processed at lower voltages showed a beaded morphology with significant variation in fiber diameter and polymer accumulation (Figures 7.1 A2 and

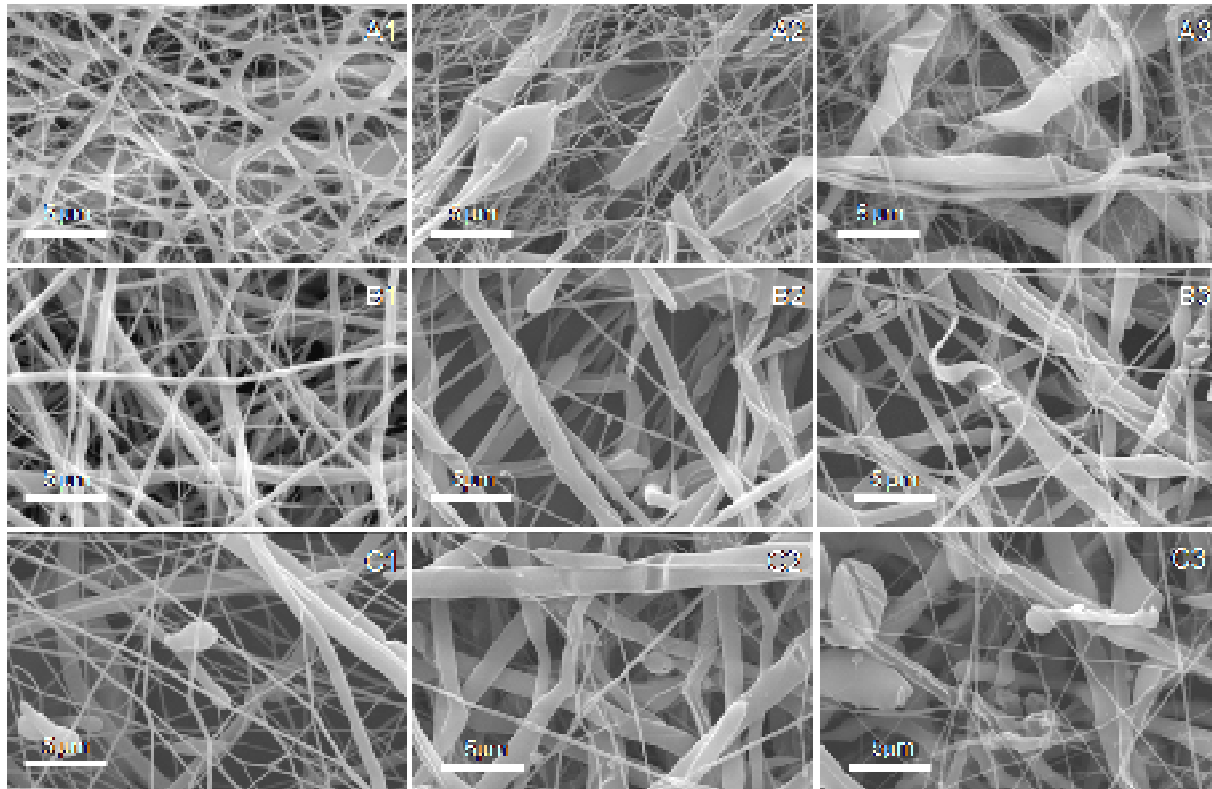


**Figure 7.1** - SEM micrographs of electrospun dual composition PCL-PEO NFM, produced with different applied tensions, from lower (**A**) to higher (**C**), without dissolution (**1**), after 2 hours (**2**) and 24 hours of dissolution (**3**) at 37 °C. Details evidenced by arrows. Original magnification of 500X.

A3). After PEO dissolution during 24 hours it is shown that the nanofibers maintain their continuity and general morphology in meshes processed at intermediate voltage. The PCL nanofibers, after the dissolution of the PEO fraction, assumed a twisted morphology (Figure 7.1 B3). The final morphology of the mesh obtained with higher voltage shows discontinuous fibers with abrupt variations of the fiber diameter and polymer accumulation points (Figure 7.1 C3). All samples presented visible surface marks caused by the dissolution of PEO fibers (Figures 7.1 A3, B3, C3). A detail of those marks is shown magnified in an insight micrograph of Figure 7.1 B3. The SEM micrographs showed that PCL-PEO meshes, when submitted to the dissolution process during 24 hours, have enhanced pore size caused by the dissolution of the PEO fraction. All subsequent dissolutions were performed during a period of 24 hours at 37 °C. Meshes were randomly selected for posterior characterization assays.

#### 7.4.1. Physical characterization

PCL and PEO solutions were simultaneously processed by electrospinning, resulting in a three-dimensional dual composition nanofibrous structure with interconnected micro-pores, and composed of uniform and randomly oriented nanofibers (Figure 7.2 A2). Applying the Kruskal-Wallis test to the fiber diameter results, we found a highly significant difference between the produced NFMs ( $p < 0.0001$ ). The Tukey's HSD test indicated that the fiber diameter distribution in PCL-PEO NFM, after PEO dissolution is comparable with the ones observed for the control PCL NFM ( $p = 0.183$ ) (Figure 7.3). It was just noticed that the PCL-PEO NFM submitted to the dissolution process showed a marginal increase in the average fiber diameter ( $\sim 157$  nm), which did not significantly affect the fiber diameter distribution when compared with the control PCL NFM.

Comparing the SEM micrographs of control PCL NFM (Figure 7.2 A1) and the dual composition PCL-PEO NFM (Figure 7.2 A2) with the PCL-PEO NFM, after PEO dissolution (Figure 7.2 A3) it was observed an apparent increment on the size of the pores, accomplished by a decrease in the number of pores. Indeed, the PCL-PEO

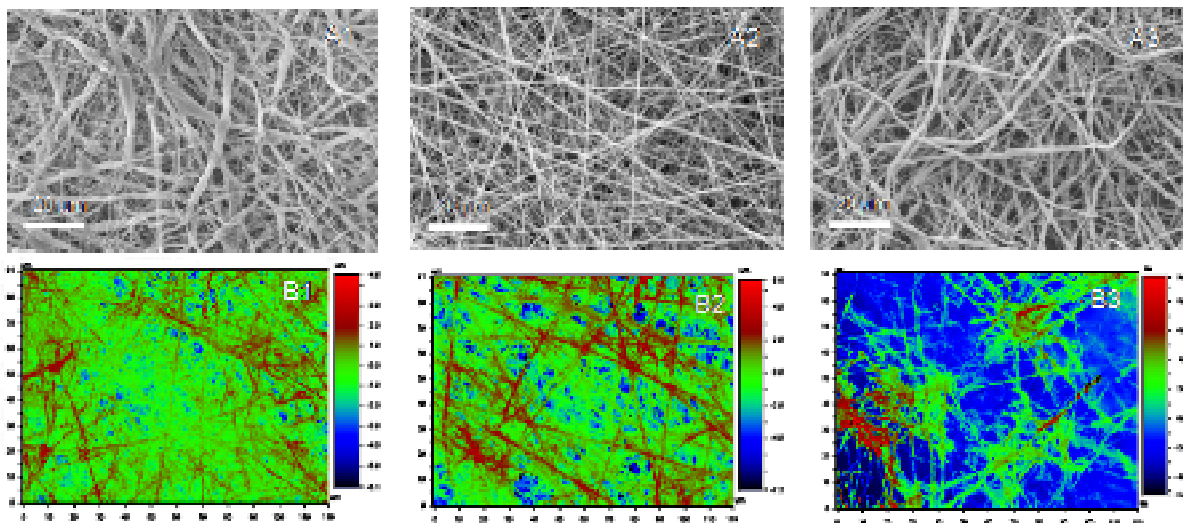


**Figure 7.2** - SEM micrographs (A) and Interferometric Optical Profilometry images (B) of electrospun control PCL NFM (1), dual composition PCL-PEO NFM (2) and PCL-PEO NFM, after PEO dissolution (3). Original magnification of 1000X and 51.8X, respectively.

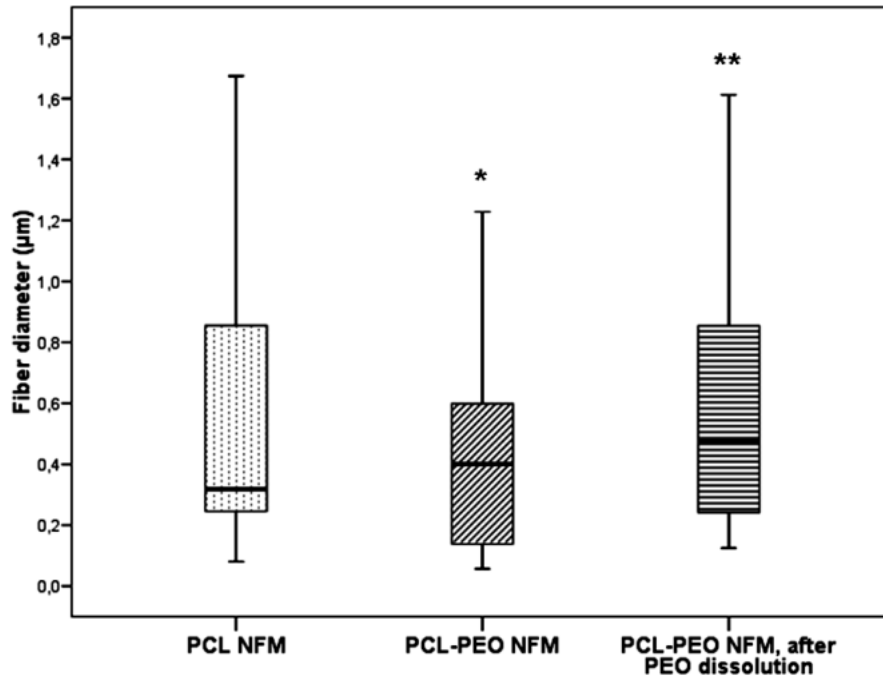


**Figure 7.3** - Box plot of fiber diameter for control PCL NFM, dual composition PCL-PEO NFM and PCL-PEO NFM, after dissolution. \*  $p < 0.01$  versus control PCL NFM; \*\*  $p < 0.01$  versus PCL-PEO NFM.

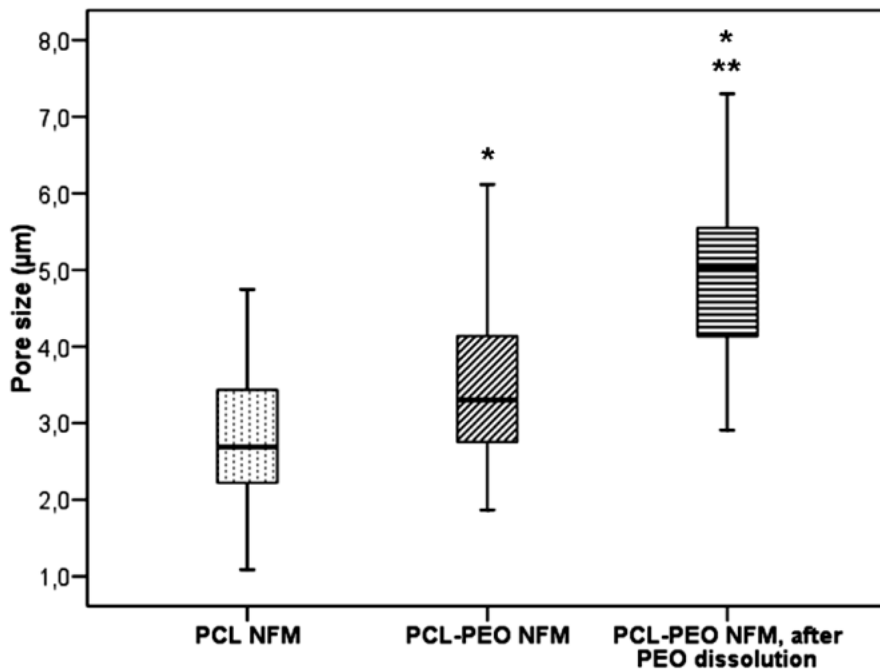


**Figure 7.4** - Box plot of pores size on control PCL NFM, dual composition PCL-PEO NFM and PCL-PEO NFM, after dissolution. \*  $p < 0.01$  versus control PCL NFM; \*\*  $p < 0.01$  versus PCL-PEO NFM.

NFM, after PEO dissolution has statistically significant larger pores ( $p < 0.001$ ), as revealed by the Tukey's HSD test (Figure 7.4). Interferometric Optical Profilometry images confirmed the pore size increment in the samples and consequent topographical alterations. The higher in depth scale of the PCL-PEO NFM, after PEO dissolution could be an indicative of a more open structure and presence of loosely connected fibers in this sample (Figure 7.2 B3). An increment of the pore size was also confirmed by the significant higher average roughness of the PCL-PEO NFM, after PEO dissolution ( $p = 0.001$ ) (Figure 7.5), also determined by Interferometric Optical Profilometry. Briefly, both SEM and Interferometric Optical Profilometry show consistent results with the increased level of pore size, when performing PEO fibers dissolution.

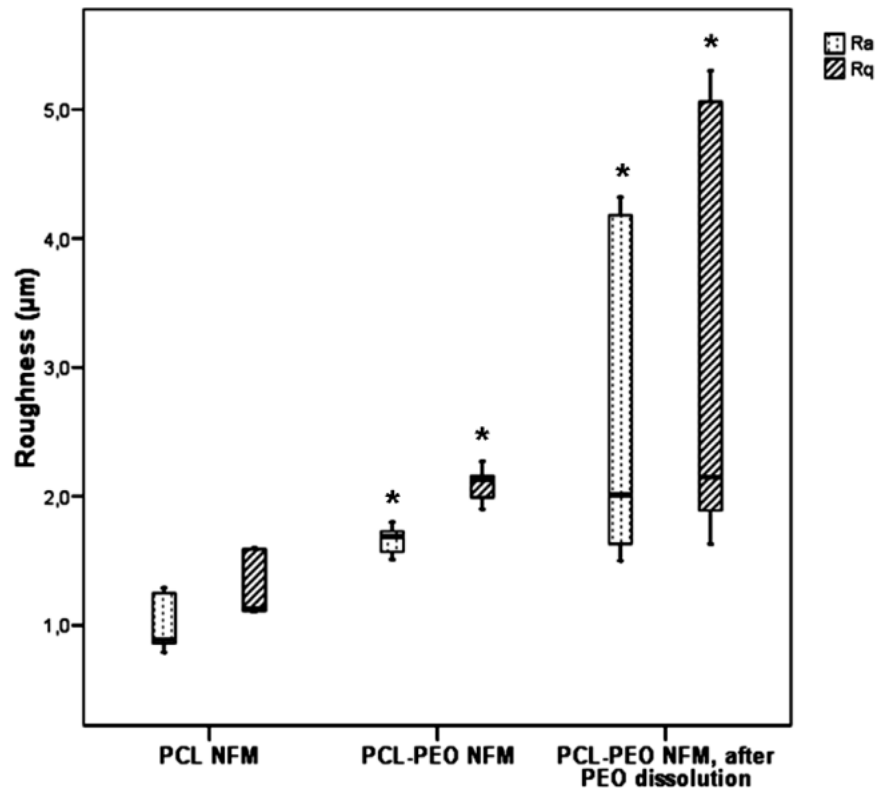


**Figure 7.5** - Box plot of roughness parameters, namely Ra (average roughness) and Rq (root mean square roughness), on control PCL NFM, dual composition PCL-PEO NFM and PCL-PEO NFM, after dissolution. \*  $p < 0.01$  versus control PCL NFM.

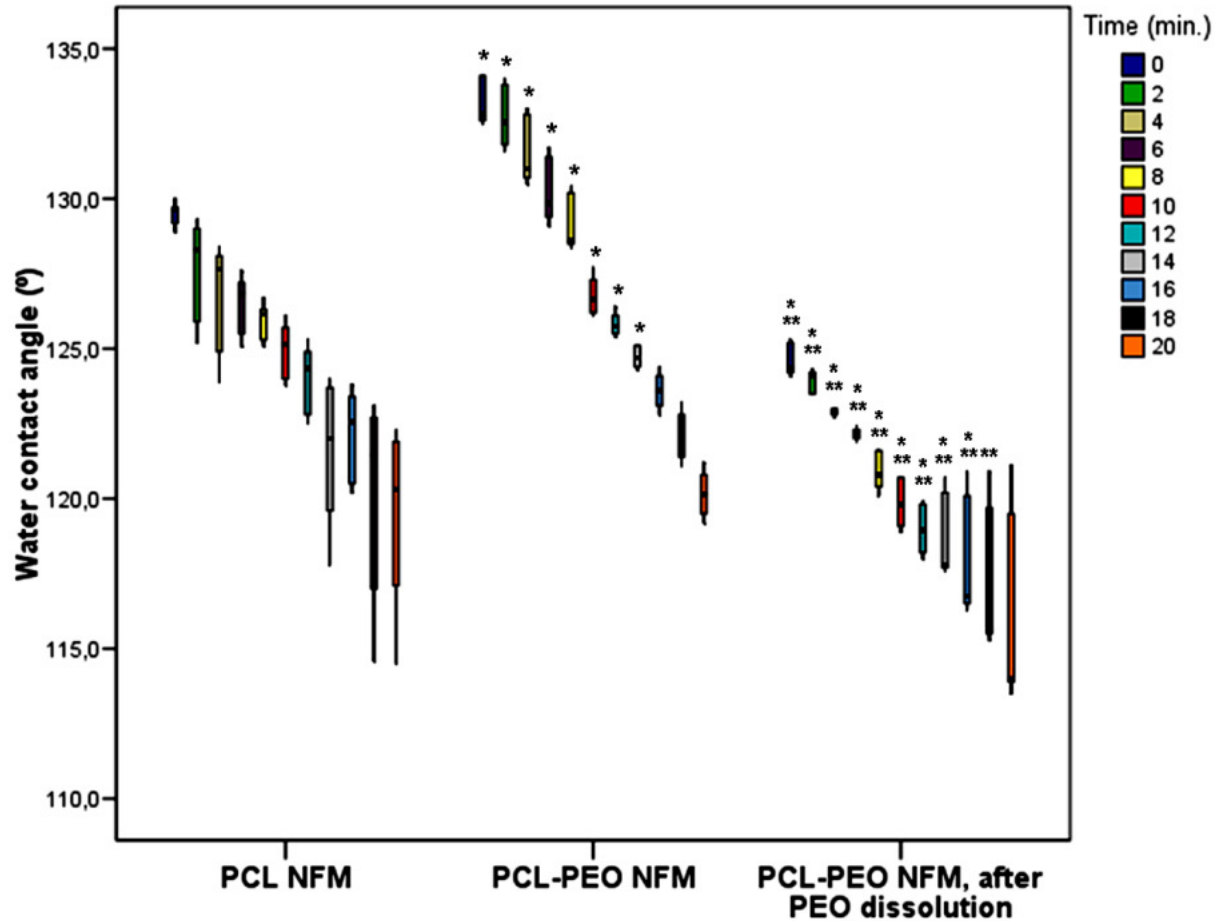


**Figure 7.6** - Box plot of water contact angle values for control PCL NFM, dual composition PCL-PEO NFM and PCL-PEO NFM, after PEO dissolution NFM, as a function of time. \*  $p < 0.01$  versus control PCL NFM; \*\*  $p < 0.01$  versus PCL-PEO NFM.

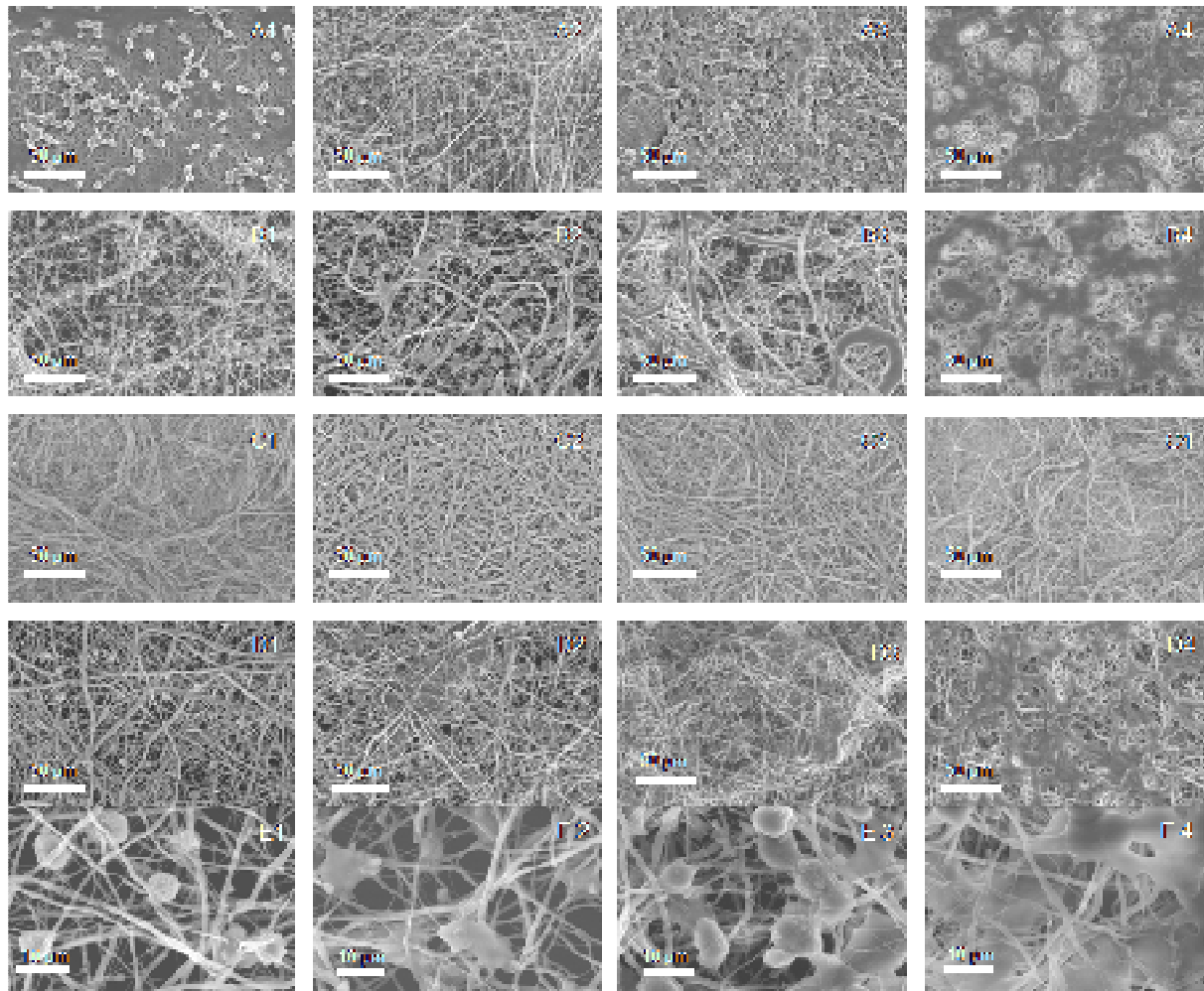
To ascertain about the influence of these topographical alterations over the hydrophobic/hydrophilic character of the samples, the water contact angle evolution during a period of 20 minutes was measured for control PCL NFM, dual composition PCL-PEO NFM and PCL-PEO NFM, after PEO dissolution (Figure 7.6). Generally, all samples show a hydrophobic character. However, the dissolution of PEO induced a statistically significant reduction of the water contact angle ( $p < 0.001$ ), as revealed by the Tukey's HSD test, until 16 minutes of wettability. At this time, there were not statistically significant differences in the water contact angle between the control PCL NFM and the dual composition PCL-PEO NFM ( $p = 0.007$ ). For the time point of 18

min was only observed statistically significant differences in the wettability between the dual composition PCL-PEO NFM and the PCL-PEO NFM, after PEO dissolution ( $p < 0.01$ ). Moreover, for the time point 20 min was observed the inexistence of statistically significant differences in the wettability between the three types of NFMs ( $p > 0.01$ ).

#### 7.4.2. *Biological assays*

The adhesion, spreading, viability and proliferation of human osteoblastic cells on the dual composition electrospun nanofiber meshes, after PEO dissolution, were all evaluated for 1, 3, 7 and 14 days of culture (control PCL NFM were include as controls). Figure 7.7 shows SEM micrographs of cultured cells on the electrospun meshes. In the case of the control PCL NFM, the adhesion only happens at the surface of the nanofiber mesh (Figure 7.7 A). Cell infiltration into the mesh is observed on PCL-PEO NFM, after PEO dissolution for longer culture periods (Figure 7.7 B3). Cells are visible in different layers of the NFM, clearly below the upper level of the nanofibers and inside the mesh structure (Figures 7.7 B3 and B4). After 14 days of culture, both samples have their top surface (seeding surface) almost fully covered with cells. Additionally, in control PCL NFM there was observed a confluent cell layer, which is not observed in the dual composition meshes.

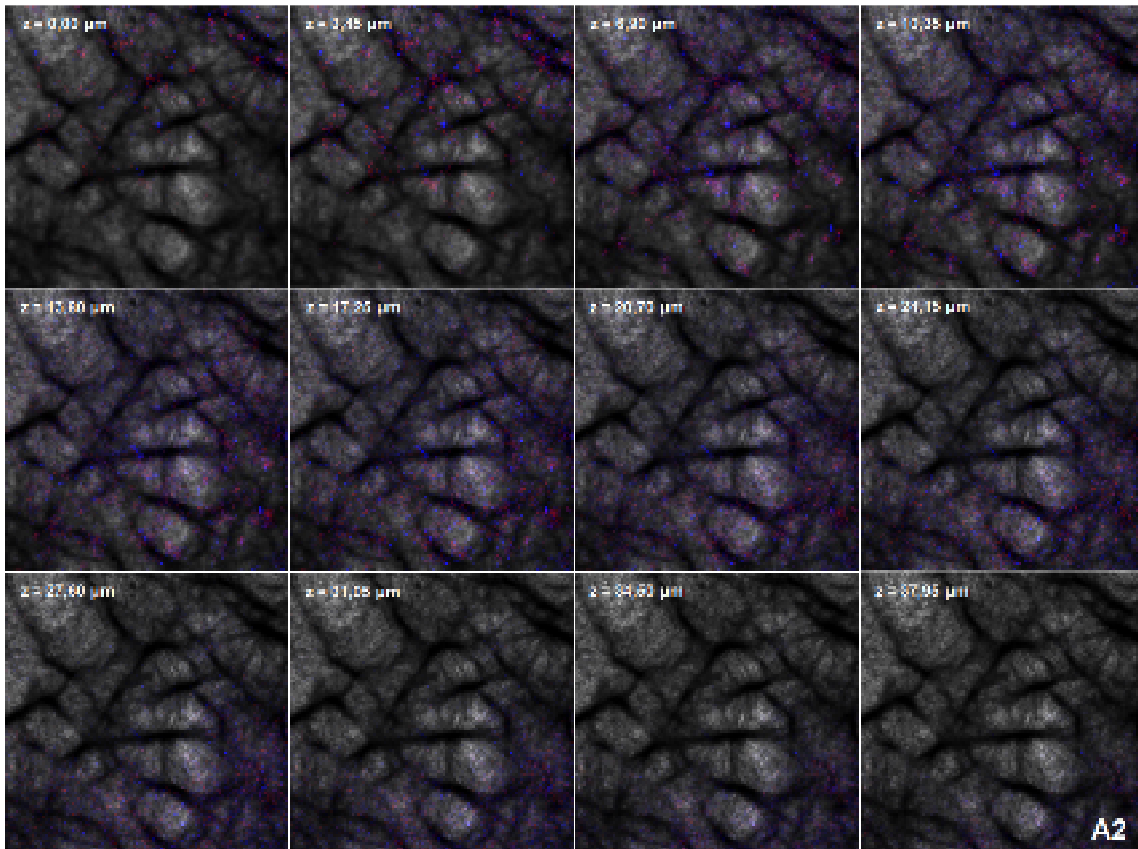
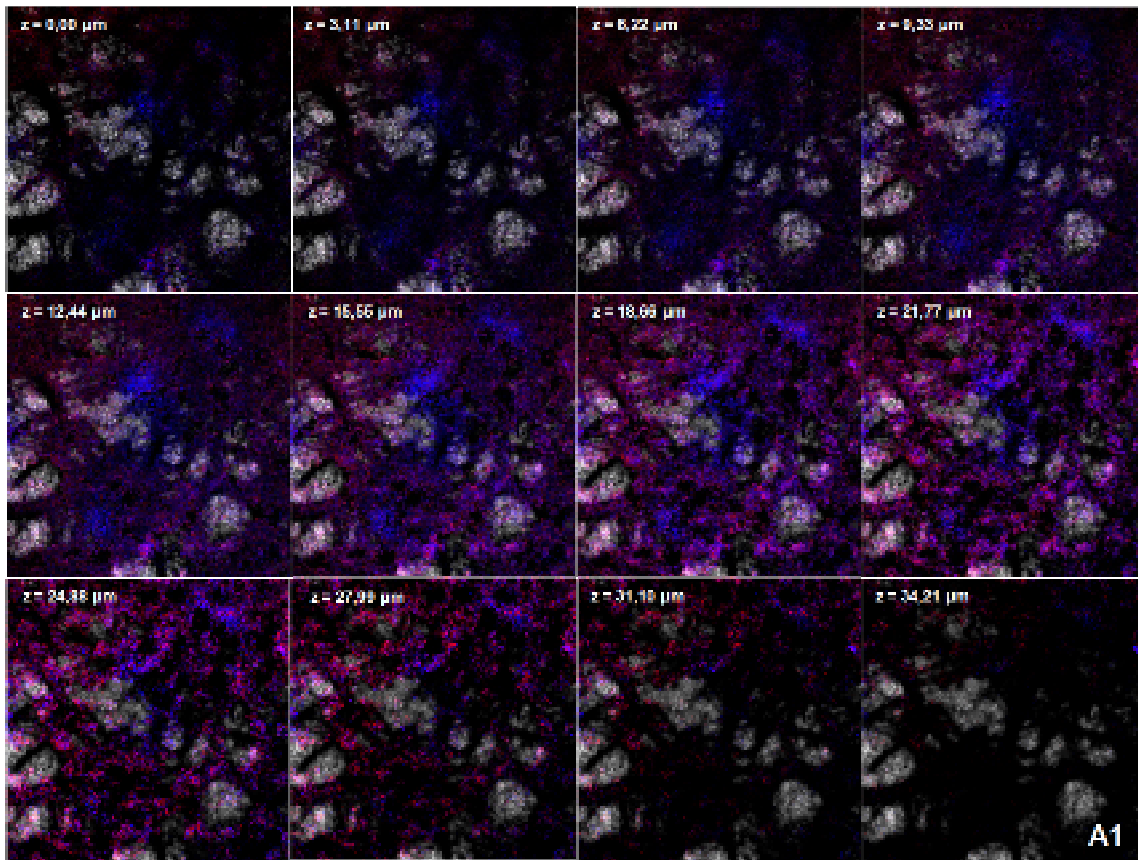
To further confirm cell penetration into the nanofiber meshes, the opposite side of the seeding surface of the meshes was also observed by SEM (Figure 7.7 C). As the seeding was performed in the area confined by the clamping silicone ring, the cells present in the opposite surface of the mesh can only migrate through the thickness of the nanofiber mesh. This results show that the increased pore size and the overall morphology of the PCL-PEO, after PEO dissolution allow the cell penetration into the mesh. For longer culture periods, it was observed an increment in the cell number at the surface of the nanofiber mesh. In this side of the mesh, it is visible a progressive infiltration of the cells, from the interior of the mesh to its surface, along the culturing periods (Figure 7.7 D). In control PCL NFM this infiltration was not observed and the cells were absent at the opposite side of the mesh (Figure 7.7 C), which also demonstrates the efficiency of the ring system in confining the cell



**Figure 7.7** - SEM micrographs of electrospun control PCL NFM (**A**) and PCL-PEO NFM, after PEO dissolution (**B**), and opposite face of control PCL NFM (**C**) and PCL-PEO NFM, after PEO dissolution (**D**) cultured with human osteoblastic cells during 1 (1), 3 (2), 7 (3) and 14 days (4). Original magnification of 500X. Details of cellular infiltration on PCL-PEO NFM, after PEO dissolution (**E**). Original magnification of 2200X.

adhesion. Detailed and further magnified micrographs illustrate cellular infiltration into the PCL-PEO NFM, after PEO dissolution (Figure 7.7 E). SEM micrographs show a progressive cell penetration during the culture periods. Cells are visible underneath several fibers and in different layers across the mesh thickness (Figures 7.7 E3 and E4).

To further confirm the cellular penetration observed in SEM, laser scanning



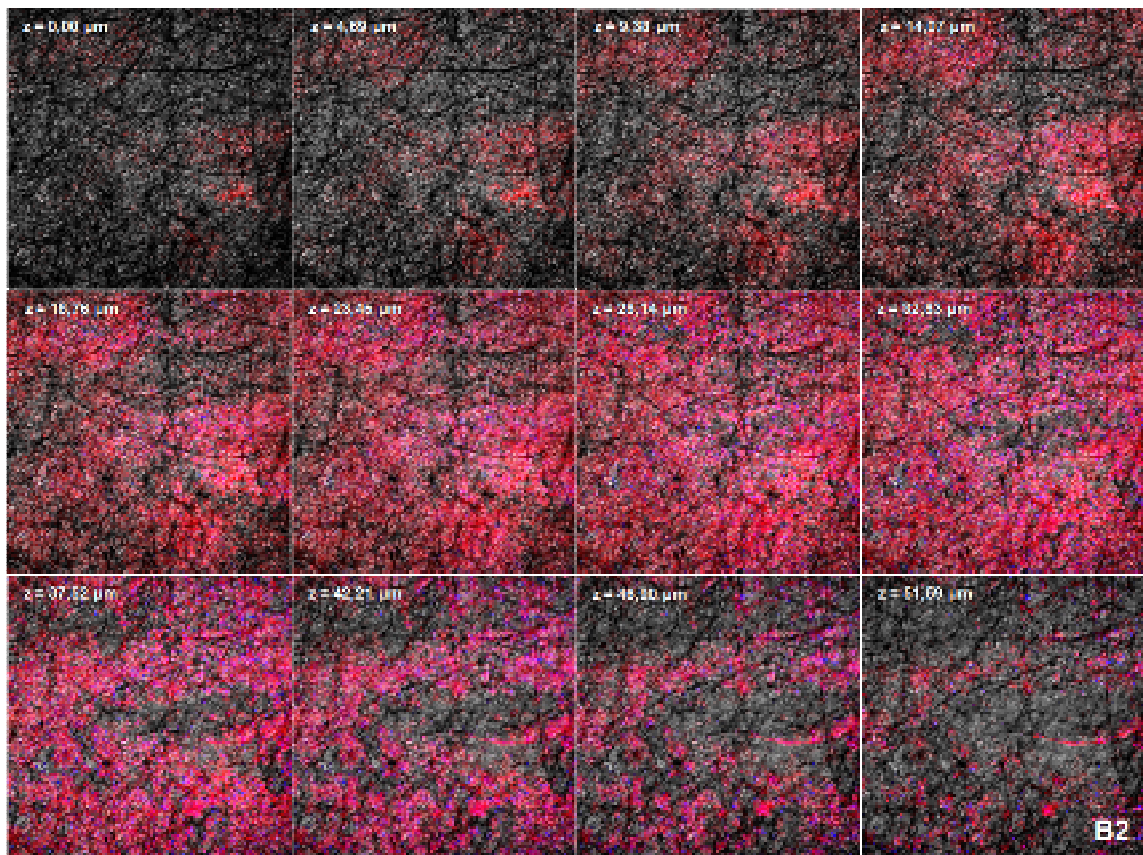
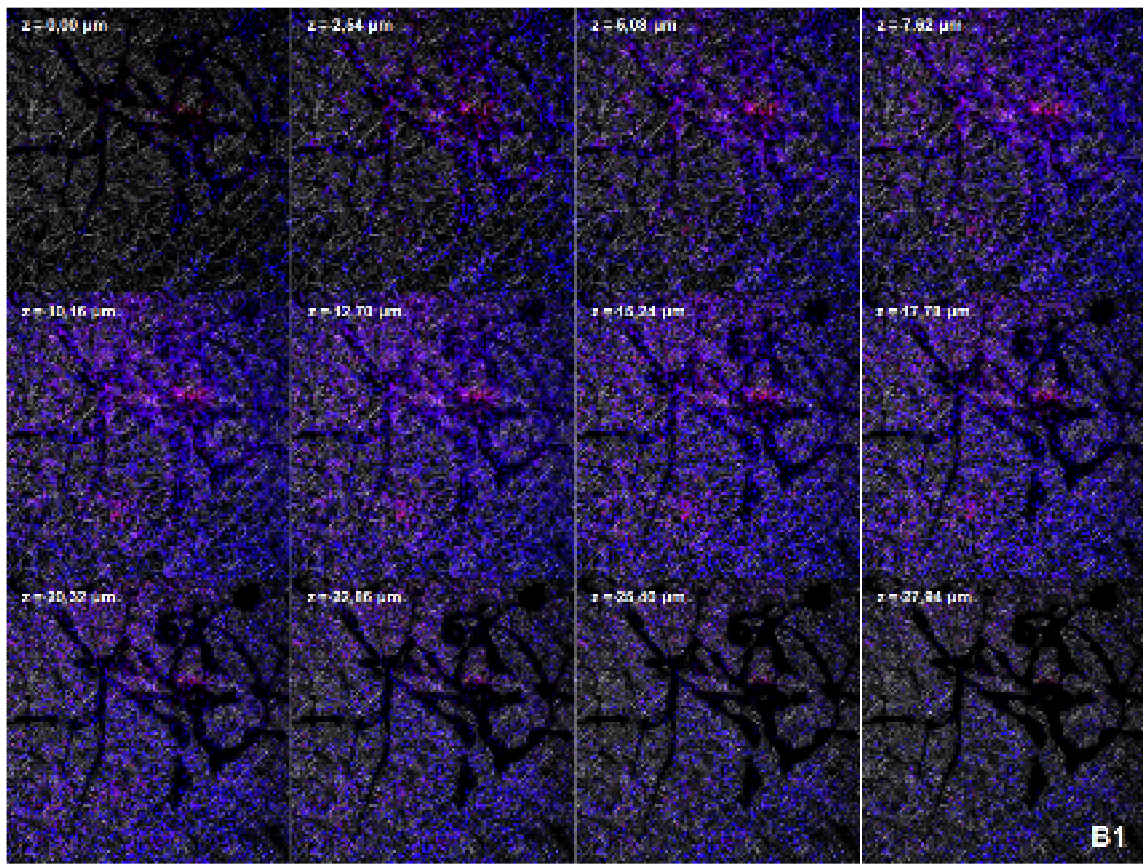


**Figure 7.8** - Laser scanning confocal microscopy images of electrospun control PCL NFM (A) and PCL-PEO NFM, after PEO dissolution (B), after 1 (1) and 7 days (2) of human osteoblastic-like cells culture. Cells nucleus were stained with DAPI and actin filaments stained with Phalloidine. Original magnification of 10X.

confocal microscopy was conducted on control PCL NFMs and PCL-PEO NFM, after PEO dissolution cultured with human osteoblastic cells (Figure 7.8). Cells appeared rounded, but uniformly distributed over the scaffolds surfaces for 1 day (Figures 7.8 A1 and B1). For longer culture periods (7 days), control PCL NFM still present cells mainly at the surface of the mesh (Figures 7.8 A2). In contrast, in PCL-PEO NFM, after PEO dissolution cells appear spread and were detected in the inner/deeper layers of the NFM (Figures 7.8 B), colonizing the full thickness of the scaffold and infiltrating into the unseeded side of the mesh. Thus, these observations corroborate the ones from SEM analysis.

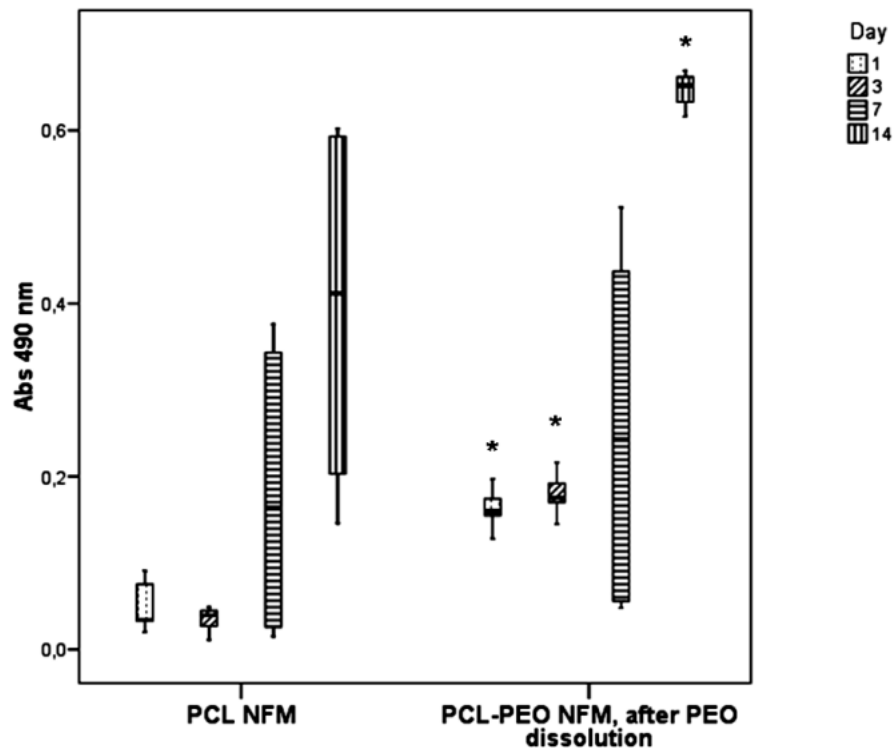


**Figure 7.9** - Box plot of human osteoblast-like cells viability cultured on control PCL NFM control and PCL-PEO NFM, after PEO dissolution. \*  $p < 0.01$  versus control PCL NFM.

The viability of the osteoblastic cells cultured on the control PCL NFMs and on the PCL-PEO NFM, after PEO dissolution was assessed by MTS assay (Figure 7.9). Cell viability was significantly higher on the PCL-PEO NFM, after PEO dissolution ( $p < 0.001$ ), as revealed by the Mann-Whitney U-test, for almost all the time points. The only exception was the culturing time 7 days, where any significant differences were found between the both NFMs ( $p = 0.063$ ). The higher viability of cells seeded PCL-PEO NFM, after PEO dissolution can be justified by the attachment and growth of cells into the open structure of the mesh. Additionally, a progressive increment of cell viability along culturing time was also observed for both nanofiber meshes.

Cellular proliferation was estimated based on the DNA quantification assay (Figure 7.10). In control PCL NFM, DNA content increases slightly until 3 days of culture, reaching the maximum value, and reducing the DNA quantity from that time point onwards. In PCL-PEO NFM, after PEO dissolution was observed a statistically significant decrease in DNA content at the 3<sup>rd</sup> day ( $p = 0.002$ ), followed by a

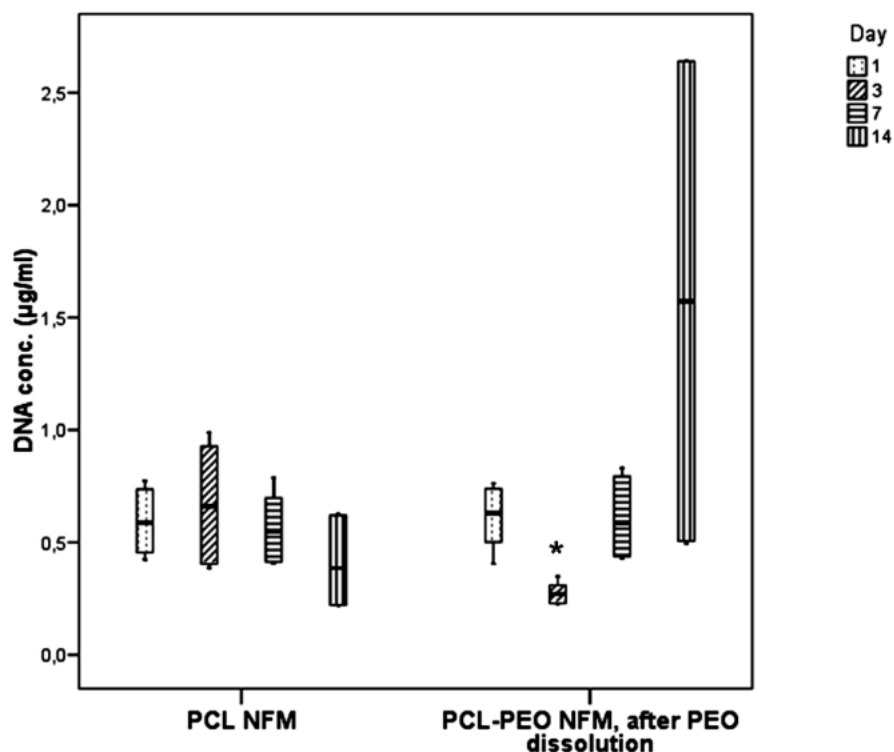


**Figure 7.10** - Box plot of cell proliferation on control PCL NFM and PCL-PEO NFM, after PEO dissolution, estimated according to the DNA quantification assay. \*  $p < 0.01$  versus control PCL NFM.

progressive increment for longer culture periods. Despite this progressive increment of DNA quantity, any statistically significant difference was found between PCL-PEO NFM, after PEO dissolution and the control PCL NFM ( $p > 0.01$ ), as revealed by the Mann-Whitney U-test.

## 7.5. Discussion

In natural tissues the cells are surrounded by the extracellular matrix (ECM), which provides structural support for the cells, controls the tissue structure and regulates cell adhesion, migration, proliferation and, consequently, tissue morphogenesis. The ECM is a dynamic and hierarchal organized structure composed of polysaccharides (glycosaminoglycans) and proteins (collagen and proteoglycans). These components are organized as an interconnected nano- or micro-ranged fibrous network [17]. In the past two decades, nanofiber meshes produced by electrospinning have been described as having a large potential in the tissue regeneration field [17, 40, 51]. Due to their nanoscale structure, electrospun meshes highly resemble the ECM and can act as a functional replacement of the ECM [17, 51]. The most serious limitation on the use of the nanofiber meshes as Tissue Engineering scaffolds in 3D tissues is probably the fact that the pores created by the random deposition of nanofibers are too small to allow cell infiltration into the inner regions of the nanofiber mesh [17, 23, 51]. Most of the reports in literature using electrospinning to produce tissue templates do not provide any strategy to overcome this problem, compromising the scaffolds effectiveness for the proposed applications.

Herein, we propose the electrospinning of a dual composition nanofibrous structure that is intentionally designed for cells penetration, obtained by the selective extraction of one material of the nanofiber mesh. This strategy would create larger pores that could promote cell infiltration to the inner region of the mesh and, at same time, maintain the structural and biological properties that resemble the ECM structure. Unlike some previously described strategies to increase pore size, such as techniques that use blowing agents [45] or post processing by laser [46], our strategy modifies the nanofiber mesh as a whole, providing an homogeneous pore size distribution. The developed system allows an independent voltage control, since the

PCL and PEO solutions have different properties and, consequently, need to be processed at different conditions. Additionally, the proposed post processing technique is very simple and does not involve any extra component that could eventually compromise the cellular behavior.

It is hypothesized that the PEO dissolution products are non-toxic and will not be detrimental for the cell viability. In fact, the dissolution of PEO nanofibers in water has revealed itself as an efficient method to obtain the selective removal. This was verified by the “fingerprinting” marks of PEO nanofibers visible on the remaining PCL fibers, constituting an important characteristic of the obtained meshes. Those marks result from the deposition of the fibers in the collector not completely dry and are caused by the overlap of PEO and PCL fibers. According to previous experimental results from the literature, the solubility of PEO in water increases in the temperature range of 20-40 °C and tends to saturate at higher temperatures [50]. Thus, the PEO dissolution was performed at the temperature of 37 °C, being also the temperature at which the biologic assays are conducted and ensuring that the PEO was successfully and completely removed at that temperature. This temperature is lower than the melt temperature of both polymers, which does not involve nanofiber morphology alterations during the process of dissolution. Due to the presence of impurities in the PEO solution, some aggregates of PEO were also observed and produced during the dissolution in water [50] which may cause morphologic alterations in the nanofiber mesh. Considering the hydrophobic character of PCL, the PCL nanofibers no significant morphological alterations are expected. To confirm this statement, different topographical properties of the electrospun meshes, namely fiber diameter, pore size and roughness, were characterized. Fiber diameter measurements show that most of the produced fibers have diameters in the range of 175-875 nm, thus in the sub-micrometric range. Considering the main aim of the present study, it is not advantageous to have very small fiber diameters since, as was already discussed [42], increasing fiber diameter results in an increase in the mean pore size. Hypothetically, the slightly higher, but not statistically significant, diameter of the fibers measured in the PCL-PEO NFM after PEO dissolution can also contribute to a larger pore size in these meshes. Even so, the electrospun nanofiber meshes have

maximum probability of being effective in mimicking the natural ECM and allowing cell infiltration.

Different methods have been proposed in the literature to measure the pore size and amount of porosity. Sieving methods [52], mercury intrusion porosimetry [53, 54] and flow porosimetry [54] are among the most used methods to determine pore size. In the present study the evaluation of the pore size was performed by quantitative image analysis of SEM micrographs to obtain the size of the pores [56]. As expected, PCL-PEO NFM, after PEO dissolution has the largest pore sizes. The dissolution of PEO fibers allows obtaining pore sizes significantly higher than similar PCL meshes, which is in agreement with the removal of half of the fibers that constitute the mesh. The enhanced pore size meshes present a median pore diameter of  $5.017 \mu\text{m}$ . This pore sizes are in the same range of values previously reported by Tzezana *et al* [56]. The PCL-PEO NFM, after PEO removal showed clearly larger pores, as depicted by the Interferometric Optical Profilometry images. These meshes also present larger topography gradients between the top and bottom fibers, which can be an indication of a more open mesh structure and of the presence of loosely connected nanofibers. Considering this higher distances and the fact that the fibers are slightly larger, it is consistent with a considerably higher average roughness of those samples, being the roughest of all three samples analyzed by this technique.

These roughness differences could have also influence in the hydrophobic/hydrophilic character of the samples and, consequently, on the cell behavior [57]. The contact angle assay showed a decrease of the hydrophobicity of the PCL-PEO NFM, after PEO dissolution, when comparing with control PCL NFM. Despite the maintenance of a hydrophobic character, the PEO dissolution turned the PCL-PEO NFM into a more hydrophilic structure. This effect can be related to the increased fiber diameter of the dual composition PCL-PEO NFM. As reported in the literature, the increase in the fiber diameter causes a decrease in the water contact angle [57]. Also, it has been shown that smaller pore sizes leads to higher air entrapment in the pore structure, which may cause an increase in water contact angle [57]. This is particularly evident on control PCL NFM. Conversely, higher pore size induced a decrement on water contact angle, as shown in our results.

The biologic performance of the PCL-PEO NFM, followed by PEO dissolution was assessed by the cellular infiltration level, cell viability and proliferation into the inner regions of the produced nanofibrous meshes. To demonstrate that human osteoblastic cells could migrate through the all thickness of the NFM, a special setup system was developed. This system was designed to have the double function of limiting the seeding area and to clamp the meshes at a certain distance from the bottom of the culture well-plate. Thus, while in control PCL NFM the cell infiltration is limited to the top surface of the nanofiber mesh (because the pore size is insufficient to allow infiltration), in the PCL-PEO NFM, after PEO dissolution the infiltration of the cells into the inner regions of the mesh was observed, mainly for longer culture periods. In these meshes, the cells are clearly visible at various depths within the nanofiber mesh and covering different levels of the mesh, as confirmed by laser scanning confocal microscopy. The extent of cell infiltration was also evaluated by SEM observation of the opposite face of the mesh that was not seeded with cells. It was observed the presence of cells in this surface only in the PCL-PEO NFM, after PEO dissolution. In fact, in the initial days of culturing, the cells are seen inside the mesh, progressing along the culturing period and reaching the opposite surface of the mesh. Conversely, control PCL NFM shows no cells in the opposite side of the mesh even for long culturing periods. This result demonstrates that the presence of cells in the opposite surface of the PCL-PEO NFM, after PEO dissolution is in fact due to cell infiltration through the mesh thickness, and not due to any other cell colonization alternative. The previously published work on dual-polymer composite fiber-aligned scaffolds [47] did not reported results showing a even distribution of cells through the scaffold thickness. Our results demonstrate unequivocally that the obtained pore size and porosity are sufficient to allow extensive cell infiltration from one face of the mesh to the other.

The enlargement of the pore size may facilitate already the cell penetration in the dual composition meshes. However, this result may also be related with the loosely connected structure of electrospun meshes that are formed by differently oriented fibers lying without physical connection with the neighboring fibers (caused by the dissolution of the PEO fibers). The removal of the PEO fibers may also lead to

discontinuities in the remaining PCL fibers. By this way, the surrounding fibers will offer only minor resistance to the migration of cells [58]. It is remarkable that the biological results herein reported are obtained using a shorter culturing period (14 days) and cells with lower migratory capabilities when comparing with mesenchymal stem cells used in other work [47]. Additionally, our results show infiltration of cells through the full thickness of the nanofiber mesh. Others, following a similar strategy, reported a gradient of cells from the edge (~ 45 % of cells remain in the outer quarter) to the center of the construct (~ 12 % of total cell population reaches the center region).

The viability of cultured cells was also assessed by the MTS test, showing significant improved cell viability in the PCL-PEO, after PEO dissolution when compared with control PCL NFM. The extra access to the inner mesh structure facilitates the attachment of cells and allowing further cell penetration. The progressive increase in cell viability also demonstrates that PEO dissolution and also PEO dissolution products do not affect negatively the cell viability. Additionally, the cellular proliferation assay shows a progressive increment in DNA content along the culture periods, with the exception of the 3<sup>rd</sup> day. Despite the differences not being statistical significant between control PCL NFM and PCL-PEO NFM, after PEO dissolution, those meshes present higher cell proliferation, which indicate easier access of inner surfaces for cells to proliferate into, than in the case PCL NFM. Additionally, these results confirm that the PEO dissolution did not affected negatively neither cell proliferation nor its viability.

## 7.6. Conclusions

We demonstrated the efficacy of a dual composition strategy to increase the pore size and solve the low cell infiltration capacity of random electrospun nanofiber meshes. This strategy consists in producing a dual composition nanofiber mesh and selectively removing one of the polymeric fibers leaving the other fraction intact. It was observed that this method indeed increases the pore size without major alterations of the mesh structure. Pore size measurements showed a significant increase of pore size (doubling) in those meshes when comparing with control PCL

NFM. The biologic assays showed that the cells not only were able to proliferate into the nanofibrous scaffold, but also were capable to migrate into the opposite side of the mesh. The approach herein proposed can be followed to successfully overcome the critical limitation of the control of the pore size in electrospun meshes for 3D Tissue Engineering applications.

## 7.7. References

1. Langer R, Vacanti, J. P. Tissue Engineering. Science 1993; 260(5110):920-926.
2. Hutmacher DW. Scaffolds in tissue engineering bone and cartilage. Biomaterials 2000; 21(24):2529-2543.
3. Agrawal CM, Ray, R. B. Biodegradable polymeric scaffolds for musculoskeletal tissue engineering Journal of Biomedical Materials Research 2001; 55(2):141-150.
4. Sachlos E, Reis, N., Ainsley, C., Derby, B., Czernuska, J. T. Novel collagen scaffolds with predefined internal morphology made by solid freeform fabrication. Biomaterials 2003; 24(8):1487-1497.
5. Wallace DG, Rosenblatt, J. Collagen gel systems for sustained delivery and tissue engineering. Advanced Drug Delivery Reviews 2003; 55(12):1631-1649.
6. Lu Q, Ganesan, K., Simionescu, D. T., Vyavahare, N. R. Novel porous aortic elastin and collagen scaffolds for tissue engineering. Biomaterials 2004; 25(22):5227-5237.
7. Endres M. HDW, Salgado A. J., Kaps C., Ringe J., Reis R. L, Sittinger M., Brandwood A., Schantz J. T. Osteogenic induction of human bone marrow-derived mesenchymal progenitor cells in novel synthetic polymer-hydrogel matrices. Tissue Engineering 2003; 9(4):689-702.
8. Tolaimate A, Desbrieres, J., Rhazi, M., Alagui, A. Contribution to the preparation of chitins and chitosans with controlled physico-chemical properties. Polymer 2003; 44(26):7939-7952.

9. Reis CC, Tuzlakoglu, K., Yang, K., Haj, A. E., Reis, R. L. Influence of Porosity/Fiber Diameter on the Degradation of Chitosan Fiber-mesh Scaffolds. *Journal of Materials Science: Materials in Medicine* 2007; 18:195-200.
10. Malafaya PB, Pedro, A. J., Peterbauer, A., Gabriel, C., Redl, H., Reis, L. R. Chitosan particles agglomerated scaffolds for cartilage and osteochondral tissue engineering approaches with adipose tissue derived stem cells. *Journal of Materials Science: Materials in Medicine* 2005; 16(1077-1085).
11. Salgado AJ, Gomes, M. E., Chou, A., Coutinho, O. P., Reis, L. R., Hutmacher, D. W. Preliminary study on the adhesion and proliferation of human osteoblasts on starch-based scaffolds. *Materials Science and Engineering C* 2002; 20(1-2):27-33.
12. Gomes ME, Ribeiro, A. S., Malafaya, P. B., Reis, R. L., Cunha, A. M. A new approach based on injection moulding to produce biodegradable starch-based polymeric scaffolds: morphology, mechanical and degradation behaviour. *Biomaterials* 2001; 22(9):883-889.
13. Balmayor E. R. TK, Marques A. P., Azevedo H. S., Reis R. L. A novel enzymatically-mediated drug delivery carrier for bone tissue engineering applications: combining biodegradable starch-based microparticles and differentiation agents. *Journal of Materials Science: Materials in Medicine* 2008; 19(4):1617-1623.
14. Liu LS, Thompson, A. Y., Heidaran, M. A., Poser, J. W., Spiro, R. C. An osteoconductive collagen/hyaluronate matrix for bone regeneration. *Biomaterials* 1999; 20(12):1097-1108.
15. Borzacchiello A, Mayol, L., Ramires, P. A., Pastorello, A., Bartolo, C. D., Ambrosio, L., Miella, E. Structural and rheological characterization of hyaluronic acid-based scaffolds for adipose tissue engineering. *Biomaterials* 2007; 28(30):4399-4408.
16. Chen LJ, Wang, M. Production and evaluation of biodegradable composites based on PHB-PHV copolymer. *Biomaterials* 2002; 23(13):2631-2639.
17. Martins A, Araújo, J. V., Reis, R. L., Neves, N. M. Electrospun Nanostructured Scaffolds for Tissue Engineering Applications. *Nanomedicine* 2007; 2(6):929-942.

18. Zhang Y, Lim, C. T., Ramakrishna, S., Huang, Z. M. Recent development of polymer nanofibers for biomedical and biotechnological applications *J Materials Science - Materials in Medicine* 2005; 16:933-946.
19. Ashammakhi N, Ndreu, A., Piras, A. M., Nikkola, L., Sindelar, T., Ylikauppila, H., Harlin, A., Gomes, M. E., Neves, N. M., Chiellini, F., Hasirci, V., Redl, H., Reis, R. L. Biodegradable Nanomats Produced by Electrospinning: Expanding Multifunctionality and Potential for Tissue Engineering. *Journal of Nanoscience and Nanotechnology* 2006; 6:2693-2711.
20. Martins A, Pinho, E. D., Faria, S., Pashkuleva I., Marques, A. P., Reis, R. L., Neves, N. M. Surface Modification of Electrospun Polycaprolactone Nanofiber Meshes by Plasma Treatment to Enhance its Biological Performance. *Small* 2009; 5(10):1195-1206.
21. Salgado AJ, Coutinho, O. P., Reis, L. R. Bone Tissue Engineering: State of the Art and Future Trends. *Macromolecular Bioscience* 2004; 4(8):743-765.
22. Alberts B, Johnson, A., Lewis, J., Raff, M., Roberts, K., Walter, P. *Molecular Biology of the Cell*. 4th Edition. New York: Garland Science, 2002.
23. Martins A, Reis, R. L., Neves, N. M. Electrospinning: processing technique for tissue engineering scaffolding. *International Materials Review* 2008; 53(5):257-274.
24. Zagrís N. Extracellular matrix in development of the early embryo. *Micron* 2001; 32(4):427-438.
25. Tang ZG, Black, R. A., Curran, J. M., Hunt, J. A., Rhodes, N. P., Williams, D. F. Surface properties and biocompatibility of solvent-cast poly(caprolactone) films. *Biomaterials* 2004; 25(19):4741-4748.
26. Mikos AG, Bao, Y., Cima, L. G., Ingber, D. E., Vacanti, J. P., Langer, R. Preparation of poly(glycolic acid) bonded fiber structures for cell attachment and transplantation. *Journal of Biomedical Materials Research* 1993; 27(183-189).
27. Kim BS, Mooney, D. J. Engineering smooth muscle tissue with a predefined structure. *Journal of Biomedical Materials Research* 1998; 41:322-332.
28. Rodrigues MT, Leonor, I. B., Viegas, C. A. A., Dias, I. R., Gomes, M. E., Reis, R. L. Osteoconductive scaffolds obtained by means of in situ surface

functionalization of wet-spun fiber meshes for bone regeneration applications. *Tissue Engineering, Part A* 2008; 14(5):765.

29. Gomes ME, Godinho, J. S., Tchalamov, A. M., Cunha, A. M., Reis, R. L. Alternative tissue engineering scaffolds based on starch: processing methodologies, morphology, degradation and mechanical properties. *Materials Science and Engineering C* 2002; 20:19-26.

30. Mooney DJ, Baldwin, D. F., Shu, N. P., Vacanti, J. P., Langer, R. Novel approach to fabricate porous sponges of poly(D, L-lactic-co-glycolic acid) without the use of organic solvents. *Biomaterials* 1996; 17(14):1417-1422.

31. Shea LD, Wang, D., Franceschi, R. T., Mooney, D. J. Engineered Bone Development from a Pre-Osteoblast Cell Line on Three-Dimensional Scaffolds. *Tissue Engineering* 2000; 6(6):605-617.

32. Mao JS, Zhao, L. G., Yin, J. Y., Yao, K. D. Structure and properties of bilayer chitosan–gelatin scaffolds. *Biomaterials* 2003; 24(6):1067-1074.

33. Ferreira BM, Sousa, R. A., Reis, R. L. Development of novel carrageenan scaffolds for tissue engineering using rapid prototyping. *Tissue Engineering, Part A* 2008; 14(5):837-838.

34. Landers R, Hubner, U., Schmelzeisen, R., Mulhaupt, R. Rapid prototyping of scaffolds derived from thermoreversible hydrogels and tailored for applications in tissue engineering. *Biomaterials* 2002; 23(23):4437-4447.

35. Lam CXF, Mo, X. M., Teoh, D., Hutmacher, D. W. Scaffold development using 3D printing with a starch-based polymer. *Journal of Materials Science and Engineering* 2002; 20:49-56.

36. Martins A, Chung, S., Pedro, A. J., Sousa, R. A., Marques, A. P., Reis, R. L., Neves, N. M. Hierarchical starch-based fibrous scaffold for bone tissue engineering applications. *Journal of Tissue Engineering and Regenerative Medicine* 2009; 3: 37-42.

37. Li M, Mondrinos, M. J., Ganghi, M. R., Ko, F. K., Weiss, A. S., Lelkes, P. I. Electrospun protein fibers as matrices for tissue engineering. *Biomaterials* 2005; 26:5999-6008.

38. Townsend-Nicholson A, Jayasinghe, S. Cell electrospinning: a unique biotechnique for encapsulating living organisms for generating active biological microthreads/scaffolds. *Biomacromolecules* 2006; 7:3364-3369.

39. Stankus JJ, Guan, J., Fujimoto, K., Wagner, W. R. Microintegrating smooth muscle cells into a biodegradable, elastomeric fiber matrix. *Biomaterials* 2006; 27(5):735-744.

40. Doshi J, Reneker, D. H. Electrospinning process and applications of electrospun fibers. *Journal of Electrostatics* 1995; 35(2-3):151-160.

41. Li D, Xia, Y. Electrospinning of Nanofibers: Reinventing the Wheel? *Advanced Materials* 2006; 16(14):1151-1170.

42. Eichhorn SJ, Sampson, W. W. Statistical geometry of pores and statistics of porous nanofibrous assemblies. *Journal of the Royal Society Interface* 2005; 2:309-318.

43. Nam J, Huang, Y., Agarwal, S., Lannutti, J. Improved cellular infiltration in electrospun fiber via engineered porosity. *Tissue Engineering* 2007; 13(9):2249-2257.

44. Lee HY, Lee, J. H., An, I. G., Kim, C., Lee, D. S., Lee, Y. K., Nam, J. D. Electrospun dual-porosity structure and biodegradation morphology of Montmorillonite reinforced PLLA nanocomposite scaffolds. *Biomaterials* 2005; 26(3165-3172).

45. Kim G, Kim, W. Highly porous 3D nanofiber scaffold using an electrospinning technique. *Journal of Biomedical Materials Research, Part B - Applied Biomaterials* 2007; 81(1):104-110.

46. Lannutti J, Reneker, D., Ma, T., Tomasko, D., Farson, D. Electrospinning for Tissue Engineering Scaffolds. *Materials Science and Engineering C* 2007; 27:504-509.

47. Baker BM, Gee AO, Metter RB, Nathan AS, Marklein RA, Burdick JA, *et al.* The potential to improve cell infiltration in composite fiber-aligned electrospun scaffolds by the selective removal of sacrificial fibers. *Biomaterials* 2008; 29(15):2348-2358.

48. Martins A, Cunha, J., Macedo, F., Reis, R. L., Neves, N. M. Improvement of Polycaprolactone Nanofibers Topographies: Testing the Influence in Osteoblastic Proliferation. *Nanotech 2006 Technical Proceedings*; Boston, MA; 2006; 2:148-151.

49. She FH, Tung, K. L., Kong, L. X. Calculation of Effective Pore Diameters in Porous Filtration Membranes with Image Analysis. *Robotics and Computer - Integrated Manufacturing* 2008; 24:427-434.

50. Farone A, Magazú, S., Maisano, G., Migliardo, P., Tettamanti, E., Villari, V. The puzzle of poly(ethylene oxide) aggregation in water: Experimental findings. *Journal of Chemical Physics* 1999; 10(3):1801-1806.

51. Zhang YZ, Su, B., Venugpal, J., Ramakrishna, S., Lim, C. T. Biomimetic and bioactive nanofibrous scaffolds from electrospun composite nanofibers. *International Journal of Nanomedicine* 2007; 2(4):623-638.

52. Bahatia SK, Smith, J. L. Geotextile Characterization and Pore Size Distribution: Part III. Comparison of Methods and Application to Design. *Geosynthetics International* 1996; 3(3):301-328.

53. Ramakrishna S, Fujihara, K., Teo, W. E., Lim, T. C., Ma, Z. An Introduction to Electrospinning and Nanofibers. World Scientific Publishing PTe Lda. Singapore, 2005.

54. Jena A, Sanders, H., Miller, J., Wimberly, R. Comparison of Mercury Porosimetry and Flow Porometry for the Testing of Battery Separator Materials. *Proceedings of the 16th Annual Battery Conference on Applications and Advances* 2001; Long Beach; 2001.

55. Ziabari M, Mottaghitalab, V., Haghi, A. K. Evaluation of Electrospun Nanofiber Pore Structure Parameters. *Korean Journal of Chemical Engineering* 2008; 25(4):923-932.

56. Tzezana R, Zussman. E., Levenberg, S. A layered ultra-porous scaffold for tissue engineering, created via hydrospinning method. *Tissue Engineering: Part C* 2008; 14.

57. Cui W, Li, X., Zhou, S., Weng, J. Degradation patterns and surface wettability of electrospun fibrous mats. *Polymer Degradation and Stability* 2008; 93(3):731-738.

58. Bhattarai SR, Bhattarai, N., Yi, H. K., Hwang, P. H., Cha, D. I., Kim, H. Y. Novel biodegradable electrospun membrane: scaffold for tissue engineering *Biomaterials* 2004; 25:2595-2602.



## Chapter 8

### hBMSCs Osteogenic Induction by Electrospun Scaffolds with Dexamethasone Release Functionality

This chapter is based on the following publication: Martins A, Duarte ARC, Faria S, Marques AP, Reis RL, Neves NM. *hBMSCs Osteogenic Induction by Electrospun Scaffolds with Dexamethasone Release Functionality*. Submitted.

## 8.1. Abstract

Electrospun structures were proposed as scaffolds owing to their morphological and structural similarities with the extracellular matrix found in many native tissues. These fibrous structures were also proposed as drug delivery systems based on the principle that the dissolution rate of a drug increases with the increase of the surface area of both the drug and the corresponding carrier. Dexamethasone (DEX), a synthetic glucocorticoid, is routinely added in culture medium aimed to induce the differentiation of stem cells towards the osteogenic lineage. Different concentrations of the drug (5, 10, 15 and 20 wt.% polymer) were incorporated into polycaprolactone (PCL) nanofibers produced by electrospinning, in a single-step process. The incorporated DEX into the polymeric carrier in an amorphous state, as determined by DSC experiments, did not influence the typical morphology of the nanofibers. *In vitro* drug release studies demonstrated that dexamethasone release was sustained over a period of 15 days.

Bioactivity of the released dexamethasone was assessed by cultivating human bone marrow mesenchymal stem cells (hBMSCs) on 15 wt.% DEX-loaded PCL NFMs, under dexamethasone-absent osteogenic differentiation medium formulation. An increased concentration of alkaline phosphatase and deposition of a mineralized matrix was observed. Phenotypic and genotypic expression of osteoblastic-specific markers corroborates the osteogenic activity of the loaded growth/differentiation factor.

Our data suggests that the electrospun biodegradable nanofibers can be used as carriers for the sustained release of growth/differentiation factors relevant for bone tissue engineering strategies.

## 8.2. Introduction

Drug release systems are used to improve the therapeutic efficacy and safety of drugs, and enhancing the quality of life of patients, by delivering them to the site of action at a rate dictated by the need of the physiological environment [1]. The

limitations of the current drug delivery systems include suboptimal availability, limited effective targeting and potential cytotoxicity resulting from deficient control of the release kinetics. Nano-scale drug delivery systems can be designed to tune the release kinetics, to regulate distribution and to minimize toxic side effects, thereby enhancing the therapeutic efficacy of a given drug. Drug delivery with polymer nanofibers is based on the principle that the dissolution rate of a drug increases with increased surface area of both the drug and the corresponding carrier [2]. Unlike common encapsulation systems involving some complex preparation process [3], electrospinning allows the convenient incorporation of therapeutic/bioactive compounds into the carrier polymer nanofibers in a single step process [4]. Indeed, it was observed that enzymes and antibiotics encapsulated in electrospun nanofibers preserved higher catalytic activity than the ones incorporated in solvent casting membranes [5, 6].

Electrospinning is considered a promising and versatile processing technique, since several polymeric systems [7, 8], proteins [9, 10] and even living cells [11] can be applied to develop functionally active nanofibrous structures. Recently, electrospun nanofibers were used as a carrier for both hydrophobic and hydrophilic drugs [6, 12-14], where the drug release profile can be controlled by the modulation of scaffold morphology, porosity, and composition. Usually, the incorporation of bioactive materials (i.e. proteins and growth factors) within electrospun fibers is achieved by “two-phase” electrospinning, where an aqueous solution of the biological molecule is mixed with an organic polymeric solution to form a biphasic suspension [10, 15-17], resulting in the encapsulation of aqueous reservoirs within the polymer fibers. In another possible alternative, two or more components can be co-electrospun through coaxial capillary channels and integrated into one core-shell composite fiber structure [8]. Consequently, obvious problems in the kinetic release, such as the burst release effect, of those bioactive molecules could be predicted [18-20]. So far, research has been conducted to obtain the controlled delivery of anti-inflammatory agents, antibiotics and anticancer agents [21]. The controlled release of growth and differentiation factors from electrospun meshes was not previously explored.

Functional and structural engineering of musculoskeletal tissue, using a tissue engineering approach, may involve the use of appropriated cells cultured with specific growth factors after seeding in biomaterial scaffolds. In fact, growth factors play a crucial role in the communication and cross-talk between cells and their microenvironment in a tissue engineering construct [22]. They modulate (i.e. regulate the stimulation or inhibition) the cellular activities including proliferation, differentiation, migration, adhesion and gene expression and by this way strongly influencing cell fate [23]. Typically, growth factors are administrated in a soluble form, usually obtained by recombinant technology, being rapidly degraded and inactivated by enzymes and other chemical and physical degradation reactions occurring at body temperature and hence have short bioavailability and biological half-lives. Matrix-bound growth factors, on the other hand, are dispensed locally where they are needed and protected from degradation and are often latent or physiologically unavailable for receptor binding. The shorter half-lives of the growth factors, their relatively large size, slow tissue penetration and their potential toxicity at high systemic levels, suggest that conventional routes of administration are unlikely to be effective for many, if not all, growth factors [22]. In fact, for regenerative and therapeutic effects, tissue must often be exposed to exogenous delivered growth factors during relatively long periods with repetitive administrations.

Tissue engineering can be viewed as a special case of drug delivery in the sense that it should immobilize cells at the injury site. Controlled release of therapeutic/bioactive molecules from biodegradable scaffolds will enhance the efficacy of tissue engineering approaches [1]. In fact, polymeric biomaterials are frequently used as delivery systems, since they can readily deliver growth factors at the desired site either by direct protein delivery approaches or indirectly by gene therapy or by cell transplantation [22]. Consequently, herein we propose the development of electrospun biodegradable nanofibers as a delivery system of an established osteogenic differentiation factor - dexamethasone - of mesenchymal stem cells (MSCs). Dexamethasone (DEX) is a synthetic glucocorticoid, which has been shown to stimulate MSCs proliferation and to support osteogenic lineage differentiation *in vitro*, together with  $\beta$ -glycerophosphate and ascorbic acid in defined

concentrations [24, 25].  $\beta$ -glycerophosphate, the organic phosphate source, play an important role in the mineralization process and in modulating osteoblast activities, such as the alkaline phosphatase (ALP) activity and in expression of osteocalcin. Moreover, ascorbic acid is also essential for increasing cell viability and to stimulate the production of Collagen type I by osteogenic cells. Therefore, the *in vitro* osteogenesis of MSCs might be more successfully established if the culturing substrate/scaffold combines at its surface the adequate physical (i.e. ECM-like nanofibers) and chemical (i.e. growth/differentiation factors) stimulus. Ultimately, we aim at improving the efficacy and reduce the total time required to regenerate a functional bone tissue.

Other authors in the literature reported on electrospun silk fibroin composite fiber scaffolds, containing bone morphogenetic protein 2 (BMP-2) and/or nanoparticles of hydroxyapatite (nHAP), and cultured them with human bone marrow-derived mesenchymal stem cells (hMSCs) [44]. The results demonstrated that those scaffolds, not only support growth and osteogenic differentiation of hBMSCs, but significantly enhance calcium deposition and mRNA transcript levels of bone-related genes. Recently, in a similar work [45], recombinant human bone morphogenetic protein-2 (rhBMP-2) was loaded into poly(D,L-lactide-co-glycolide)/hydroxylapatite (PLGA/HAp) composite electrospun fibrous scaffolds. Cell culture experiments with BMSCs showed that the encapsulation of HAp could enhance cell attachment to scaffolds and lower cytotoxicity effect. Both works described electrospun fibrous as delivery system incorporating a growth/differentiation factor with known clinical potential (FDA approved) for bone and cartilage repair [46]. However, the required cocktail of BMPs able to induce a controlled osteogenic differentiation of mesenchymal stem cells is still to be defined.

### **8.3. Materials & Methods**

#### *8.3.1. Production of Nanofiber Meshes Loaded with Dexamethasone*

A polymeric solution of poly( $\epsilon$ -caprolactone) (PCL) (TONE™, Union Carbide Chemicals and Plastics Division; New Jersey) 17 % (w/v) was prepared using a

mixture of chloroform and dimethylformamide (7:3), as described elsewhere [26]. Different quantities (5, 10, 15 and 20 wt.% polymer) of dexamethasone (Sigma-Aldrich, Germany) were added to the polymeric solution previously prepared, and let to stir until complete dissolution was achieved (approximately during 20 min). A tension of 9.5 kV, a current of 3.32  $\mu$ A, a needle tip-to-ground collector distance of 20 cm and a flow rate of 1 ml/h were defined as optimized processing conditions for the specific material being processed.

### *8.3.2. Characterization of Dexamethasone-loaded PCL Nanofiber Meshes*

DEX-loaded electrospun PCL nanofiber meshes were gold sputter-coated (model SC502, Fisons Instruments; England) for 2 min at 15 mA. Samples were analyzed using a Scanning Electron Microscope (model S360, Leica Cambridge; England). Micrographs were recorded at 15 kV with magnifications ranging from 100 to 5000 times.

Fourier Transform Infra-Red Spectroscopy (FTIR) analysis was performed with the DEX-loaded electrospun PCL nanofiber meshes. The samples were powdered, mixed with KBr, and processed into pellets. FTIR spectra were recorded at 48 scans with a resolution of 2  $\text{cm}^{-1}$  (Shimadzu – IR Prestige 21)

Differential Scanning Calorimetry (DSC) experiments were carried out using a DSC Q100 equipment (TA Instruments – ELNOR). The experiments were conducted under a nitrogen atmosphere on samples (5-10 mg) packed in aluminium capsules. The samples were heated in two stages at a constant heating rate of 10  $^{\circ}\text{C}/\text{min}$  from room temperature up to 300  $^{\circ}\text{C}$ . The samples were kept at this temperature for a period of 2 minutes and cooled at the same rate to the initial temperature.

### *8.3.3. Dexamethasone Kinetic Release Studies*

DEX-loaded PCL nanofiber meshes (with 4  $\text{cm}^2$ ) were weighted and incubated at 37  $^{\circ}\text{C}$  in 30 ml of phosphate buffer solution stirred at 60 rpm. Aliquots of 3 ml were retrieved in predetermined time intervals and the same volume of fresh medium was added to the suspension. The samples were analysed by UV-Vis spectroscopy at 242

nm (Shimazu UV 1601). The DEX concentration of each sample was calculated using a standard curve (concentrations ranging from 0.0 to 72  $\mu\text{g/ml}$ ), relating the quantity of DEX with the intensity of light absorbance. The results presented are an average of three measurements. Calculations of the amount of drug released took into account the replacement of aliquots with fresh medium.

#### *8.3.4. Expansion, Seeding and Osteogenic Differentiation of Human Bone Marrow Mesenchymal Stem Cells*

Human bone marrow mesenchymal stem cells (hBMSCs) (Biopredic International, France) were isolated and characterized according to the method established by Delome and Charbord [27]. hBMSCs were expanded in basal medium consisting of MEM alpha medium ( $\alpha$ -MEM; Gibco, GB) supplemented with 10 % heat-inactivated fetal bovine serum (FBS; Biochrom AG, Germany) and 1 % antibiotic/antimycotic solution (final concentration of penicillin 100 units/ml and streptomycin 100  $\mu\text{g/ml}$ ; Gibco, GB). Cells were cultured at 37 °C in an atmosphere of 5 %  $\text{CO}_2$ .

Before the *in vitro* studies, PCL nanofiber meshes loaded with 15 wt.% dexamethasone were cut in samples with areas of approximately 1  $\text{cm}^2$  and sterilized by UV irradiation during 1 h on each side of the mesh. Confluent hBMSCs at passage 4 were harvested for seeding onto the DEX-loaded PCL NFMs at a density of  $1.0 \times 10^5$  cells/ $\text{cm}^2$  of the nanofiber mesh. Unloaded PCL nanofiber meshes were used as controls. The DEX-loaded PCL NFMs-hBMSCs constructs were cultured under static conditions, in basal and dexamethasone-absent osteogenic differentiation media (basal medium supplemented with 50  $\mu\text{g/ml}$  ascorbic acid and 10 mM  $\beta$ -glycerophosphate). The control PCL NFMs-hBMSCs constructs were also cultured under static condition, in basal and standard osteogenic differentiation media (basal medium supplemented with 50  $\mu\text{g/ml}$  ascorbic acid, 10 mM  $\beta$ -glycerophosphate and  $10^{-7}$  M dexamethasone). The constructs were retrieved at different culture times: 7, 14 and 21 days.

### *8.3.5. Cell Morphology and Distribution, and Chemistry of Deposited Matrix*

For scanning electron microscopy (SEM) observation, the samples were fixed with 2.5 % Glutaraldehyde (Sigma; USA) in a Phosphate Buffer Saline solution (Sigma; USA) during 1h at 4 °C. The samples were further dehydrated through increasing series of ethanol concentrations and let to dry overnight. Previous to the analysis by SEM (model S360, Leica Cambridge; England) equipped with an energy dispersive spectrometer (EDS; link-eXL-II), the samples were gold or carbon sputter coated (sputter coater model SC502, Fisons Instruments; England).

### *8.3.6. Cell Viability and Proliferation Assessment*

Cell viability for each culturing time was determined using the CellTiter 96<sup>®</sup> AQueous One Solution Cell Proliferation Assay (Promega; USA). This assay is based on the bioreduction of a tetrazolium compound, 3-(4,5-dimethylthiazol-2-yl)-5-(3-carboxymethoxyphenyl)-2-(4-sulfofenyl)-2H-tetrazolium [MTS], into a water soluble brown formazan product. The absorbance was measured at 490 nm in a microplate reader (Synergie HT, Bio-Tek; USA), being related with the quantity of formazan product and directly proportional to the number of living cells in the constructs. Three samples of each nanofiber mesh per time point were characterized.

Cell proliferation was quantified by the total amount of double-stranded DNA, along the culturing time. Quantification was performed using the Quant-iT<sup>™</sup> PicoGreen dsDNA Assay Kit (Invitrogen<sup>™</sup>, Molecular Probes<sup>™</sup>; Oregon, USA), according to the instructions of the manufacturer. Briefly, cells in the construct were lysed by osmotic and thermal shock and the supernatant used for the DNA quantification assay. The fluorescence of the dye was measured at an excitation wavelength of 485/20 nm and at an emission wavelength of 528/20 nm, in a microplate reader (Synergie HT, Bio-Tek; USA). Triplicates were made for each sample and per culturing time. The DNA concentration for each sample was calculated using a standard curve (DNA concentration ranging from 0.0 to 1.5 µg/ml) relating quantity of DNA and fluorescence intensity.

### 8.3.7. Alkaline Phosphatase Quantification

The concentration of alkaline phosphatase (ALP) was determined for all time culture periods, using the lysates used for DNA quantification. Briefly, the ALP quantity was assessed using the *p*-nitrophenol assay, in which the colourless nitrophenyl phosphate disodium salt (pnPP; Sigma, USA) is hydrolysed by the ALP (Sigma, USA) at pH 10.5 and temperature of 37 °C to form yellow free *p*-nitrophenol. The reaction was stopped by addition of 2M NaOH (Panreac Quimica, Spain) and the absorbance read at 405 nm in a microplate reader (Bio-Tek, Synergie HT; USA). Standards were prepared with 10 µmol/ml *p*-nitrophenol (pNP; Sigma, USA) solution, to obtain a standard curve ranging from 0 to 0.250 µmol/ml. Triplicates of each sample and standard were made, and the ALP concentrations read off from the standard curve.

### 8.3.8. Alizarin Red Staining

After culture, the DEX-loaded nanofiber meshes-hBMSCs constructs were fixed in 10 % formalin solution neutral buffer (Sigma-Aldrich, Germany) for 30 min and maintained in phosphate buffer saline (PBS) until further use. The constructs were further stained with a 2 % Alizarin Red solution (Merk, Germany) in distilled water for 5 min, and finally washed with distilled water. Stained constructs were observed under an optical microscope (BX61, Olympus Corporation, Germany) and images captured by a digital camera (DP70, Olympus Corporation, Germany).

### 8.3.9. Immunodetection of Bone-specific Proteins

Immunocytochemistry was performed following the streptavidin-biotin-peroxidase complex approach (R.T.U. Vectastain<sup>®</sup> Universal Elite<sup>®</sup> ABC kit; Vector Laboratories Inc., Burlingame, CA), using a rabbit polyclonal antibody against osteopontin (Abcam Ltd., Cambridge, UK; dilution 1:1500), a mouse monoclonal antibody against osteocalcin (clone OC4-30, Abcam Ltd., Cambridge, UK; dilution 1:100) and a rabbit polyclonal antibody against bone sialoprotein II (Chemicon<sup>®</sup>

International Inc., Germany; dilution 1:2500). Prior to the immunocytochemistry procedure, constructs were fixed in 10 % formalin solution neutral buffer (Sigma-Aldrich, Germany) for 30 min and maintained in phosphate buffer saline (PBS) until further use. The constructs were treated with 0.3 % hydrogen peroxide in methanol during 30 min to inactivate the endogenous peroxidases. After washing with PBS, the constructs were blocked with 2.5 % normal horse serum for 20 min at room temperature to avoid unspecific reactions. Primary antibodies were incubated overnight at 4 °C. Negative controls were set in the absence of primary antibodies incubation. After washing in PBS, the samples were incubated for 30 min with biotinylated secondary antibody anti-rabbit/mouse IgG, followed by incubation with streptavidin-peroxidase complex (Elite ABC Reagent). The immune reaction was visualized using DAB as a chromogen (DAB Substrate Reagent from Peroxidase Substrate Kit; Vector Laboratories Inc, Burlingame, CA). The constructs were observed under an optical microscope (BX61, Olympus Corporation, Germany) and images captured by a digital camera (DP70, Olympus Corporation, Germany).

#### *8.3.10. RNA isolation and Real-Time Quantitative Polymerase Chain Reaction*

Total RNA from the constructs was extracted using the Trizol<sup>®</sup> (Invitrogen, Life Technologies Inc., UK) method according to the manufacturer's directions. Briefly, at each culturing time the constructs were washed with PBS, immersed in Trizol and storage at -80 °C until further use. Proteins were removed with chloroform extraction, and the RNA pellets were washed once with isopropyl alcohol and once with 70 % ethanol. The total RNA pellets were reconstituted in Rnase free water (Gibco, Invitrogen, UK).

Reverse transcriptase (RT)-PCR was performed according to the protocol from iScript<sup>™</sup> cDNA synthesis kit (BioRad, Hercules, CA, USA). Briefly, a reaction mixture consisting of 1X iScript Reaction Mix, 1 µl iScript Reverse Transcriptase, RNA template (300 ng total RNA) and nuclease-free water was prepared, in 20 µl of total volume. The single-strand cDNA synthesis occurred by incubating the complete reaction mixture 5 min at 25 °C, followed by 30 min at 42 °C and terminated by an incubation at 85 °C for 5 min.

**Table 8.1** - Primers list of osteogenic markers.

<b>Gene</b>		<b>Primer sequences (5'-3')</b>	<b>T<sub>m</sub> [°C]</b>
<i>ALP</i>	sense	CTCCTCGGAAGACACTCTG	60,0
	antisense	AGACTGCGCCTGGTAGTTG	
<i>OP</i>	sense	GGGGACA AACTGGAGTGAAAA	58,4
	antisense	CCCACAGACCCTTCCAAGTA	
<i>BSP</i>	sense	CAACAGCACAGAGGCAGAAAAC	59,9
	antisense	CCTCGTATTCAACGGTGGTG	
<i>OC</i>	sense	CTGAGAGGAGCAGAACTGG	61,4
	antisense	GGCAGCGAGGTAGTGAAGAG	
<i>Runx2</i>	sense	TTCCAGACCAGCAGCACTC	58,1
	antisense	CAGCGTCAACACCATCATTC	
<i>Osterix</i>	sense	CCCTTTACAAGCACTAATGG	57,1
	antisense	ACACTGGGCAGACAGTCAG	
<i>GAPDH</i>	sense	ACAGTCAGCCGCATCTTCTT	58,4
	antisense	GACAAGCTTCCCGTTCTCAG	

Amplification of the target cDNA for real-time PCR quantification were performed according to manufacturer, using 2 µl RT cDNA products, 1 µM each primer (bone-specific primer sets listed in Table 8.1), 1X iQ SYBR Green Supermix (BioRad, Hercules, CA, USA) and nuclease-free water, in a final volume of 25 µL. Forty-four cycles of denaturation (95 °C, 10 s), annealing (temperature dependent on the gene, 30 s) and extension (72 °C, 30 s) were carried out in the gradient thermocycler MiniOpticon real-time PCR detection system (BioRad, Hercules, CA, USA) for all genes. The transcripts expression data were normalized to the housekeeping gene glyceraldehydes-3-phosphate-dehydrogenase (*GAPDH*) and the relative quantification calculated by the  $\Delta C_T$  method.

### 8.3.11. Statistical Analysis

Statistical Analysis was performed using the SPSS statistic software (Release 15.0.0 for Windows). Firstly, a Shapiro-Wilk test was used to ascertain about the data normality. The results indicated that nonparametric tests should be used for all comparisons. A Kruskal-Wallis test followed by Turkey's HSD test were performed to analyze the effect of the DEX-loaded electrospun nanofibrous meshes on the

hBMSCs' viability and proliferation, ALP quantification, and osteogenic genotype. *P* values lower than 0.01 were considered statistically significant.

## 8.4. Results

### 8.4.1. Physicochemical Properties of the Dexamethasone-loaded Electrospun PCL Nanofiber Meshes

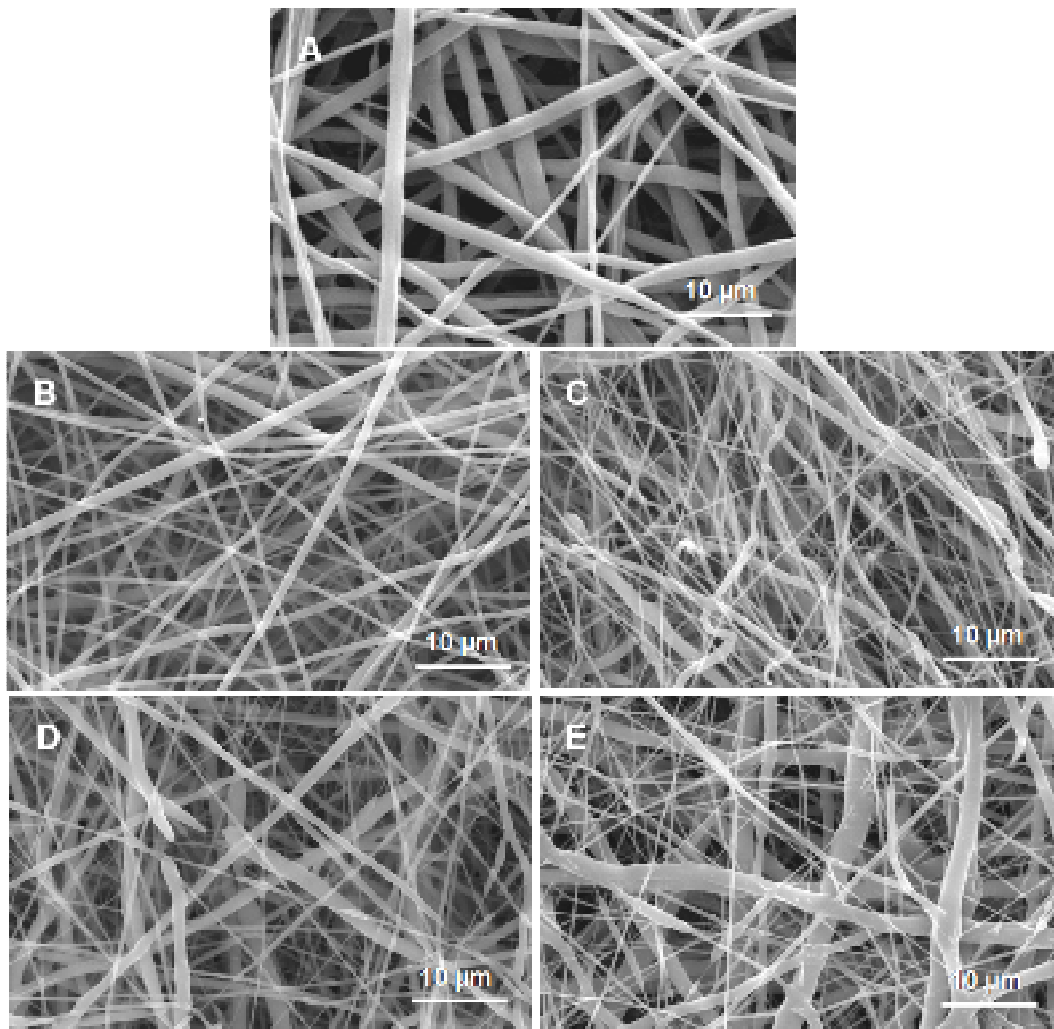


**Figure 8.1** – Morphological characterization of a typical electrospun PCL nanofiber mesh (A) and the electrospun nanofiber meshes incorporating different concentrations of dexamethasone: 5 wt.% (B), 10 wt.% (C), 15 wt.% (D) and 20 wt.% (E).

In the present work, a glucocorticoid drug - dexamethasone - was dissolved at different concentrations (5, 10, 15 and 20 wt.% polymer) in the polymeric solution to be electrospun. A mesh-like structure composed by randomly distributed fibers with diameters ranging from 150 nm – 1.6  $\mu\text{m}$  (Figures 8.1 B-E) was produced. The incorporation of dexamethasone at concentrations ranging from 5 to 15 wt.% (Figures 8.1 B-D) shows the appearance of thinner fibers in large number than in the control nanofiber meshes (Figure 8.1 A). However, those differences in morphology are probably not sufficient to induce any specific cell response. This observation was expected since the solvent is able to dissolve simultaneously the polymer and the incorporated drug. In this way, the drug is very well dispersed in the bulk polymeric matrix of the electrospun nanofibers without inducing significant morphological variation of the electrospun fibers. Relevant morphological alterations, namely an increment of nanofibers diameter, was observed only in the electrospun meshes incorporation 20 wt.% DEX (Figure 8.1 E).

To confirm the presence of dexamethasone incorporated in the electrospun PCL nanofibers a FTIR analysis was performed. Figure 8.2 shows the spectra of PCL

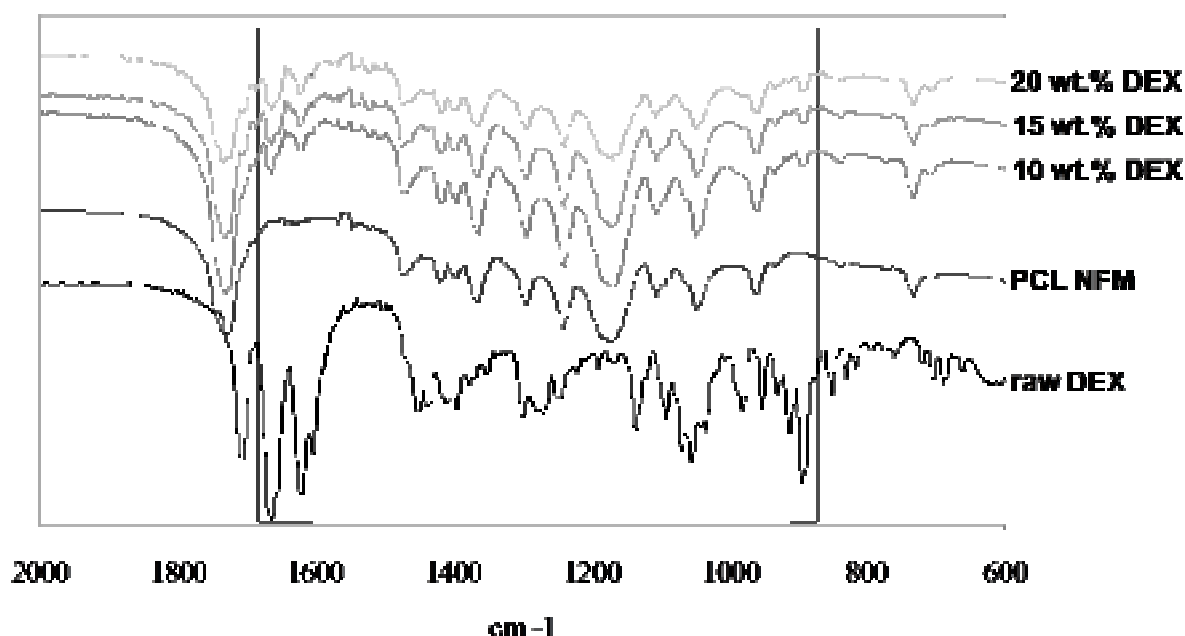


**Figure 8.2** - FTIR spectra of raw dexamethasone, control PCL NFMs, DEX-loaded PCL NFMs at 10 wt.%, 15 wt.% and 20 wt.%.

nanofibers, raw dexamethasone and also of the different DEX-loaded electrospun PCL nanofiber meshes. The characteristic peaks of dexamethasone at 900 and 1650  $\text{cm}^{-1}$  are observed in the nanofiber meshes prepared with the different DEX concentrations, which confirms the presence of the glucocorticoid in the polymeric matrix.

Thermal analysis of the DEX-loaded nanofiber meshes was carried out to ascertain about the crystalline state of the incorporated dexamethasone. Figure 8.3 A shows the DSC thermograms of PCL nanofiber meshes and raw dexamethasone. In this graph is possible to observe the melting peaks of the polymer at 56.9 °C and of dexamethasone at 262.2 °C. However, the characteristic endothermic peak of dexamethasone is not present in the DEX-loaded nanofiber meshes (Figure 3 B). These thermal properties of DEX-loaded PCL nanofiber meshes suggest that dexamethasone, precipitated from the polymeric/organic solution during the electrospinning processing, is not in its crystalline state when incorporated in the nanofiber meshes. This is a typical observation, since the mobility of the DEX inside the fibers is highly hindered.

#### 8.4.2. Release Kinetics of Dexamethasone from the Electrospun PCL Nanofiber Meshes

The release profile of dexamethasone from the different DEX-loaded PCL NFM

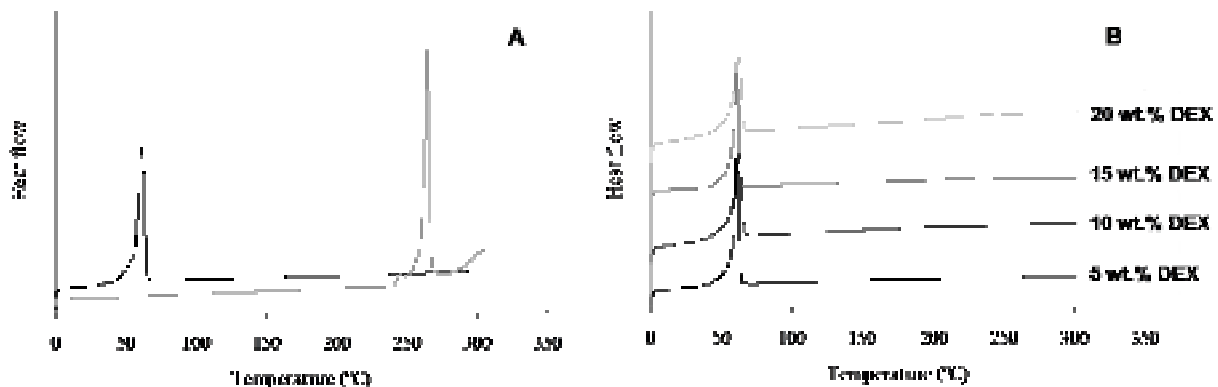


**Figure 8.3** – DSC thermogram of control PCL NFMs (black line) and raw dexamethasone (grey line) (A), and DEX-loaded PCL nanofibers at 5 wt.%, 10 wt.%, 15 wt.% and 20 wt.% (B).

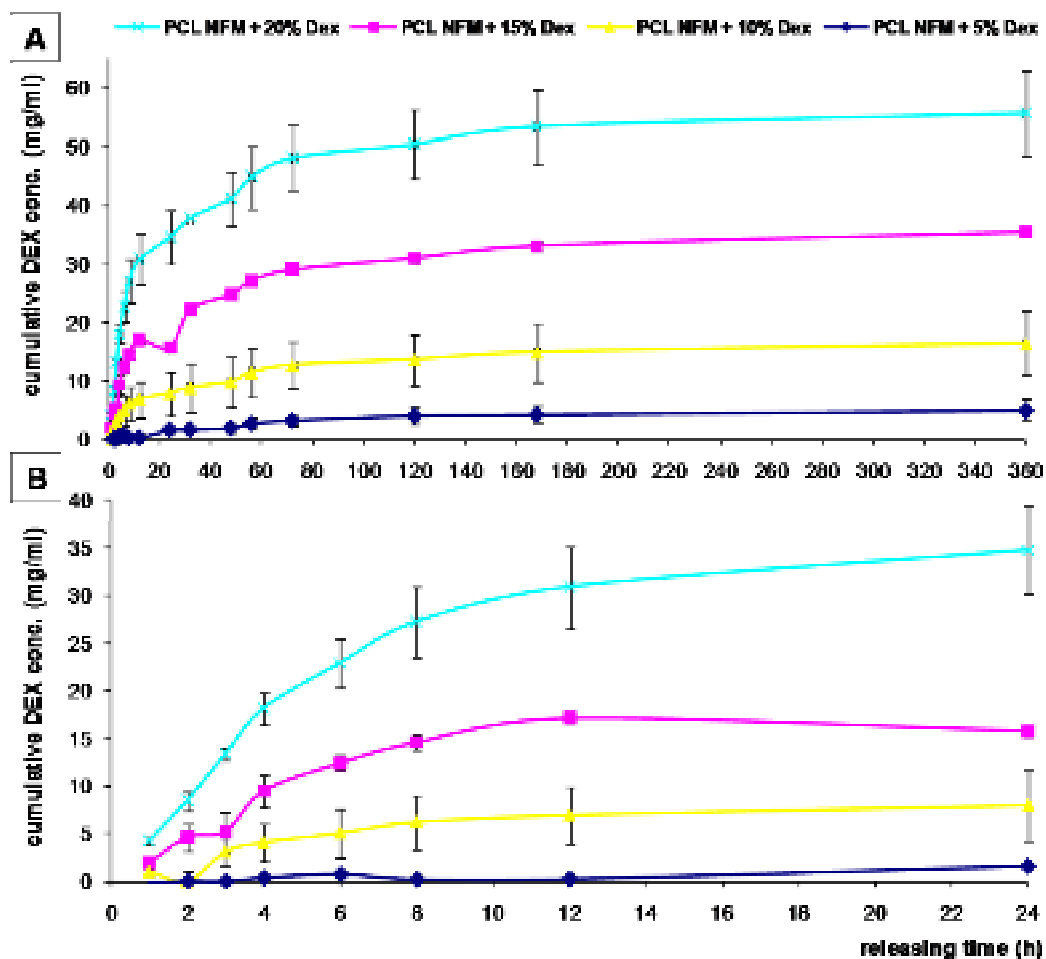


**Figure 8.4** – Release profile of the different dexamethasone concentrations incorporated into the electrospun PCL nanofiber meshes during 360h (**A**); zoom up of the initial 24h of dexamethasone release (**B**).

was followed during 21 days, in accordance with the culture time usually needed to observe a complete osteogenic differentiation of MSCs *in vitro*. As depicted in Figure 8.4 B, a significant initial release of dexamethasone - burst release - was observed in the case of PCL NFMs incorporating above 5 wt.% of the growth/differentiation factor. It was noticed that a higher amount of drug lead to a faster release rate (Figure 8.4 A). After 100h, a slow sustained release of dexamethasone was observed for all release systems. Considering the release profiles of the different DEX-loaded PCL NFMs, the dexamethasone concentrations achieved and the morphology of the nanofiber meshes, the 15 wt.% DEX-loaded PCL NFMs was chosen for further *in vitro* biological assays.

### 8.4.3. Biological Activity of the Dexamethasone Released from the Electrospun Nanofiber Meshes

To ascertain about the biological activity, and inherent structural integrity, of the released dexamethasone from the electrospun PCL NFMs, human bone marrow mesenchymal stem cells (hBMSCs) were cultured on 15 wt.% DEX-loaded PCL NFMs. From the MTS assay data (Figure 8.5) it was possible to observe that, until the 14<sup>th</sup> day of culture, the different culture conditions did not induce significant changes over hBMSCs viability ( $p > 0.01$ ). However, at day 21, hBMSCs cultured on DEX-loaded NFMs on dexamethasone-absente osteogenic differentiation medium (*NFM+DEX\_Osteo*), on DEX-loaded NFMs (*NFM+DEX\_Basal*) and on control PCL NFMs (*NFM\_Basal*) on basal medium showed significant lower viability than those cultured on standard osteogenic differentiation medium (*NFM\_Osteo*) ( $p < 0.01$ ).

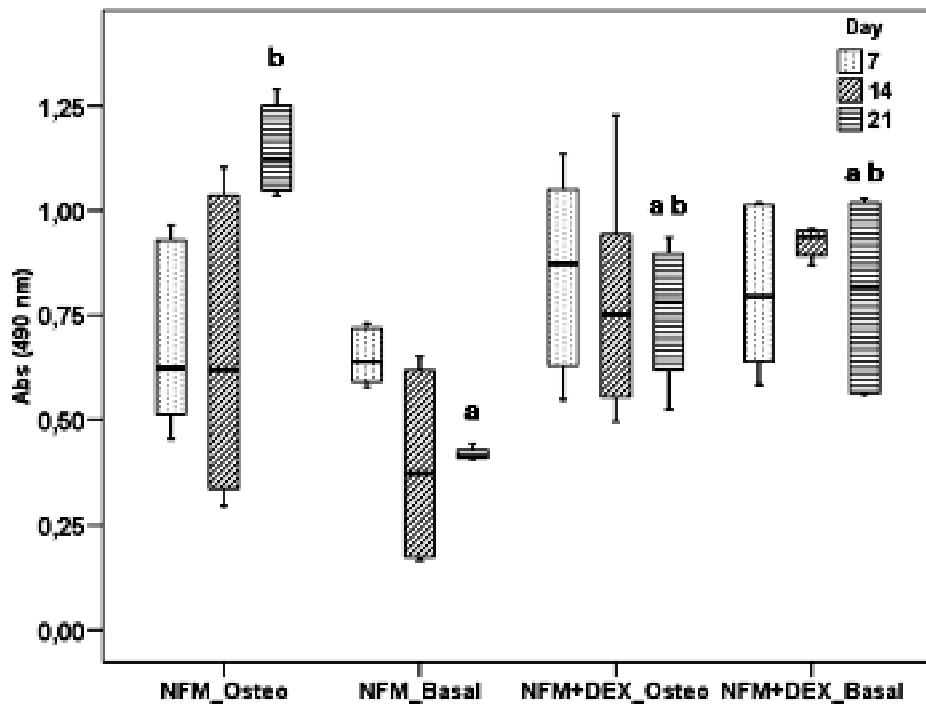


**Figure 8.5** – Box plot of the hBMSCs viability (MTS assay) cultured on *NFM\_Osteo*, *NFM\_Basal*, *NFM+DEX\_Osteo* and *NFM+DEX\_Basal*, after 7, 14 and 21 days. Data were analyzed by nonparametric way of a Kruskal-Wallis test followed by Tukey's HSD test: **a** denotes significant differences compared to *NFM\_Osteo*; **b** denotes significant differences compared to *NFM\_Basal*.

Moreover, for this culturing time, DEX-loaded NFMs cultured on basal (*NFM+DEX\_Basal*) and dexamethasone-absent osteogenic differentiation media (*NFM+DEX\_Osteo*) presented significantly higher hBMSCs' viability than those cultured on control PCL NFMs under basal conditions (*NFM\_Basal*) ( $p < 0.01$ ). Complementary to the analysis of hBMSCs' viability along the course of the experiment, the proliferation or replication rate of those cells was also quantified based on the DNA content (Figure 8.6). DEX-loaded NFMs constructs cultured on dexamethasone-absent osteogenic differentiation medium (*NFM+DEX\_Osteo*) present significant lower proliferation capability than hBMSCs cultured under all the other conditions ( $p < 0.01$ ). Conversely, control PCL NFMs cultured under basal medium (*NFM\_Basal*) demonstrated significantly higher DNA concentration than all

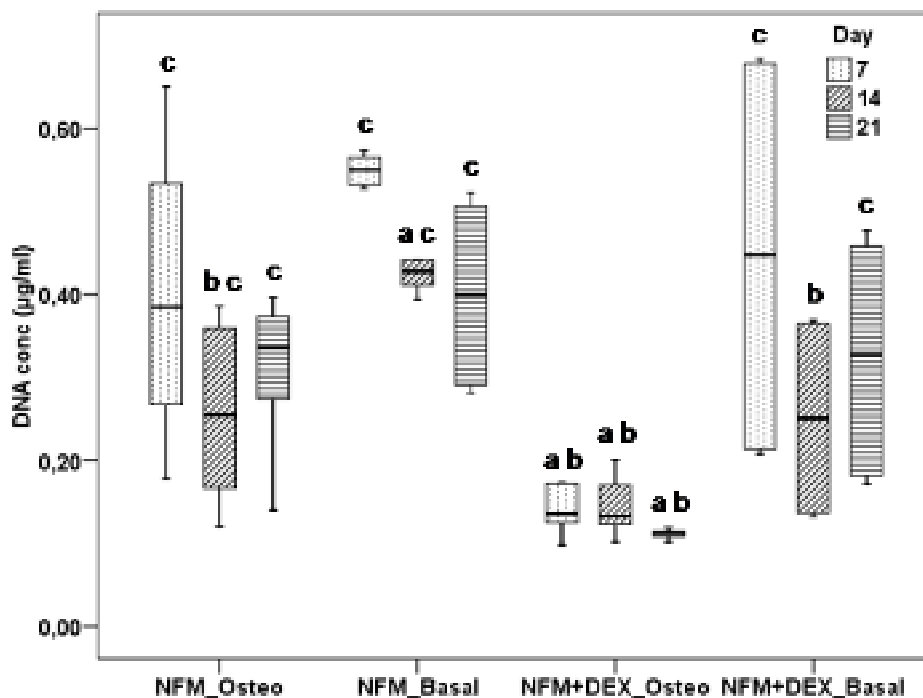


**Figure 8.6** – Box plot of the hBMSCs proliferation (DNA concentration) cultured on *NFM\_Osteo*, *NFM\_Basal*, *NFM+DEX\_Osteo* and *NFM+DEX\_Basal*, after 7, 14 and 21 days. Data were analyzed by nonparametric way of a Kruskal-Wallis test followed by Tukey's HSD test: **a** denotes significant differences compared to *NFM\_Osteo*; **b** denotes significant differences compared to *NFM\_Basal*; **c** denotes significant differences compared to *NFM+DEX\_Osteo*.

the other substrates and corresponding culture medium ( $p < 0.01$ ), just for the 14<sup>th</sup> day.

Despite the above described proliferative cell population cultured on the DEX-loaded PCL NFMs under basal (*NFM+DEX\_Basal*) or dexamethasone-absent osteogenic differentiation media (*NFM+DEX\_Osteo*), the expression of alkaline phosphatase (ALP) is similar to the one observed in control PCL NFMs cultured on standard osteogenic differentiation medium (*NFM\_Osteo*) ( $p > 0.01$ ) (Figure 8.7). An exception was observed for the 14 days of culture: hBMSCs cultured on DEX-loaded NFMs under dexamethasone-absent conditions (*NFM+DEX\_Osteo*) produced significant higher quantities of ALP than the control PCL NFMs under osteogenic conditions (*NFM\_Osteo*) ( $p < 0.01$ ). Undifferentiated hBMSCs cultured on the control

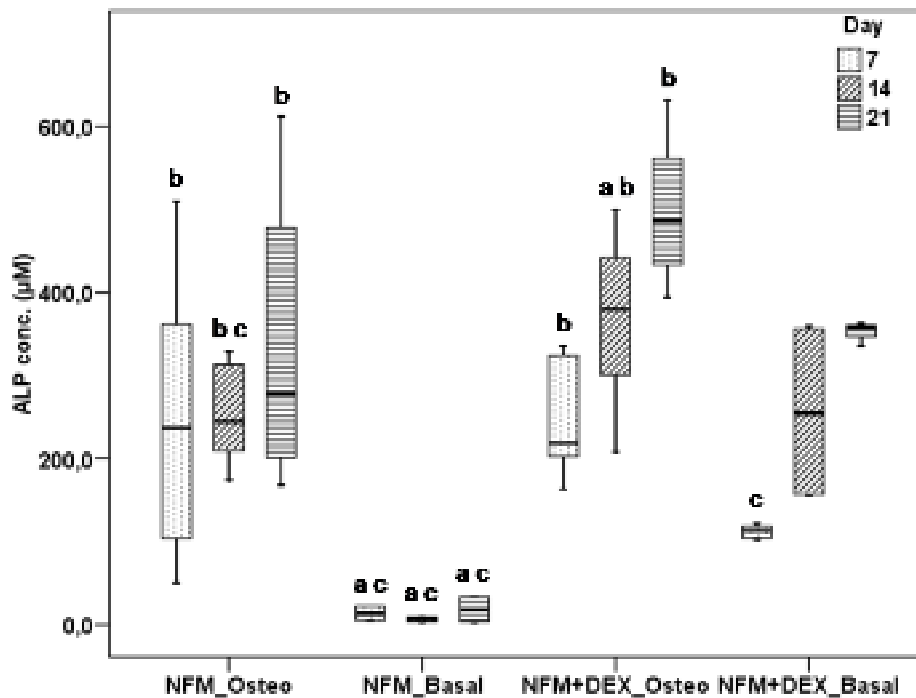


**Figure 8.7** – Box plot of the alkaline phosphatase (ALP) produced by hBMSCs cultured on *NFM\_Osteo*, *NFM\_Basal*, *NFM+DEX\_Osteo* and *NFM+DEX\_Basal*, after 7, 14 and 21 days. Data were analyzed by nonparametric way of a Kruskal-Wallis test followed by Tukey's HSD test: **a** denotes significant differences compared to *NFM\_Osteo*; **b** denotes significant differences compared to *NFM\_Basal*; **c** denotes significant differences compared to *NFM+DEX\_Osteo*.

PCL NFMs (*NFM\_Basal*) produce negligible quantities of ALP, as depicted by the significant lower ALP concentration compared to all the other substrates and corresponding culture medium ( $p < 0.01$ ). Consequently, from this test on further characterization of the osteogenic phenotype and genotype do not includes this condition.

The morphology and distribution of the hBMSCs cultured on DEX-loaded NFM was analyzed by SEM. The cells interacted with the fibrous structure, bridging contiguous fibers and formed a dense cellular construct that was clearly visible at day

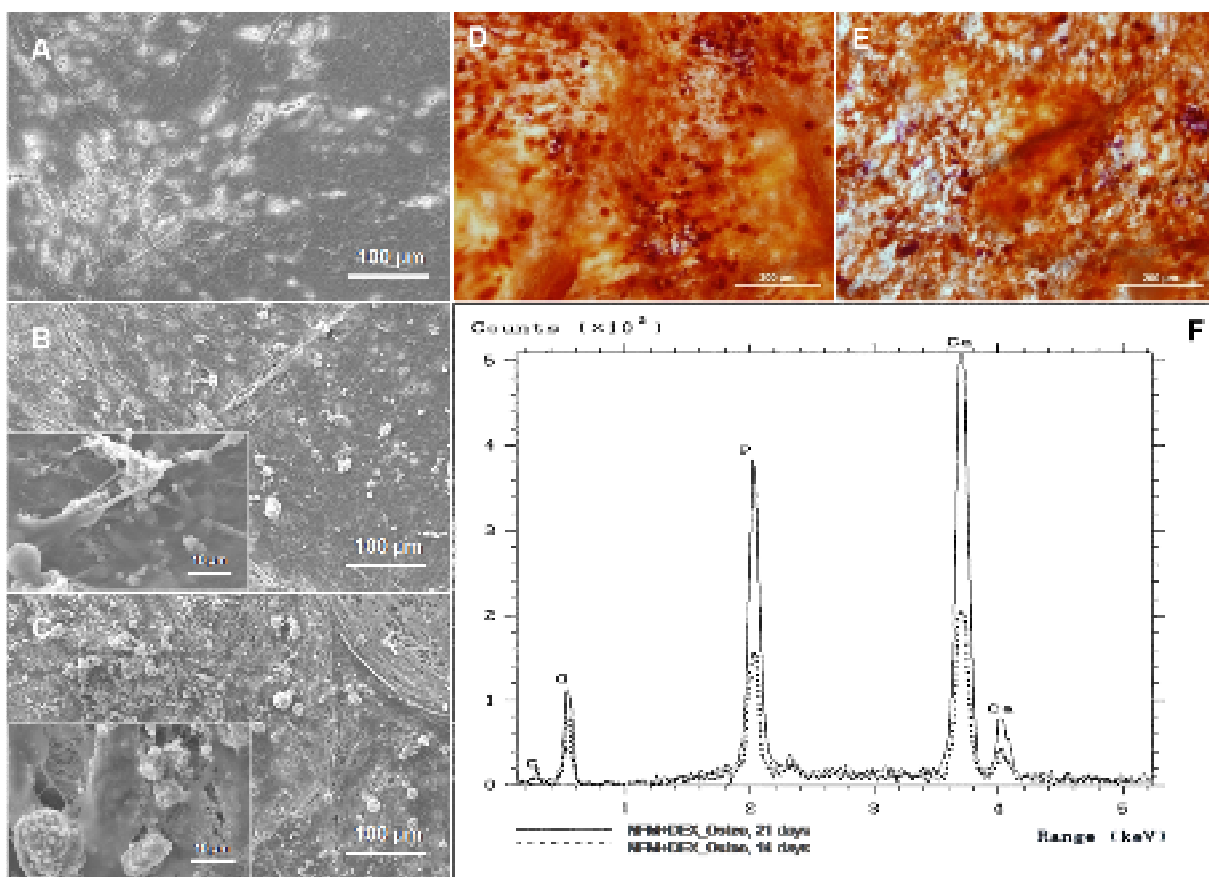


**Figure 8.8** – SEM micrographs of hBMSCs cultured on DEX-loaded NFMs during 7 (A), 14 (B) and 21 days (C). Higher magnifications are shown to evidence the mineralization nodules produced by the hBMSCs. Alizarin red staining of the DEX-loaded NFMs-hBMSCs constructs after 14 (D) and 21 days (E). Energy dispersive spectrometer (EDS) spectra of the calcium phosphates nodules produced by hBMSCs cultured on DEX-loaded NFMs after 14 and 21 days (F).

7 (Figure 8.8 A). It was also possible to observe deposition of minerals over the dense cellular layer from day 14 onward (Figures 8.8 B and C), resulting from the matrix mineralization that occurs along the differentiation of hBMSCs into osteoblasts. To confirm the matrix mineralization, an alizarin red staining was performed to specifically detect the calcium presented in those mineralized nodules. The intense red/purple dots dispersed in the construct correspond to the mineralized nodules, after 14 and 21 days of hBMSCs culture on DEX-loaded NFM under dexamethasone-absent osteogenic differentiation medium formulation (Figures 8.8 D and E). Using an Energy Dispersive Spectrometer (EDS) it was possible to identify the elemental composition of the minerals deposited on the DEX-loaded PCL NFM-hBMSCs constructs (Figure 8.8 F). EDS data confirms the presence of Calcium and Phosphorous deposition by the adjacent cells, and the increasing amount from day 14 to 21 of hBMSCs culture under dexamethasone-absent osteogenic differentiation medium formulation. Those observations were not found in control PCL NFM cultured with hBMSCs under standard osteogenic differentiation conditions, nor in the DEX-loaded PCL NFM culture with hBMSCs on basal medium (data not included here).

The osteogenic phenotype of hBMSCs seeded onto DEX-loaded nanofiber meshes was also assessed by the immunodetection of some specific osteoblastic proteins, namely osteopontin, bone sialoprotein and osteocalcin. Photomicrographs seem to show a progressive expression of the specific osteoblastic glycoprotein osteopontin on the DEX-loaded NFMs-hBMSCs constructs during the 21 days of culture (Figure 8.9). In the case of the bone sialoprotein and osteocalcin protein, its maximum expression seems to be achieved at the 14<sup>th</sup> day of hBMSCs culture under dexamethasone-absent osteogenic differentiation medium. Similar osteoblastic protein expression pattern was observed in the control PCL NFM cultured with hBMSCs under standard osteogenic differentiation conditions and, also, in the DEX-loaded PCL NFM culture with hBMSCs in basal medium (data not showed).

Complementary to the phenotypic analysis, a genotypic quantification of the expression of some bone-specific genes was performed to ascertain about the differentiation level of seeded hBMSCs on DEX-loaded PCL NFMs. The relative expression of those genes was normalized against the housekeeping gene *GAPDH*

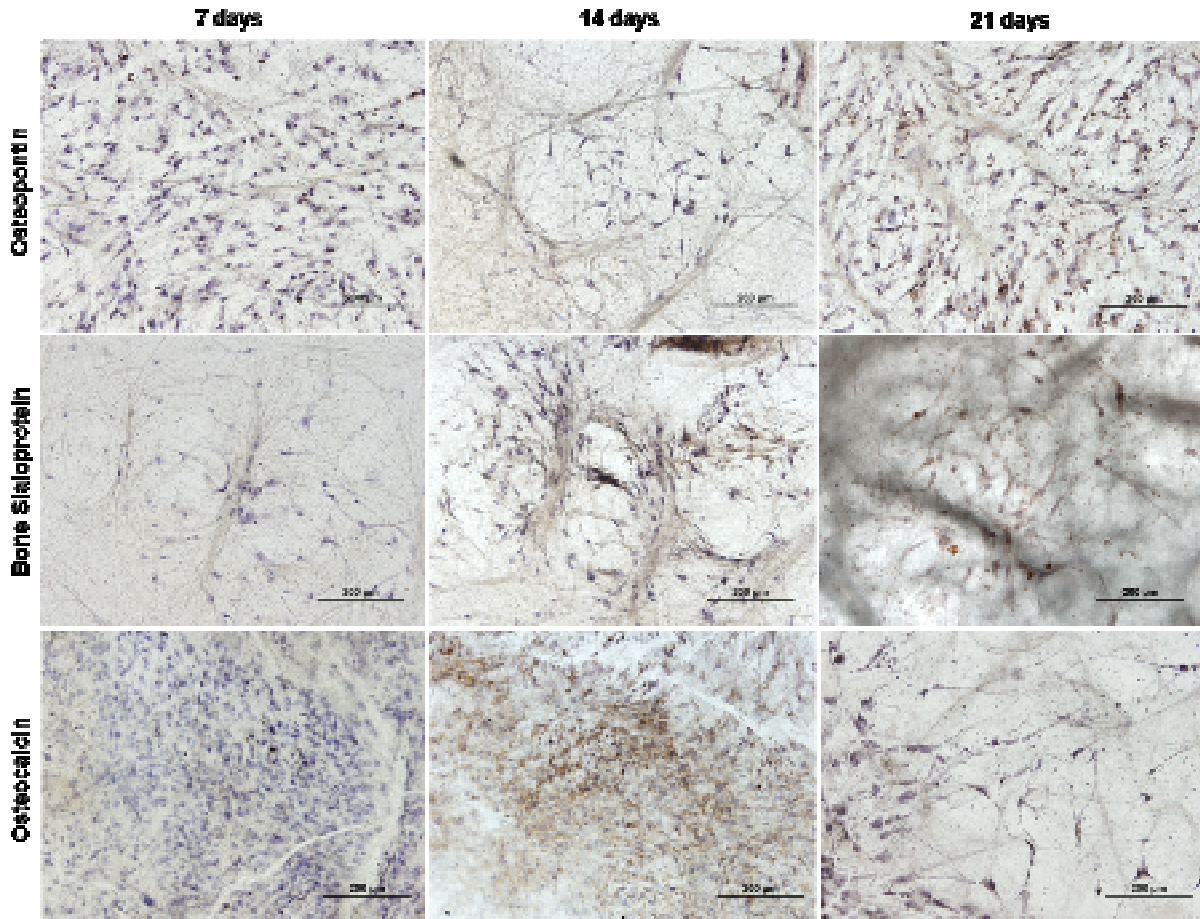


**Figure 8.9** – Immunodetection of some bone-specific proteins, namely Osteopontin, Bone Sialoprotein and Osteocalcin, expressed by hBMSCs cultured on DEX-loaded NFMs during 7, 14 and 21 days.

and compared to hBMSCs cultured on control PCL NFM under standard osteogenic differentiation conditions. A constitutive expression of all mRNA transcripts (i.e. *Alkaline Phosphatase*, *Osteopontin*, *Bone Sialoprotein*, *Osteocalcin*, *Runx-2* and *Osterix*) was observed during the 21 days of culture. Although *Alkaline Phosphatase* was present in a stable fashion, its expression is significant lower by hBMSCs cultured on DEX-loaded PCL NFMs, in both culture conditions ( $p < 0.01$ ) (Figure 8.10). Between those bone-specific genes, *Bone Sialoprotein* and *Osterix* were the highest expressed, followed by the *Osteopontin* gene.

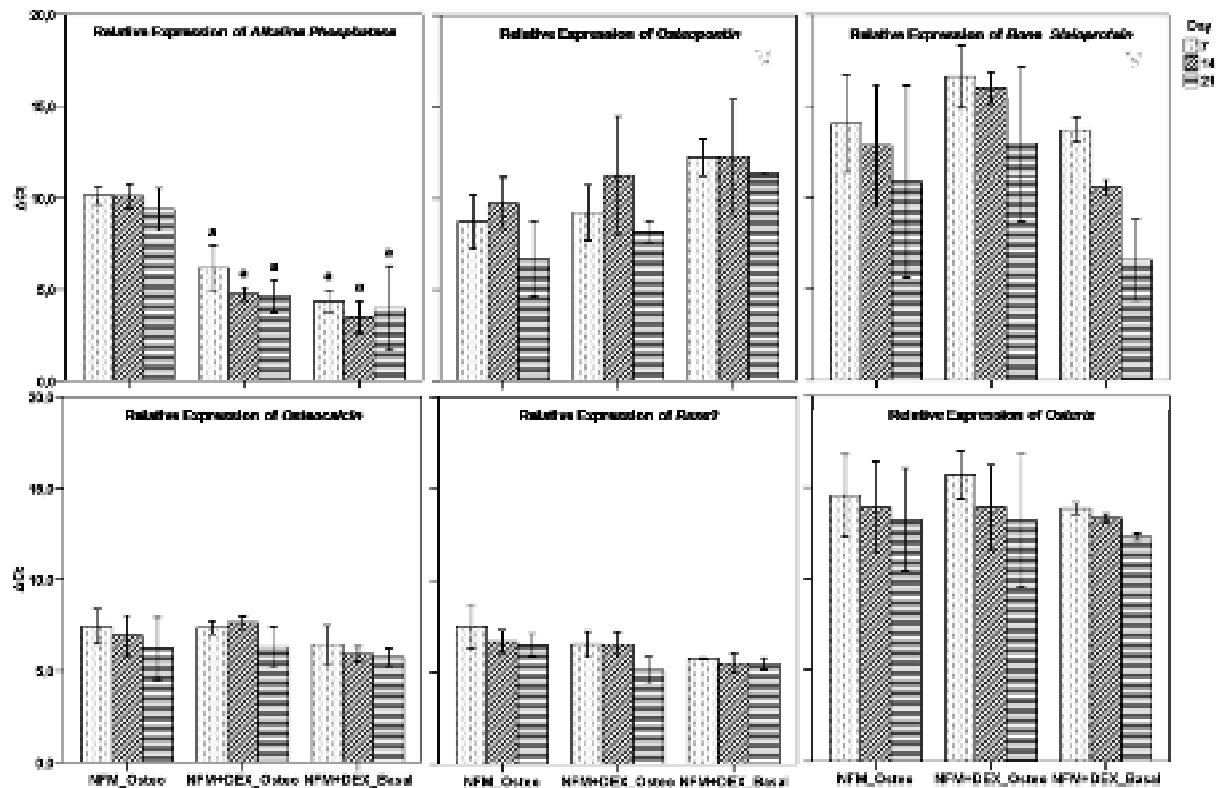


**Figure 8.10** - Relative expression of bone-specific transcripts, namely *Alkaline Phosphatase*, *Osteopontin*, *Bone Sialoprotein*, *Osteocalcin*, *Runx2* and *Osterix*, by hBMSCs cultured on *NFM\_Osteo*, *NFM+DEX\_Osteo* and *NFM+DEX\_Basal*, after 7, 14 and 21 days. The expression of these genes was normalized against the housekeeping gene *GAPDH* and calculated by the  $\Delta\text{CT}$  method. Data were analyzed by nonparametric way of a Kruskal-Wallis test followed by Tukey's HSD test: **a** denotes significant differences compared to *NFM\_Osteo*.

## 8.5. Discussion

### 8.5.1. Electrospun PCL Nanofiber Meshes Incorporating and Releasing Dexamethasone

The rate of drug release depends on a multitude of factors, such as the nature of the polymer matrix (i.e. chemical composition, backbone stability and water solubility), matrix architecture, loading capacity and drug-matrix interaction. Therefore, for the development of an ideal drug delivery system, the polymer should

be biodegradable, have appropriate degradation rate, nontoxic degradation products, appropriate solubility and simplicity of fabrication [28]. The herein developed drug carrier was based on the convenient processing of nanofibrous structures by electrospinning, using an adequate organic solvent to simultaneously dissolve the biodegradable polymer - polycaprolactone - and the incorporated drug - dexamethasone. This drug delivery system allows a suitable interaction between the PCL and the dexamethasone, being the drug well distributed in a polymer matrix. Consequently, the drug presents a good physicochemical interaction with the polymer. Thus, the structural integrity of the differentiation factor, as well as its biological activity could be maintained during the processing step. The large surface area associated with the nanofiber mesh allows fast and efficient solvent evaporation, which provides to the incorporated drug a limited period of time to recrystallize, favouring the formation of amorphous dispersed phase [2, 6, 13]. The presence of amorphous dexamethasone in our polymeric carrier was also observed in our DCS data.

The most widely investigated delivery system for the encapsulation of bioactive compounds is micro- and nano-particles. Nanoparticles have facility to diffuse through cell membranes, allowing controlling or modifying the cell activity. The osteogenic differentiation factor herein incorporated in electrospun biodegradable nanofibers was already studied, by our group and others [29-37], in other drug delivery systems, including micro- and nano-particles and scaffolds. Those polymeric drug delivery systems are based in starch-polycaprolactone (SPCL) microparticles or carboxymethylchitosan/poly(amidoamine) dendrimer (CMChT/PAMAM) nanoparticles. Both devices were intended to be used as part of an injectable system or in a polymeric 3D scaffold. In the present work was presented a novel dexamethasone delivery system, based on electrospun biodegradable nanofibers as carrier. It is aimed at developing a system that simultaneously acts as a scaffold for mesenchymal stem cells differentiation toward the osteogenic lineage. The next generation of engineered tissues relies on the development of biodegradable scaffolds as physical supports to deliver bioactive molecules that control cell attachment, proliferation and differentiation [38].

Due to the relatively slow wetting, as a consequence of the highly hydrophobic character of the PCL NFM, and its slow degradation rate it was possible to deduce that dexamethasone release occurred primarily by diffusion, demonstrating that a biodegradable nanofibrous system can be used to obtain a release profile that was effective in differentiating stem cells. The burst release effect common in polymer-based release systems, is connected to the high gradients of concentration observed on the initial stages of release. In the system of 20 wt.% DEX-loaded PCL NFMs, the burst release effect may be primarily caused by an imperfect distribution/entrapment of the dexamethasone into the polymer matrix or by their tendency to migrate to the nanofiber surface during the electrospinning process [39]. As the nanofibers are placed in an aqueous environment, at the initial stage water penetrates into the nanofibers surface and a large amount of dexamethasone is faster released due to the initial surface erosion. Subsequently, water permeates into the bulk of the nanofibers causing polymer swelling, bond cleavage and bulk erosion, generating interconnecting pores and channels within nanofibers that allow the slow sustained release of the remaining dexamethasone [39].

#### *8.5.2. Bioactivity of the Dexamethasone Released from the Electrospun Nanofiber Meshes*

Drug delivery systems are developed to maximize the therapeutic activity while minimizing the toxic side effects of drugs. However, the scope of those devices is limited for targeting tissues rather than individual cells [1]. In tissue engineering, the required bioactive molecules are typically supplied to the cells growing on the scaffold in the culture medium, in the soluble form. The present drug carrier was designed to operate as a synthetic extracellular matrix - scaffold - for mesenchymal stem cell growth and, simultaneously, to allow directly supplying the differentiation factor to the adherent cells. This may it is intended to supply locally the required amount to promote the proliferation and differentiation towards the osteogenic lineage. To validate this hypothesis, an osteogenic differentiation study was conducted. The osteogenic differentiation is sensitive to the dose and duration of glucocorticoid exposure [40]. Jaiswal *et al.* [25] suggested that the effective concentration of DEX for

the osteogenic differentiation of MSCs should be in the range of 10 nM to 100 nM, showing toxic effects at 1000 nM.

The electrospun PCL NFMs loaded with 15 wt.% dexamethasone were cultured with hBMSCs under dexamethasone-absent osteogenic differentiation medium formulation. Our biological results confirm the biological activity of the incorporated dexamethasone, as shown by the increased amount of deposited calcium phosphates produced by the differentiated cells (also stained by alizarin red and identified by EDS). Additionally, the increasing concentration of the enzyme alkaline phosphatase (ALP) also confirms the osteoblastic differentiation and mineralization of hBMSCs cultured on DEX-loaded PCL NFMs. In fact, this enzyme catalyses the splicing of phosphate from non-phosphoric esters, constituting a biochemical indicator of the osteoblasts' presence and the deposition of mineralized ECM, since MSCs produce negligible amounts of this enzyme, as depicted by our results. This hypothesis of osteoblastic differentiation was confirmed by the expression of specific osteoblastic glycoproteins, namely osteopontin and bone sialoprotein, which are also present in the ECM of bone. The deposition and mineralization of ECM, previously observed in the SEM micrographs, stained with alizarin red and chemically identified by EDS, were also confirmed by the immunodetection of the osteocalcin protein, which binds strongly to apatite and calcium.

In the literature three periods were identified on the osteogenic differentiation of embryonic stem (ES) cells [41], corresponding to the expression pattern of the osteoblastic markers: a proliferative phase, followed by the period of matrix deposition and the mineralization phase. The highest expression peak of *Osteopontin* mRNA at 14 days of hBMSCs culture determines the end of the matrix deposition phase and the beginning of the mineralization phase. The very high expression level of *Bone Sialoprotein* confirms the presence of mature osteoblasts, corresponding to the mineralization phase. Finally, this phase was confirmed by the expression of *Osteocalcin* mRNA, which is designed as the essential marker of the mineralization phase, reaching a maximum expression just before or during tissue mineralization [31]. Therefore, considering our results and the differences in the cell type used, the

most important genes involved in the osteogenic differentiation process were constitutively expressed, confirming the matrix deposition and mineralization by hBMSCs cultured and differentiated on DEX-loaded NFMs. The main specific transcription factors involved in the osteogenesis were also quantified by qPCR, namely the core binding factor  $\alpha$  1/runt-related gene (*Cbfa1/Runx2*) and *Osterix* (*Osx*). *Cbfa1/Runx2* was already shown to be involved in the two steps of the differentiation process: driving stem cells into preosteoblasts and also preosteoblasts into osteoblasts. *Osterix* acts only during the last stage involving the transition preosteoblast/osteoblast [42, 43]. Our results showed that *Osterix* was one of the bone-specific transcripts with the highest expression level, similar to *Bone Sialoprotein* gene. This result further corroborates the successful differentiation of hBMSCs into osteoblasts on DEX-loaded NFMs. Similar osteoblastic gene expression patterns were observed for hBMSCs culture on DEX-loaded NFMs under basal conditions. This surprising result corroborates the hypothesis that even a transient exposure of stem cells to DEX (specifically during the 1<sup>st</sup> week) may be effective in inducing and maintaining the osteoblastic phenotype [25].

## 8.6. Conclusions

We report herein the development of electrospun biodegradable nanofibers has a delivery system of an established osteogenic differentiation agent of hBMSCs - dexamethasone. Dexamethasone was incorporated at different concentrations (5, 10, 15 and 20 wt.% polymer) in the polymeric nanofibers, and released accordingly in an amorphous state. The 15 wt.% delivery system was selected for cell studies to assess the bioactivity of the released dexamethasone. An increased alkaline phosphatase concentration and deposition of mineralized matrix was observed on dexamethasone releasing nanofibrous system cultured with hBMSCs in dexamethasone-absent osteogenic differentiation medium. The phenotypic and genotypic expression of osteoblastic-specific markers confirmed the osteogenic inducing potential of the loaded growth/differentiation factor. Thus, a novel osteogenic inductive scaffold was developed aimed for bone tissue engineering strategies.

## 8.7. References

1. Goldberg M, Langer R, Jia XQ. Nanostructured materials for applications in drug delivery and tissue engineering. *Journal of Biomaterials Science - Polymer Edition* 2007; 18(3):241-268.
2. Venugopal J, Low S, Choon AT, Ramakrishna S. Interaction of cells and nanofiber scaffolds in tissue engineering. *Journal of Biomedical Materials Research, Part B - Applied Biomaterials* 2008; 84(1):34-48.
3. Koo OM, Rubinstein I, Onyuksel H. Role of nanotechnology in targeted drug delivery and imaging: a concise review. *Nanomedicine* 2005; 1(3):193-212.
4. Sill TJ, von Recum HA. Electrospinning: applications in drug delivery and tissue engineering. *Biomaterials* 2008; 29(13):1989-2006.
5. Xie JB, Hsieh YL. Ultra-high surface fibrous membranes from electrospinning of natural proteins: casein and lipase enzyme. *Journal of Materials Science* 2003; 38(10):2125-2133.
6. Kenawy ER, Bowlin GL, Mansfield K, Layman J, Simpson DG, Sanders EH, *et al.* Release of tetracycline hydrochloride from electrospun poly(ethylene-co-vinylacetate), poly(lactic acid), and a blend. *Journal of Controlled Release* 2002; 81(1-2):57-64.
7. Huang ZM, Zhang YZ, Kotaki M, Ramakrishna S. A review on polymer nanofibers by electrospinning and their applications in nanocomposites. *Composites Science and Technology* 2003; 63(15):2223-2253.
8. Zhang YZ, Su B, Venugopal J, Ramakrishna S, Lim CT. Biomimetic and bioactive nanofibrous scaffolds from electrospun composite nanofibers. *International Journal of Nanomedicine* 2007; 2(4):623-638.
9. Mareschek S, Greiner A, Kissel T. Electrospun biodegradable nanofiber nonwovens for controlled release of proteins. *Journal of Controlled Release* 2008; 127(2):180-187.
10. Zeng J, Aigner A, Czubyko F, Kissel T, Wendorff JH, Greiner A. Poly(vinyl alcohol) nanofibers by electrospinning as a protein delivery system and the retardation of enzyme release by additional polymer coatings. *Biomacromolecules* 2005; 6(3):1484-1488.

11. Townsend-Nicholson A, Jayasinghe SN. Cell electrospinning: a unique biotechnique for encapsulating living organisms for generating active biological microthreads/scaffolds. *Biomacromolecules* 2006; 7(12):3364-3369.
12. Xu X, Chen X, Wang Z, Jing X. Ultrafine PEG-PLA fibers loaded with both paclitaxel and doxorubicin hydrochloride and their in vitro cytotoxicity. *European Journal of Pharmacy and Biopharmacy* 2009; 72(1):18-25.
13. Verreck G, Chun I, Peeters J, Rosenblatt J, Brewster ME. Preparation and characterization of nanofibers containing amorphous drug dispersions generated by electrostatic spinning. *Pharmaceutical Research* 2003; 20(5):810-817.
14. Katti DS, Robinson KW, Ko FK, Laurencin CT. Bioresorbable nanofiber-based systems for wound healing and drug delivery: Optimization of fabrication parameters. *Journal of Biomedical Materials Research, Part B - Applied Biomaterials* 2004; 70B(2):286-296.
15. Dong B, Smith ME, Wnek GE. Encapsulation of multiple biological compounds within a single electrospun fiber. *Small* 2009; 5(13):1508-1512.
16. Sanders EH, Kloefkorn R, Bowlin GL, Simpson DG, Wnek GE. Two-phase electrospinning from a single electrified jet: Microencapsulation of aqueous reservoirs in poly(ethylene-co-vinyl acetate) fibers. *Macromolecules* 2003; 36(11):3803-3805.
17. Chew SY, Wen J, Yim EK, Leong KW. Sustained release of proteins from electrospun biodegradable fibers. *Biomacromolecules* 2005; 6(4):2017-2024.
18. He CL, Huang ZM, Han XJ. Fabrication of drug-loaded electrospun aligned fibrous threads for suture applications. *Journal of Biomedical Materials Research* 2009; 89(1):80-95.
19. Jiang H, Hu Y, Li Y, Zhao P, Zhu K, Chen W. A facile technique to prepare biodegradable coaxial electrospun nanofibers for controlled release of bioactive agents. *Journal of Controlled Release* 2005; 108(2-3):237-243.
20. Zhang YZ, Wang X, Feng Y, Li J, Lim CT, Ramakrishna S. Coaxial electrospinning of (fluorescein isothiocyanate-conjugated bovine serum albumin)-encapsulated poly(epsilon-caprolactone) nanofibers for sustained release. *Biomacromolecules* 2006; 7(4):1049-1057.

21. Martins A, Araujo JV, Reis RL, Neves NM. Electrospun nanostructured scaffolds for tissue engineering applications. *Nanomedicine* 2007; 2(6):929-942.
22. Tayalia P, Mooney DJ. Controlled growth factor delivery for tissue engineering. *Advanced Functional Materials* 2009; 21:1-17.
23. Alberts B, Johnson A, Lewis J, Raff M, Roberts K, Walter P. *Molecular Biology of the Cell*. Fourth Edition. London, UK: Garland Science, 2002.
24. Salgado AJ, Oliveira JT, Pedro AJ, Reis RL. Adult stem cells in bone and cartilage tissue engineering. *Current Stem Cell Research & Therapy* 2006; 1(3):345-364.
25. Jaiswal N, Haynesworth SE, Caplan AI, Bruder SP. Osteogenic differentiation of purified, culture-expanded human mesenchymal stem cells in vitro. *Journal of Cellular Biochemistry* 1997; 64(2):295-312.
26. Martins A, Pinho ED, Faria S, Pashkuleva I, Marques AP, Reis RL, *et al.* Surface modification of electrospun polycaprolactone nanofiber meshes by plasma treatment to enhance biological performance. *Small* 2009; 5(10):1195-1206.
27. Delome B, Charbord P. Culture and characterization of human bone marrow mesenchymal stem cells. *Methods in Molecular Medicine* 2007; 140:67-81.
28. Venugopal J, Prabhakaran MP, Low S, Choon AT, Zhang YZ, Deepika G, *et al.* Nanotechnology for nanomedicine and delivery of drugs. *Current Pharmaceutical Design* 2008; 14(22):2184-2200.
29. Balmayor ER, Feichtinger GA, Azevedo HS, van Griensven M, Reis RL. Starch-poly- $\epsilon$ -caprolactone Microparticles Reduce the Needed Amount of BMP-2. *Clinical Orthopaedics and Related Research* 2009; 267(12):3138–3148.
30. Balmayor ER, Tuzlakoglu K, Azevedo HS, Reis RL. Preparation and characterization of starch-poly-epsilon-caprolactone microparticles incorporating bioactive agents for drug delivery and tissue engineering applications. *Acta Biomaterialia* 2009; 5(4):1035-1045.
31. Balmayor ER, Tuzlakoglu K, Marques AP, Azevedo HS, Reis RL. A novel enzymatically-mediated drug delivery carrier for bone tissue engineering applications: combining biodegradable starch-based microparticles and differentiation agents. *Journal of Materials Science* 2008; 19(4):1617-1623.

32. Oliveira JM, Sousa RA, Kotobuki N, Tadokoro M, Hirose M, Mano JF, *et al.* The osteogenic differentiation of rat bone marrow stromal cells cultured with dexamethasone-loaded carboxymethylchitosan/poly(amidoamine) dendrimer nanoparticles. *Biomaterials* 2009; 30(5):804-813.

33. Oliveira JM, Kotobuki N, Marques AP, Pirraco RP, Benesch J, Hirose M, *et al.* Surface engineered carboxymethylchitosan/poly(amidoamine) dendrimer nanoparticles for intracellular targeting. *Advanced Functional Materials* 2008; 18(12):1840-1853.

34. Duarte ARC, Mano JF, Reis RL. Dexamethasone-loaded scaffolds prepared by supercritical-assisted phase inversion. *Acta Biomaterialia* 2009; 5(6):2054-2062.

35. Eroglu H, Kas HS, Oner L, Turkoglu OF, Akalan N, Sargon MF, *et al.* The in-vitro and in-vivo characterization of PLGA:L-PLA microspheres containing dexamethasone sodium phosphate. *Journal of Microencapsulation* 2001; 18(5):603-612.

36. Yoon JJ, Kim JH, Park TG. Dexamethasone-releasing biodegradable polymer scaffolds fabricated by a gas-foaming/salt-leaching method. *Biomaterials* 2003; 24(13):2323-2329.

37. Silva GA, Costa FJ, Neves NM, Coutinho OP, Dias AC, Reis RL. Entrapment ability and release profile of corticosteroids from starch-based microparticles. *Journal of Biomedical Materials Research* 2005; 73(2):234-243.

38. Habibovic P, de Groot K. Osteoinductive biomaterials--properties and relevance in bone repair. *Journal of Tissue Engineering and Regenerative Medicine* 2007; 1(1):25-32.

39. Abidian MR, Martin DC. Multifunctional nanobiomaterials for neural interfaces. *Advanced Functional Materials* 2009; 19(4):573-585.

40. Beresford JN, Joyner CJ, Devlin C, Triffitt JT. The effects of dexamethasone and 1,25-dihydroxyvitamin D3 on osteogenic differentiation of human marrow stromal cells in vitro. *Archives of Oral Biology* 1994; 39(11):941-947.

41. zur Nieden NI, Kempka G, Ahr HJ. In vitro differentiation of embryonic stem cells into mineralized osteoblasts. *Differentiation* 2003; 71(1):18-27.

42. Ryoo HM, Lee MH, Kim YJ. Critical molecular switches involved in BMP-2-induced osteogenic differentiation of mesenchymal cells. *Gene* 2006; 366(1):51-57.

43. Satija NK, Gurudutta GU, Sharma S, Afrin F, Gupta P, Verma YK, *et al.* Mesenchymal stem cells: molecular targets for tissue engineering. *Stem Cells and Development* 2007; 16(1):7-23.



## **Section VI**

GENERAL CONCLUSIONS AND FURTHER WORK



## Chapter 9

### Concluding Remarks

## 9.1. Conclusions

The three common strategies employed in cell-based therapies for tissue regeneration are infusion of isolated cells, treatment with molecules inducing tissue-morphogenesis, and implantation of a cell-scaffold hybrid construct. Of the three strategies, the use of cell-scaffold hybrids generally leads to a more controlled outcome. In contrast to the infusion of cells, the scaffold acts as a synthetic extracellular matrix (ECM) substitute in which the cells can proliferate, migrate and/or differentiate, produce a mature matrix and a functional tissue, recapitulating the normal tissue development process and allowing cells to mature their own preferred microenvironments.

Much attention has been given recently to the production of scaffolds that mimic the extracellular microenvironment. Indeed, the design and production of polymeric structures that resemble the hierarchical composite structure of the natural extracellular matrix remains a challenging task. At the macroscopic level, a scaffold should impart a 3D geometry, having adequate mechanical properties to support the physiologic loads developing at the tissue site. At the microscopic level, a highly porous structure is needed for diffusion of cells, nutrients and metabolic products throughout the scaffold. The optimal pore size should be tailored to the specific cell type and be large enough to allow for cell infiltration and ECM formation yet not being so small that lead to pore occlusion. The scaffold surface morphology and chemistry should facilitate cell adhesion and migration through the scaffold, provide developmental signals to the cells, and promote cell recruitment from the surrounding tissue. Additionally, in most cases the scaffold should be constructed from a degradable nontoxic, non-immunogenic and biocompatible material. To this end, numerous natural and synthetic materials have been proposed for use in tissue scaffolds.

Among the various nanostructured scaffolds recently developed, enabled by the advent of the nanotechnology and nanoscience, membranes made of nanofibers from synthetic and natural-origin polymers have received increased attention due to their easy fabrication and the ability to control their compositional, structural and

functional properties. Herein, the resurged polymer processing technique – electrospinning – was exploited in the development of nanofibrous structures and, subsequently, testing its applicability in the tissue engineering field. The key advantage of producing fibers with extremely small diameters is their very high specific surface area, high porosity and micro-range pore size. Besides the topographical properties of the electrospun nanofiber meshes, the fibers surface chemistry also plays an important role on cell adhesion. In fact, the presence of functional chemical groups facilitates the adhesion of protein and cell adhesion. To enhance the biofunctionality of electrospun synthetic NFMs, they were submitted to different plasma treatments including the gas used ( $O_2$  and Ar), the electrical power, and the exposure time. SEM micrographs and surface roughness analysis demonstrated the induction of some unintended topographical alterations by the plasma treatments. The contact angle analysis revealed that the electrospun NFMs became generally more hydrophilic after the applied modifications, being the most significant changes in the wettability observed for  $O_2$ -treated NFMs. XPS results indicated higher oxygen-contents at the surface of plasma-treated NFMs, including hydroxyl (-OH) and carbonyl (-C=O) functionalities. Three model cell types, namely fibroblasts (L929 cell line), chondrocytes (ATDC5 cell line), and osteoblast-like (Saos-2) cells, were used to study the effect of plasma treatments over the morphology, cell adhesion, and proliferation. From the biological results it was possible to define treatment conditions leading to significantly enhanced cell adhesion and faster proliferation, namely  $O_2$  at 30W for 5 min and Ar at 20W for 5 min. Despite the often claimed morphological similarity of NFMs to natural ECMs, both those plasma treatment conditions could enhance the biological performance showing that the surface chemistry is at least as important as the surface morphology.

It is frequently mentioned in the literature that the typical random distribution of the electrospun nanofibers in a mesh-like structure resembles the topography of the native collagen ECM of various connective tissues. However, the complex ordered organization of the ECM is not usually replicated in this typical randomly aligned nanofibrous structure. Herein we presented an ordered microporous fibrous structure composed of both random/orthogonal and parallel/uniaxial aligned fibers, designated

as patterned nanofiber meshes. In fact, those patterned structures were initially developed in an attempt to control the topography and, consequently, the mechanical properties of the nanofiber meshes. It is shown that this elaborated structure induces guidance of human bone marrow mesenchymal stem cells (hBMSCs) along the uniaxially aligned fibers, mainly at earlier culturing periods under basal and osteogenic differentiation conditions. Although it was demonstrated that the cells are somewhat sensitive to the topography of the supporting surface, the exact reasons for this observation are still unclear. Additionally, the results from phenotypic and genotypic characterization demonstrated the effectiveness of P-NFM on the differentiation of hBMSCs into osteoblastic cells and, consequently, in the deposition of mineralized ECM. Our results undoubtedly represent a new and enhanced functional outcome of the patterned electrospun nanofiber meshes.

Ideally, to create a tissue-engineered scaffold capable of regenerate a fully functional tissue, it should mimic both the fibrous morphology and the complex structure/functionality of the native ECM. This ECM analogue should have topographical features and geometry on the macro-, micro and even nanoscale levels, as each may influence cell response to the scaffold. Electrospun nanofibrous structures, due to their inherent planar structure, could compromise a successful reconstruction or regeneration of bone tissue. Herein, multi-scale polymeric fibrous structures were developed by integrating microfibrillar structures, produced rapid prototyping or fiber bonding techniques, with electrospun nanofiber meshes. In this study, novel hierarchical starch-based scaffold were obtained by a combination of starch-polycaprolactone (SPCL) micro- and polycaprolactone (PCL) nano-motifs, respectively produced by rapid prototyping (RP) and electrospinning techniques. These scaffolds were characterized by a 3D structure of parallel aligned rapid prototyped microfibrils, periodically intercalated by randomly distributed electrospun nanofibers. The integration of these nano-motifs resulted in an 11 % decrease of the scaffold porosity, although maintaining the necessary interconnectivity. The integrated nanofiber meshes provide topological cues at the ECM level, whereas the micro 3D fibrous structure provides the required mechanical stability. Human osteoblast-like cells presented significantly higher proliferation and maturation when dynamically

seeded on these hierarchical starch-based fibrous scaffolds. Particularly, SEM micrographs demonstrated that the osteoblastic cells preferentially adhered and spread on the nanofiber meshes, constituting an innovative strategy to enhance cell seeding efficiency/cell adhesion into the microfibrinous scaffolds. Ultimately, this nanofiber mesh integration will significantly improve the potential application of such 3D fibrous structures in bone tissue-engineering strategies.

Current attempts to replicate the complexity and hierarchical organization of natural ECM are mostly restricted to dispensing nanofibers in existing implants and biomedical devices or used as random nanofibrous meshes. In another study, we developed novel highly functional fibrous composite scaffolds by the integration of electrospun chitosan (Cht) nanofibers within biodegradable polymeric microfibers (poly(butylene succinate) - *PBS* and *PBS/Cht*), assembled in a fiber mesh structure. The influence of electrospun chitosan nanofiber reinforcement on the biological performance of *PBS* and *PBS/Cht* microfibrinous scaffolds was assessed, using hBMSCs under osteogenic differentiation inductive conditions. Biological data demonstrated that the electrospun chitosan nanofibers used to reinforce the microfibers, although improving the mechanical and degradation properties of the composite fibers, still preserve the excellent *in vitro* biological performance already described for *PBS/Cht* fiber mesh scaffolds. Among the developed fiber meshes, only the *PBS/Cht*-based scaffolds sustained an ECM deposition and mineralization, as suggested by the increased amount of calcium phosphates produced by the osteogenic differentiated hBMSCs. Therefore, while a detailed mechanism to explain this behaviour is beyond the scope of this work (i.e. nanofiber reinforcement), the biological performance of the biodegradable nanofibrous reinforced microfibrinous scaffolds is mainly a function of the physicochemical (e.g. roughness and chemical composition) surface properties. These data represent the first report on the biological functionality of biodegradable nanofiber-reinforced composite scaffolds, envisaging the applicability of the developed structures for bone tissue engineering.

As previously mentioned, the main properties of electrospun nanofiber meshes were the extremely small fibers diameters and, consequently, their very high specific surface area, high porosity and micro-range pore size. However, electrospun

nanofiber meshes present a critical limitation hindering its application in 3D tissue engineering applications: the obtained pore size is typically too small to allow for cell infiltration into the inner regions of the nanofibrous scaffold. To overcome this problem, we proposed the simultaneous electrospinning of PCL and PEO solutions to obtain a dual composition random fiber mesh, followed by the selective dissolution of the PEO fraction to increase the porosity. It was observed that this method indeed increases the pore size without major alterations of the mesh structure. Pore size measurements shown a significant increase of pore size (doubling) in those meshes when comparing with control PCL NFM, and confirmed by interferometric optical profilometry. A novel clamping system was developed to have the double function of limiting the seeding area and to clamp the meshes at a certain distance from the bottom of the culture well-plate. By scanning electron microscopy and laser scanning confocal microscopy it was observed that the meshes allow for the infiltration of human osteoblastic cells into the 3D structure, migrating from one side of the mesh into the opposite side. Those cultured cells present enhanced viability and proliferation due to the colonization of the entire thickness of the fibrous scaffold. Consequently, a fully cellularized electrospun nanofiber mesh was obtained, being also appropriated for 3D Tissue Engineering applications.

The chemical and topographical properties of the scaffolds should provide an appropriated environment for tissue development, allowing also for the incorporation of biological signals to enhance tissue formation. This is still today one of the main challenges in the field. Electrospun fibrous structures were also proposed as drug release systems based on the concept that the dissolution rate of a drug increases with the increase of the surface area of both the drug and the corresponding carrier. We report herein the development of electrospun biodegradable nanofibers as a release system of an established osteogenic differentiation agent of hBMSCs - dexamethasone. Dexamethasone was incorporated at different concentrations (5, 10, 15 and 20 wt.% polymer) in the polymeric nanofibers, being the 15 wt.% system selected for cell studies because of its sustained release. An increased alkaline phosphatase concentration and deposition of mineralized matrix was observed on dexamethasone releasing nanofibrous system cultured with hBMSCs in

dexamethasone-absent osteogenic differentiation medium. The phenotypic and genotypic expression of osteoblastic-specific markers confirmed the osteogenic inducing potential of the loaded growth/differentiation factor. Thus, a novel osteogenic inductive scaffold was developed aimed for bone tissue engineering strategies.

As a final remark, we can say that many of the challenges discussed in the review paper were touched during the course of the work leading to the present PhD thesis. We believe that the contributions herein compiled helped to improve our knowledge on the ways not only to overcome the limitations of electrospun nanofiber scaffolds but, in some cases, to take advantage of those limitations to present new solutions to specific challenges of designing highly functional scaffolds for specific TE problems.

## **9.2. Future work**

The scientific and technology development processes are a never-ended journey. Each closed research project opens a new range of questions that can be exploited in multiple directions. The work developed in the scope of this thesis is not an exception.

By using patterned meshes we believe that new opportunities may be explored for the regeneration of more complex and ordered tissues (e.g. bone and skin) involving more than one cell communities. In a similar approach, the application of hierarchical fibrous scaffolds could be an outstanding point on the *in vitro* generation of hierarchically structured tissues, namely vascularised tissues like bone. The strategy of dual composition nanofiber mesh, followed by the selective removal of one fraction, can be systematically implemented to successfully overcome the critical limitation of the control of the pore size in electrospun meshes. The electrospun nanofiber mesh incorporating a growth/differentiation factor only release one of the supplements of a standard osteogenic differentiation medium. More complex release system, incorporating those differentiation factors, could be developed based on a co-electrospinning strategy.

Several nanofibrous-based structures were developed, namely complex ordered scaffolds, highly porous nanofiber meshes and bioactive electrospun nanofibers, and tested biologically *in vitro*. However, in the nanofibrous-based scaffolds studied with cell lines the obtained data should be further confirmed using primary cells, prior to the *in vivo* studies. The studies where mesenchymal stem cells were differentiated into the osteogenic lineage, it is desired to observe the *in vivo* performance of the corresponding nanofibrous-based scaffolds.

Considering the diversity of developed scaffolds with independent physical or chemical properties, the conjugation of those properties into one structure will theoretically improve its biological performance. As an example, the optimum surface plasma modifications could be applied for any presented nanofibrous-based scaffold. The functional complexity of the hierarchical fibrous scaffolds could be also improved by the incorporation of biological factors into the nanofibers. Specifically in the case of hierarchical fibrous scaffold, the opportunity of incorporation biological factors into electrospun nanofibers makes possible to spatially and temporally control, layer by layer, the differentiation of progenitor cells toward desired lineages.

It is also important to mention that some of those strategies are being followed for some of my group colleagues. For ethical reasons and intellectual property protection, any more details will be presented in this thesis.